Determination and selective decomposition of alkyl hydroperoxides for the selective oxidation of hydrocarbons

Bahhaj Alshammari

Thesis submitted to the University of Sheffield for degree of Doctor of Philosophy in Science

School of Mathematical and Physical Sciences

October 2024

Author’s Declaration

I, Bahhaj Alshammari, confirm that the Thesis is my own work. I am aware of the University’s Guidance on the Use of Unfair Means (www.sheffield.ac.uk/ssid/unfair-means). This work has never before been submitted for an award at this university, or any other, university.

Acknowledgments

First and foremost, I would like to extend my deepest gratitude to my supervisor Dr.Marco Conte whose unwavering support and guidance have been invaluable throughout this journey. During some of the most difficult times, when I faced significant challenges and was on the verge of giving up, Marco was there offering not just academic advice but also kindness and patience that kept me moving forward. His belief in me meant more than words can express. From the bottom of my heart, I want to say thank you for everything you've done for me. You are truly an amazing person. "Thank you" doesn't feel like enough to express my gratitude, but please know how much your support has meant to me.

I would also like to express my gratitude to the department staff for their support throughout my research. Special thanks go to: Ms. Anna Foster (University of Sheffield) for ICP analysis, Dr. Craig Robertson (University of Sheffield) for XRD analysis, Dr. Khalid Doudin (University of Sheffield) for support and training for NMR analysis. I would then like to thank Dr. Naoko Sano (University of Newcastle) for XPS analysis, Prof. Xi Liu (Shanghai Jiao Tong University) for TEM data and data analysis, Dr. Marco Conte (University of Sheffield) for data analysis for XRD, XPS and textural properties. Additionally, I would like to thank acknowledge Dr. Simon Thorpe and Mr. Joe Quick for the training with gas cylinders and the support provided in the laboratory where I have worked at the University of Sheffield. I am deeply appreciative of everyone who contributed, and I offer my sincere thanks to all.

I would like to express my sincere gratitude to my sponsor, the University of Hafr Albatin in Saudi Arabia, for their financial support and for granting me this invaluable opportunity to expand my knowledge.

I am also deeply grateful to my parents and my family, each and every one of them, for their unwavering support, constant encouragement, and for always being proud of me. You have been my backbone throughout this journey and your belief in me has

been a source of strength. Thank you all for being there for me, through thick and thin. To my dear husband and my wonderful children, Diyam and Talal, thank you from the bottom of my heart for always being there for me. Your love, patience, and constant support have made even the most challenging times feel lighter and more manageable. I am incredibly grateful for each of you, and this achievement is as much yours as it is mine.

I want to extend my heartfelt thanks to my dear friend Raged from Iraq. Your unwavering support during my difficult times has meant a lot to me. I truly appreciate everything you've done it has made all the difference. Thank you, Mengyuan. It has been a wonderful coincidence and a stroke of luck to have you as both a friend and co-worker. I truly appreciate your constant support, your willingness to listen, and your openness in sharing throughout this journey. Your friendship has made all the difference, and I am so grateful to have had you by my side through the ups and downs.

Finally, Thank you to all my friends and colleagues for your support, encouragement, and the wonderful times we've shared together. They mean so much to me. I can't mention each of you personally due to space, but you all hold a special place in my heart.

Abstract

This study focusses on the design of supported metal nanoparticle catalysts in a solvent free system under mild reaction conditions, as well as the selective oxidation of alkanes and cyclic alkanes utilising molecular oxygen as the oxidant. The projects' goal is to develop supported metal nanoparticle catalysts for the direct oxidation of hydrocarbons, enabling the synthesis of oxygenated products such as alcohol and ketone. These compounds serve as important products in the production of fibres, fragrances and pharmaceuticals. With this objective, supported Ag metal particles were synthesized, showing the ability to activate both molecular oxygen O_2 and the organic substrate. In specific terms, Ag/Nb_2O_5 was designed for the oxidation of ethylbenzene, cyclooctane, and *p*-xylene. An extensive study was conducted to assess Ag and Nb_2O_5 catalytic efficacy in the oxidation of ethylbenzene. This involved characterising the metal and support using XPS, XRD, and TEM, as well as a methodical assessment of the impact of alcohol or 1-phenyl ethyl alkyl hydroperoxide residues in ethylbenzene. 1-phenyl ethyl alkyl hydroperoxide (EBHP) is a significant oxidation product generated through the autoxidation of ethylbenzene. Due to the weak O-O bond in EBHP, a detailed investigation of its decomposition was conducted using gas chromatography-mass spectrometry (GC-MS), along with method development and validation using nuclear magnetic resonance (NMR) spectroscopy for quantitative analysis. Method development for the characterization of EBHP was validated, demonstrating that the use of Ag/Nb_2O_5 catalyst enables the selective formation of the desired ketone product. With a total selectivity of approximately 70% to 75% from these substrates, this catalyst shows significant potential for application in the manufacturing of products that contain oxygen, particularly ketone. As a result of these significant findings, the role of supported Ag particles and Nb_2O_5 in the oxidation process was carefully studied. Interestingly, Ag^0 was shown to have the ability to activate molecular oxygen producing reactive superoxide species ($O2^{\bullet-}$), and Ag^+ was participating in the C-H bonds activation. The supported metal oxide Nb_2O_5 was proved to be effective for the decomposition of the intermediate 1-Phenyl ethyl alkyl hydroperoxide to generate the desired products ketone in our case with a higher selectivity. This intriguing result aligns with the objective of developing a metallic

partner that helps the initiation of the reaction and another that enhances its selectivity. Consequently, this leads to the practical realization of a bifunctional catalyst.

List of abbreviations

AP	Acetophenone
BDE	Bond Dissociation Energy
BET	Brunauer-Emmet-Teller
BSTFA	N,O-bis (trimethylsilyl) trifluoroacetamide
COSHH	Control of Substances Hazardous to Health
CMB	Carbon Mass Balance
DCM	Dichloromethane
EBHP	1-phenyl ethyl alkyl hydroperoxide
EB	Ethylbenzene
1-Ph	1-phenylethanol
GC-MS	Gas Chromatography-Mass Spectrometry
ICP-MS	Inductively coupled plasma – mass spectroscopy
M: S	Metal to substrate ratio
NIST	National Institute of Standards and Technology
NMR	Nuclear Magnetic Resonance
KA Oil	Ketone-Alcohol oil
tBHP	tert Butyl Hydroperoxide
Q-TOF	Quadrupole Time of Flight
SMSI	Strong Metal Support Interaction

List of abbreviations

TEM	Transmission Electron Microscopy
TGA	Thermogravimetric Analysis
TPA	Terephthalic acid
TPP	Triphenylphosphine
TPPO	Triphenylphosphine oxide
WI	Wet impregnation
XPS	X-ray Photoelectron Spectroscopy
XRPD	X-ray Powder Diffraction

Thesis contents

Chapter 1: Introduction

Selective oxidation of hydrocarbons serves as a crucial method for adding functional groups to generate various oxygenated products, including aldehydes, alcohols, ketones, and carboxylic acids. However, achieving high yields of the desired product under mild reaction conditions remains a significant challenge. This chapter focuses on several key aspects: i) it is fundamentally important to understand the process by which alkanes or cyclic alkanes oxidise and the challenges associated with achieving selective oxidation (the activation of O_2 and dissociation of C-H bonds); ii) building on point i), this study will show various catalytic systems suitable for oxidation. This investigation is aimed at developing supported metal nanoparticle catalysts, with a subsequent analysis of how the properties of these catalysts influence their catalytic activity, providing valuable insights for catalyst design; iii) Nb_2O_5 was selected as either the active phase or the support material after a thorough analysis of the literature on supported metal catalysts for hydrocarbon oxidation and earlier studies by our group. It was expected that supported silver (Ag) nanoparticles would improve molecular oxygen activation. This thesis suggests using a unique Ag/Nb_2O_5-supported metal nanoparticle system for hydrocarbon oxidation in light of these findings. 1-phenyl ethyl alkyl hydroperoxide plays a key role in this chemistry, representing the initial semi-stable products formed during hydrocarbon autoxidation. These compounds are integral to numerous industrial and laboratory applications due to their ability to generate free radicals, which drive many chemical reactions. However, alkyl hydroperoxides have a weak oxygen-oxygen bond that is highly susceptible to decomposition. Therefore, as this work focuses on the autoxidation of hydrocarbons, which leads to the formation of these species, we begin by studying their reactivity in detail for quantitative purposes in chapter 3. 1-phenyl ethyl hydroperoxide (EBHP) are significant oxidation products formed through the autoxidation of ethylbenzene and serve as important intermediates in understanding the decomposition of these compounds as illustrated in scheme 1.1. 1-phenylethyl alkyl hydroperoxide releases free radicals due to autoxidation processes that are closely linked to radical pathways and interaction of intermediate with molecular oxygen in its triplet ground state ($3O_2$).

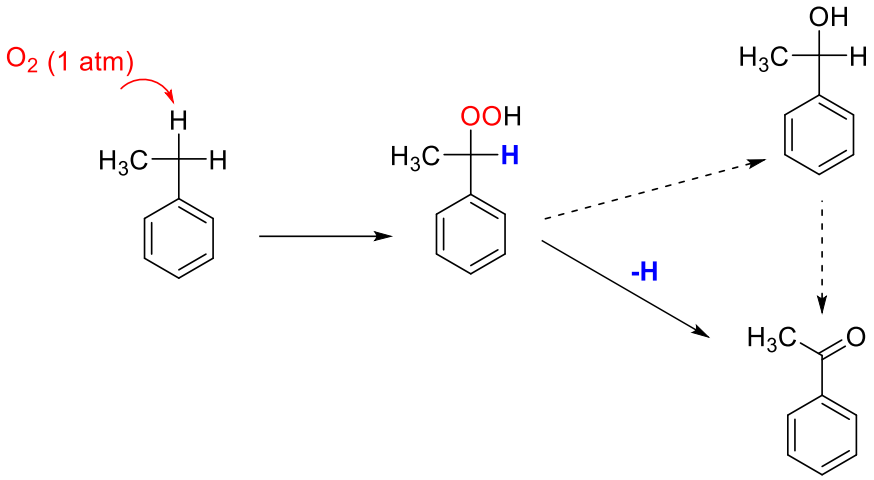

Scheme 1.1: A simplified pathway for the ethylbenzene oxidation to 1-phenyl ethyl hydroperoxide and this decomposes to acetophenone R=O and 1-phenylethanol R-OH.

A challenge arises because EBHP can decompose via catalytic reactions or thermally. However, many analytical techniques such as gas chromatography-mass spectrometry (GC-MS) one of the most widely used methods for characterizing products due to its low detection limit (1-10 ppt), and hydrocarbon products are quantified with high accuracy. However, the high temperatures involved in GC-MS can decompose alkyl hydroperoxide intermediates during analysis rather than during the actual reaction. However, NMR offers faster screening techniques despite having higher detection limits than GC-MS. Additionally, NMR measurements are typically conducted at ambient temperature, reducing the risk of initiating unwanted reactions and preventing the decomposition of intermediates. Thus, with the aim of studying various analytical techniques to develop fast and reliable characterization protocols for analyzing different hydrocarbons and understanding the reactivity of this intermediate. After achieving this goal, In order to selectively oxidise alkanes or cyclic alkanes, our next goal is to create supported metal oxide catalysts. Industrial materials can be manufactured using these catalysts to produce corresponding alcohols or ketones. A significant portion of the modern chemical industry relies on catalytic selective oxidation, as illustrated in figure 1.1. Over 60% of chemicals and intermediates produced globally through catalytic processes result from oxidation[1]. Aromatic hydrocarbons such as ethylbenzene and *p*-xylene, along with cyclooctane are widely used in the laboratory and petrochemical industry. These compounds serve as crucial precursors for numerous products such as nylons, and polyester [2-3].

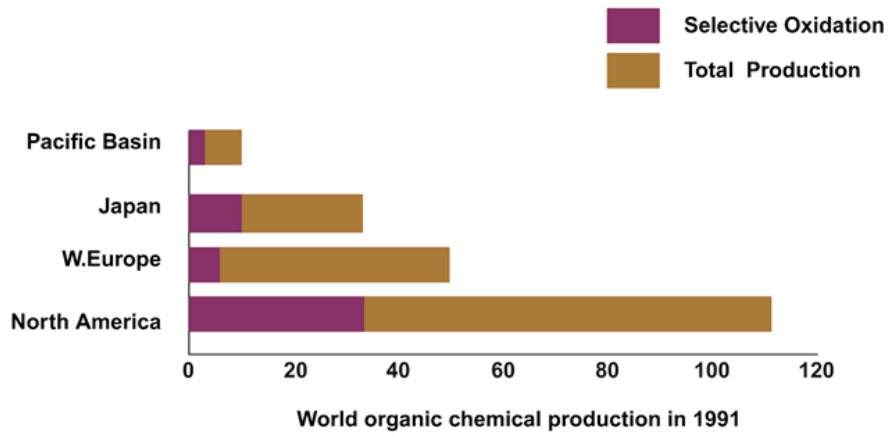

Figure 1.1: Selective oxidation constitutes a substantial portion of the global market (data as of 1991). Of this, 25% was achieved using heterogeneous catalysts, with one of the most significant applications being the functionalization of hydrocarbons [177].

1.1 Activation of hydrocarbons

Compounds of hydrogen and carbon that fall into several subcategories are known as hydrocarbon molecules. They can exist in a linear or cyclic form and can be either saturated or unsaturated. Different states contain hydrocarbons: gaseous (e.g., methane), liquid (e.g., ethylbenzene), or solid (e.g., polymers), each with different properties. Naturally occurring hydrocarbons are the main components of fossil fuels such as natural gas and petroleum, which are also found in plants and trees. Primarily, hydrocarbons serve as a crucial source of energy. Activating the inert C-H bonds in these molecules to generate functional groups like hydroxyl or carbonyl is an important reason to use them as precursors for chemicals instead of fuels. This transformation converts them into valuable molecules for the drug, food, and pharmaceutical industries [4-5]. The oxidation of hydrocarbons can be categorized into two main types: total oxidation resulting in CO_2 (known as combustion) and partial or selective oxidation. Our work specifically studies partial and selective oxidation aiming to produce more valuable products while minimizing the formation of CO_2. Throughout the process one of the primary challenges is the chemo-selective activation of C-H bonds. The high activation energy required for C-H bonds in hydrocarbons (as shown in table 1.1), typically ranges from 395-410 kJ mol^{-1} [6-7], means that breaking these bonds is generally challenging and this needs high temperatures and pressures, as well as the use of corrosive and costly media [8].

Table 1.1: Dissociation energy of the C-H bonds in a range of significant organic compounds [7].

Compound	Formula	C-H bond energy (kJ mol^{-1})
Benzene	C_6H_5-H	473
Toluene	$C_6H_5CH_2$-H	377
Cyclooctane	C_8H_{15}-H	385
Ethylbenzene	C_6H_5-CH_2-CH_3	343
Cyclohexane	C_6H_{11}-H	414

For example, terephthalic acid is produced by oxidizing *p*-xylene with air in an acetic acid solvent conducted at temperatures between 175 and 225 °C and pressures of 15 to 30 bar [9]. As a result of these conditions, it is often difficult to control the reaction leading to the formation of thermodynamically stable undesired products such as CO_2 and H_2O. Taking these factors into account, ethylbenzene was selected as the primary substrate for this thesis. Ethylbenzene contains one CH_2 group and one CH_3 group, Activation of the primary C-H bond is particularly challenging because it has the highest energy compared to other C-H bonds in the ethylbenzene, as illustrated in scheme 1.2. The energy difference between primary CH_2 and secondary CH_3 bonds is 67 kJ mol^{-1}. Consequently, it is expected that the internal position will be oxidized first, producing a mixture of alcohol and ketone.

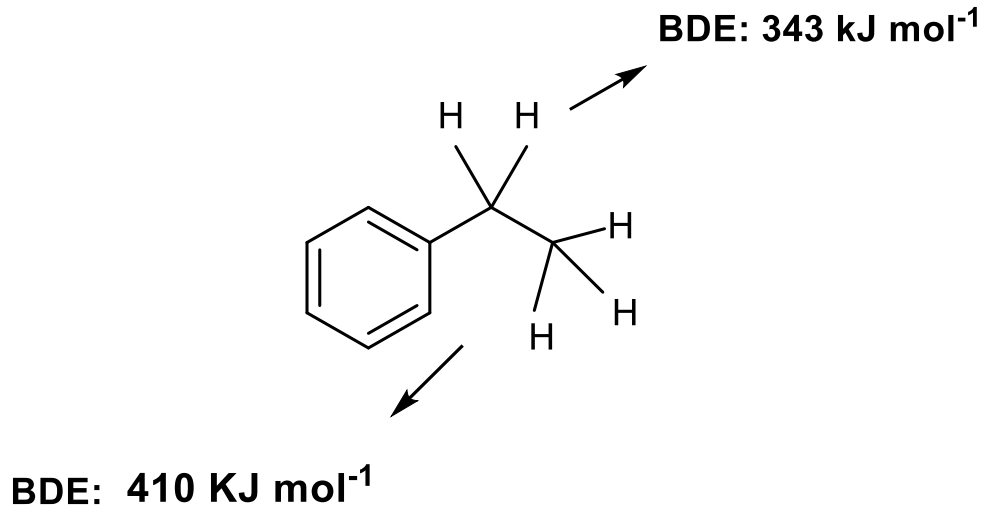

Scheme 1.2: Bond dissociation energy (BDE) in main and secondary C-H bonds is displayed in the ethylbenzene structure [10].

Due to this, it is of great significance that C-H bonds are selectively functionalized under mild reaction conditions (lower temperature, pressure) to generate functionalized products. Typically, saturated hydrocarbons do not display basic or

acidic properties and are generally unreactive towards nucleophiles or electrophiles, except when exposed to certain highly reactive species like super acids (e.g., antimony pent-fluoride in the oxidation of benzene) [11-12]. Considering this, the direct aerobic oxidation of hydrocarbons with air or O_2 as an oxidant is fundamentally an environmentally friendly process. It is also more cost-effective compared to other oxygen transfer reagents like H_2O_2 and tBHP, which are generally expensive, limit industrial applications, and often produce undesirable by-products [13-14]. In light of these considerations, a major field of research is the development of an efficient catalytic technique for the aerobic oxidation of hydrocarbons using molecular O_2. Depending on the hydrocarbon involved, catalyst design can focus on generating steric interactions or creating specific reactive sites capable of functionalizing the primary C-H bond without causing over-oxidation.

1.2 Selective oxidation of hydrocarbons

Selective oxidation reactions are essential in today's organic synthesis and chemical industry [15-16]. After polymerization, oxidation is the second most significant process accounting for approximately 30% of the industry's total production [17]. Selective oxidation catalysis is used to produce many essential chemicals and intermediates including alcohols, aldehydes, ketones, and organic acids. In today's chemical industry, some of the most well-known selective oxidation processes include the oxidation of ethylbenzene to acetophenone and *p*-xylene to terephthalic acid, and the oxidation of cyclohexane to cyclohexanone. The chemical industry needs to enhance selectivity to minimize the generation of non-selective by-products, particularly CO_2. This improvement is crucial for reducing waste and increasing process efficiency. The catalytic oxidation of alcohols to aldehydes or ketones is a key transformation in organic chemistry. Traditionally, about 70% of the oxidation process depends on stoichiometric reagents like permanganate and dichromate to produce products [16]. However, these stoichiometric oxidants are costly and /or toxic and generate substantial amounts of heavy metal waste. For instance, the oxidation of *p*-xylene using potassium permanganate would generate millions of tons of waste annually, specifically, Mn_2O_3 and NaOH, if this reaction (Scheme 1.3) were still used industrially. This is because $KMnO_4$ acts as a non-recyclable reagent being consumed in large quantities without regeneration.

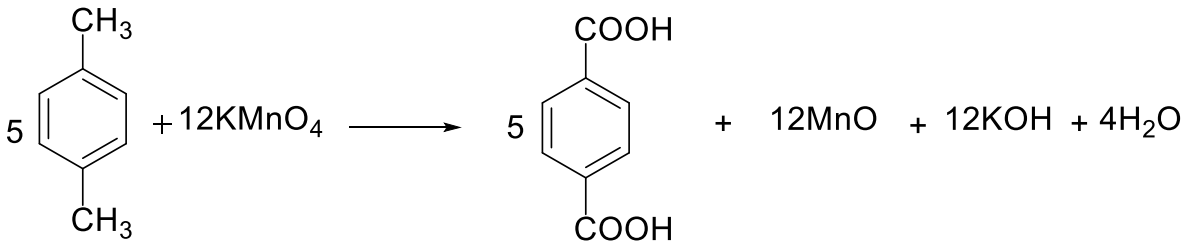

p-xylene

Scheme 1.3: Oxidation of *p*-xylene by $KMnO_4$ as the oxidizing agent, leading to the production of significant waste by-products such as MnO and KOH and water. $KMnO_4$ is not regenerated but and consumed in large quantities as stoichiometric reagent.

The scientific community is prioritizing and minimizing the environmental impact of oxidation processes in the synthesis of fine and commodity chemicals [18]. Molecular oxygen is an attractive oxidant due to its low cost and environmentally friendly by-

products it generates such as H_2O [19]. In chemistry, using O_2 as a partial oxidant is still a challenge. The process must effectively control the reaction to prevent complete oxidation. Once the C-H bond is activated, further oxidation reactions become thermodynamically favourable, driven by the significantly negative standard free energy associated with the formation of oxidation products [20]. The challenge is to either (i) slow down the rate of over-oxidation, which may reduce the overall reaction rate when aiming for selectivity, or (ii) develop a catalyst and methodologies that facilitate a reaction pathway capable of desorbing the product before it undergoes further oxidation.

In industry, aerobic oxidations for producing chemicals are typically autoxidation that follows radical pathways. Among the successful examples are terephthalic acid and cyclohexanone. Terephthalic acid (TPA) is synthesized by reacting *p*-xylene with oxygen in the presence of a catalytic mixture of trivalent cobalt and manganese acetate salt, along with an ammonium bromide co-catalyst, all dissolved in acetic acid (Scheme 1.4). Bromine free radicals are produced, which activate the methyl groups of p-xylene leading to the formation of aromatic aldehydes. These aldehydes are subsequently oxidized to carboxylic acids [21]. Almost all of the 30 million tons of TPA produced annually is utilized as a precursor in the manufacture of polyethylene terephthalate, which is a key material in plastic bottles and synthetic fibres [22-23].

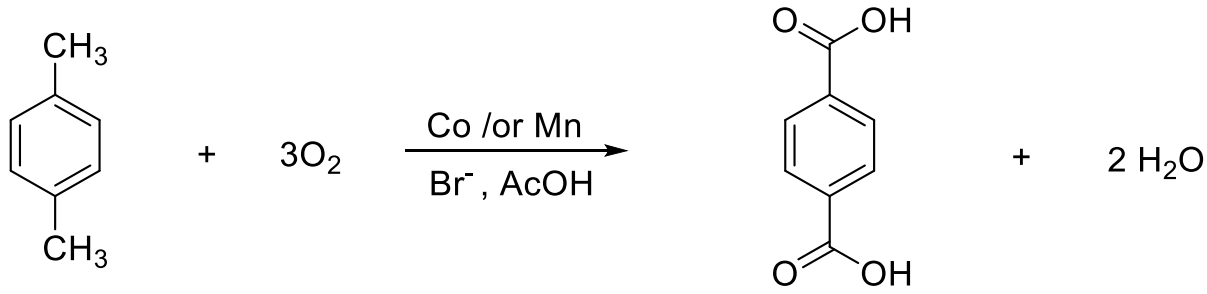

Scheme 1.4: Terephthalic acid (TPA) is synthesized by reacting *p*-xylene with oxygen in the presence of a catalytic mixture of trivalent cobalt /or manganese acetate salts along with ammonium bromide co-catalyst in an acetic acid media.

In addition, air is used as an oxidant to produce cyclohexanone and cyclohexanol known as K/A oil. When cyclohexane reacts with oxygen in the presence of cobalt or

manganese acetate salts as catalysts, it initially forms a cyclohexyl hydroperoxide intermediate. This intermediate then further reacts to yield both an alcohol and a ketone (Scheme 1.5).

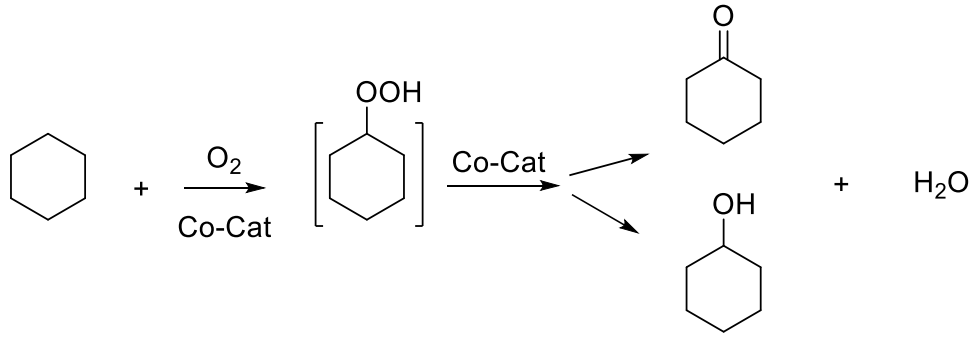

Scheme 1.5: Cyclohexane reacts with oxygen and cobalt acetate salts as catalysts to form a cyclohexyl hydroperoxide intermediate, which then produces an oxidative mixture comprising an alcohol and a ketone.

The majority of the K/A mixture produced globally is utilized as a precursor in making nylon 6.6 which is essential for developing fabrics and other materials [24-25]. Both examples of industrial aerobic oxidations are types of autoxidation's are limited to substrates that are ready for selective radical reactions. For terephthalic acid (TPA), the reaction occurs efficiently because the benzylic C-H bonds are the reactive sites in the molecule and the resulting carboxylic acid product is stable [16]. In the cyclohexane reaction, the conversion to K/A oil is restricted to 10-12% to avoid the formation of over-oxidation by-products like acids. Any unreacted cyclohexane will be distilled and recycled [26]. These examples illustrate that using O_2 as an odd-electron oxidant presents both challenges and limitations. Most organic molecules are in a singlet ground state, meaning their electrons are paired. O_2, being a triplet in its ground state, requires a spin flip to react with these singlet molecules. This "spin-forbidden" nature often slows down reactions with O_2 unless specific catalysts are used to facilitate spin-crossover. There is a need for new methods that can be widely applied to various organic substrates. As a result, there is significant interest in developing oxidation processes that utilize molecular oxygen in large-scale chemical manufacturing, due to its environmentally friendly nature and high atom efficiency. Successfully developing such methods would significantly impact the synthesis of both fine and bulk chemicals by enabling the selective oxidation of low-carbon feedstock.

1.2.1 Autoxidation of saturated hydrocarbons

One of the objectives of this work is to use molecular oxygen to selectively oxidise hydrocarbons. We aimed to minimize autoxidation phenomena as much as possible since they can occur during the oxidation of hydrocarbons. The impact of autoxidation on the reaction mixtures will be discussed in this study.

An autoxidation is the process of oxidizing a substance auto-catalytically, which may occur if there are remnants of an initiator or a promoter (such as the reactor's walls , residual alkyl hydroperoxide in solution, etc.) [27], along with a substrate and molecular oxygen. This reaction is significant as it can occur wherever molecular oxygen is available, and if not controlled it can significantly reduce the selectivity of a reaction. This occurs due to a free-radical mechanism initiated by the homolytic breaking of the O-O bond in alkyl hydroperoxide intermediates, often without the presence of a confined active site [28]. Autoxidation is also possible through the interaction of hydroperoxides with transition metals like Mn, Fe and Co [29-30]. These trace metals induce the generation of free radicals, such as alkoxy $RO^{\bullet}$ and alkyl peroxyl ($ROO^{\bullet}$), in the presence of hydroperoxides. This interaction triggers a process known as free radical chain reaction or autoxidation, which involves further reactions with the substrate. Autoxidation was initially investigated through the degradation of rubber and natural oils and later adopted by the petrochemical industry. Ideally, it should be completely avoided because of its limited selectivity by nature when oxidizing hydrocarbons. Product distribution is frequently expressed as the molar ratio between ketone and alcohols or serves as an initial indicator of whether an oxidation reaction is proceeding via autoxidation. In the autoxidation consistent ratio of ketone and alcohols (1:1) suggests that the reaction is occurring through autoxidation only [31]. For instance, autoxidation was detected during the oxidation of cyclohexane when ClO_2^- and manganese porphyrin complex were present [32]. Autoxidation was confirmed by detecting a 1:1 ratio of ketone to alcohol, which is diagnostic of the occurrence of hydrocarbon autoxidation (in this instance, ethylbenzene). On the other hand, the non-autoxidative route generated just the alcohol [32]. R.A.Sheldon In 1991 described three mechanisms for oxidation [33-34]; i) auto-oxidation via a free radical chain reaction ; ii) oxidation of a substrate bound to a metal ion followed by the re-oxidation of the reduced metal; iii) catalytic oxygen transfer. The primary focus of this project is on the first mechanism, which involves auto-oxidation through a free-radical chain reaction.

This process is not catalytic; rather it consists of three distinct stages: initiation, propagation, and termination, which are depicted in the equations shown in figure 1.2. During the initiation step, a free radical species is generated through the homolytic cleavage of a substrate or a radical initiator. This radical then reacts with an additional substrate or initiator, producing more radicals that propagate the reaction. Oxidation occurs when oxidative radicals are formed, the generation of radicals can be catalysed by suitable radical initiators. Several radical initiators, including alkyl peroxide serve as sources of oxygen. Oxygen can also be sourced from sacrificial oxidants or atmospheric O_2, the specific process depends on the species involved. The presence of trace amounts of alkyl hydroperoxide residues in the starting ingredients can cause autoxidation to begin [27], as illustrated in eq.1. 2. Additionally, it can be promoted by metal surfaces such as the walls of a reactor or trace metals found even in glassware in the absence of additional initiator. Alkyl peroxy radicals are created when the produced $R^{\bullet}$ radicals interact with ground state oxygen. This interaction is considered an energetically barrier less step, primarily controlled by diffusion limitations [35]. Then, peroxy radicals' abstract hydrogen atoms from the substrate, regenerating $R^{\bullet}$ and producing alkyl hydroperoxides. These hydroperoxides can undergo homolytic cleavage to form $RO^{\bullet}$ and $^{\bullet}OH$ radicals, both of which are highly reactive and continue to propagate the autoxidation process. This process is actually a branching reaction that generates an increasing number of radicals, unless termination occurs, it can theoretically continue indefinitely until all reagents are consumed. The termination step involves the reaction between two alkyl peroxides, resulting in the production of ketone and alcohol in equal ratio. As a result, at low conversion, the anticipated molar ratio of alcohol to ketone for a specific hydrocarbon substrate would be 1, assuming there are no parallel reaction pathways and no catalysts present that could influence selectivity [4-27]. Moreover, the reaction may be controlled by diffusion of O_2 under autoxidation conditions. As a result, the oxidation happens in a diffusion regime rather than a kinetic regime, which may have unfavourable effects on the product distribution. This should be considered when using the product distribution for structure-activity correlations in catalyst development and design. Therefore, controlling the catalytic decomposition of alkyl hydroperoxide can serve as a significant method to adjust selectivity patterns in autoxidation reactions [36]. Our main study will investigate the autoxidation of ethylbenzene to acetophenone and 1-phenylethanol through the decomposition of 1-phenylethyl alkyl hydroperoxide.

Initiation

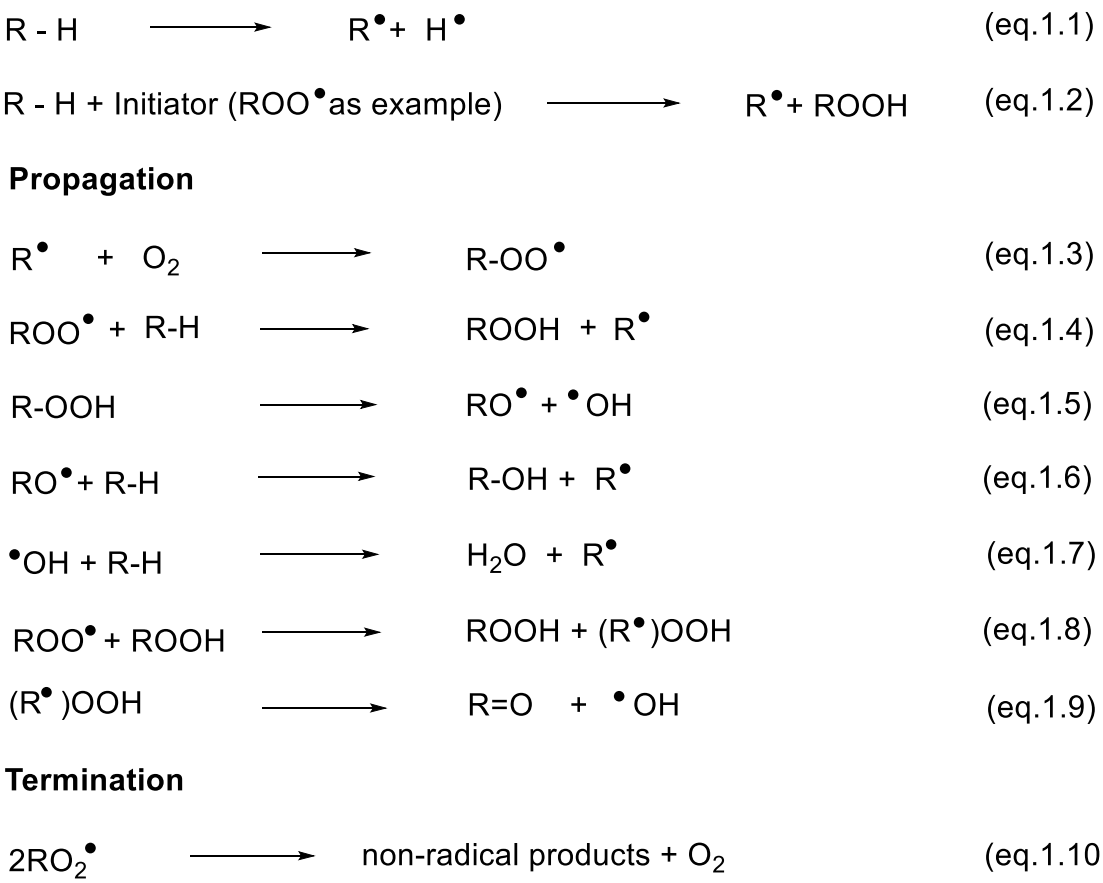

Scheme 1.6: Simplified process of hydrocarbon autoxidation without the use of additional initiators or catalysts. The reaction initiation occurs through 1-phenyl alkyl hydroperoxide acting as initiators (as per eq. 1.2). The 1-phenyl alkyl hydroperoxide undergo O-O bond cleavage (eq.1. 5), resulting in alcohols, while the abstraction of α-H (eq.1. 8) from 1-phenyl alkyl hydroperoxide leads to the formation of ketone.

Nevertheless, despite its widespread use, the simplified scheme fails to cover further interactions among the intermediates produced throughout the procedure or their interactions with reactor walls. Typically, any reaction mixture resulting from autoxidation consistently exhibits an excess of ketone, typically in a molar ratio of 2:1 respect to alcohols [37-38-39]. It is worth mentioning that characterizing the reaction products is essential for study the reaction mechanisms. This is a challenging process because the autoxidation of hydrocarbons, including acids and esters, can result in the formation of over 40% of by-products [40]. These by products can also react with each other, for example an alcohol can be dehydrated by an acid leading to double bond formation which can further react to produce additional by products.

1.3 Oxidation of alkyl aromatics

Alkyl aromatics encompass a wide range of chemical compounds. Alkyl aromatics are abundant and relatively cheap, due to begin produced as by-products in the petrochemical industry, which makes them an attractive chemical feedstock [41]. Alkyl aromatics can undergo partial oxidation reaction to yield a plethora of compounds that have applications in pharmaceuticals, agriculture, and fine chemicals. There are, however, some challenges associated with partial oxidation reactions. The reasons for this are both thermodynamic and kinetic. In the same way as alkanes, alkyl aromatics are also stable and non-reactive. As a result, strong C-H bonds must be cleaved to enable the reaction to occur. The strength of this bond is influenced by various factors, such as its location and its environment. As mentioned in section 1.1, in the alkyl chain of an alkyl aromatic the C-H bond in a CH_2 group usually has a bond strength of approximately 343 kJ mol^{-1}. In contrast, C-H bonds in a CH_3 group are stronger, with bond strengths around 410 kJ/mol^{-1}, making terminal position oxidation more challenging. In the aromatic portion of the molecule, the bond strength between C-H can vary depending on where they sit in relation to the alkyl chain and adjacent rings. Naphthalene, for example, possess a bond strength of ~ 465 kJ mol^{-1} for the C-H bonds on alpha carbons , whereas those on beta carbons exhibit a bond strength of ~ 464 kJ mol^{-1} [42]. These bonds can be cleaved at elevated reaction temperatures, however, this may result in a significant loss in selectivity. Additionally, once significant temperatures to oxidise C-H bond has been achieved, it becomes susceptible to further oxidation since this process is thermodynamically favourable. This can lead to over-oxidation, where complete combustion results in the formation of CO_2 and water, thereby loss of yield. As we know, a catalyst affects only the kinetics of a reaction, not its thermodynamics. Thus, although a catalyst cannot alter the thermodynamic favourability of complete combustion, it can enable the reaction to proceed at a lower temperature, thereby reducing the rate of over-oxidation. An ideal heterogeneous catalyst would enable the partially oxidized product to desorb before undergoing the over-oxidation reaction. Nevertheless, it might still be essential to limit the conversion process in order to maintain high selectivity. Reaction selectivity can also be affected by steric hindrance, particularly in the case of polyaromatic compounds or branched alkyl chains. This research will centre on the oxidation of ethylbenzene, *p*-xylene and cyclooctane.

1.4 Potential oxidants for hydrocarbon oxidation

The use of stoichiometric oxidation reagents such as $KMnO_4$, or CrO_3 are not environmentally friendly for reasons mentioned earlier in section 1.2. Consequently, catalytic methods that enable low-temperature, highly selective partial oxidation which can limit the generation of unwanted by-products and can use air or molecular oxygen (O_2) as the oxygen source have become highly desirable. Additionally, hydrogen peroxide (H_2O_2) and tert-butyl hydroperoxide (tBHP) are also viable oxygen sources due to their advantages in oxidation reactions. The use of these oxidants generally involves a radical pathway, which is challenging to control due to the nature of radical reactions. Therefore, it is crucial to develop a catalyst that can both initiate the radical mechanism and manage its propagation. The development of new heterogeneous catalytic systems requires an understanding of the reaction mechanism on the catalyst's surface. The selection of oxidants depends on factors such as reaction conditions, the substrate, and the established mechanism. H_2O_2 and tBHP are relatively inexpensive and environmentally friendly, while O_2 is an abundant and extremely cost-effective resource. However, activating O_2 can be more challenging.

1.4.1 Hydrogen peroxide (H_2O_2)

H_2O_2 is a fundamental inorganic molecule widely utilized in the fine chemical industry and commonly used in daily life as a bleaching agent and disinfectant. From a chemistry perspective, H_2O_2 in preferable because its decomposition produce only water as a by-product. This specificity lends the molecule a distinctively green characteristic. Shulpin and Nizova demonstrated that peroxy radical species can be formed by using O_2 in conjunction with a transition metal complex as a catalyst [43]. H_2O_2 can generate highly active radical species, by simplifies the reaction by avoiding the need to create peroxy species from O_2. The drawback of H_2O_2 is its thermodynamic instability, leading it to decompose into water and O_2. Many factors such as high temperatures, and solubility in organic media, certain catalysts can accelerate the decomposition of H_2O_2, making its use challenging. Furthermore, in this study H_2O_2 does not supply any activation energy for the cleavage of C-H bonds. The implications of this oxidant (H_2O_2) are investigated in chapter 4.

1.4.2 Tert-butyl hydroperoxide (tBHP)

Tert-butyl hydroperoxide (tBHP) is a more complex organic molecule compared to H_2O_2 and is commonly used in oxidation processes. The molecule has organic properties because of the tert-butyl group making it soluble in both aqueous and organic media. For oxidation reactions, the combination of tBHP and catalysts such as transition metals is very effective. It is believed that the catalyst's role is to activate tBHP, producing free radical species. Singh et al. demonstrated that their catalyst, $LaMO_3$ (with M= Cr, Co, Fe, Mn, and Ni), can generate radicals from tBHP, which then oxidize alkyl aromatic molecules into benzylic ketones [44]. The main advantage of using tBHP over H_2O_2 is its higher reactivity. H_2O_2 and tBHP require different activation energies for the radical pathway, highlighting the importance of the catalyst's role and the reaction conditions. Tert-butyl hydroperoxide is a strong oxidant and is more reactive than H_2O_2 and O_2. This behavior has been attributed to a variety of explanations [45-46]. Alirio E. Rodrigues stated a system in which H_2O_2 decomposed rapidly, whereas the tBHP radical remained stable long enough to initiate the reaction [47]. According to Escola *and co-workers* [48], tBHP oxidizes 1-dodecene better than H_2O_2 for 2-dodecanone production. Their study also noted the generation of complexes involving tBHP and Pd in the system. These complexes demonstrated different oxidizing properties, which could account for the superior oxidizing performance of tBHP [48]. On the other hand, Singh and co-workers outlined a system in which H_2O_2 was around three times more effective than tBHP. This increased activity was attributed by H_2O_2 more aqueous properties enabling it to interact more effectively with the hydrophilic sites of the catalyst [49]. The tBHP or H_2O_2 radical species often leads to the formation of decomposition products. The decomposition product of H_2O_2 is water, which typically does not interfere desired reaction. In contrast, tBHP can generate by-products such as tert-butanol or methanol, which may exhibit reactivity based on the reaction conditions. Additionally, this by product being a flammable chemical, it must be disposed of properly [50]. Thus, selecting the appropriate oxidant should consider the specific substrate, the desired target products, and the reaction conditions. Each of these factors plays a crucial role in determine the efficiency and selectivity of the oxidation process, ensuring a good outcome in the reaction. More thorough details and data regarding the usage of tBHP in the oxidation of ethylbenzene will be thoroughly discussed in chapter 4.

1.4.3 Molecular Oxygen (O_2)

Molecular oxygen O_2 garnered significant research interest due to its natural abundance, safety, cost-effectiveness, and environmentally friendly attributes, which contribute to sustainability [51]. Molecular oxygen is readily available in the air, constituting approximately 21% of the volume [52]. Other oxidants are often preferred because they are easier to activate. Typically, stronger conditions, such as high temperatures are required to activate O_2, while milder conditions are sufficient for oxidants like H_2O_2. Active oxygen species, depicted in Figure 1.2 include chemically reactive forms of oxygen that can activate stable molecules through their reactivity. To design a system that effectively activates O_2, it is crucial to comprehend its interaction with the catalyst and substrate during the activation process. Research has primarily centred on utilizing O_2 as an oxidant in heterogeneous catalytic systems. Some heterogeneous systems have demonstrated that some metals can be active under milder conditions when using O_2 as an oxidant. However, these systems typically achieve only low conversion rates. Many studies have highlighted the capability of Au-based catalysts to activate O_2. For instance, Schroeder and co-workers demonstrated that CO could be oxidised at room temperature by the activation of O_2 using an Au/TiO_2 catalyst [53]. Adding an additional transition metal such as Pd, Fe or Ag showed improved O_2 activation under mild conditions. Different Au/TiO_2 catalysts were examined to understand how the size and shape of the Au clusters, as well as their interaction with TiO_2, affect the activation of O_2 [53].

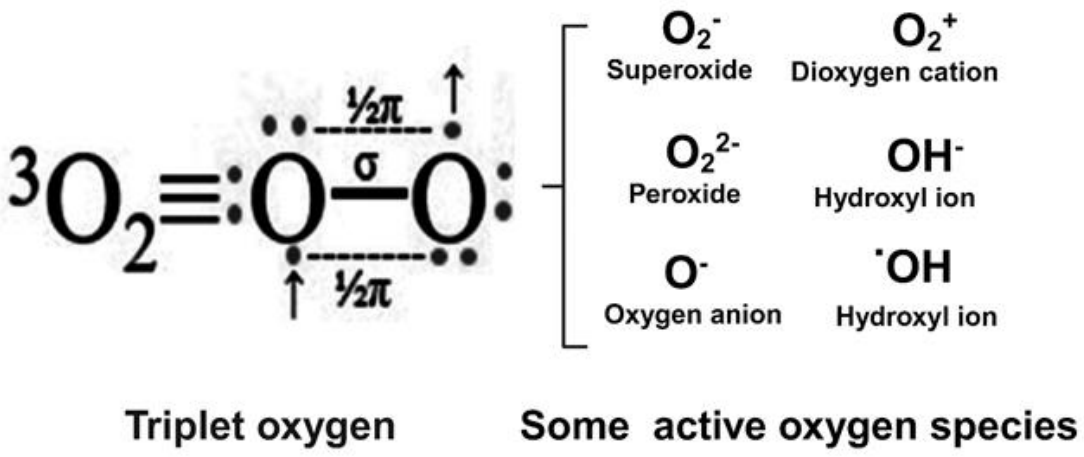

Figure 1.2: This diagram illustrates the structure of molecular oxygen (O_2) and highlighting its triplet state and some reactive species containing oxygen [54-55].

1.5 Concept of Catalysis

Catalytic reactions have been studied since the late 18th century. As early as 1835, Berzelius coined the term catalysis. He described it as the ability of a molecule to enable a reaction to take place under conditions where it otherwise would not, without the molecule itself being altered. He explained the term based on numerous scientific papers, which claimed that the catalyst could not be involved in chemical reactions. Generally, catalysis is defined as the acceleration of a reaction rate by an additional substance known as a catalyst. However, the catalyst is not consumed during the reaction. Various scientists, including industrialists, study the use of catalysis. For instance, a patent from Phillips suggested using Pt as a catalyst in sulphuric acid production. As research into catalytic reactions expanded, scientists recognized that catalysis could be applied to a wide variety of processes. In 1877, Lemoyne clarified the thermodynamics of catalysis, explaining that while the reaction rate changes, the reaction equilibrium remains unchanged. The process of catalysis is ubiquitous in nature, including within the human body where proteins called enzymes function as catalysts. In all cases, a catalyst acts by providing an alternative pathway with reduced activation energy ($Ea.$), as illustrated in figure 1.3 [56]. The rate constant, k (eq.1.11) can be increased by lowering the activation energy Ea (considered here as Gibbs free energy), increasing the frequency factor A or both when catalysis involves adsorbed species on a surface, activation entropy decreases, which helps maintain a high pre-exponential factor.

$$k = A \times exp(-\frac{Ea}{\mathrm{RT}}) \quad (eq.1.11)$$

Where A represents the pre-exponential factor, Ea showed the activation energy, R is the gas constant and T is the reaction temperature.

The catalyst stabilizes intermediates or transition states in the reaction, thereby lowering the activation energy needed for the process. Increasing the proportion of reactants that meet the lower energy barrier results in an increase in rate. As a result, a catalyst affects reaction kinetics, but thermodynamics remain the same. It is based on this principle that all catalysts work. Catalysis can be divided into three types: homogeneous, heterogeneous, and enzyme-based. Homogeneous catalysts are substances that share the same phase as the reactants, usually in the liquid phase.

For instance, the production of ethylene glycol from water and ethylene oxide occurs in a water based environment, catalysed by sulphuric acid [57]. Homogeneous catalysts typically demonstrate high activity; nevertheless, their removal from the reaction mixture which includes both reactants and products can be challenging and costly. As a result, it is especially important when the catalyst has a high cost or contains materials that are harmful to the environment, such as heavy metals [58]. Heterogeneous catalyst are molecules in a different phase than the reactants, such as a solid catalyst with liquid phase reactants. In general, it is significantly simpler to extract heterogeneous catalysts from reaction mixtures compared to homogeneous ones. This prevents catalyst loss and eliminates the need for costly and complex separation procedures. After separation, the heterogeneous catalyst can be restored if needed and reused. Among the industrial applications of heterogeneous catalysts are Haber-Bosch ammonia synthesis processes using porous iron-based catalysts [59-60], and nickel catalysts employed in producing synthesis gas from carbon dioxide and hydrogen .

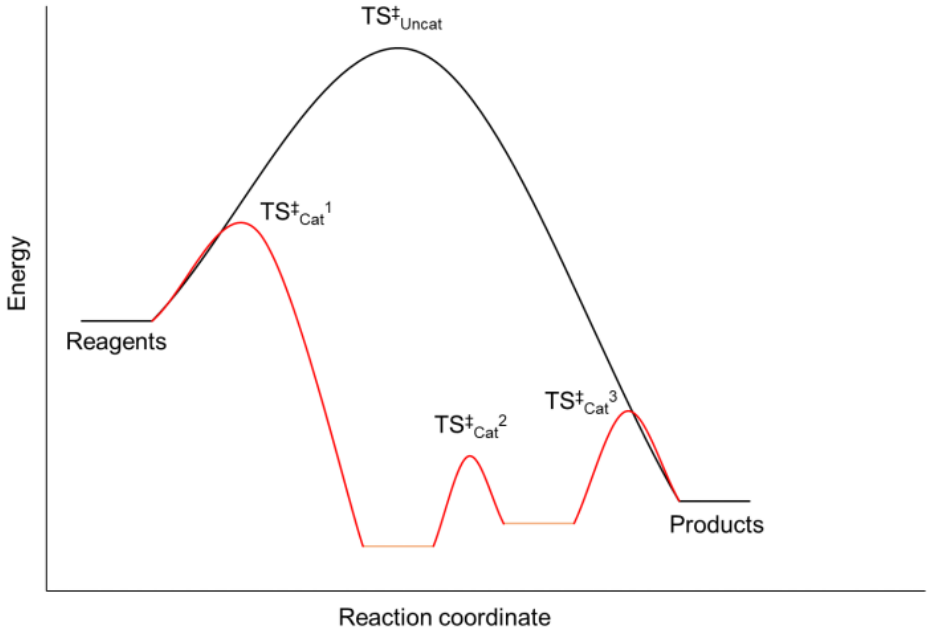

Figure 1.3: A schematic illustrating how a heterogeneous catalyst can influence the activation energy required for a reaction to proceed. Additional transition states may appear due to adsorption and intermediates that are not present in the un-catalysed reaction. The overall standard Gibbs free energy (ΔG) of the reaction remains unchanged with the use of a catalyst. A catalyst influences only the reaction kinetics not the thermodynamic equilibrium [56].

1.5.1 Homogeneous catalysis

Homogeneous catalysts are catalysts that share the same phase as reactants and products. All catalytic sites are able to interact with the substrates since these catalysts are fully dissolved in the reaction medium. Usually, these catalysts are complex, consisting of several organic ligands bound to a metal. The ligands ensure the stability of the metal catalyst complex and can be modified to improve the catalyst's selectivity for producing a specific desired product [61]. A significant achievement of a homogeneous catalyst is its ability of produce a product with over 90% selectivity and a high conversion rate. This is achieved by carefully choosing the metal centre ligands, reaction parameters, and an appropriate substrate [62]. Despite the numerous benefits of selectivity in homogeneous catalysis, scientists are focusing heavily on heterogeneous catalysts because separating homogeneous catalysts from reaction mixtures is challenging and costly. Homogeneous catalysts can lead to corrosion of the reaction reactors with some catalysts accumulating on the reactor walls. Consequently, the workup process for homogeneous catalysts is often complex as seen in (figure 1.4).

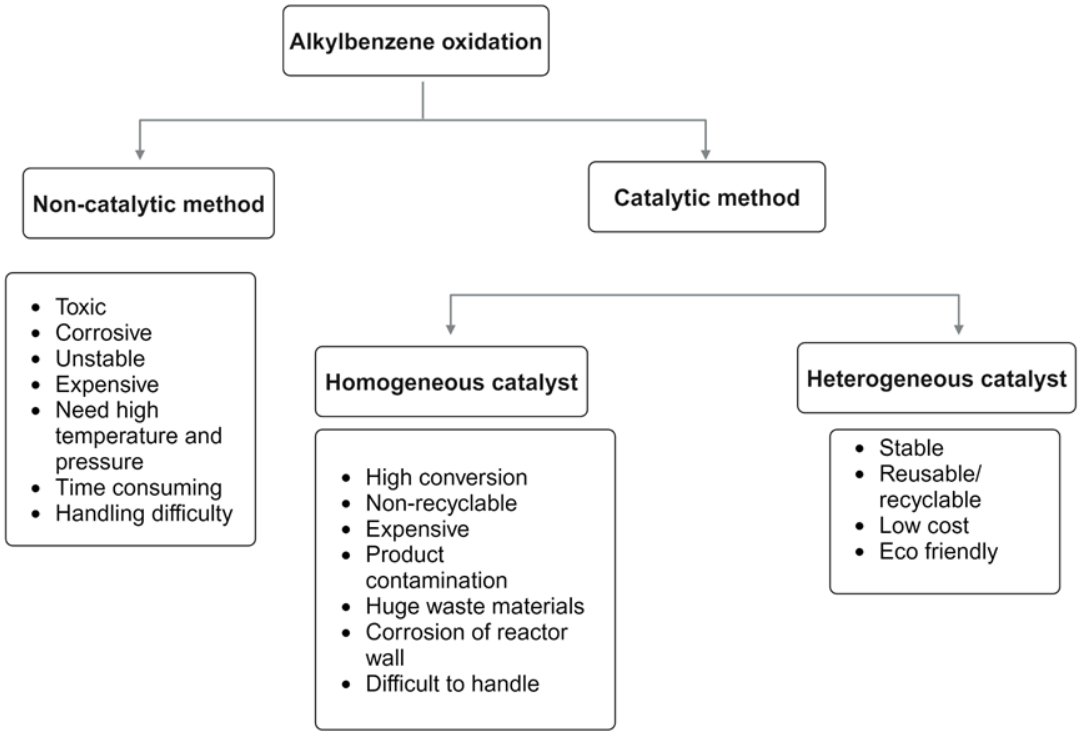

Figure 1.4: a comparison of non-catalytic and catalytic methods in alkyl benzene oxidation; the non-catalytic approach typically requires unstable conditions and results in lower efficiency and selectivity. In contrast, the catalytic method utilized a homogeneous or heterogeneous catalyst to study reaction under milder conditions leading to higher efficiency and selectivity in producing the desired products.

1.5.2 Heterogeneous catalysis

While homogeneous catalysts offer high activity with more readily available active sites for reactant interaction, heterogeneous catalyst are favoured in industrial applications due to their easier separation and recovery as well as their suitability for continuous flow processes making them more economically advantageous. However, heterogeneous catalysis may have certain drawbacks that can restrict its broader application. These consist of the loss of active species in solution and the sintering of supported metal species [63], mass transfer limitations [64], undesired changes in oxidation states or phase transitions and complexity of studying and identifying mechanisms due to the multiphase nature of reactions [65]. These factors must be considered when applying and designing heterogeneous catalysts, particularly if the goal is to maintain both high reactivity and selectivity. Nearly 90% of chemical processes involve catalysts with a usage ratio of approximately 3:1 between homogeneous and heterogeneous catalysis in these procedures [65-66]. As discussed earlier, a key reason for favouring heterogeneous catalysts, particularly in scale up or industrial applications is their ease of separation of the catalyst from reactants and products after the reaction. Additionally, when the reaction is conducted in a continuous flow process (in our work batch to batch) the use of a catalytic bed becomes feasible a possibility that is not available with homogeneous catalysts [67]. A typical heterogeneous catalytic cycle exemplified by the oxidation of carbon monoxide [68] (as shown in scheme 1.7) includes the subsequent steps: i) the diffusion of reactants from the fluid phase to the catalyst surface; ii) the surface adsorption of reactants on the catalytic; iii) the chemical reaction and formation of products; iv) the desorption of products from the catalytic surface, and v) the return of products to the solution through diffusion. However, it is important to note that porous materials are frequently used to enhance the interaction between reactants and active sites and to provide a broad surface area for the deposition of catalytically active species, usually metal centres. Conversely, this can lead to challenges related to the internal diffusion of reactants and products. Heterogeneous catalysis are currently highly utilised in oil refining and the manufacture of bulk chemicals, such as ethylene oxide, acrylonitrile and maleic anhydride [69]. Sheldon et al. [70], classified heterogeneous catalysis in organic synthesis into five different categories: solid-acid catalysis, solid-base catalysis, catalytic hydrogenation, catalytic oxidation, and catalytic C-C bond formation

[70]. Among these selective catalytic oxidation reactions such as the oxidations and alcohols are particularly crucial in fine chemistry.

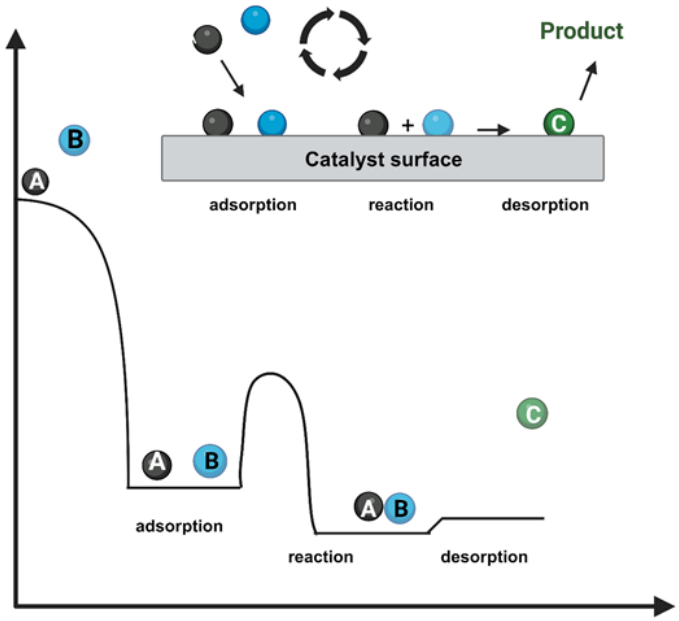

Scheme 1.7: An illustration of a heterogeneous catalytic cycle's phases that has been simplified. This graphic illustrates the cycle, including reactant adsorption onto the catalyst surface, reactant-product interaction, and product desorption [68].

Supported metal catalysts a type of heterogeneous catalyst has been used and researched for the oxidation of hydrocarbons and their corresponding alcohols. Various noble and transition metals including Au, Pt, Pd, Co, Fe, and Mn have been employed in these applications. These metals exhibit unique properties when supported as metal or metal oxide nanoparticles. For instance, supported gold catalysts with particle sizes under 5 nm can demonstrate exceptional activity in selective oxidation reactions, such as propene epoxidation or the oxidation of higher alkanes like cyclohexane , styrene, and cyclooctane [71-72]. Cobalt-based catalysts have demonstrated significant activity in the oxidation of alkenes. Numerous studies have been conducted on cobalt oxide supported on various materials, such as Co/MCM-41 and Co/SBA-15 to enhance their performance [73-74]. From this viewpoint, Ag is an attractive catalytic system and has been used in various reactions, such as ethylene epoxidation [75-76], styrene epoxidation [77-78] and carbon monoxide oxidation [79], as well as on soot removal [80-81]. However, Ag has received limited attention in the oxidation of hydrocarbons such as ethylbenzene, cyclooctane, and p-xylene. We will study this topic in this thesis for a novel application. Currently, silver is industrially used for the

epoxidation of ethylene to produce ethylene oxide, achieving up to 80% selectivity. Ethylene oxide is a valuable intermediate in the production of ethylene glycol (a component of antifreeze), poly (ethylene oxide), and surfactants [82]. Additionally, silver is employed in the dehydrogenation of methanol to formaldehyde [83]. These applications highlight the industrial potential of supported silver catalysts. Given the promising results of Ag-based catalysts, section 1.6 presents a detailed literature review on the effects of Ag nanoparticles. This forms the basis for our primary focus on developing supported Ag nanoparticles for hydrocarbon oxidation.

1.5.3 Enzymatic catalysis (Bio-catalysis)

Enzymes or intricate protein molecules are commonly used as biocatalysts. It is naturally occurring and aids in reactions within living cells. The structure of the enzyme is determined by the peptide bonds that bind the amino acids that make up proteins. A cavity within the protein molecule's structure, bordered by different amino acids, typically functions as the enzyme's active site. After bonding, the reaction takes place, and products are formed. In order to adhere to their substrates, enzymes use four distinct kind of interactions: hydrophobic, van der Waals, hydrogen bonding, and electrostatic forces. Enzymes are highly effective catalysts that, due to the unique shape of their active sites, are selective for specific reactions. An enzyme can normally complete about 1000 catalytic cycles in a second. Because of this, biocatalysts are highly valuable commercially, particularly in the food and pharmaceutical industries where they are employed in the manufacturing of a variety of medications, food additives, flavourings, and scents. Enzymes provide added advantages as they can be utilized outside biological systems, functioning as isolated compounds in both aqueous and organic solvents [68]. However, care is required during reactions because enzymes are often sensitive to heat. Excessive heat can denature the weak bonds that preserve the enzyme's functional shape, thereby destroying its active site [84].

1.6 The use of supported catalysts for oxidation reactions

1.6.1 Principles and development of supported catalysts

Typically, supports used in heterogeneous catalysis should meet certain physical criteria, which include high specific surface area to facilitate the formation of well-dispersed metal nanoparticles, stability under high temperature and pressure, mechanical resistance to friction, especially for batch-to-batch processes involving stirring, and cost effectiveness. Figure 1.5 illustrates that the growth of small particles by itself can lead to a decrease in active surface area. However, applying the active component on a support helps to stabilize the active surface area. It is important to note that in some chemical reactions, the support can be an active participant. For instance, CeO_2 can facilitate the complete combustion of volatile organic compounds, converting them into CO_2 and H_2O [85]. In the development of supported metal nanoparticle catalysts, metal oxides are commonly used as supports. They significantly influence both the characteristics and effectiveness of the catalysts in reactions. Laursen and Linic [86] suggested that The electron charge transfer from oxygen vacancies at the TiO_2 interface to the supported Au nanoparticles alters the nanoparticles' electronic structure. This modification facilitates O_2 activation and enhances oxidation reactions. Defect sites, such as surface oxygen vacancies in metal oxide supports, play a critical role in influencing the adsorption energy, particle morphology, and the electronic properties of the metal nanoparticles they host. These effects in turn enhance the catalytic activity [86- 87]. As a result, it has been observed that metals such as Au and Pt when supported on reducible oxides (like TiO_2, CeO_2, and MoO_3) show greater catalytic activity compared to those supported on irreducible oxides (such as SiO_2 and Al_2O_3) [86]. Of particular significance, given the focus of this thesis on the use of Ag with various metal oxide supports (such as TiO_2, CeO_2, Nb_2O_5 and SiO_2). For instance, the catalyst reducibility can be enhanced by synergistic interactions between Ag and manganese oxide supports, which promote the generation of abundant active lattice oxygen. This leads to improved catalytic performance, particularly in the complete oxidation of toluene, facilitating the removal of hazardous organic compounds [88]. In this context, the interactions between supported Ag nanoparticles and the support can influence the distribution of oxygen vacancies (both bulk and surface). The activity of supported Ag/CeO_2 was regulated by surface vacancies near the nanoparticles in an oxygen-rich environment, while bulk

oxygen vacancies played a more significant role under low oxygen conditions [89]. Another important factor for catalysts based on silver is the relative proportion of supported Ag and Ag_2O. This is significant for several reasons: surface Ag can transform into Ag_2O, while Ag_2O can readily revert to Ag through thermal decomposition. Ag and Ag^+ species may also exhibit varying levels of reactivity. The support affects the active metal's effective oxidation state, much like it does for other heterogeneous catalysts. For example, Ag_2O is extensively distributed on the surface of CeO_2, whereas metallic Ag tends to form preferentially on ZrO_2 and Al_2O_3. This is due to the strong interaction between Ag and CeO_2 can inhibit the decomposition of Ag_2O into Ag [81]. Likewise, the metallic Pt nanoparticles stability and oxidation state are affected by the support. Pt^{2+} is predominantly found in Pt/ZrO_2 and Pt/SiO_2, whereas Pt/CeO_2 displays a highly oxidized state (Pt^{4+}), and a strong contact between CeO_2 and Pt nanoparticles is indicated by higher binding energies [90].

Beatriz [91] summarized the effects of catalyst supports on reaction activity based on existing research: i) enhancing metal nanoparticle stability to prevent sintering, preventing their aggregation into inactive macroparticles; ii) impacting the structure and morphology of nanoparticles (the physical properties),; iii) providing oxygen vacancies necessary for reactions (e.g.,MoO_3, CeO_2) stabilizing the active species of nanoparticles during reaction into the impact of supports on reaction processes, identifying heterogeneous catalysts' surface active sites remains a significant challenge [92].

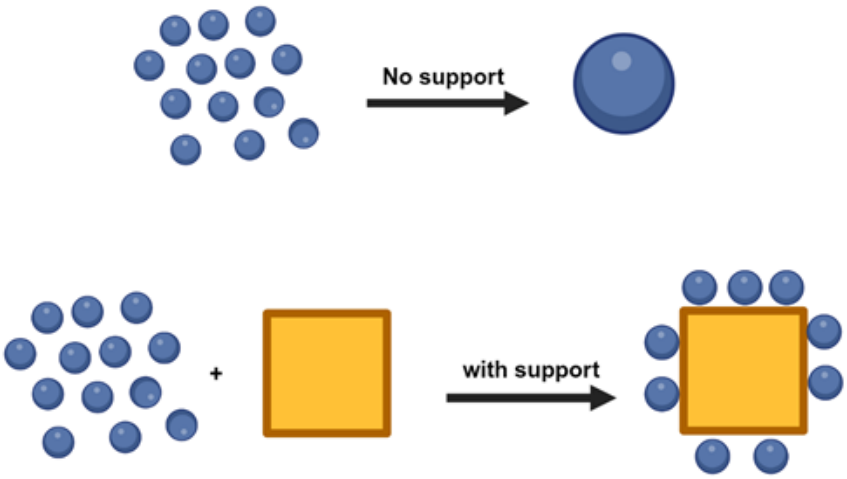

Figure 1.5: Example showing that while the growth of small particles alone can lead to a decrease in the active surface area, a stabilization of the active surface area can be achieved by utilizing the active components on a support [70-74].

1.6.2 Impact of oxidation states on active metals in catalysis

Research has shown that in supported metal catalysts, the active species is typically not the pure metal but rather its corresponding metal oxide (e.g., RuO_2 and PtO_x in the oxidation of CO to CO_2 under oxygen-rich conditions [93-94]. This finding highlights the significance of identifying reactive species in supported metal catalysts, a crucial aspect for the advancement of catalyst design. For instance, Gong et al. [95-96] demonstrated that metal oxides exhibited greater reactivity compared to their metal counterparts. The conclusion resulted from a comparison of the energetics and reaction pathways in CO oxidation catalyzed by metals, including Pd, Pt, Ru, and Rh, and their oxides, RuO_2, RhO_2, PdO_2, and PtO_2. Jason R. et al. found that Pt oxides on Pt/ZrO_2 nanoparticle catalysts were effective in methanol oxidation, indicating that catalyst reduction may not be needed [97]. Studies on the reaction of propane with a PdO film indicated that the C-H bond dissociation was facilitated, accelerating the propane oxidation process. This occurred due to the strong interaction between propane molecules and the PdO film surface, following a donor-acceptor mechanism that initiated the cleavage of the C-H bond [98]. These findings highlight the need to determine if the oxidation process is driven by metal oxides (MeO_x) or the metallic form when evaluating practical applications. In the context of this thesis, Ag also exhibits these phenomena. Specifically, in the oxidation of cyclooctane and cyclohexane using Ag-based supported catalysts, it has been observed that the valence of Ag significantly influences the reaction performance. For example, Ag^0 in Ag/Al_2O_3 primarily drives the oxidation of ammonia at temperatures below 140°C. However, at temperatures above 140 °C, Ag^+ likely becomes the active species possibly due to the oxidation of Ag^0 at these higher temperatures [98]. Furthermore, in supported Ag/CeO_2 catalysts prepared using the impregnation method, different valence states of Ag (Ag^{2+}, Ag^+, Ag^0) are observed. In contrast, Ag^{2+} is not present in catalysts prepared by the deposition-precipitation method. This difference accounts for the superior reaction performance of the impregnated catalyst in the oxidation of propylene, and soot, attributed to the presence of three redox couples: Ag^{2+}/Ag^+, Ag^0, and Ag^+/Ag^0 [99]. The oxidation state of supported catalysts can be influenced by factors such as preparation methods and the type of support material. In our study on Ag nanoparticles, we employed different metal oxides as supports, primarily Nb_2O_5 b connected with Brønsted acid sites, and Lewis acid can be found in all supported Nb_2O_5 catalysis while in some specific catalysis

systems there is only Brønsted acid, along with other metal oxides like CeO_2, TiO_2, and SiO_2 In view of this, there is a promising application of Nb_2O_5 in acid catalysed reaction.

1.6.3 Additional factors including the effects of particle shape and composition

In addition to the above mentioned factors, there are other elements that affect catalytic properties, thereby affecting its activity and selectivity. For instance, the use of Ag nanoparticles with different natures (cubic, truncated triangular nanoplates, and near-spherical) for the oxidation of styrene demonstrates that the nanocube particles exhibit the highest reaction rate, being fourteen times faster than the nanoplates and four times faster than the nearly spherical particles. This is due to the different reaction activities of the facets, with (100) facets on nanotube nanoparticles having a higher reaction activity than (111) facets on nanoplates [100]. Haruta et al. [101] observed that the method used to prepare supported gold nanoparticles plays a key role in controlling their shape. Hemispherical gold particles on TiO_2 produced via the deposition-precipitation method exhibited superior performance in CO oxidation compared to spherical gold particles created through the impregnation protocol. According to these results, the perimeter interfaces around gold nanoparticles probably affect catalytic reactivity.it is also observed that the preparation method affects the shape of the supported Ag nanoparticles on ZrO_2 [80]. Hemispherical Ag particles are unevenly distributed on the surface of ZrO_2, whereas spherical Ag nanoparticles formed relatively uniformly through the chemical reduction method demonstrate higher activity for soot oxidation. Additionally, the composition of catalysts has been widely studied, including bimetallic and multimetallic systems, to reduce the use of noble metals for economic reasons and to enhance activity and selectivity. It has been observed that CeO_2 can serve as a promoter in supported Ag nanoparticle catalysts for alcohol oxidation [102]. When compared to monometallic catalytic characteristics of bimetallic catalysts can be enhanced, and the electronic impact resulting from charge transfer is a significant factor [103-104-105]. Bimetallic catalysts have been studied for various reactions including the liquid phase oxidation of methane to methanol using Au-Pd/MgO [106], as well as Au-Ag catalysts for CO oxidation[107] and Pd-Ag catalysts for the selective oxidation of benzyl alcohol [108]. It is essential to recognize that the presence of two or more metals in a catalyst can produce synergistic effects that incorporating

two or more metals into a catalyst can create synergistic effects, which can modify the electronic properties of the nanoparticle catalysts and potentially boost their reaction activity. However, these effects might also have no overall impact or could even be detrimental if they change the electron density in an inefficient manner. In this work, we examined a supported Ag-based catalyst (Ag + Fe) for ethylbenzene oxidation to compare its performance with monometallic supported Ag catalysts and further optimize the catalytic reactivity of Ag-based systems. However, it is essential to emphasize that our aim was not only to create a bimetallic catalyst but also a bi-functional one. This mean that one site of the catalyst is designed to initiation step while another site is focused on controlling selectivity. Based on the discussion above, supported metal nanoparticle catalysts have demonstrated exceptional performance in oxidation reactions. The catalytic behavior of these nanoparticles is influenced by several factors, such as their size, the nature of the support material, the oxidation states of the active metals, as well as their morphology, composition, and the surrounding chemical environment of the metal atoms. Figure 1.6 Illustrate how the optical properties of Ag nanoparticles vary with size [109]. Hence, by adjusting these parameters, it is possible to develop supported metal nanoparticle catalysts that are highly active, selective, recyclable, and environmentally friendly.

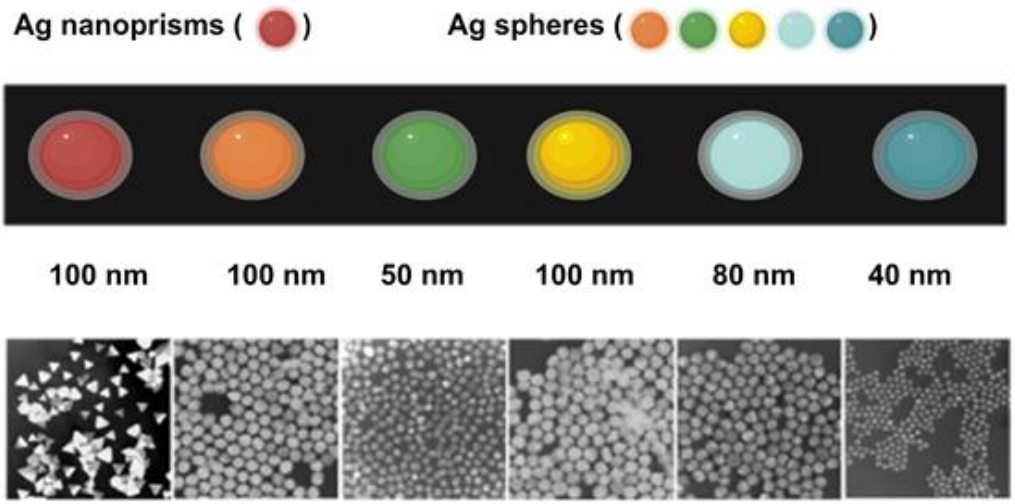

This statement is illustrated here by considering the Rayleigh light-scattering properties of various nanoparticles (quoted nanoparticle sizes are all approximate)

Figure 1.6: Typical sizes and shapes of Ag nanoparticles. The dimensions and form of nanoparticles can impact their optical and chemical properties at the nanometre scale (using Rayleigh light-scattering properties of different nanoparticles) [109].

1.6.4 Challenges in the application of supported metal catalysts

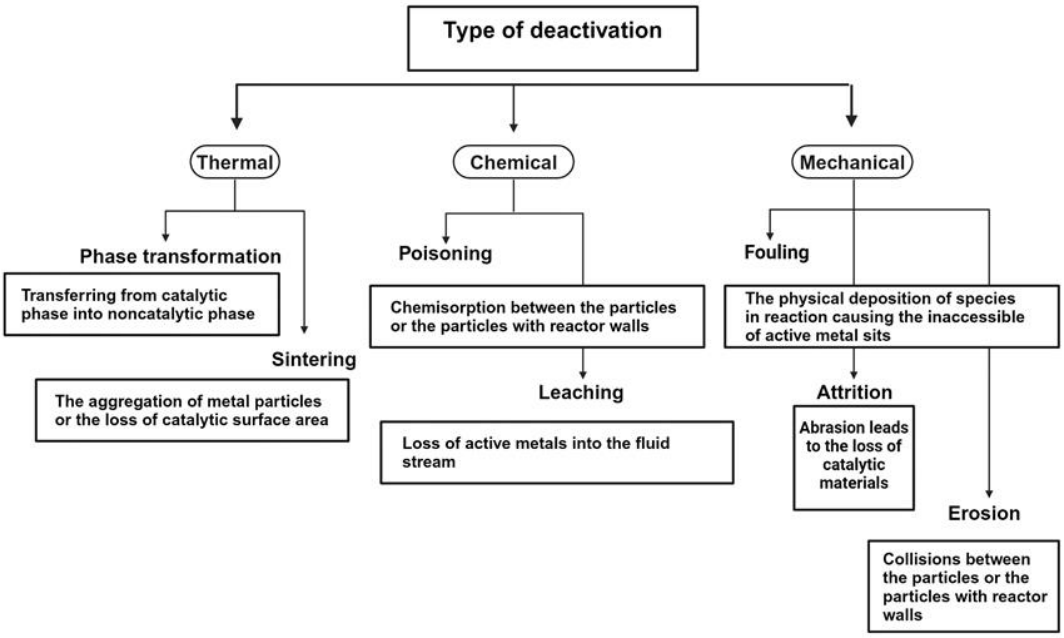

Figure 1.7: Different types of catalyst deactivation, with the causes of deactivation being classified by type and mechanism. In our research, metal leaching is a primary concern, as it is frequently happens and significantly impacts the reduction of activity in supported metal nanoparticle catalysts.

While supported metal nanoparticles demonstrate different properties and enhanced reaction performance compared to bulk metals, they still face several significant issues that cannot be overlooked in practical applications. A major concern is the deactivation or decline in catalytic reactivity and selectivity over time. Figure 1.7 provides an overview of the different types of deactivation [63-110-111]. For example , it has been observed that Pt-based catalysts can become deactivated by adsorbed side products, such as those resulting from aldol condensation or the oligomerization of carbonyl compounds during alcohol oxidation [112-113]. Additionally, reactivity is reduced on supported Pd/C catalysts when an inactive surface oxide layer forms, because of the strong attraction between Pd nanoparticles and oxygen; this issue can be mitigated by adding bismuth [114]. Metal nanoparticle aggregation during preparation or reaction processes presents a challenge since nanoparticles are thermodynamically unstable, leading to a loss of activity. This is particularly problematic because uniformly dispersed nanoparticles tend to exhibit superior reaction performance [115]. Due to the loss of activity in soot oxidation this issue has been documented in the sintering of Ag nanoparticles in Ag/ZrO_2 [80]. For instance, the migration of supported cobalt particles

to the external surface and their subsequent sintering into larger particles results in a loss of reactivity [116]. Increasing the particles dispersion across a high surface area support and using a strong support to guarantee that substrate molecules can reach active surface locations are crucial steps in preventing aggregation, or conducting reactions under milder conditions, such as lower temperatures [117]. Furthermore, metal leaching into liquid-phase media is a common problem for both metal and metal oxide catalysts, as evidenced by studies on the deactivation of supported metal catalysts. This problem is a major factor in the catalysts' instability [118]. As a matter of fact, all reactions covered in this thesis have had this phenomenon thoroughly researched. Metal leaching can lead to several consequences ;(i) a decline in catalyst reactivity as the reaction progresses, (ii) difficulties in regenerating and recycling catalysts, (iii) contamination of the products [119 - 120], and (iv) the possible onset of a homogeneous reaction pathway if the leached species is reactive. The C-C Suzuki cross-coupling reaction by palladium catalysts is a frequently cited case in the literature that sparked a debate regarding the reaction mechanism [121-122]. In the Suzuki-Miyaura cross-coupling reaction, high catalytic reactivity of leached Pd has been observed, indicating that both supported Pd nanoparticles and soluble Pd^{2+} species contribute to the catalytic process [123]. From an industrial standpoint, metal leaching restricts practical reusability, regardless of whether the leached species are active or inert, and should therefore be minimized. Conversely, it is crucial to assess the impact of leached metal on the reaction if leaching occurs. The presence of leached metal could lead to discussions regarding the mechanism in a catalytic process that involves both homogeneous and heterogeneous catalysis, due to the complexity of the reaction. Gruber-Wölfer et al. [124] outlined the techniques for monitoring metal leaching and its impact on reactions, as detailed in table 1.2. In this thesis, metal leaching analysis for silver (Ag) was performed using ICP-MS. Control tests were conducted with $AgNO_3$ to investigate how leached Ag species in the Ag^+ state effect the oxidation process. Additionally, the reaction mixture contained the supporting catalysts, which were recovered, dried and reused in subsequent oxidation reactions under identical conditions to evaluate their catalytic stability.

Table 1.2: Control test and methods to assess leaching species on the reaction were analysed using several techniques. This table indicates that metal leaching into the reaction mixture was quantitatively analysed using ICP, and a series of test were conducted to assess the reusability of catalyst in our study.

Techniques	An explanation of the procedure	Results
Test for hot filtering	Observed the activity of the filtrate by removing active particles through filtration.	The observed conversion may suggest that the leached species are active. However, this does not confirm that the reaction occurs by heterogeneous catalysis, as the leached species could redeposit on the support and remain undetected by this method [125-126].
ICP-OES analysis	After the reaction mixture is dried, the residue is dissolved in nitric acid and the concentration of metal species is analysed.	Quantitative analysis of the leached metal in the reaction mixture if significant leaching occurs during the reaction.
Three –phase test	A covalently immobilized reaction partner is added to the soluble reagent in the presence of a supported catalyst[127-128].	This technique can provide analysis for monitoring active homogeneous metal species. The covalently immobilized reagent will undergo conversion if leaching takes place.
Catalyst reusability	Recovering the catalyst from the reaction mixture after the reaction and then performing tests with a fresh substrate.	Reusability is a crucial factor in assessing catalyst stability. A noticeable decline in catalytic activity due to leaching would be evident after numerous test cycles if the activity is affected by quantity of active species present.
Test in different solvent	Evaluating the catalysts for the same model reaction using different solvents.	The catalytic reactivity and the extent of leached metals can be affected by the solvent used [129-130]. It is proposed that solvent polarity and high temperature may not impact Pd leaching.
Catalyst poisoning	Introducing catalyst poisons into the reaction system while the catalysts are present	Catalyst deactivation will be observed if metal leaching takes place as the leached species can be rendered inactive by poisons.

1.7 The use of Nb_2O_5 as supported metal catalysts

Metal oxides such as TiO_2, CeO_2, SiO_2, and MgO are commonly used as supports for creating metal nanoparticles due to their unique properties: i) their thermal and mechanical stability is essential for long-term use and scaling up; ii) their high surface area facilitates metal nanoparticles dispersion and helps prevent sintering or aggregation by enhancing the interaction between the support and deposited nanoparticles; iii) the presence of oxygen vacancies may influence partial oxidation reactions. For instance, it has been observed that the oxygen vacancies in CeO_2 can enhance activity because oxygen can be adsorbed and activated at these sites, resulting in the formation of (O_2^-) species [131-132]. Additionally, a new route suggests that during CO oxidation , O_2 is adsorbed on Au-Ce^{3+} bridge sites [133]. In the absence of O2, the oxidation of CO suggests that lattice oxygen from CeO2 is involved [134-135]. The presence of oxygen vacancies during the liquid phase oxidation of ethylbenzene in TiO_2 has been shown to enhance the chemisorption of O_2, which is beneficial for the oxidation process. However, it is important to consider that neutral oxygen vacancies could potentially trap radicals. This phenomenon has been observed in catalysts like V_2O_5 and CuO, where the vacancies act as quenchers for peroxy radicals, thereby inhibiting the oxidation reaction. Consequently, both surface and bulk vacancies can significantly influence the catalytic performance [136- 137-138]. With the aim to designing a new catalyst system for hydrocarbon oxidation, this thesis work has widely used Nb_2O_5 a support that has been relatively overlooked thus far. There have been reports of strong metal-support interaction (SMSI) between this support and Pt nanoparticles, which can affect the dispersion of the metal nanoparticles, resulting in a more uniform distribution of smaller Pt particles [139], and influence catalytic reactivity, either enhancing or suppressing it [140]. In the hydrodeoxygenation of 1, 6-hexanediol, the SMSI effect, which involves charge transfer from Nb_2O_5 to Pt nanoparticles, lowers the electron density on Pt and improves selectivity for n-hexane and 1-hexanol [141]. Moreover, this interaction does not always play a promoting role, as evidenced by the fact that nickel supported over Nb_2O_5 suppresses hydrogenation reaction activity. As a result of their unique optical, electronic, and chemical properties, Niobium oxide materials have garnered a lot of interest and have shown significant potential in numerous fields, including catalysis, solid electrolytic capacitors, and photochromic devices [142]. However, knowledge about these oxygen compounds and their

applications remains limited. Niobium exhibits three oxidation state in its oxides: 2^+.4^+ and 5^+, corresponding to NbO, NbO_2 and Nb_2O_5, respectively. Of these, Nb_2O_5 is the most thermodynamically stable [142]. The properties of niobium oxides, which vary with different oxidation states, are significantly influenced by factors such as phase, polymorphism, and stoichiometry. For instance, niobium oxides typically exhibit an octahedral NbO_6 coordination structure, but NbO_7 and NbO_8 structures can also be observed [143]. Additionally, Nb_2O_5 can adopt several different phase, including TT-pseudohexagonal, T-orthorhombic, and M-tetragonal, B-monoclinic, and H-monoclinic, depending on the temperature conditions [143]. This variability suggests that niobium oxide samples may contain a mixture of these different phase. In our project, which focuses on developing a new material for the selective oxidation of hydrocarbons, we have utilized Nb_2O_5 due to its significant thermodynamic stability as a support material. Given that Nb_2O_5 is known for its favourable properties in this context, we studied it both as an active species and as a support for the deposition of nanoparticles. This dual role of Nb_2O_5 aims to enhance the efficiency and selectivity of the oxidation process, making it a crucial component in our design of advanced catalytic materials for hydrocarbon oxidation.

1.7.1 An overview of the fundamental properties of Nb_2O_5

Considering the role that the metal oxide will have in this thesis, it is important to describe its properties in depth. Its crystal structure is depicted in figure 1.8, The orthorhombic unit cell in this crystalline form has a volume of 708 $Å^3$ [144]. Niobium atoms are connected to oxygen atoms through both distorted octahedral and pentagonal bipyramidal linkages. Eight niobium ions in deformed octahedral and eight niobium ions in pentagonal bipyramids are present in each unit cell. Lewis acid sites are linked to Nb=O double bonds in highly deformed NbO_6 structures , whereas slightly distorted NbO_6, as well as NbO_7 and NbO_8 structures, contain only Nb-O bonds, which are linked to Brønsted acid sites [143]. There are Lewis acid sites in every Nb_2O_5 catalyst that is supported, whereas some specific catalytic systems such as Nb_2O_5/Al_2O_3 and Nb_2O_5/SiO_2, contain only Brønsted acid sites [145-146]. Niobium pentoxide (Nb_2O_5) features a conduction band derived from the empty Nb^{5+}4d orbitals, with a band gap of approximately 3.4 eV. This is 0.2-0.4 eV higher than that of titanium dioxide (TiO_2), suggesting that Nb_2O_5 can still absorb light in the UV region. This characteristic indicates its potential as a photocatalyst under UV light, although this application has

not yet been studied in detail [142-147].

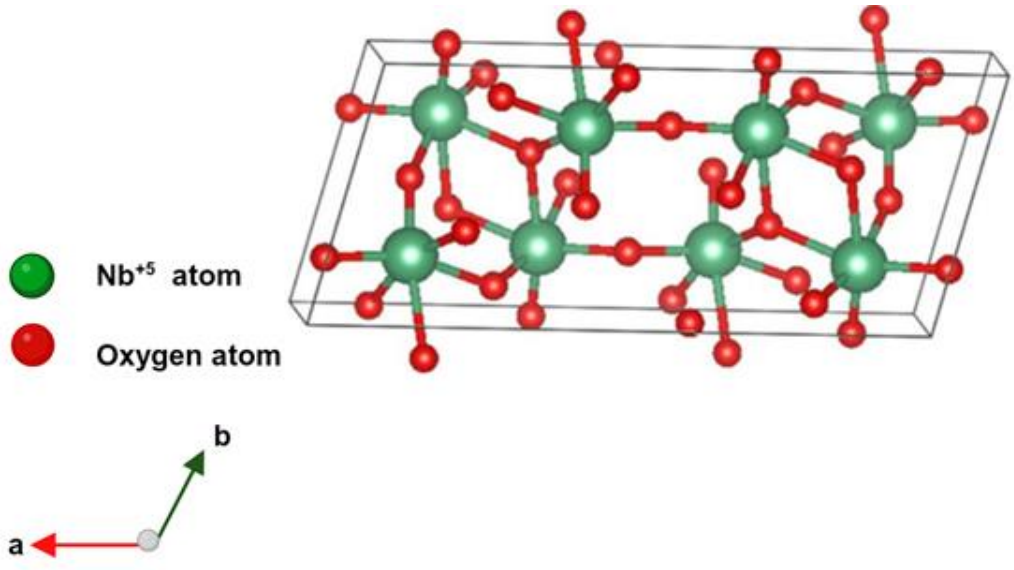

Figure 1.8: From the crystal structure of NbO_5, Niobium atoms are bonded to oxygen atoms by distorted octahedral coordination.

Given this Nb_2O_5 has promising applications in acid-catalysed reactions (e.g., 1-butene isomerization [148] and ethylene oxide (hydration) to produce monoethylene glycol)[149] through the adjustment of its acid properties. Schäfer et al. [150] noted that an O/Nb ratio of 2.5 can result from various combinations of octahedral linkages, leading to multiple crystal structures of Nb_2O_5. Nb_2O_5 demonstrated a range of polymorphisms, transitioning from an amorphous state to various polymorphs as the temperature increases during the crystallization process as illustrated in figure 1.9. There are multiple typical polymorphs of Nb_2O_5: TT-Nb_2O_5 in a pseudohexagonal crystal structure, T-Nb_2O_5 in an orthorhombic crystal structure, and monoclinic H-Nb_2O_5. The TT (Tetragonal crystalline phase) or T (Hexagonal phase) typically forms at a crystallization temperature of about 500°C from amorphous Nb_2O_5. This is succeeded by a conversion into the M phase which has a tetragonal crystal structure, and monoclinic B-Nb_2O_5 at 800°C. The monoclinic H phase is formed at temperatures exceeding 1000°C [147-151]. Among these polymorphs, it has been observed that the crystal structure of bulk Nb_2O_5 formed at higher temperatures is more ordered compared to that formed at lower temperatures [151]. Amorphous Nb_2O_5 features slightly distorted NbO_6, NbO_7, and NbO_8 structures, and it can facilitate the formation of radical peroxo species through its interaction with hydrogen peroxide [152]. The TT and T phases exhibit similar X-ray diffraction patterns, but some reflection peaks are split in

T-Nb_2O_5 compared to those observed in TT-Nb_2O_5 [143]. For instance, in the X-ray diffraction patterns of the T phase of Nb_2O_5, the peaks corresponding to the 2θ= 29° (180) plane and the 37° (181) plane are observed to be split [153]. The TT phase is less crystalline compared to the T phase and is typically stabilized by impurities such as OH^-, Cl^-, or oxygen vacancies. In T-Nb_2O_5, the Nb atoms are located in distinct, closely spaced, and equivalent sites, which may lead to broader peaks compared to the similarly split peaks observed in T-Nb_2O_5 [147-151]. Heat treatment at temperatures higher than 1000°C can produce H-Nb_2O_5, the most thermodynamically stable phase, from any Nb_2O_5 polymorph. In contrast, the TT or T phase of Nb_2O_5 are relatively more metastable by comparison [151]. Furthermore, it is important to emphasize that the preparation methods, the properties of the starting, existing impurities, and interactions with other components can all influence the crystal structure of Nb_2O_5 [151]. These factors are highlighted here because they can impact the physical and chemical properties (e.g., reducibility and acidity) relevant to catalytic applications. Therefore, different polymorphisms of Nb_2O_5 are likely to influence its performance in catalytic reactions.

In our work, we studied the reactivity of Nb_2O_5, with purity (99.99%) in the oxidation of ethylbenzene, *p*-xylene and cyclooctane. This study allowed us to assess how Nb_2O_5 influence its catalytic effectiveness in this oxidation process.

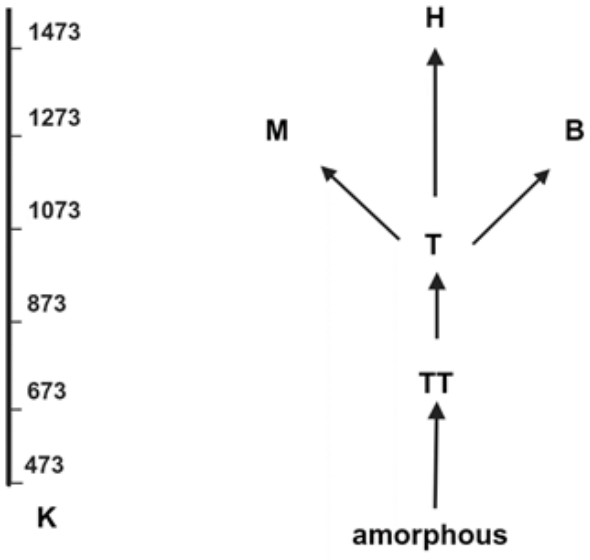

Figure 1.9: Polymorphism of Nb_2O_5 and its phase transformations as temperature increases [143].

The ability of a solid material to exist in several crystal structures is known as polymorphism, and it is commonly seen in a wide range of materials, including metals, minerals, and polymers [154]. This phenomenon greatly affects the physical and chemical properties of materials, thereby influencing their behavior. In various applications and contributing to the diverse range of material characteristics observed in both research and industrial contexts

1.7.2 The use and application of bulk Nb_2O_5 in catalytic process

However, there are only a few rare instances where Nb_2O_5 is used directly in chemical reactions. For instance, Tanabe et al[148] and Wachs et al [145-146] were among the pioneers in studying the use of niobium species in catalysis. Their research demonstrated that niobium compounds can serve as promoters or active species, as well as supports and solid acid catalysts in catalytic processes. Nb_2O_5 shows promising potential as a promoter or support in heterogeneous catalysts for a variety of reactions, such as esterification, alcohol oxidation, and the photooxidation of hydrocarbons in the presence of a solvent [155-156]. Despite its promising prospects as a catalyst, acting as a promoter, active phase, or support, Nb_2O_5 receives less attention compared to other transition metal oxides like CeO_2, MoO_3, and TiO_2 and MgO. The understanding of Nb_2O_5 roles in catalysis remains limited [147], highlighting its significant potential for further research in this field. Moreover, the direct oxidation of hydrocarbons with molecular oxygen in the presence of catalysts based on niobium oxide without the need for an initiator or solvent has received little attention. This indicates potential for further study of Nb_2O_5 in hydrocarbon oxidation. Therefore, in our study, we investigated the use of Nb_2O_5 as an active phase or support in the direct oxidation of hydrocarbons to gain insights into the feasibility of Nb_2O_5 in this application. In table 1.3 we provide an overview of the application of Nb_2O_5 in the field of oxidation. According to the literature, Nb_2O_5 has several roles in influencing catalyst properties and catalytic reactivity, summarized as follows: i) Nb_2O_5 exhibits promise in photooxidation, acting either as an active phase or as a support in the oxidation of hydrocarbons or alcohols. in this process radicals are generated by the transfer of electron from the surface electron donor to the conduction band under photo irradiation [157]; ii) oxidising substances such as H_2O_2 and tBHP can interact with bulk amorphous Nb_2O_5, resulting in the formation of peroxy species (Nb_2O_5). This reaction typically involves a color change from white to yellow, indicating the presence of active

intermediates for the reaction[152]; iii) the robust interaction between the metal-support influences the dispersion and size of metal nanoparticles on the Nb_2O_5 surface, enhancing the catalyst's activity [139]; iv) In the presence of an initiator, supported Nb_2O_5 nanoparticles can function as active species in the photo-oxidation of both saturated and unsaturated hydrocarbons [155]. Following existing literature and our research, while Nb_2O_5 is used as an active phase or support for hydrocarbon oxidation, usually, photo-irradiation or an initiator are used to carry out these reactions, which restricts large-scale production. As a result, we will examine the bulk Nb_2O_5 reactivity in the oxidation of hydrocarbons, focusing on ethylbenzene, p-xylene, and cyclooctane. Additionally, we will develop an innovative catalyst system that employs Nb_2O_5 as a support to selectively catalyse the oxidation process for the production of the desired products.

Table 1.3: Outlines of the various functions of Nb_2O_5 and its impact on reactions. This table highlights the promising outcomes when Nb_2O_5 is used either as a support or an active phase and its strong metal-support interaction (SMSI) with supported metals.

Catalyst	Results
Nb_2O_5, TiO_2	Nb_2O_5 catalysed the photooxidation of hydrocarbons with O_2, solvent free, showing increase in ethylbenzene conversion, even outperforming TiO_2. Photogenerated positive holes and electrons facilitated the formation of alkyl radicals, suggesting Nb_2O_5 is a promising photocatalyst [155].
Pt/Nb_2O_5	Nb_2O_5 served as a support and a strong metal-support interaction (SMSI) was noted between Pt nanoparticles and Nb_2O_5. This interaction can generate electron deficient Pt species, which create new active sites at the interface and promote a more uniform dispersion of particles resulting in enhanced activity during the dehydrogenation process [158-159].
Cu/Nb_2O_5, Nb_2O_5	Nb_2O_5 functioned as either the active phase or support for catalysts used in the solvent-free photooxidation of alcohols with O_2. Radicals were generated through direct electron transfer from the surface electron donor to the conduction band, while alcohol molecules were adsorbed onto the Lewis acid sites (Nb^{5+}) to form alkoxide species. The inclusion of Cu significantly improved photo-activity [157-160].
Nb species as inhibitor	Adding small amounts of Nb^{+5} can lead to formation of active metal-Nb-Ox species, which enhances the selectivity and stability of the catalyst structure. However, in some cases, the doped Nb species might interact with active metals to form undesirable phase, such as $VVNbO_4$ and $VNbO_5$ in V/Nb mixed oxide catalysts [161-162].
Amorphous and crystalline Nb_2O_5	This type used for glycerol and some hydrocarbon oxidation with H_2O_2.amorphous Nb_2O_5 formed peroxo species with H_2O_2 enabling substrate conversion. In contrast crystalline Nb_2O_5 lacked peroxo species, resulting in lower reactivity [163].

1.8 Catalysts based on supported Ag nanoparticles

As a result of their antiseptic properties, silver and silver-based compounds play an important role in antimicrobials. Much research on silver metal focuses on its applications in biological sciences and optoelectronics [164]. However, supported Ag nanoparticles garner increasing interest for their use in heterogeneous catalysis. They show great potential for the selective oxidation of alkanes and alkenes, which aid in the formation of oxygen-containing compounds [165-166]. Compared to other supported metal nanoparticles like Au, Pt, Cu, and Ni, the use of supported Ag nanoparticles is still in its early stages. Nonetheless, there is significant potential for developing this catalyst for various reactions. Studying the reaction mechanisms involving supported Ag and their interactions with oxygen or metal oxide supports presents a promising and challenging area for investigation [167]. The most recognized application of Ag-based catalysts is in the industrial process of ethylene epoxidation, where ethylene oxide is produced with selectivity rates of up to 80%. Ethylene oxide is subsequently utilized in the production of ethylene glycol (a component in antifreeze), poly (ethylene oxide), and surfactants [82], as well as in the dehydrogenation of methanol to produce formaldehyde [168], which is extensively used in producing resins for the wood panel industry [169]. Previous studies have shown that the catalytic activity of supported Ag catalysts can be influenced by the oxidation state of Ag, as well as the size and morphology of the nanoparticles. These factors are affected by the preparation methods and the type of support used. For instance, silver is mainly stabilized in the oxide state on CeO_2, whereas it tends to form a metallic state on Al_2IO_3 due to CeO_2 reducibility. Additionally, the distribution of Ag/Ag_2O affects their activity in soot oxidation [81]. In supported Ag/CeO_2 catalysts prepared by the impregnation method, three silver species are observed: Ag^{2+}, Ag^{+} and Ag^{0}. However, Ag^{2+} formation requires nitrate in the precursor and oxygen migration from the support during calcination at temperatures above 400°C, therefore the range of temperature used was 300°C [99]. Additionally, it's important to recognize that Ag nanoparticles play a crucial role in activating O_2. During the oxidation process involving O_2, two proposed mechanisms describe how reactive oxygenated species are formed [170-171]; i) the O_2 molecule becomes activated at active sites including the surface of metal particle, oxygen vacancies, or metal/oxide interfaces, resulting in the creation of species such as superoxide (O_2^{-}) and peroxide (O_2^{2-}); ii) the release of O from the metal oxide lattice

(Mars-van Krevelen mechanism). According to reports, supported Ag can adsorb oxygen onto the Ag species, activating molecular oxygen to form superoxide [80-167-170]. According to Luca et al. [170] research, oxygen molecules can either strongly adsorb at oxygen vacancy sites on CeO_2/TiO_2 to form peroxide or weakly adsorb on silver particles as superoxide (figure 1.10). CeO_2 capacity to store and release electrons can facilitate the breakdown of the O-O bond by lowering the activation barriers for oxygen reduction, which is accomplished by charge transfer from the vacancies to O_2. Supported Ag particles produce oxygen vacancies on the surface, which makes it easier for O_2 to adsorb reductively. Consequently, both the silver particles and the oxygen vacancies created by the interaction between Ag and the reducible support are susceptible to O_2 activation. In our research project, where O_2 is used as an oxidant without any initiator, the effect of Ag on O_2 activation suggests that Ag species (Ag^+) could facilitate the conversion of ground triplet molecular oxygen into reactive oxygen species.

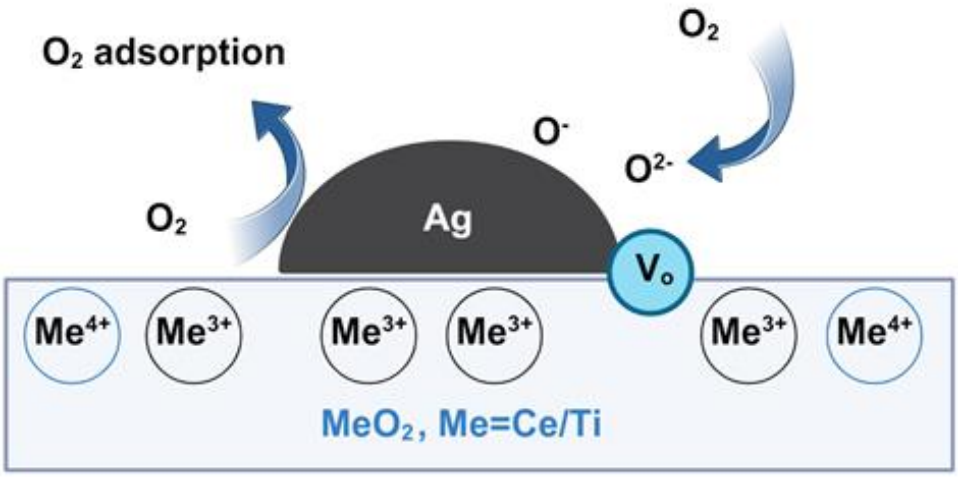

Figure 1.10: Activation of O_2 by supported Ag on the surface of metal oxides. V_o represents the oxygen vacancies in the metal oxide caused by the deposition of Ag [170].

In this case, table 1.4 summarises the utilisation of supported Ag on metal oxides in oxidation applications. These research indicate that the following are the consequences of supported Ag ; i) enhanced efficiency in activating molecular oxygen by adsorbing it onto particles and the oxygen vacancies generated through the interaction between particles and the metal oxide support [170]; ii) Interactions between supported Ag nanoparticles and support may impact the oxygen vacancy distribution, further influencing reaction performance [89]; iii) Redox couples are enhanced when

different states of Ag (Ag^+, Ag^0) are present in the catalyst., thereby improving activity. Furthermore, because it is less costly than other noble metals like Au, Pd, and Pt, Ag has an economic advantage. Given the description above, Ag exhibits promise for advancement in the selective oxidation of hydrocarbons utilising molecular oxygen in the absence of an initiator since, given the right circumstances, activated oxygen species are probably able to start the reaction.

Table 1.4: Applications of Ag metal catalysts with support in oxidation. As was already noted, the preparation and support techniques can affect the supported Ag's characteristics, such as its oxidation state and particle size.

Supported Ag catalyst	Preparation	Reaction
Ag/SiO_2 [172]	Impregnation method	CO oxidation
Ag/CeO_2 [99]	Impregnation and deposition method	CO oxidation
Ag/SiO_2 (Al_2O_3, MgO) [173]	Impregnation method	Alcohols oxidation
Ag/CeO_2 [89-81]	Impregnation method	Soot oxidation
Ag/SiO_2 [174]	Sol immobilization	Ethylbenzene oxidation
Ag/Al_2O_3 , MgO	Impregnation and Sol immobilization method	Styrene oxidation
Ag/TiO_2 , CeO_2	Impregnation method	Ethylene oxidation

1.9 Leaching

As previously mentioned , Assessing supported metals requires consideration of leaching [124-175]. If a metal leaches into a reaction mixture, it can have several consequences, including the pathway of alternative homogeneous mechanisms, reduced conversions with repeated usage, and potential safety hazards if toxic heavy metals or metal complexes contaminate the products. Supported metal oxides are widely used and relatively easy to synthesize. However, there is a risk that the active metal may leach into the reaction mixture, thereby losing its heterogeneous nature[176]. For instance, Sheldon et al. emphasized the significance of leaching studies. In their research on the oxidation of α-pinene using a CrAPO-5 catalyst (a porous material made of chromium-doped aluminium phosphate) they observed that chromium could oxidize with tBHP but not with larger oxidizing agents. Although they initially believed the reaction was taking place within the pores, they discovered that the reaction with tBHP caused leaching, resulting in homogeneous reactions occurring outside the pores. This example illustrates that thorough leaching tests are crucial, as they can

fundamentally alter our comprehension of a mechanism. We study the effect of leaching on our catalyst in detail in Chapter 4.

1.10 Project aims and objectives

This project will focus on developing analytical techniques to establish fast and reliable characterization protocols for analysing intermediates in hydrocarbon oxidation, specifically targeting alky hydroperoxide. This intermediate is unstable and may decompose during analysis rather than during the reaction. Since GC-MS is commonly used in hydrocarbon studies due to its high detection limit, we investigate the decomposition of alkyl hydroperoxide during GC-MS analysis and compare these results with those obtained from NMR spectroscopy. Following that, we will develop a novel catalyst designed for the selective oxidation of ethylbenzene, p-xylene, and cyclooctane. The objective is to create a catalyst that achieves high selectivity to ketone in our case Acetophenone, while running under milder conditions (120°C) compared to those used in current industrial practices, and without requiring additional initiators. For example, the conventional synthesis of Acetophenone involves Friedel–Crafts acylation of aromatic hydrocarbons using anhydrides or acyl halides with $AlCl_3$ as a catalyst, alongside stoichiometric oxidants like permanganates or dichromate's. However, this method faces challenges such as high reagent costs, low reactivity, equipment corrosion, and secondary pollution from harmful by-products. Thus, a key challenge is to enhance selectivity and consequently yield for specific products by reducing waste and improving energy efficiency. Supported metal oxide catalysts have been used in oxidation reactions, with silver (Ag) showing particularly promising results due to their ability to activate O_2 and interact with the support. However, their application remains limited and a deep understanding of the reaction mechanisms including interactions with the support and size effects is still needed. It has been reported that the performance of supported Ag catalysts largely depends on the oxidation state, particle size, and the characteristics of the support. Taking these aspects into consideration, our research will focus on the development of a novel silver-based catalyst for hydrocarbon oxidation and the role of Ag species during oxidation. Additionally, literature and prior research within our group indicate that Nb_2O_5 when used as a support exhibits strong metal-support interactions that significantly impact the properties of the supported and consequently the reaction

outcomes. The use of Nb_2O_5 as either an active phase or support in oxidation process demonstrates its impact on the reaction with promising results. Despite this, Nb_2O_5 based catalysts are largely underutilized for the direct selective oxidation of hydrocarbons with molecular oxygen without initiators, and there is insufficient knowledge about the mechanisms of C-H bond activation or the decomposition of alkyl hydroperoxides by Nb_2O_5 during oxidation. Based on the properties and applications of Ag and Nb_2O_5, a novel catalyst system with significant potential for hydrocarbon oxidation is being studied.

1.11 References

1 S. T. Oyama, *Factors Affecting Selectivity in Catalytic Partial Oxidation and Combustion Reactions,* ACS Publications, 1996.

2 M. Arshadi, M. Ghiaci, A. A. Ensafi, H. Karimi-Maleh and S. L. Suib, *J. Mol. Catal. A Chem.*, 2011, **338**, 71–83.

3 R. A. F. Tomas, J. C. M. Bordado and J. F. P. Gomes, *Chem. Rev.*, 2013, **113**, 7421–7469.

4 B. P. C. Hereijgers and B. M. Weckhuysen, *J. Catal.*, 2010, **270**, 16–25.

5 D. Belluš and B. Ernst, *Angew. Chemie Int. Ed.*, 1988, **27**, 797–827.

6 R. H. Crabtree, *Chem. Rev.*, 1995, **95**, 987–1007.

7 S. J. Blanksby and G. B. Ellison, *Acc. Chem. Res.*, 2003, **36**, 255–263.

8 I. Hermans, *Alkane CH activation by single-site metal catalysis*, Springer Science & Business Media, 2012, **38**.

9 M. Arshadi, M. Ghiaci, A. A. Ensafi, H. Karimi-Maleh and S. L. Suib, *J. Mol. Catal. A Chem.*, 2011, **338**, 71–83.

10 I. Hermans, J. Peeters and P. A. Jacobs, *Top. Catal.*, 2008, **50**, 124–132.

11 G. Brilmyer and R. Jasinski, *J. Electrochem. Soc.*, 1982, **129**, 1950.

12 J. W. Larsen, *J. Am. Chem. Soc.*, 1977, **99**, 4379–4383.

13 D. Munz and T. Strassner, *Inorg. Chem.*, 2015, **54**, 5043–5052.

14 E. Roduner, W. Kaim, B. Sarkar, V. B. Urlacher, J. Pleiss, R. Gläser, W. Einicke, G. A. Sprenger, U. Beifuß and E. Klemm, *ChemCatChem*, 2013, **5**, 82–112.

15 C. Freund, W. Herrmann and F. E. Kühn, *Organomet. Oxid. Catal.*, 2007, 39–77.

16 B. Meunier, G. Brudvig, J. L. Mclain, S. Murahashi, V. L. Pecoraro, D. Riley, A.

Robert, J. A. Rodriguez, R. A. Sheldon and J. S. Valentine, *Biomimetic oxidations catalyzed by transition metal complexes*, World Scientific, Imperial College Press, 2000.

17 Z. Guo, B. Liu, Q. Zhang, W. Deng, Y. Wang and Y. Yang, *Chem. Soc. Rev.*, 2014, **43**, 3480–3524.

18 C. J. Rolle, *Selective aerobic oxidations catalyzed by manganese(III) complexes using redox-active ligands*, University thesis work, Georgia Institute of Technology, 2011.

19 S. S. Stahl, *Angew. Chemie Int. Ed.*, 2004, **43**, 3400–3420.

20 J. A. Dean, *Lange's handbook of chemistry*, University of Tennessee, Knoxville: McGrawHill, Inc, 1999.

21 K. Weissermel and H. J. Arpe, *Synth. Synth. Org. Chem.*, 2004, 1127.

22 Q. Wang, Y. Cheng, H. Xu, L. Wang and X. Li, *Ind. Eng. Chem. Res.*, 2007, **46**, 7367–7377.

23 P. Raghavendrachar and S. Ramachandran, *Ind. Eng. Chem. Res.*, 1992, **31**, 453–462.

24 B. P. C. Hereijgers, R. F. Parton and B. M. Weckhuysen, *Acs Catal.*, 2011, **1**, 1183–1192.

25 J. Li, Y. Shi, L. Xu and G. Lu, *Ind. Eng. Chem. Res.*, 2010, **49**, 5392–5399.

26 K. Weissermel and H.-J. Arpe, *Industrial organic chemistry*, John Wiley & Sons, 2008.

27 D. G. Hendry, C. W. Gould, D. Schuetzle, M. G. Syz and F. R. Mayo, *J. Org. Chem.*, 1976, **41**, 1–10.

28 X. Liu, Y. Ryabenkova and M. Conte, *Phys. Chem. Chem. Phys.*, 2015, **17**, 715–731.

29 P. Chen and E. I. Solomon, *J. Am. Chem. Soc.*, 2004, **126**, 4991–5000.

30 N. Lehnert, R. Y. N. Ho, Que Lawrence and E. I. Solomon, *J. Am. Chem. Soc.*, 2001, **123**, 8271–8290.

31 T. Naicker and H. B. Friedrich, *J. Porous Mater.*, 2013, **20**, 763–775.

32 N. Kosinov, C. Liu, E. J. M. Hensen and E. A. Pidko, *Chem. Mater.*, 2018, **30**, 3177–3198.

33 R. A. Sheldon, *Chemtech*, 1991, **21**, 566–576.

34 I. Arends and R. A. Sheldon, *Appl. Catal. A Gen.*, 2001, **212**, 175–187.

35 M. S. Stark, *J. Am. Chem. Soc.*, 2000, **122**, 4162–4170.

36 C. Futter, E. Prasetyo and S. A. Schunk, *Chemie Ing. Tech.*, 2013, **85**, 420–436.

37 I. Hermans, T. L. Nguyen, P. A. Jacobs and J. Peeters, *ChemPhysChem*, 2005, **6**, 637–645.

38 G. A. Olah, Á. Molnár and G. K. S. Prakash, *Hydrocarbon Chemistry, 2 Volume Set*, John Wiley & Sons, 2017.

39 I. Hermans, P. A. Jacobs and J. Peeters, *Chem. - A Eur. J.*, 2006, 12, 4229–4240.

40 C. J. Hammond, J. R. L. Smith, E. Nagatomi, M. S. Stark and D. J. Waddington, *New J. Chem.*, 2006, **30**, 741–750.

41 M. J. Beier, B. Schimmoeller, T. W. Hansen, J. E. T. Andersen, S. E. Pratsinis and J.-D. Grunwaldt, *J. Mol. Catal. A Chem.*, 2010, **331**, 40–49.

42 C. Barckholtz, T. A. Barckholtz and C. M. Hadad, *J. Am. Chem. Soc.*, 1999, **121**, 491–500.

43 G. B. Shulpin, G. V. Nizova, *React. Kinet. Catal. Lett.*,1992, **48**, 333–338.

44 S. J. Singh and R. V Jayaram, *Catal. Commun.*, 2009, **10**, 2004–2007.

45 A. Dhakshinamoorthy, M. Alvaro and H. Garcia, *J. Catal.*, 2009, **267**, 1–4.

46 J. Zhang, Z. Wang, Y. Wang, C. Wan, X. Zheng and Z. Wang, *Green Chem.*, 2009, **11**, 1973–1978.

47 D. Kishore and A. E. Rodrigues, *Catal. Commun.*, 2009, **10**, 1212–1215.

48 J. M. Escola, J. A. Botas, J. Aguado, D. P. Serrano, C. Vargas and M. Bravo, *Appl. Catal. A Gen.*, 2008, **335**, 137–144.

49 R. K. Jha, S. Shylesh, S. S. Bhoware and A. P. Singh, *Microporous Mesoporous Mater.*, 2006, **95**, 154–163.

50 C. Samanta, *Appl. Catal. A Gen.*, 2008, **350**, 133–149.

51 K. Zhao, L. Zhang, J. Wang, Q. Li, W. He and J. J. Yin, *J. Am. Chem. Soc.*, 2013, **135**, 15750–15753.

52 W. R. Whitney, *J. Am. Chem. Soc.*, 1903, **25**, 394–406.

53 N. Weiher, A. M. Beesley, N. Tsapatsaris, L. Delannoy, C. Louis, J. A. van Bokhoven and S. L. M. Schroeder, *J. Am. Chem. Soc.*, 2007, **129**, 2240–2241.

54 O. Augusto and S. Miyamoto, *Princ. Free Radic. Biomed.*, 2011, **1**, 19–42.

55 H. Taube, *J. Gen. Physiol.*, 1965, **49**, 29–50.

56 E. Roduner, *Chem. Soc. Rev.*, 2014, **43**, 8226–8239.

57 S. Rebsdat and D. Mayer, *Ullmann's Encycl. Ind. Chem.*

58 P. A. Kobielska, A. J. Howarth, O. K. Farha and S. Nayak, *Coord. Chem. Rev.*, 2018, **358**, 92–107.

59 F. Haber and G. Van Oordt, *Zeitschrift für Anorg. Chemie*, 1905, **44**, 341–378.

60 J. W. Erisman, M. A. Sutton, J. Galloway, Z. Klimont and W. Winiwarter, *Nat. Geosci.*, 2008, **1**, 636–639.

61 M. A. M. Hossain, M. E. Ali, S. B. Abd Hamid and M. M. Rahman, *Adv. Mater. Res.*, 2015, **1109**, 248–252.

62 J. A. Dumesic, G. W. Huber and M. Boudart, *Handb. Heterog. Catal. Online*.

63 M. D. Argyle and C. H. Bartholomew, *Catalysts*, 2015, **5**, 145–269.

64 S. E. Davis, M. S. Ide and R. J. Davis, *Green Chem.*, 2013, **15**, 17–45.

65 B. Cornils and W. A. Herrmann, *J. Catal.*, 2003, **216**, 23–31.

66 I. Fechete, Y. Wang and J. C. Védrine, *Catal. Today*, 2012, **189**, 2–27.

67 J. K. Nørskov, F. Studt, F. Abild-Pedersen and T. Bligaard, *Fundamental concepts in heterogeneous catalysis*, John Wiley & Sons, 2014.

68 I. Chorkendorff and J. W. Niemantsverdriet, *Concepts of Modern Catalysis and Kinetics*, Wiley, 2017.

69 R. A. Sheldon, in *Studies in Surface Science and Catalysis*, Elsevier, 1991, vol. 59, pp. 33–54.

70 R. A. Sheldon and H. Van Bekkum, *Fine chemicals through heterogeneous catalysis*, John Wiley & Sons, 2008.

71 M. D. Hughes, Y.-J. Xu, P. Jenkins, P. McMorn, P. Landon, D. I. Enache, A. F. Carley, G. A. Attard, G. J. Hutchings and F. King, *Nature*, 2005, **437**, 1132–1135.

72 Y.-J. Xu, P. Landon, D. Enache, A. F. Carley, M. W. Roberts and G. J. Hutchings, *Catal. Letters*, 2005, **101**, 175–179.

73 Q. Tang, Q. Zhang, H. Wu and Y. Wang, *J. Catal.*, 2005, **230**, 384–397.

74 H. Cui, Y. Zhang, Z. Qiu, L. Zhao and Y. Zhu, *Appl. Catal. B Environ.*, 2010, **101**, 45–53.

75 M. O. Ozbek, I. Onal and R. A. Van Santen, *J. Catal.*, 2011, **284**, 230–235.

76 M. O. Özbek and R. A. Van Santen, *Catal. Letters*, 2013, **143**, 131–141.

77 P. A. N. Zhenyan, H. U. A. Li, Q. Yunxiang, Y. Hanmin, Z. Xiuge, F. Bo, Z. H. U. Wenwen and H. O. U. Zhenshan, *Chinese J. Catal.*, 2011, **32**, 428–435.

78 S. Rojluechai, S. Chavadej, J. W. Schwank and V. Meeyoo, *Catal. Commun.*, 2007, **8**, 57–64.

79 A.-Q. Wang, C.-M. Chang and C.-Y. Mou, *J. Phys. Chem. B*, 2005, **109**, 18860–18867.

80 M. Haneda and A. Towata, *Catal. today*, 2015, **242**, 351–356.

81 E. Aneggi, J. Llorca, C. de Leitenburg, G. Dolcetti and A. Trovarelli, *Appl. Catal. B Environ.*, 2009, **91**, 489–498.

82 H. H. Lou, J. Chandrasekaran and R. A. Smith, *Comput. Chem. Eng.*, 2006, **30**, 1102–1118.

83 L. Kundakovic and M. Flytzani-Stephanopoulos, *Appl. Catal. A Gen.*, 1999, **183**, 35–51.

84 G. Rothenberg, *Catalysis: concepts and green applications*, John Wiley & Sons, 2017.

85 Z. Feng, Q. Ren, R. Peng, S. Mo, M. Zhang, M. Fu, L. Chen and D. Ye, *Catal. Today*, 2019, **332**, 177–182.

86 S. Laursen and S. Linic, *Phys. Rev. Lett.*, 2006, **97**, 26101.

87 M. Chen and D. W. Goodman, *Acc. Chem. Res.*, 2006, **39**, 739–746.

88 Z. Qu, Y. Bu, Y. Qin, Y. Wang and Q. Fu, *Appl. Catal. B Environ.*, 2013, **132**, 353–362.

89 S. Wu, Y. Yang, C. Lu, Y. Ma, S. Yuan and G. Qian, *Eur. J. Inorg. Chem.*, 2018, **2018**, 2944–2951.

90 J. R. Croy, S. Mostafa, J. Liu, Y. Sohn, H. Heinrich and B. R. Cuenya, *Catal. Letters*, 2007, **119**, 209–216.

91 B. R. Cuenya, *Thin Solid Films*, 2010, **518**, 3127–3150.

92 G. Zhao, F. Yang, Z. Chen, Q. Liu, Y. Ji, Y. Zhang, Z. Niu, J. Mao, X. Bao and

P. Hu, *Nat. Commun.*, 2017, **8**, 14039.

93 M. S. Chen and D. W. Goodman, *Science (80-.).*, 2004, **306**, 252–255.

94 B. L. M. Hendriksen and J. W. M. Frenken, *Phys. Rev. Lett.*, 2002, **89**, 46101.

95 X.-Q. Gong, R. Raval and P. Hu, *Phys. Rev. Lett.*, 2004, **93**, 106104.

96 X.-Q. Gong, Z.-P. Liu, R. Raval and P. Hu, *J. Am. Chem. Soc.*, 2004, **126**, 8–9.

97 J. R. Croy, S. Mostafa, H. Heinrich and B. R. Cuenya, *Catal. Letters*, 2009, **131**, 21–32.

98 J. F. Weaver, S. P. Devarajan and C. Hakanoglu, *J. Phys. Chem. C*, 2009, **113**, 9773–9782.

99 M. Skaf, S. Aouad, S. Hany, R. Cousin, E. Abi-Aad and A. Aboukaïs, *J. Catal.*, 2014, **320**, 137–146.

100 R. Xu, D. Wang, J. Zhang and Y. Li, *Chem. Asian J.*, 2006, **1**, 888–893.

101 M. Haruta, *J. New Mater. Electrochem. Syst.,* 2004, **35**, 163–172.

102 M. J. Beier, T. W. Hansen and J.-D. Grunwaldt, *J. Catal.*, 2009, **266**, 320–330.

103 N. Toshima and T. Yonezawa, *New J. Chem.*, 1998, **22**, 1179–1201.

104 G. Sharma, A. Kumar, S. Sharma, M. Naushad, R. P. Dwivedi, Z. A. ALOthman and G. T. Mola, *Sci*, 2019, **31**, 257–269.

105 Z.-Q. Zhang, J. Huang, L. Zhang, M. Sun, Y.-C. Wang, Y. Lin and J. Zeng, *Nanotechnology*, 2014, **25**, 435602.

106 C. Williams, J. H. Carter, N. F. Dummer, Y. K. Chow, D. J. Morgan, S. Yacob, P. Serna, D. J. Willock, R. J. Meyer and S. H. Taylor, *ACS Catal.*, 2018, **8**, 2567–2576.

107 Y. Iizuka, R. Inoue, T. Miura, N. Morita, N. Toshima, T. Honma and H. Oji, *Appl. Catal. A Gen.*, 2014, **483**, 63–75.

108 L. F. Liotta, A. M. Venezia, G. Deganello, A. Longo, A. Martorana, Z. Schay and L. Guczi, *Catal. today*, 2001, **66**, 271–276.

109 C. A. Mirkin, *Small*, 2005, **1**, 14–16.

110 S. Kim, Y. F. Tsang, E. E. Kwon, K.-Y. A. Lin and J. Lee, *Korean J. Chem. Eng.*, 2019, **36**, 1–11.

111 C. H. Bartholomew, *Appl. Catal. A Gen.*, 2001, **212**, 17–60.

112 T. Mallat and A. Baiker, *Chem. Rev.*, 2004, **104**, 3037–3058.

113 T. Mallat, Z. Bodnar, P. Hug and A. Baiker, *J. Catal.*, 1995, **153**, 131–143.

114 M. Besson, F. Lahmer, P. Gallezot, P. Fuertes and G. Fleche, *J. Catal.*, 1995, **152**, 116–121.

115 J. A. Widegren and R. G. Finke, *J. Mol. Catal. A Chem.*, 2003, **198**, 317–341.

116 P. Munnik, P. E. De Jongh and K. P. De Jong, *J. Am. Chem. Soc.*, 2014, **136**, 7333–7340.

117 J. Liu, *Acs Catal.*, 2017, **7**, 34–59.

118 D. B. Eremin and V. P. Ananikov, *Coord. Chem. Rev.*, 2017, **346**, 2–19.

119 S. Schauermann, J. Hoffmann, V. Johánek, J. Hartmann, J. Libuda and H. Freund, *Angew. Chemie Int. Ed.*, 2002, **41**, 2532–2535.

120 L. D. Pachon and G. Rothenberg, *Appl. Organomet. Chem.*, 2008, **22**, 288–299.

121 A. V Gaikwad, A. Holuigue, M. B. Thathagar, J. E. ten Elshof and G. Rothenberg, *Chem. Eur. J.*, 2007, **13**, 6908–6913.

122 J.-S. Chen, A. N. Vasiliev, A. P. Panarello and J. G. Khinast, *Appl. Catal. A Gen.*, 2007, **325**, 76–86.

123 T. Borkowski, J. Dobosz, W. Tylus and A. M. Trzeciak, *J. Catal.*, 2014, **319**, 87–94.

124 H. Gruber-Wölfler, P. F. Radaschitz, P. W. Feenstra, W. Haas and J. G. Khinast, *J. Catal.*, 2012, **286**, 30–40.

125 M. Lamblin, L. Nassar-Hardy, J. Hierso, E. Fouquet and F. Felpin, *Adv. Synth. Catal.*, 2010, **352**, 33–79.

126 N. T. S. Phan, M. Van Der Sluys and C. W. Jones, *Adv. Synth. Catal.*, 2006, **348**, 609–679.

127 J. Rebek and F. Gavina, *J. Am. Chem. Soc.*, 1974, **96**, 7112–7114.

128 J. Rebek, D. Brown and S. Zimmerman, *J. Am. Chem. Soc.*, 1975, **97**, 454–455.

129 Y. Ji, S. Jain and R. J. Davis, *J. Phys. Chem. B*, 2005, **109**, 17232–17238.

130 A. Corma, H. García and A. Leyva, *Appl. Catal. A Gen.*, 2002, **236**, 179–185.

131 Z.-Y. Pu, X.-S. Liu, A.-P. Jia, Y.-L. Xie, J.-Q. Lu and M.-F. Luo, *J. Phys. Chem. C*, 2008, **112**, 15045–15051.

132 C. Bozo, N. Guilhaume and J.-M. Herrmann, *J. Catal.*, 2001, **203**, 393–406.

133 H. Y. Kim, H. M. Lee and G. Henkelman, *J. Am. Chem. Soc.*, 2012, **134**, 1560–1570.

134 G. Sedmak, S. Hočevar and J. Levec, *J. Catal.*, 2004, **222**, 87–99.

135 G. Sedmak, S. Hočevar and J. Levec, *J. Catal.*, 2003, **213**, 135–150.

136 G. Zhang, D. Zhao, J. Yan, D. Jia, H. Zheng, J. Mi and Z. Li, *Appl. Catal. A Gen.*, 2019, **579**, 18–29.

137 L. Dall'Acqua, I. Nova, L. Lietti, G. Ramis and E. Giamello, *Phys. Chem. Chem. Phys.*, 2000, **2**, 4991–4998.

138 M. Conte, H. Miyamura, S. Kobayashi and V. Chechik, *Chem. Commun.*, 2010, **46**, 145–147.

139 S. Shanmugapriya, P. Zhu, C. Yan, A. M. Asiri, X. Zhang and R. K. Selvan,

Adv. Mater. Interfaces, 2019, **6**, 1900565.

140 R. Wojcieszak, A. Jasik, S. Monteverdi, M. Ziolek and M. M. Bettahar, *J. Mol. Catal. A Chem.*, 2006, **256**, 225–233.

141 J.-W. Jun, Y.-W. Suh, D. J. Suh and Y.-K. Lee, *Catal. Today*, 2018, **302**, 108–114.

142 C. Nico, T. Monteiro and M. P. F. Graça, *Prog. Mater. Sci.*, 2016, **80**, 1–37.

143 I. Nowak and M. Ziolek, *Chem. Rev.*, 1999, **99**, 3603–3624.

144 K. Kato and S. Tamura, Acta Crystallogr. Sect. B Struct. Crystallogr. Cryst. Chem., 1975, **31**, 673–677.

145 J.-M. Jehng and I. E. Wachs, *Catal. Today*, 1990, **8**, 37–55.

146 J. M. Jehng and I. E. Wachs, *J. Phys. Chem.*, 1991, **95**, 7373–7379.

147 R. A. Rani, A. S. Zoolfakar, A. P. O'Mullane, M. W. Austin and K. Kalantar-Zadeh, *J. Mater. Chem. A*, 2014, **2**, 15683–15703.

148 T. Iizuka, K. Ogasawara and K. Tanabe, *Bull. Chem. Soc. Jpn.*, 1983, **56**, 2927–2931.

149 Y. Li, S. Yan, W. Yang, Z. Xie, Q. Chen, B. Yue and H. He, *J. Mol. Catal. A Chem.*, 2005, **226**, 285–290.

150 H. Schäfer, R. Gruehn and F. Schulte, *Angew. Chemie Int. Ed. English*, 1966, **5**, 40–52.

151 E. I. Ko and J. G. Weissman, *Catal. Today*, 1990, **8**, 27–36.

152 M. Ziolek, I. Sobczak, P. Decyk and L. Wolski, *Catal. Commun.*, 2013, **37**, 85–91.

153 S. M. A. H. Siddiki, M. N. Rashed, M. A. Ali, T. Toyao, P. Hirunsit, M. Ehara and K. Shimizu, *ChemCatChem*, 2019, **11**, 383–396.

154 P. W. Bridgman, *J. Appl. Phys.*, 1956, **27**, 659.

155 S. Furukawa, T. Shishido, K. Teramura and T. Tanaka, *J. Phys. Chem. C*, 2011, **115**, 19320–19327.

156 T. Shishido, T. Miyatake, K. Teramura, Y. Hitomi, H. Yamashita and T. Tanaka, *J. Phys. Chem. C*, 2009, **113**, 18713–18718.

157 S. Furukawa, Y. Ohno, T. Shishido, K. Teramura and T. Tanaka, *ChemPhysChem*, 2011, **12**, 2823–2830.

158 D. A. G. Aranda, A. D. Ramos, F. B. Passos and M. Schmal, *Catal. today*, 1996, **28**, 119–125.

159 R. Brown and C. Kemball, *J. Chem. Soc. Faraday Trans.*, 1996, **92**, 281–288.

160 S. Furukawa, A. Tamura, T. Shishido, K. Teramura and T. Tanaka, *Appl. Catal. B Environ.*, 2011, **110**, 216–220.

161 N. Ballarini, F. Cavani, C. Cortelli, C. Giunchi, P. Nobili, F. Trifirò, R. Catani and U. Cornaro, *Catal.Today*, 2003, **78**, 353–364.

162 V. V Guliants, R. Bhandari, A. R. Hughett, S. Bhatt, B. D. Schuler, H. H. Brongersma, A. Knoester, A. M. Gaffney and S. Han, *J. Phys. Chem. B*, 2006, **110**, 6129–6140.

163 M. Ziolek, P. Decyk, I. Sobczak, M. Trejda, J. Florek, H. G. W. Klimas and A. Wojtaszek, *Appl. Catal. A Gen.*, 2011, **391**, 194–204.

164 J. M. Campelo, D. Luna, R. Luque, J. M. Marinas and A. A. Romero, *ChemSusChem Chem. Sustain. Energy Mater.*, 2009, **2**, 18–45.

165 H. Zhao, J. Zhou, H. Luo, C. Zeng, D. Li and Y. Liu, *Catal. Letters*, 2006, **108**, 49–54.

166 F. W. Zemichael, A. Palermo, M. S. Tikhov and R. M. Lambert, *Catal. Letters*, 2002, **80**, 93–98.

167 M. Lamoth, M. Plodinec, L. Scharfenberg, S. Wrabetz, F. Girgsdies, T. Jones, F. Rosowski, R. Horn, R. Schlögl and E. Frei, *ACS Appl. nano Mater.*, 2019, **2**, 2909–2920.

168 L. Lefferts, J. G. Van Ommen and J. R. H. Ross, *Appl. Catal.*, 1986, **23**, 385–402.

169 G. J. Millar and M. Collins, *Ind. Eng. Chem. Res.*, 2017, **56**, 9247–9265.

170 L. Brugnoli, A. Pedone, M. C. Menziani, C. Adamo and F. Labat, *J. Phys. Chem. C*, 2020, **124**, 25917–25930.

171 A. R. Almeida, J. A. Moulijn and G. Mul, *J. Phys. Chem. C*, 2011, **115**, 1330–1338.

172 X. Zhang, Z. Qu, X. Li, M. Wen, X. Quan, D. Ma and J. Wu, *Sep. Purif. Technol.*, 2010, **72**, 395–400.

173 V. Raji, M. Chakraborty and P. A. Parikh, *Ind. Eng. Chem. Res.*, 2012, **51**, 5691–5698.

174 V. Raji, M. Chakraborty and P. A. Parikh, *Ind. Eng. Chem. Res.*, 2012, **51**, 5691–5698.

175 H.-U. Blaser, A. Indolese, A. Schnyder, H. Steiner and M. Studer, *J. Mol. Catal. A Chem.*, 2001, **173**, 3–18.

176 R. A. Sheldon, M. Wallau, I. Arends and U. Schuchardt, *Acc. Chem. Res.*, 1998, **31**, 485–493.

177 G. Centi, F. Cavani, F. Trifirò, G. Centi, F. Cavani and F. Trifirò, *Sel. Oxid. by Heterog. Catal.*, 2001, 1–24.

Chapter 2: Experimental

2.1 Introduction

This chapter outlines the experimental procedures employed in the study. The initial section of this chapter provides information about the synthesis and characterization and quantification of 1-phenyl ethyl alkyl hydroperoxide (EBHP). Next, analytical methods were developed and used to identify and quantify EBHP by GC-MS and ^{1}H-NMR. Then, the process of catalyst preparation, along with the theory and techniques employed for characterizing the prepared catalysts.

2.2 Materials Used

The reagents were used without further purification unless otherwise specified.

2.2.1 Catalyst metal precursors

- Copper (II) acetylacetonate ($C_{10}H_{14}CuO_4$, 98% w/w, Alfa-Aesar)
- Chloro (pyridine) cobaloxime ($C_{13}H_{19}ClCoN_5O_4$, 98% w/w, Sigma-Aldrich)
- Fluorene [$(C_6H_4)_2CH_2$)], ≥ 99% w/v, Sigma-Aldrich)
- Gold (III) acetate (Au ($O_2CCH_3)_3$, 99.9% w/w, Sigma-Aldrich)
- Gallium (III) nitrate hydrate (Ga ($NO_3)_3.xH_2O$, 99.99% w/w, Sigma-Aldrich)
- Iron (III) acetylacetonate (Fe ($C_5H_7O_2)_3$, 99% w/w, Sigma-Aldrich)
- Iron (III) nitrate (Fe ($NO_3)_3$, 99% w/w, Sigma-Aldrich)
- Manganese (III) acetate ($C_6H_9MnO_6$.2 (H_2O), ≥ 99% w/w, Alfa-Aesar)
- Palladium (II) acetate (Pd ($OCOCH_3)_2$, ≥ 99.8% w/w, Sigma-Aldrich)
- Platinum (II) chloride ($PtCl_2$, ≥ 98% w/w, Alfa-Aesar)
- Palladium (II) nitrate (Pd ($NO_3)_2$, ≥ 99.8% w/w, Sigma-Aldrich)
- Potassium iodide (KI, ≥ 99.5% w/w, Sigma-Aldrich)
- Silver acetate ($AgC_2H_3O_2$, 99% w/w, Sigma-Aldrich)
- Silver nitrate ($AgNO_3$, ≥ 99.8% w/w, Sigma-Aldrich)
- Sodium sulfate ($Na_2S_2O_3$, 99.99% w/w, Sigma-Aldrich)

- Sulfur (S, 99.98 % w/w, Sigma-Aldrich)
- Triphenylphosphine [$(C_6H_5)_3P$], 99% w/w, Sigma-Aldrich)
- Triphenylphosphine oxide ($(C_6H_5)_3PO$, ≥ 98.5% w/w, Sigma-Aldrich)

2.2.2 Metal oxides and supports

- Copper (I) oxide (Cu_2O, 99.999% w/w, Sigma-Aldrich)
- Cerium (IV) oxide (CeO_2, 99.9%, w/w, Sigma-Aldrich)
- Chromium (III) oxide (Cr_2O_3, 99.9% w/w, Sigma-Aldrich)
- Iron (III) oxide powder (Fe_2O_3, 99% w/w, Sigma-Aldrich)
- Manganese (III) oxide (MnO_2, ≥ 99.99% w/w, Sigma-Aldrich)
- Manganese (III) oxide (Mn_2O_3, ≥ 99.99% w/w, Sigma-Aldrich)
- Molybdenum trioxide (MoO_3, 99% w/w, Sigma-Aldrich)
- Nitric acid (HNO_3, 68% w/v, VWR)
- Niobium (V) oxide (Nb_2O_5, 99.9% w/w, Sigma-Aldrich)
- Platinum (IV) oxide (PtO_2, 99.995% w/w, Sigma-Aldrich)
- Palladium (IV) oxide (PdO_2, 99.995% w/w, Sigma-Aldrich)
- Silver (I) oxide (Ag_2O, ≥ 99.99% w/w, Sigma-Aldrich)
- Silica dioxide (SiO_2, 99.8% w/w, Sigma-Aldrich)
- Titanium dioxide (TiO_2, Rutile, ≥ 99.9% w/w, Sigma-Aldrich)
- Zeolite [(SiO_2) (AlO_2) x] M x/n, Acros organic)

2.2.3 Reagents and solvents

- Acetophenone ($CH_3COC_6H_5$, 98% w/v, Sigma-Aldrich)
- Cyclooctane (C_8H_{16}, ≥ 99% w/v, Sigma-Aldrich)
- Chloroform ($CHCl_3$, ≥ 99% w/v, Sigma-Aldrich)
- Deuterated chloroform ($CDCl_3$, 99.8% D, VWR)
- Dichloromethane (CH_2Cl_2, HPLC grade, Sigma-Aldrich)

- Diethyl ether ($C_4H_{10}O$, ≥ 99.8% w/v, Honeywell)
- Ethylbenzene ($C_6H_5CH_2CH_3$, 99% w/v, Alfa-Aesar)
- Hydrogen Peroxide (H_2O_2, > 30% w/v Sigma-Aldrich)
- Hydrochloric acid (HCl, 35% w/v, VWR)
- N,O-bis(trimethylsilyl) trifluoroacetamide $CF_3C=NSi(CH_3)_3OSi(CH_3)_3$, ≥ 99% w/v, Sigma-Aldrich)
- 1-phenyl ethanol (C_6H_5CH (OH) CH_3, 96% w/v, Sigma-Aldrich)
- P-xylene (C_6H_4 $(CH_3)_2$, 99% w/v, Sigma-Aldrich)
- Pyridine (C_5H_5N ,anhydrous, 99.8% w/v, Sigma-Aldrich)
- Sodium hydroxide (NaOH, ≥ 98% w/w, VWR)
- Sulphuric acid (H_2SO_4, ≥ 96% w/v, VWR)
- tert-Butyl hydroperoxide ($C_4H_{10}O_2$, 70 wt% in H_2O Sigma-Aldrich)
- Trifluorotoluene ($C_6H_5CF_3$, 99% w/v, Sigma-Aldrich)

2.2.4 Gases

- O_2 (99.5% v/v, BOC limited)

2.3 Definitions

2.3.1 Gas chromatography- mass spectroscopy (GC-MS) calculation:

The following equations can be used to quantify conversion and selectivity using GC-MS.

$$Conversion\ (\%)\ = \frac{Reactant\ \ converted}{Total\ original\ reactant\ at\ time\ 0} \times\ 100\%\ \ (\ eq.2.1)$$

The observed molar selectivity (S_i) is described as the ratio of moles of the desired product (p_i) to the total moles of all detected products in the reaction mixture (p_f) based on equation 2.2:

$$Selectivity\ (S_i)\ )\%\ = \frac{[p_i]}{\Sigma\ [p_f]} \times\ 100\%\ \ (eq.2.2)$$

2.3.2 Nuclear magnetic resonance (NMR) calculation:

Equations 2.3 and 2.4, respectively, can be used to define conversion and selectivity, where A p_i represents the product's area and the number of protons in the corresponding signal for a particular substance is denoted by n_H .

$$Conversion\ \%\ = \frac{\Sigma \frac{A_{pi}}{n_H}}{\frac{A_{left,R}}{n_R} + \Sigma \frac{A_{pi}}{n_H}} \times 100\% \quad (eq.2.3)$$

$$Selectivity\ (Si)\%\ = \frac{\frac{Api}{n_H}}{\Sigma i\ \frac{A_{pi}}{n_H}} \times 100\%\ \ (eq.2.4)$$

When applying these equations (eq.2.3 and 2.4) for determining conversion and selectivity in hydrocarbon oxidation, the carbon mass balance should be close to 100% within experimental error if no decarboxylation occurs. To verify the validity of these calculations, carbon mass balance (CMB) calculations were performed with an internal standard 1, 1, 2, 2 tetrachloroethane (TCE), based on eq. 2.5.

$$CMB\% = \frac{\Sigma_i C_i P_i \ + C_R n_{R,L}}{C_R n_{R,0}} \times 100 \quad (eq. 2.5)$$

Where:

In a molecule, $C_i P_i$ is the number of carbon atom products, $C_R n_{R,L}$ is the number of carbon atoms in the reactant left, $C_R n_{R,0}$ represents number of carbon atoms in the reaction mixture at the start of the reaction at a time zero.

2.4 Synthesis of 1-phenyl ethyl alkyl hydroperoxide (EBHP)

Due to a limited availability of suppliers for alkyl hydroperoxides, 1-phenyl ethyl alkyl hydroperoxide (C_6H_5CH (O_2H) CH_3) was synthesized in the laboratory and subsequently purified. The synthesized compound was then used assess its stability during analysis conditions and reactivity during reaction conditions by using analytical techniques such as GC-MS and ^{1}H-NMR. 1-phenyl ethyl alkyl hydroperoxide is synthesized (figure 2.1) according to literature procedures.[1]

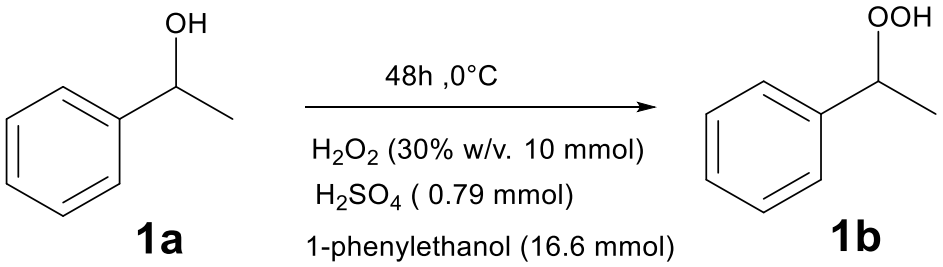

Figure 2.1 : Schematics of the Synthesis of ROOH (1b): A 48h reaction at ambient temperature involving the addition of 1-phenylethanol (1a) to a cooled solution of H_2O_2 and H_2SO_4, followed by extraction, purification, and flash chromatography.

1- Phenylethylhydroperoxide. To a cooled (0°C) solution of H_2O_2 (10.6 mL, 0. 10 mmol, 30% wt. in H_2O) and H_2SO_4 (0.44 mL, 0.79 mmol) 1-phenylethanol was added (2 mL, 16.6 mmol). The reaction mixture was stirred vigorously for 48h at ambient temperature and partitioned between Et_2O (20 mL) and water (30 mL). The aqueous layer was extracted with Et_2O (2 × 20 mL) and the combined organic layers were washed with 1 N aq. NaOH (2×10 mL) and brine (20 mL). The resulting solution was dried over $MgSO_4$, concentrated in a vacuum using a rotavapor, and purified by flash chromatography (hexanes/EtOAc 9:1).

Details of the flash chromatography are: silica gel was first added to the column,

followed by the eluent (Petroleum Ether/EtOAc, 9:1), allowing the silica to settle. The crude mixture was carefully added along the walls of the column, followed by a layer of sand to protect the silica gel from disturbance during elution. The purification process was monitored by thin-layer chromatography (TLC), with the compound showing an Rf value of 0.26. Differences in the behavior of the compounds were observed, indicating variations in the mixture. The product was collected in test tubes. The purified compound was then vacuum-dried and analyzed for purity by NMR.

2.4.1 Characterization of 1-phenyl ethyl hydroperoxide (EBHP)

1.1.1.1 Stability test at room temperature

To determine whether 1-phenylethylhydroperoxide (EBHP), is stable or not weather during analysis or reaction conditions, an EBHP of 96% purity was used. EBHP (0.02 mL) was typically analysed by using 1H-NMR including the addition of an internal standard 1,1,2,2-Tetrachloroethane ($C_2H_2Cl_4$, 0.02 mL) dissolved in 0.06 mL of $CDCl_3$ and spectra collected on a monthly basis. NMR data were collected by using a Bruker Advance IIIHD 400 spectrometer operating at 400 MHz.

2.4.2 Quantification of 1-phenylethylhydroperoxide (EBHP)

1.1.1.2 By titration

Titration can be used to quantitatively identify peroxides like CHP, H_2O_2, tBHP, including EBHP. Idometric titration with sodium thiosulfate ($Na_2S_2O_3$) was used to calculate the concentration of pure EBHP as follows:

A diluted reaction solution of EBHP 1 mL (with a dilution ratio of 100), 4 mL KI (100 $g.L^{-1}$), and 1 mL H_2SO_4 was pipetted into a narrow mouth flask with a tapered stopper, this precaution is recommended to prevent product loss due to evaporation. The mixture was allowed to sit for 10 minutes at a dark, temperature of 69°C by slow stirring, and left it cool down for 5 min until a yellow solution was obtained before being titrated with $Na_2S_2O_3$ (0.04 M) with a few drops of starch solution present [3]. When the combination turned colourless, it had achieved the endpoint. At the titrations end point, the volume (V_4) of the $Na_2S_2O_3$ solution was recorded, and then using the formula (eq.2.6) to calculate the EBHP concentration:

$$C_{ROOH=}\frac{1}{2}\times\frac{C_{Na_2S_2O_3}}{V_{ROOH}}\times D_2 = 10\times CNa_2S_2O_2\times V_4 \quad (eq.2.6)$$

Where $C_{Na_2S_2O_3}$ is the concentration (mol·L^{-1}), V_4 (mL) is the volume of $Na_2S_2O_3$ solution, while V_{ROOH} (mL) and D_2 (=100) are the volumes and dilution ratio of ROOH solution. For example: the determination of 1-phenylethylhydroperoxide (EBHP) content using 0.04 M $Na_2S_2O_3$, reaction condition before being titrated with 0.1 M $Na_2S_2O_3$ (1 mL of EBHP in 1 mL of H_2SO_4, 4 mL of KI added into narrow mouth flask as described previously in this section, the result showed that the actual purity was 100 ± 5 and this result match with NMR purity at same range.

1.1.1.3 The determination of Ethylbenzene alkyl hydroperoxide by Triphenylphosphine (TPP)

One of the most developed methods for the determination and quantification of ROOH is Iodometric titration. There are several limitations to the method, including low reproducibility, utilising large volumes of organic solvent, and the lengthy, tedious process of determining the endpoint [2]. Alternatively, EBHP quantification can be carried out via the triphenylphosphine (TPP) method (figure 2.2), in which the TPP reacts quantitatively with hydroperoxide in a sample to form triphenylphosphine oxide (TPPO), which is then detected using the GC-MS method according to literature procedures [3].

Preparation of solution A: TPP (0.060 mmol) (1.2 M) and fluorene (1.5 M) (0.075 mmol) were dissolved in $CHCl_3$ (50 mL).

Reaction A

A solution of ROOH (0.1 mL, 0.011 g, 0.078 mmol) in 50 mL of $CHCl_3$ (0.0016 M) was prepared. Solution A (50 mL) was added to the solution of peroxide and the mixture was vigorously shaken for 10 minutes.

Reaction B

A solution of S_8 (0.316 g, 0.0095 mmol) in 50 mL of $CHCl_3$ (0.19 M) was prepared. Solution A (50 mL) was added to the solution of sulfur and the mixture was vigorously

shaken for 10 minutes.

GC Sample preparation: 0.25 mL aliquots of the reaction mixtures from reactions A and B were combined in a gas chromatography (GC) vial and the contents were shaken vigorously for an additional 15 min. Following the 15-minute reaction time, the resulting mixture was analysed by GC/MS. TPPO peak area to internal standard peak area was used for quantification.

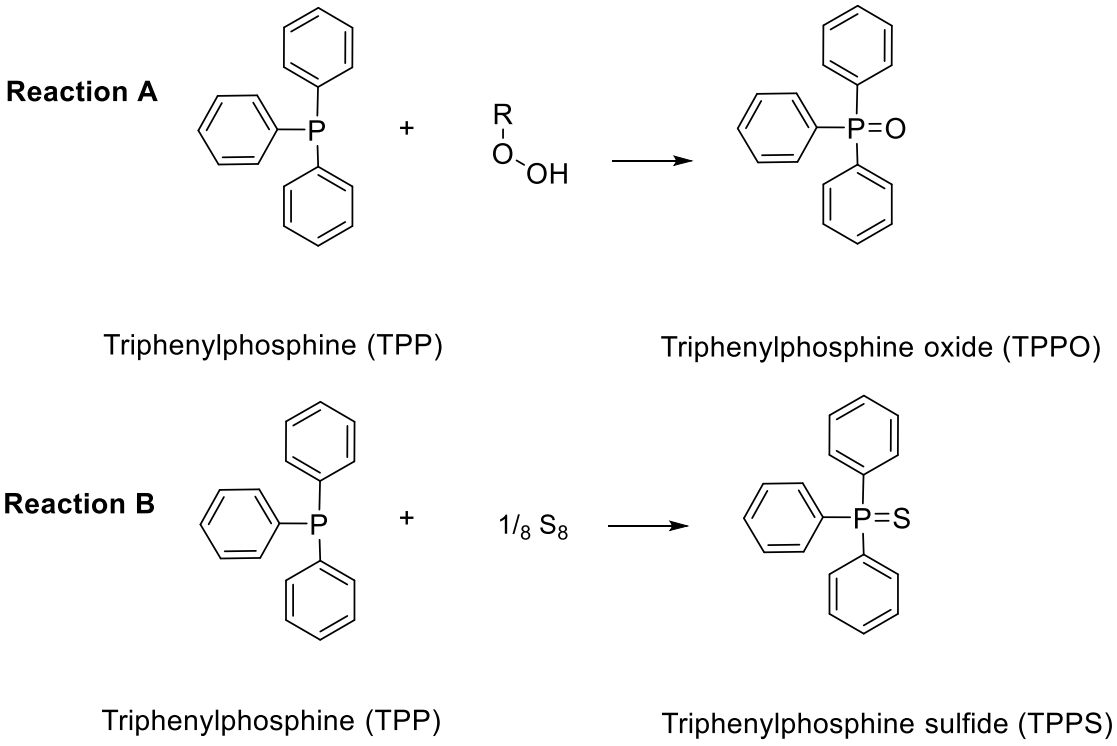

Figure 2.2 Quantification of hydroperoxide via the triphenylphosphine (TPP) method. Solution A, containing TPP is reacted with the ROOH sample in $CHCl_3$, leading to the formation of TPPO. This reaction is compared to reaction where S8 is reacted similarly, serving as a control. The resulting solutions are analysed using GC-MS according to literature procedures [3] .

In this experiment, we tested whether TPP was the limiting reagent. We used 0.06 mmol of TPP and 0.078 mmol of ROOH, with 0.018 mmol of ROOH remaining to continue the reaction. To confirm our hypothesis that no TPP was left, we conducted a secondary reaction (Reaction B) by adding 1/8 of S_8 to the reaction mixture. The absence of TPPS formation confirmed that no TPP was present.

2.5 Product analysis: quantitative analysis of reactive intermediates (EBHP) of hydrocarbon oxidation

The main objective of this study is to assess the suitability of gas chromatography (GC) for analyzing reaction mixtures containing alkyl hydroperoxides (ROOH) [4]. Alkyl hydroperoxides (EBHP) are sensitive compounds that may decompose during analysis, and this potential issue raises questions about the reliability of GC for such mixtures. To address this, the study will compare GC with nuclear magnetic resonance (NMR) spectroscopy, a method that, although more complex, is expected to avoid decomposition of Alkyl hydroperoxides during the analytical process. By directly comparing the performance and accuracy of these two techniques, this study aims to determine whether GC can be reliably used for reactions involving alkyl hydroperoxides, or if alternative methods like NMR are necessary to prevent decomposition and provide accurate results.

2.5.1 Gas chromatography

A syringe is used to collect a liquid sample and this is injected though a septum into an injector with the help of a carried gas (He in our case) figure 2.3. In our study, the injectors are heated at different temperatures. As a result, the liquid sample is vaporized and homogenized. It is recommended that the inlet sleeve be packed with an inert material, such as glass wool, which traps solid contaminants (such as fragments of the septum) as they pass into the column [5]. The mixture is introduced into a column and transported by a carrier gas, serving as the mobile phase. Inside the column, the stationary phase, which coats its interior, interacts with the analytes. As the compounds move through the column, they undergo repeated partitioning between the stationary and mobile phases. The nature and extent of these interactions vary for each compound, leading to differential retention. As a result, individual compounds elute from the column in distinct bands. The time required for each compound to elute, known as the retention time, allows for the separation and identification of the components. It is therefore crucial to select an appropriate stationary phase for the appropriate separation of a mixture of different compounds. It is possible to further optimize the separation process by adjusting the column length and diameter, the column lining thickness, the carrier gas pressure and flow rate, and the column temperature. Consequently, the column is located into a temperature

programmable oven where pressure and flow rates are monitored and controlled. Moreover, the type of GC column can be either capillary or packed. Nowadays, in gas chromatography, capillary columns are most commonly used because of their higher resolution, and firstly introduced by Golay in 1958 [6]. Generally, capillary columns are constructed from quartz tubes with diameters between 50 μm and 500 μm for the internal one , and lengths between 5 m and 200 m [7]. In order to minimize breakage, the columns are coated on the outside with polyamide. The inner surface of the column is coated with a stationary phase. In this study, the capillary column DB-5ms-UI column from Agilent was used. The backbone of the stationary phase used in this column is made of 5% Phenyl and 95% dimethylpolysiloxane (figure 2.4), with the use of different functional groups, the resolution of the components in the mixture is optimized. The stationary phase is chemically bonded to the column surface by a silane bond.

Eluates from the column then passes through a detector at the end of the column.

If resolved every peak in a chromatogram represents one component of the sample mixture. If the observed signal is compared with known values, the area of each peak can be associated to the amount of the substance in the injected sample; usually in mass or molar concentration.; thus, it can be used to quantify the amount of product present (figure 2.6). Peaks are often normalized to a standard to counteract variation in injection volume. This can be achieved by adding an internal standard (a compound that is not present in the reaction mixture) to an analytical sample throughout the reaction, and it must be stable and non-reactive with predictable and reproducible retention times and areas. Reactions were studied in the presence of an internal standard to help the assessment of carbon mass balance. *n*-decane was chosen as a standard since it did not interfere with the components of the reaction mixture, nor with the chromatographic phase and eluted from the column at a different time from the compounds studied. The amount was 0.02 mL of internal standard and 0.02 mL of undiluted reaction solutions were added to the GC vial and used 0.96 mL of DCM as solvent.

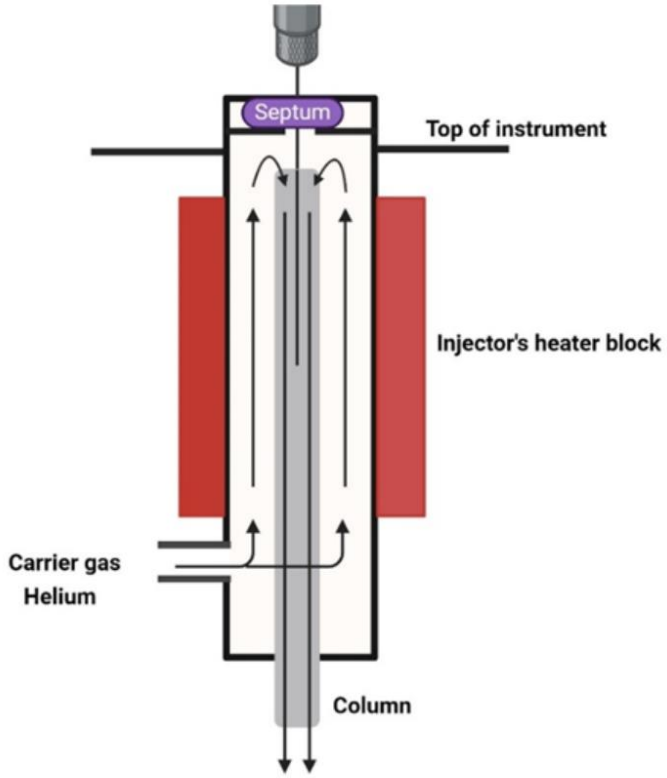

Figure 2.3 Schematic representation of a Gas Chromatography GC injector. The device introduces the sample into column via vaporization, assisted by helium gas as a carrier gas.

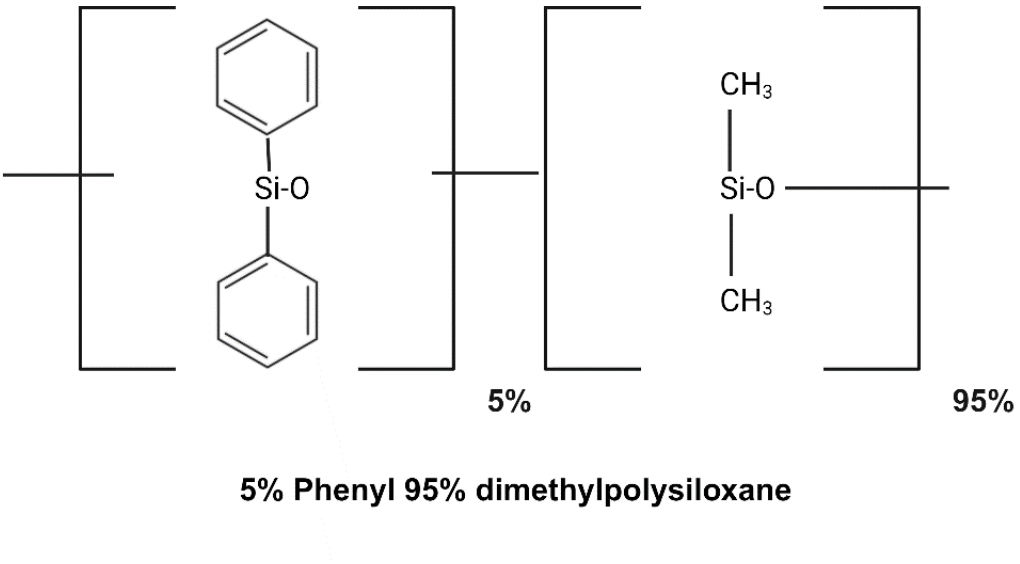

Figure 2.4 GC stationary phases described as "5% phenyl 95% dimethylpolysiloxane" are relatively non-polar GC phases containing a minor amount of phenyl groups for enhancing polarity.

2.5.2 The instrument gas chromatography-mass spectrometer (GC-MS)

In gas chromatography-mass spectrometry (GC-MS), a gas chromatograph and a mass spectrometer are combined to separate and identify compounds in liquid or gaseous mixtures [8]. As described in section 2.5.1, the components are separated first via gas chromatography, then a further split can occur by isolating different masses The GC-MS apparatus for liquid sample analysis is schematically shown in figure 2.5.

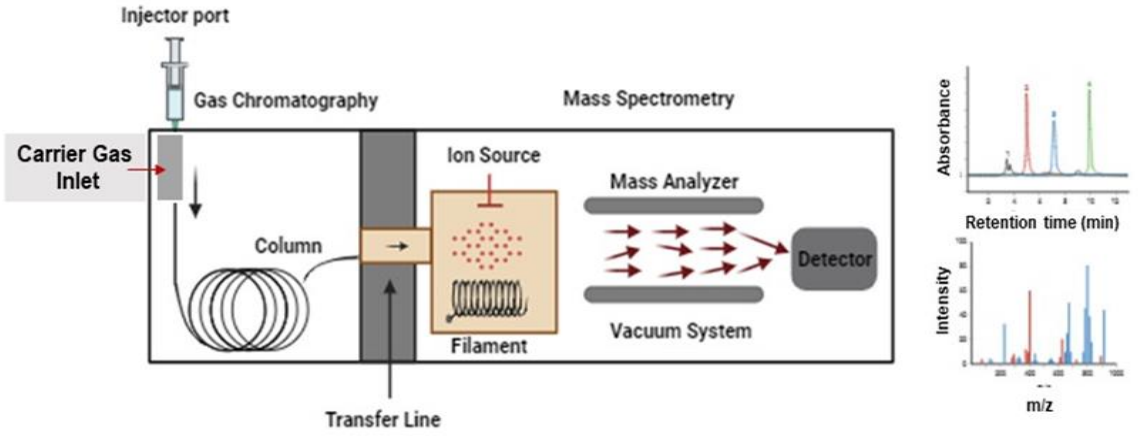

Figure 2.5: The schematic on the centre illustrates the process of separation in gas chromatography, where compounds are separated based on differential migration through the column. The chromatogram shows the output of the separation process, while the mass spectrum pattern provides molecular identification by ionizing the separated compounds and analyzing their mass-to-charge ratios through mass spectrometry. On the right a chromatogram and a mass spec pattern, together, these techniques enable both the separation and identification of compounds in a mixture.

After the components have been firstly separated per retention time, they are then analysed in a mass spectrometer and further separated, or resolved, per their mass to charge ratio and the ion source ionizes the analyte. Various methods can be employed based on the operational conditions and the type of sample. The most common method for GC-MS is using electron ionization (EI), which provides high fragmentation and detailed spectra, but is dependent on a vacuum to work. Electrons are liberated by providing a current to a heated filament in an EI source. The particles are then accelerated towards the trap electrode to create a beam. Through the beam at a 90-degree angle, the sample is fragmented and ionized and is then repelled toward the mass analyser by a repeller electrode [9]. Among the many types of mass analysers, Q-TOF (Quadrupole Time of Flight Mass Spectrometry), is one of the most common methods for separating ions according to their mass-to-charge ratio (m/z). During their passage into the Q-TOF analyser, the sample ions are exposed to a known electric field. Ions with a higher mass accelerate less than those with a lighter

mass and as such they need more time to reach the detector after passing through the system ; as a result, they spend longer 'in-flight'. The time spent 'in-flight' of each fragment is recorded, and this, along with known instrumental parameters, can be used to calculate mass-to-charge ratios. By plotting the relative ion intensity against the fragmentation pattern, a compound's fragmentation pattern can be determined, figure 2.6 illustrates the meaning of retention time and the corresponding peaks and figure 2.7 shows a simplified mass spectrum.

The gas chromatographic-mass spectrometry analysis was performed on a gas chromatograph (Agilent 7200) coupled to a mass spectrometer, namely a Quadrupole Time of Flight Mass analyser. A fused silica, capillary column was used (30 m $\times$ 0.25 mm $\times$ 0.25 μm film thickness) using helium as carrier gas at a flow rate of 1.2 mL min^{-1}. The ionization source was in positive ionization mode (electron impact energy: 70 eV), and the detection was performed in full-scan mode. The inlet and the transfer line temperatures were both maintained at 230 °C while the ion source was kept at 230 °C. Samples were injected in split mode (100:1) and separated using a temperature gradient program as follows: 50-90 °C for 4 °C min^{-1}, to 102 °C at 2 °C min^{-1}, and then maintained at 250 °C for 30 °C for a total run time of 36 min. the last step at high temperature is used to essentially to clean the column before the next sample.

The National Institute of Standards and Technology (NIST) mass database was used to analyse mass spectra. An analysis of GC-MS spectra of the structures obtained from the samples was compared to accepted standards and with NIST library standards corresponding to their spectra.

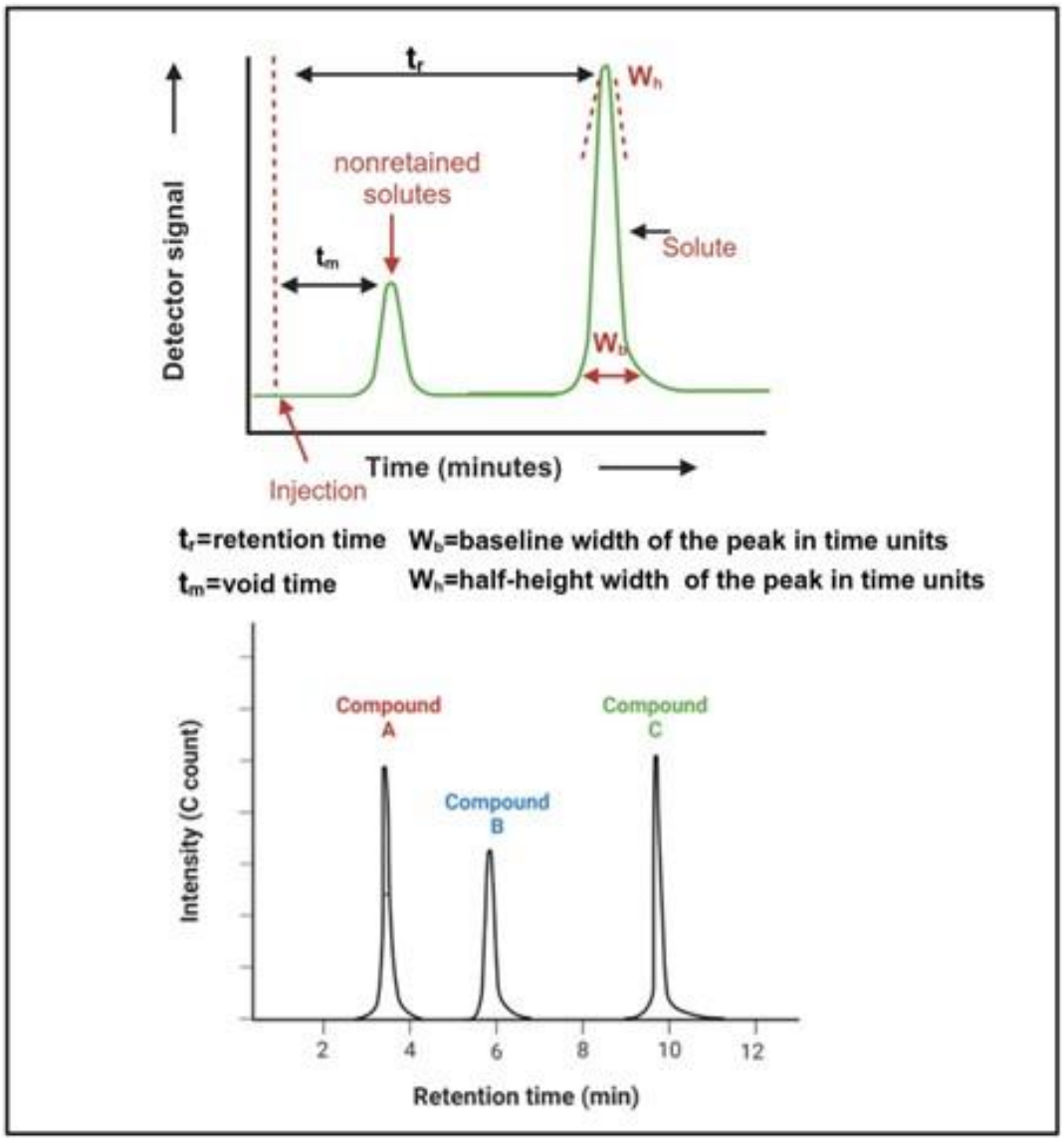

Figure 2.6: Series of chromatograms illustrating the meaning of retention time and the corresponding peaks. Retention time describes the time it takes a particular compound to elute from a chromatographic column. Analytes are separated into peaks based on their retention times and concentrations in the chromatogram. Each peak corresponds to a specific compound detected within the sample, allowing for qualitative and quantitative analysis in chromatography.

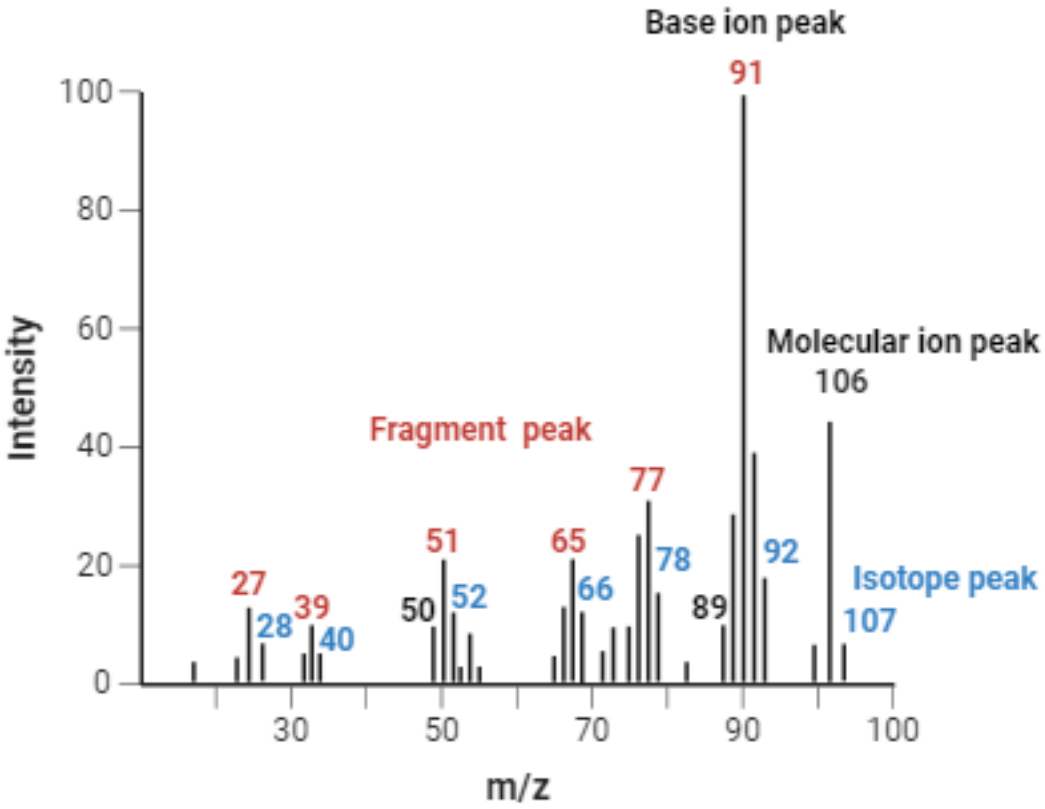

Figure 2.7: Representative ethylbenzene mass spectrum. Fragment peaks are highlighted in red from 91-27 m/z, while isotope peaks are highlighted in blue on the right-hand side. The peak at m/z 91 corresponds to the ethylbenzene molecular ion (C_8H_{10}) after the loss of a hydrogen atom. The m/z 77 peak is attributed to the phenyl ion ($C_6H_5^+$), resulting from the cleavage of the ethyl group. The m/z 51 peak represents the ethyl cation ($C_2H_5^+$), indicating the loss of the benzene ring, while the m/z 27 fragment corresponds to the ethyl radical (C_2H_3). The base ion peak is the most intense peak at 91 m/z+, while the total molecular ion is shown in black at 106 m/z+.

2.6 A study of the factors that may influence EBHP decomposition in the GC

In this section, we will detail the practical work undertaken to investigate the decomposition of alkyl hydroperoxides in GC. Various experimental variables were examined, including injector settings, column temperature, and the choice of detectors. Each of these factors plays a critical role in the analysis process.

Evaluation of the effects of the injector temperature and the vaporization of the analyte were conducted at six different injector temperatures: 70°C, 80°C, 90°C, 120°C, 150°C, and 250°C. An injection volume of 0.1 μL at a constant split ratio of 100:1 which is suitable for our quantitative analysis. In all cases, 0.02 mL of the sample, was mixed with 0.02 mL of *n*-decane as an internal standard (IS), this solution was then diluted with DCM to give 1 mL total volume.

The flow rate of the carrier gas can also have an effect on the resolution, a high flow rate reduces retention times, but this can lead to poor separation [10]. As such we examined the effects of different flow rates of 1.2 mL min^{-1}, 1.5 mL min^{-1}, and 2 mL min^{-1}, at the 70°C Injector and 230°C transfer line.

During the separation process the temperature of the column is systematically changed. This can increase the resolution and assist in evaluating any possible decomposition of EBHP during the analysis. The oven temperature programme used for the analysis is as follows: 50-90 °C for 4 °C min^{-1}, to 102 °C at 2 °C min^{-1}, and then maintained at 250°C for 30°C for a total run time of 36 min. The inlet and the transfer line temperatures were both maintained at 230°C while the ion source was kept at 230 °C with 1 min solvent delay.

2.7 Derivatization method for identification and determination of ethylbenzene alkyl hydroperoxide to be used in GC-MS

2.7.1 Overview

Due to the potential instability of EBHP during GC conditions a derivatization method aimed to identify whether an unknown compound is a peroxide or not was employed. To this scope, we used derivatives of N, O-bis (trimethylsilyl) trifluoroacetamide BSTFA (figure 2.8), that can converted the ROOH to $C_{11}H_{18}O_2Si$ and analysed by GC-MS without thermal decomposition [11].

The silyation reaction involves replacing a reactive hydrogen atom in OH, ROOH with a silyl group, most commonly trimethylsilyl (TMS) [12]. To conduct our method and to ensure safety, we used N, O-bis (trimethylsilyl) trifluoroacetamide (BSTFA) figure 2.8. A significant benefit of silyation in chromatography is the reduction of analyse polarity, its increase in stability, and improvement of GC performance [13].

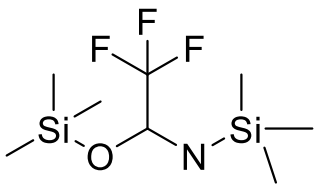

BSTFA : $C_8H_{18}F_3NOSi_2$
Mw: 257.40

Figure 2.8: Structure of N, O-bis (trimethylsilyl) trifluoroacetamide (BSTFA), used in our method to ensure safety during the analysis. The use of BSTFA facilitates the derivatization process, improving the stability of EBHP.

In detail, the synthesis is according to the method reported by Andresen et al [14]. For synthesis of $C_{11}H_{18}O_2Si$, we have used Dichloromethane (0.1 mL, 15.6 mol L^{-1}) with the internal standard Decane (0.02 mL) and ROOH (0.1 mL, 0.13 mol L^{-1}) transferred by syringe into a GC vial. Following this step BSTFA and Pyridine are added to the sample (0.5 mL, 0.27 mol L^{-1}) of BSTFA and 0.5 mL of Pyridine. The vial is then tightly closed and heated at 65 °C for approximately 20 minutes to ensure the derivatization reaction has been completed, with a maximum heating time of 30 minutes recommended. Following heating, the sample is allowed to cool to room temperature

before being injected into the GC/MS. The experiment was conducted using various ratios of the reactants, specifically 1:1, 1:0.26, 3:1, and 4:0.26, to assess the impact of different proportions on the reaction outcome.

2.7.2 Nuclear magnetic resonance (NMR)

If compared to GC-MS methods, NMR has a lower detection limit. However, NMR works at room temperature and typical ^{1}H spectra are obtained for concentration ranges of 10^{-3} –10^{-4} M, though it can reach up to 10^{-6} (unlike GC-MS where typical and minimal are 10^{-9} to 10^{-12}) within a short timeframe (about 5-10 minutes for routine spectra collection) [15-16].

In addition molecule structure and dynamics can be studied using NMR spectroscopy using the magnetic properties of atom nuclei as long as the angular momentum of some atoms is not zero. NMR can be used to analyse primarily liquids and in some cases solids. The most common types of NMR are ^{1}H and ^{13}C. As part of a typical ^{1}H NMR experiment, a small amount of sample (0.02 mL) is placed in a NMR tube with deuterated solvent for liquids. The resulting spectra will not include deuterium, which has a nuclear spin of zero. For quantitative analysis, an internal standard can also be included. The standard needs to be not reactive nor to lead to peaks overlap, providing a distinct signal against which all others can be compared. The samples are placed in holders and magnetic fields are applied (figure 2.11). The ‘spin active’ nuclei (those with $I \neq 0$) align with (+) or against (–) this field. Depending on their energy level, they are either in a higher (-) or lower (+) state known as -½ and +½ respectively. In the presence of an external magnetic field there is a difference in energy between these states called ΔE [17] as described in figure 2.10. The nuclei then relax back, releasing energy into the surrounding region (spin-lattice relaxation) or to other nuclei (spin-spin relaxation). The resulting frequency of the electromagnetic signal is thus influenced by the magnetic environment in which the nuclei are located. Nuclei in the same magnetic environment resonate at similar frequencies, and their electromagnetic signals appear together as a spectrum [17]. Accordingly, the number of magnetic surroundings found in the nuclei is equivalent to the number of signals observed in an NMR spectrum. Figure 2.9 shows a spectrum of Ethylbenzene at ^{1}H NMR as an example.

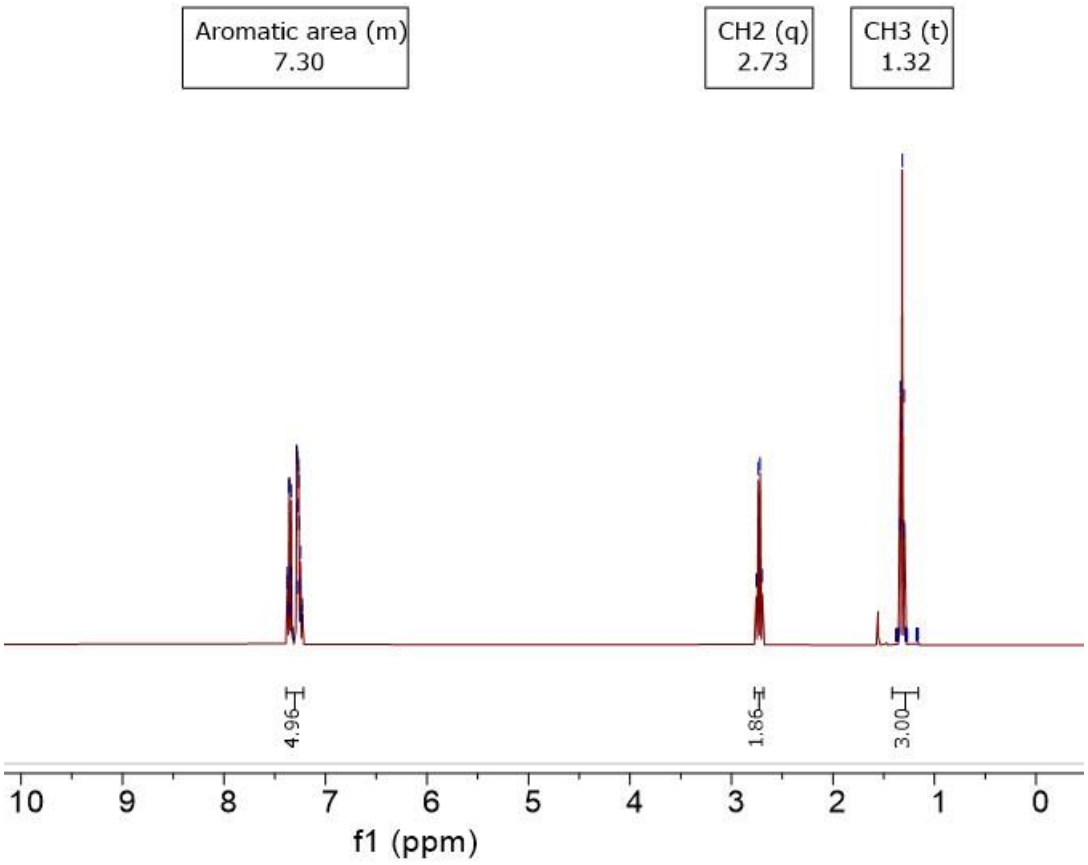

Figure 2.9: Example of a ^{1}HNMR spectrum of Ethylbenzene recorded in deuterated chloroform ($CDCl_3$) as the solvent. The spectrum displays characteristic peaks at different chemical shifts. In this spectrum, signals reflect various proton environments: aromatic protons (m) be seen at 7.30 ppm, CH_2 (q) protons be seen at 2.73 ppm, and CH_3 (t) protons are seen at 1.32 ppm. Each signal represents a magnetic environment experienced by the protons, demonstrating the principle that the number of signals in NMR spectrum corresponds to the number of distinct proton environments present in the molecule.

The chemical shift, shown on the x-axis, represents a relative measurement based on the difference between the signal frequency of the sample being analyzed and that of a reference standard (in our case $C_2H_2Cl_4$) and it is expressed in ppm. It is possible to identify functional groups based on the chemical shifts they produce, which allow them to be differentiated. As a result of the integration of the signals, we can determine how many nuclei are present in each environment. Depending on the magnetic environment, a multiple-line signal can be generated. In this case, multiple magnetic nuclei interact with and influence the magnetic field of others nearby. This can be expressed as the spin-spin coupling constant, J, measured in Hz. The spectrum displays three peaks, corresponding to three distinct environments of the hydrogens in the CH_3 and CH_2 groups as well as in the aromatic region. Chemical shifts, peak integrations, and J values can all be used to identify the structure of a sample's molecule (or molecules). Therefore, NMR spectroscopy is widely used in chemistry,

especially if associated to the synthesis of new compounds. In this study, $CDCl_3$ was used as a solvent to run analytical samples on a Bruker Advance III 400 spectrometer fitted with a 5 mm PABBO BB/19F-1H/D-GRD probe and a frequency of 400 Hz. Spectra were analysed using MestReNova and Top Spin software.

For a nucleus $I = {}^1/_2$ with an energy difference$\triangle E$, the energy splitting is provided by (eq.2.7):

$$\triangle E = \frac{\gamma h B_0}{2\pi} \quad (eq\ 2.7)$$

B_0 : is the external magnetic field strength

γ: response factor that measures the nucleus' gyromagnetic ratio

h: is the Planck's constant (6.626 x 10^{-34} J·s)

Electromagnetic radiation induce the molecule to resonate between these two energy levels producing a resonance frequency (ν) that corresponds to the magnetic field strength and the gyromagnetic ratio as described by the following equation (eq. 2.8):

$$2\pi\nu = \gamma B_0 \quad (eq.2.8)$$

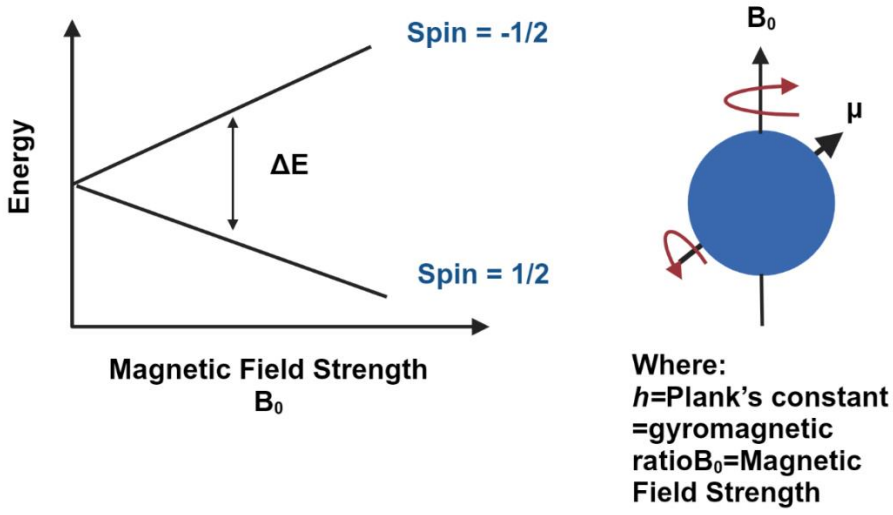

Figure 2.10: NMR-active nuclei shown in a plot showing that the energy difference between the two spin states corresponds to the strength of the magnetic field. Right: in the presence of an external l magnetic field B_0, a nucleus is spinning along its own axis while simultaneously performing a processional motion (orbit) along the direction of B_0.

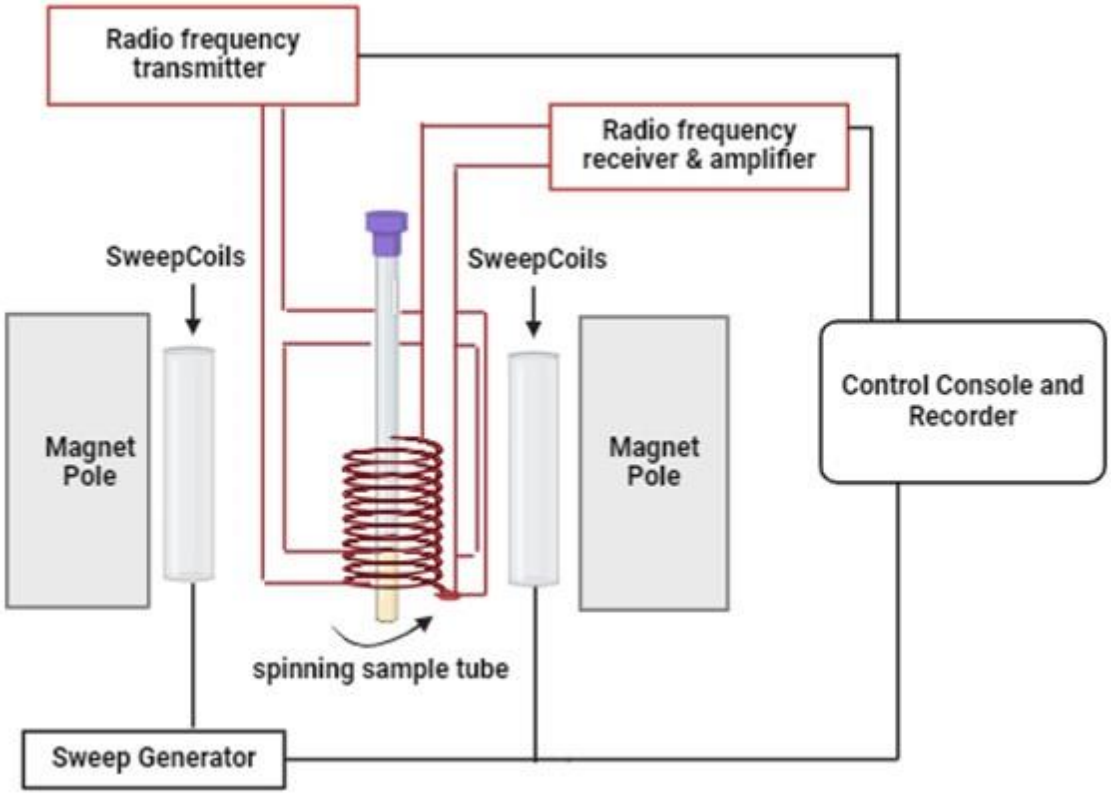

Figure 2.11: Schematics of an NMR spectrometer, NMR spectroscopy works by varying the emitted frequency of a machine while maintaining a constant magnetic field inside a sample. Within the magnet, the sample is surrounded by superconducting coils, and then a frequency from the radio wave source is applied. As soon as the results are received at the main console, a detector interprets them.

For the purpose of estimating the experimental error during analysis, a known concentration of product was analyzed three times. An analysis of a standard liquid sample from a reaction was also conducted periodically to ensure the stability and robustness of the results. The error of analysis was estimated to be around 5% based on multiple experiments. Similarly liquid samples were subjected to gas-chromatography analysis to verify and validate the data obtained from ^{1}H-NMR analysis.

2.7.3 ^{1}H-NMR parameters for relevant compounds in this thesis work

In this thesis, we focus on three relevant compounds: ethylbenzene, cyclooctane and *p*-xylene. Each of these compounds presents unique proton environments that show a spectral characteristics, allowing for the interpretation of their molecular structures and interactions.

Ethylbenzene

^{1}H NMR (400 MHz, $CDCl_3$): δ 7.44 – 7.14 (m, 5H), 2.73 (q, *J* = 7.6 Hz, 2H), 1.32 (d, *J* = 7.6, 1.2 Hz, 3H) ppm.

1-Phenylethanol

^{1}H NMR (400 MHz, $CDCl_3$): δ 7.30-7.39 (m, 5H) δ 4.87 (q, J=6.48, 1H) 1.50 (d, J= 6.48, 3H) ppm

Acetophenone

^{1}H NMR (400 MHz, $CDCl_3$): δ 8.00 – 7.91 (m, 2H), 7.60 – 7.52 (m, 1H), 7.46 (d, J = 8.3, 6.8, 1.1 Hz, 2H), 2.60 (s, 3H) ppm

Ethylbenzene alkyl hydroperoxide

^{1}H NMR (400 MHz, $CDCl_3$): δ 7.80 (s, 1H), 7.38-7.45 (m, 5H), δ 5.11 (q, J=6.6, 1H), 1.50 (d, J= 6.6, 3H) ppm

Cyclooctane

^{1}H NMR (400 MHz, $CDCl_3$): δ1.2 – 2.3 (s, 16H) ppm

Cyclooctanone

^{1}H NMR (400 MHz, $CDCl_3$) δ 1.2 – 2.3 (m, 10 H), 2.43 (t, 4H) ppm,

Cyclooctanol

^{1}H NMR (400 MHz, $CDCl_3$): δ 1.2 – 2.3 (m, 14H), 3.88 (m, 1H) ppm

Cyclooctyl peroxide

^{1}H NMR (400 MHz, $CDCl_3$): δ 1.2 – 2.3 (m, 14H), 4.15 (m, 1H) ppm.

1, 2-cyclooctadione

^{1}H NMR (400 MHz, $CDCl_3$): δ 1.2 – 2.3 (m, 8H), 2.68 (t, 4H) ppm.

Cis-9-oxabicyclononane

^{1}H NMR (400 MHz, $CDCl_3$): δ 1.2 – 2.3 (14H), 2.89 (t, 4H) ppm.

p-xylene

^{1}H NMR (400 MHz, $CDCl_3$): δ 7.10 (s, 4H), 2.34 (s, 6H) ppm

p-Toluic Acid

^{1}H NMR (400 MHz, $CDCl_3$): δ 7.27 (d, 2H, J = 8.0 Hz), 7.15 (d, 2H, J = 8.0 Hz), 2.40 (s, 3H)

p-Methylbenzyl alcohol

^{1}H NMR (400 MHz, $CDCl_3$): δ 7.26 – 7.20 (m, 4H, Ar-H), 4.65 (s, 2H, CH_2), 2.34 (s, 3H, CH_3), 1.85 (s, 1H, OH) ppm.

p-Tolualdehyde

^{1}H NMR (400 MHz, $CDCl_3$): δ 9.97 (s, 1H, CHO), 7.82 (d, 2H, J = 8.0 Hz, Ar-H), 7.26 (d, 2H, J = 8.0 Hz, Ar-H), 2.45 (s, 3H, CH_3) ppm.

p-Hydroxymethylbenzoic acid

^{1}H NMR (400 MHz, DMSO-d6): δ 12.98 (s, 1H, COOH), 7.94 (d, 2H, J = 8.0 Hz, Ar-H), 7.17 (d, 2H, J = 8.0 Hz, Ar-H), 4.56 (s, 2H, CH_2OH), 4.29 (s, 1H, OH) ppm.

P-Carboxybenzaldehyde

^{1}H NMR (400 MHz, DMSO-d6): δ 10.10 (s, 1H, CHO), 8.13 (d, 2H, J = 8.0 Hz, Ar-H), 8.05 (d, 2H, J = 8.0 Hz, Ar-H), 13.20 (s, 1H, COOH) ppm,

Terephthalic acid

^{1}H NMR (400 MHz, DMSO): δ 13.30 (s, 1H), 8.05 (s, 2H) ppm.

2.8 Catalyst synthesis: principles of deposition of supported metals and metal oxides

As this thesis work involved the preparation of some heterogeneous-based catalysts, the specifics of some of the techniques used to prepare these materials as well as the basics of alternative methods are briefly reported here.

Enhancing the catalytic properties of a material means increasing its catalytic activity, tailoring its selectivity towards the desired reaction products, and making it more stable, thereby extending its lifetime [18].

In the case of support meal species, order to increase catalytic activity, high dispersion of the metal nanoparticles over a support, most often a metal oxide support is often an important requirement, since smaller nanoparticles have greater surface area per mass of the catalyst. In addition, supported nanoparticle catalysts often contain highly expensive group metals, like Au, Pt, Pd, or Ag like in this work or rare transition metals as active metals, and increasing metal dispersion ensures that more active metals are positioned at the surface and readily available for catalysis instead of being hidden in the bulk. There is however a well-known tendency for small nanoparticles to sinter, especially at high temperatures, which reduces their surface area and catalytic activity. To prevent nanoparticle migration and sintering, the preparation route for small metal nanoparticles must ensure a strong interaction with the support as well as high dispersion. In order to optimize catalyst materials, industry faces challenges such as increasing metal dispersion, reducing nanoparticle size, lowering precious metal content, and increasing metal-support interfacial regions without compromising active catalytic sites [19]. There are three main methods of doping metal onto a support that can affect its catalytic activity: wet impregnation (WI), Co-precipitation, and sol-immobilization (SI).

The impregnation method (figure 2.12) involves wetting a solution containing the active metal salt onto the metal oxide support. During wet impregnation (WI), metal precursors (e.g. metal nitrates) are dissolved in a solvent (typically water, or ethanol). The support (e.g. metal oxide, silica) is then added (in varying quantities depending on the desired metal loading) to this solution to form a slurry, and the solvent is then

slowly dried by gently heating below its boiling point [20-21] .

The 'incipient wet impregnation' (IWI) is a variant of this protocol. The solution volume is equal to the pore volume, which allows the metal dopant to be deposited only within the pores of the support instead of the outside of it. In industry, IWI are preferred due to the minimal need for solvent, as well as the fact that they promote nearly full metal deposition into the support, resulting in minimal waste (especially for precious metal deposition) [22-18].

A co-precipitation method uses two precursor salts to precipitate active metals and metal oxide supports at the same time. There are, however, numerous washing steps necessary to remove the precursor salt, which creates large amounts of contaminated waste solvent with the co-precipitation method [23] .

In Sol immobilization method : Extensive literature shows that this method allows for more precise control of particle size, yielding narrower size distributions and achieving higher surface dispersion compared to the other protocols mentioned. However, the preparation process is more complex, involving the addition of a reducing agent to form colloids, with the resulting metal nanoparticles initially protected from aggregation using ligands (e.g., polyvinyl alcohol), which must later be removed [23-24].

As a result, metal precursors are dispersed across the support. These are then calcined to produce the desired metal/metal oxide.

Based on the procedure described here, supported Ag/Nb_2O_5 (5 wt%) was prepared (denoted as $WI\text{-}Ag/Nb_2O_5$, others would be specified.) 5 g of catalyst were prepared by dissolving 0.40 g of $AgNO_3$ in water (50 mL), then mixing Nb_2O_5 (4.75 g), thus to obtain a metal weight loading of 5 wt%. The slurry was left at 80 °C under gentle stirring. After heating the solid at 120 °C for 16 h in an oven, it was calcined at temperatures ranging between 180 °C and 300 °C 4 h. The procedure was the same for all other dopants (Cu, Fe) and supports (TiO_2, CeO_2, and SiO_2) but adjusting the relative amounts accordingly to a desired loading

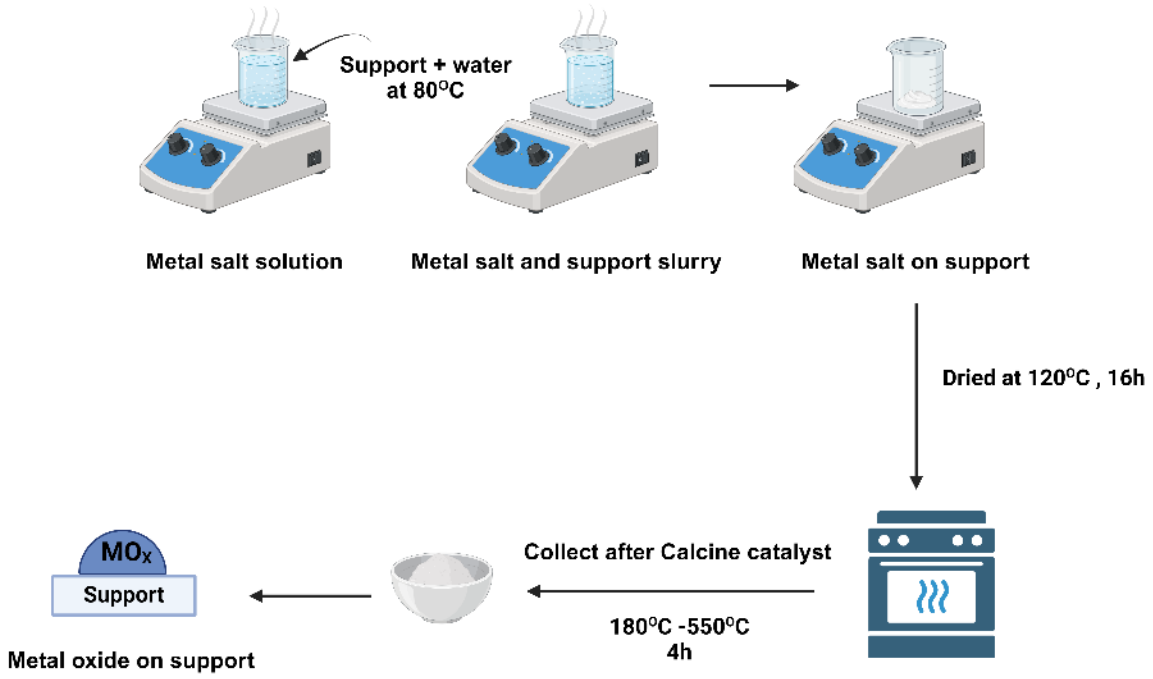

Figure 2.12: The Schematic shows the steps involved in the wetness impregnation process and what the dopant/support would look like during some of those steps [20].

2.9 Oxidation reactions and Catalytic tests

Safety was a top priority because hydrocarbons are flammable [24]. Ethylbenzene, for instance, has a low flammability limit of 2.1% in ambient air [25]. COSHH forms, risk assessments, and standard operating procedures were created as part of the work described here, closely adhering to operating safety protocols. Given these crucial health and safety regulations, catalytic texts were conducted with substrate amounts ranging from 0.5 to a maximum of 5 mL.

2.9.1 Ethylbenzene

1.1.1.4 Atmospheric tests

In a typical reaction, ethylbenzene (3 mL, 25 mmol) was oxidized to acetophenone in a round bottom flask, using a Radley's Starfish reactor set up (figure 2.13). The catalyst is added to it and heated to a given temperature usually between 110 and 130°C while stirring for 24h, and then allowed to cool. In order to separate the solid catalyst from the solution, an aliquot of the mixture was collected and centrifuged. The separated supernatant solution was used for analysis and characterization.

1.1.1.5 Aerobic oxidation by flow of oxygen

A typical reaction involves an addition of a catalyst (mass adjusted for loading) to ethylbenzene (3 mL, 25 mmol) kept in a screw cap pressure resistant round bottom flask with a bubbler. After stirring for 5 minutes under oxygen (P O_2 0.5 bar-2 bar, where P is the pressure as measured by a pressure gauge on an oxygen cylinder), the mixture was purged, and the pressure was increased by 0.5 bar at a time until the specified pressure was reached. A Radley's Starfish reactor set-up (figure 2.14) was used to heat the reaction mixture while stirring for 24-48 hours. In order to separate the solid catalyst, the mixture of ethylbenzene was stirred at the temperature for 24-48 hours, cooled, and centrifuged. ^{1}H NMR was used to analyse the resulting solution.

1.1.1.6 Effect of alcohol in ethylbenzene oxidation

A typical reaction was carried out by adding varying concentrations of 1-phenylethanol (5%, 10%, and 20%) to 3 mL of ethylbenzene. The mixture was then subjected to 120°C, at atmospheric pressure with continuous stirring at 600 rpm for 24 hours. Following the reaction, the samples were collected and analyzed by NMR

spectroscopy using deuterated chloroform ($CDCl_3$) as the solvent.

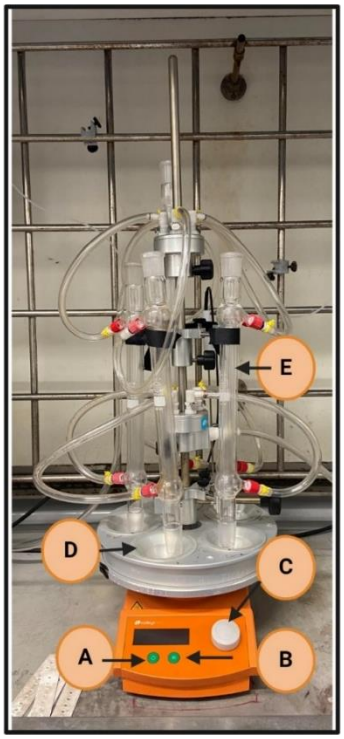

Figure 2.13: An illustration of the Radley's reactor used in this study, **A**: stirring plate, **B**: temperature plate body, **C**: controller for fixing bot temperature and stirring, **D**: aluminium heating block, **E**: condenser open to air.

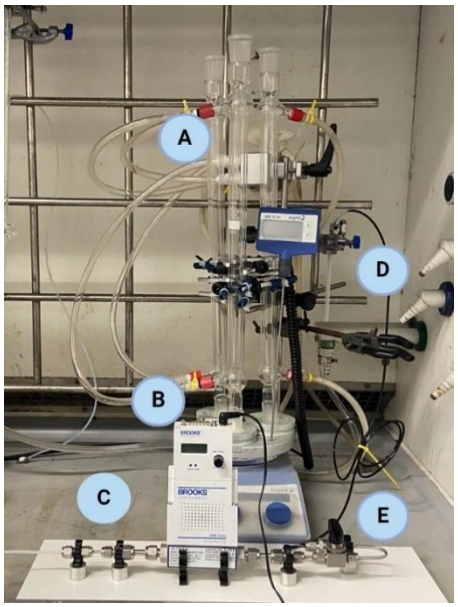

Figure 2.14: For aerobic reactions, batch reactors with an air/oxygen flow and ambient pressure are used. **A**: cooling condenser: it is connected to a two-neck flask which contains the substrate/catalyst and a stirring bar. **B**: Mass flow controller to maintain constant flow rates of reagent air / O_2. **C/D**: A steel needle connected to the other end of the mass flow controller will be perpendicularly inserted into the reaction mixture from the side neck, which is covered with a rubber cape. **E**: A controller for stopping the flow of oxygen if necessary.

2.9.2 Cyclooctane and *p*-xylene oxidation

For oxidising cyclooctane and *p*-xylene, the procedure is the same to that reported for oxidising ethylbenzene. The reaction temperature and initial oxygen pressure for the oxidation of ethylbenzene was 130 °C and 2 bar, respectively, with a specific reaction time of 24 hours. Furthermore, the reaction temperature and O_2 pressure for the oxidation of cyclooctane and *p*-xylene were optimized

In the cyclooctane oxidation tests, the addition of 3 mL of cyclooctane, 22.3 mmol, at 1-2 bar of pressure. The reaction temperature of was 120°C. And same protocol was used for the oxidation of *p*-xylene (3 mL, 25 mmol).

2.10 Ag^+ leaching control tests

In catalysis, leaching refers to the dissolution of metal species from the catalyst surface into the surrounding solution. This process is crucial in catalytic reactions, as the leached metals can affect both the catalyst's activity and its long-term performance stability. Leaching metal species can contribute to the process and act as catalysts in addition to influencing the catalyst lifetime. Therefore, control tests were carried out to determine if Ag^+ species could leach into the solution. The procedures were identical to the ethylbenzene oxidation procedure with $AgNO_3$ as the catalyst. In this control test, the only a minimal amount of metal salt is typically used (often less than 0.5 mg). To reduce experimental errors in these tests, a concentrated $AgNO_3$ solution is first prepared in water, and a measured volume of this solution is then added to a round bottom flask containing the required amount of Ag. Following the drying of the flask at 100 °C, it was cooled, and the organic substrate was introduced. More details about leaching determination in chapter 5 section 5.5.

2.11 Estimate of phase transfer of H_2O_2 and TBHP into Ethylbenzene

Ethylbenzene liquid phase oxidation rate and selectivity are greatly depends on the substrate, the solvent, the oxidant, the time, and the temperature [26]. Therefore, H_2O_2 and TBHP as oxidants have been study of their phase transfer into ethylbenzene. Experimental procedure (figure 2.15): Stirring 5 mL of EB with 5 mL each of H_2O_2 (30% v/v) and tBHP (70 w/v) separately for 1 hour at room temperature and leaving the

mixture for layer separation. After the layer separation is complete, 50 µL of the organic layer is taken into an NMR tube using $CDCl_3$.

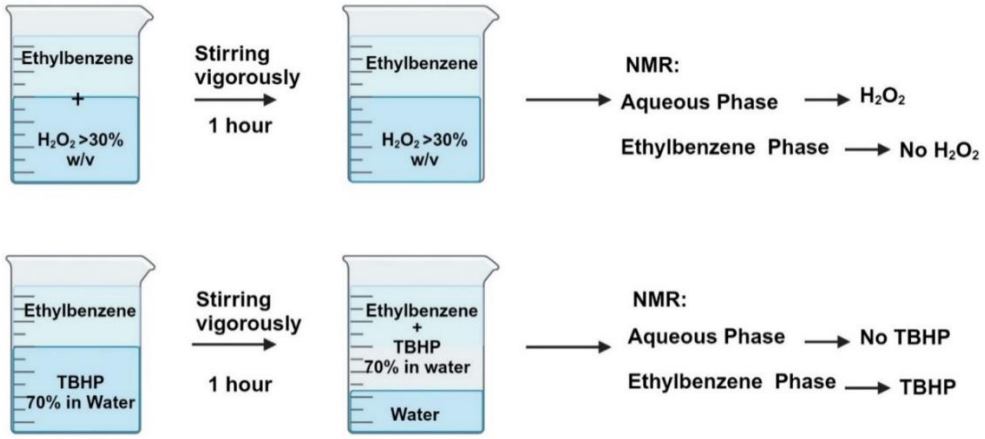

Figure 2.15: Experimental sequence for the assessment of solubility of H_2O_2 and TBHP as oxidant for ethylbenzene oxidation, followed by layer separation and NMR analysis.

2.12 Diffusion test

Diffusion is an unavoidable feature in any heterogeneous catalytic process, occurring when reactants transfer from a fluid phase to the catalyst surface, and products transfer from the catalyst surface to the fluid phase. It could have a significant impact on the reaction rate or selectivity, especially in large-scale production[27]. Therefore, diffusion test of ethylbenzene oxidation with Ag_2O by changing molar M:S ratio and stirring rate was carried out. Ethylbenzene with different M:S molar ratio and reaction condition, 3 mL of ethylbenzene using Ag_2O as catalyst M:S ratio: 1:1300,1:1000, 1:750, 1:500, 1:300, 1:100, 1:12 and 1:10 with 120 °C and 24 hours, stirring rate: 600 rpm; as well as changing in stirring rate of ethylbenzene oxidation from 400 to 800 rpm.

2.13 Catalyst characterisation

2.13.1 X-ray powder diffraction (XRPD)

Powder X-ray diffraction (XRPD) is a method of bulk characterisation that uses monochromatic X-ray radiation to identify compounds' structure and composition. Samples can be characterised based on their crystal structure, atomic spacing, and

unit cell dimensions [28].

X-rays are produced by a cathode ray tube and then filtered to produce monochromatic energy, which is directed at the sample. As these X-rays pass through an ordered lattice, they are scattered by atoms. Since X-rays can penetrate solids, they are diffracted by multiple crystal planes within the solid, and they can interfere by scattering from different crystal planes. According to Bragg's relation (eq. 2.9), incoming X-rays exhibit constructive interference when the separation between the crystal planes corresponds to an integer multiple of the wavelengths [28].

$$n\lambda = 2dsin\,\theta\ (eq.2.9)$$

This equation has the following parameters: n is an integer; the order of reflection, λ represents the wavelength of incoming X-rays, *d* represents the distance between lattice planes, and represents the angle between incoming X-rays and crystal planes.

X-ray source and detector are kept at the same distance while intensity is measured based on angle by rotating the incident radiation, the detector or both (the latter like in our case). An x-ray patterns are measured and displayed as a function of 2θ which allows the lattice spacing to be calculated according to Bragg's relation, figure 2.16. Ordered solids have a unique *d*-spacing, and thus can be identified by comparing samples of different *d*-spacing [29].

In order to obtain X-ray diffraction data, a Bruker D8 Advance diffractomer using a θ-θ, Bragg-Brentano geometry was used, using a Cu Kα radiation source operating at 40 kV and 40 mA. A typical analysis involved a 1h scan between 2θ values of 10 to 80° using wafers made of amorphous silicon are used to support the samples. Set parameters, 2θ: 15 – 80 °, t (per step): 0.6 s, primary opening: 0.3 °, secondary opening: 9.5 mm, no anti-scatter slit.

The International Centre for Diffraction Data (ICDD) database was used to identify phase diffraction patterns, which were analysed using an Analytical X'pert Pro software.

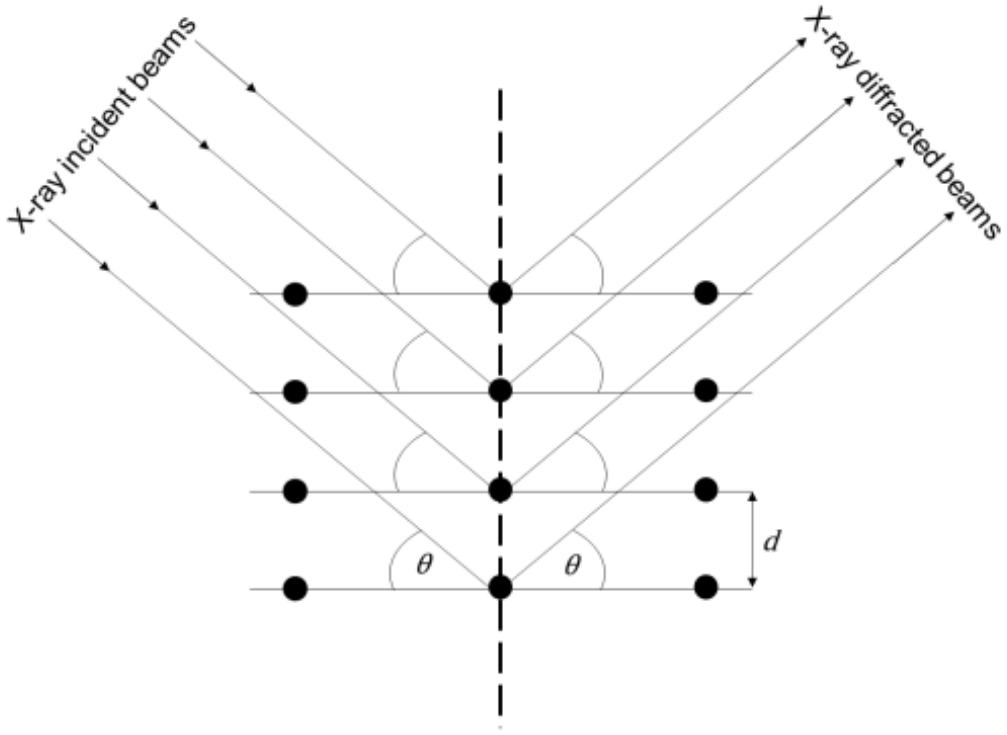

Figure 2.16: Schematic representation of X-ray diffraction (XRD) based on Bragg's theory. The angle (θ) between the incident X-ray beams and the normal to the lattice planes is used to determine inter-layer spacing (d) in the material. This diagram highlights the fundamental principle of XRD, where constructive interference occurs when the path difference between the reflected beams satisfies Bragg's law. Diagram reused with permission from E. Ameh [30].

2.13.2 Transmission Electron Microscopy (TEM).

An electron microscope can be used to determine the size, shape, and composition of particles supported on a surface or the morphology of a material [31]. This is possible because the characteristic wavelength of electrons is less than 1Å, which makes them capable of monitoring atomic detail to a considerable degree [32]. Although transmission electron microscopy employs an electron beam rather than visible light, it is founded on the same principles as light microscopy (figure 2.17).

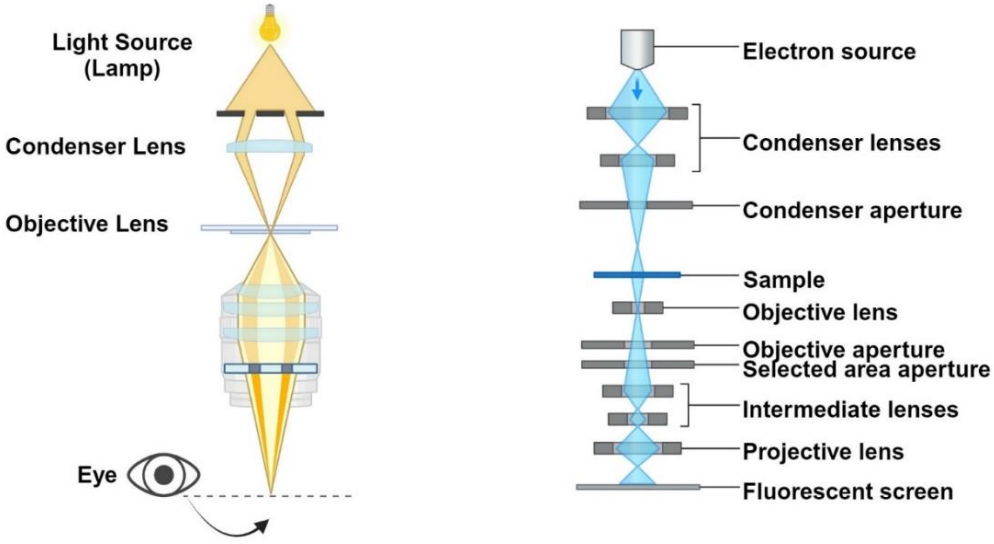

Figure 2. 17: Comparison between an optical microscope and TEM: Optical microscopes use visible light and glass lenses for magnification, suitable for larger structures. TEM, utilizing electron beams, provides much higher magnification and resolution, allowing detailed imaging at the atomic level.

As electrons are irradiate from an emitter, they pass through a condenser consisting of electromagnetic lenses to become focussed into thin beams. As the beam hits the sample, several types of electrons reflect from the surface and disappear (figure 2.18) [33]. Electrons that pass through the material are magnified by electromagnetic lenses and hit a fluorescent screen at the bottom of the microscope to create a TEM image.

Using a camera or a microscope, the operator can examine the image directly. Different atoms in the sample interact with the transmitted electrons, resulting in contrasts in the TEM image reflections. In our case only electrons that have crossed the samples will be considered, leading in fact to transmission electron microscopy. In this case the signal is affected by the atomic number and the density of the material, and as a rule of thumb species having a higher density also appearing darker in the image.

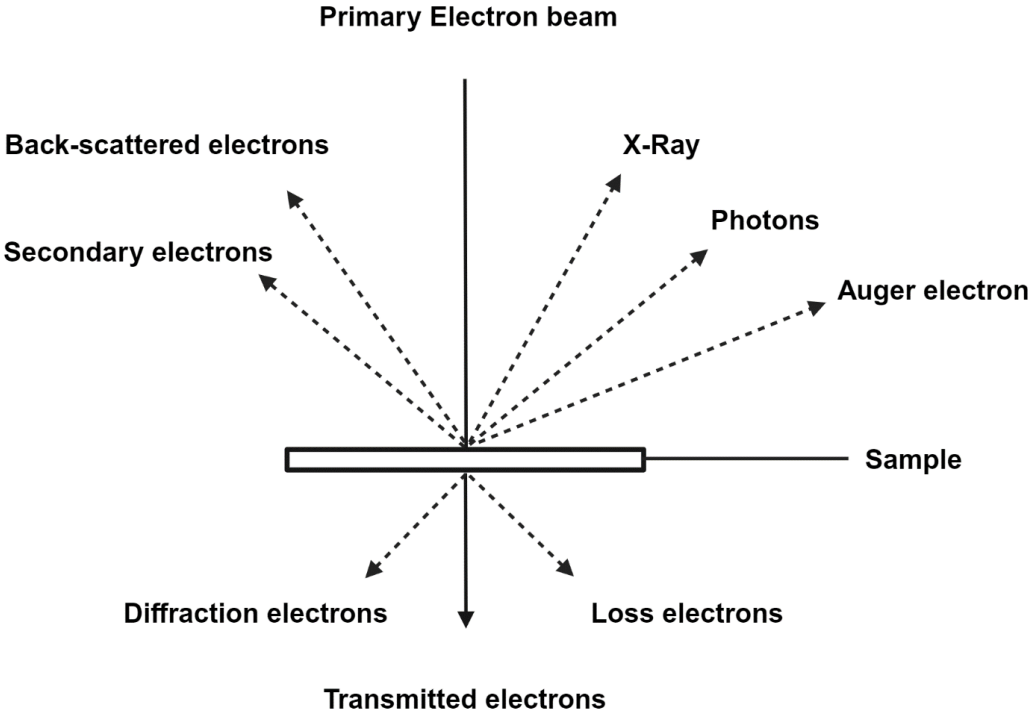

Figure 2.18: In TEM, a beam of electrons passes through an ultrathin specimen, interacting with the sample's atoms. These interactions cause electrons to scatter, with some passing through while others are absorbed or deflected.

Even though TEM has a vast array of applications, it does have a number of drawbacks. A highly energetic electron beam (typically 1 eV) [34]. Interaction with a sample under an electron microscope may result in permanent structural changes or it is possible that the region analysed does not represent the entire sample due to the relatively small view field. On the other hand, the high resolution of transmission electron microscopy makes it one of the most commonly used techniques for the characterization of catalysts despite these limitations.

A drop of the suspension was allowed to dry on a Cu grid after the catalyst powders were dispersed and sonicated in high purity ethanol for around ten minutes in order to prepare the samples for transmission electron microscopy (TEM) analysis. A collection of 200 particles was used to determine the frequency count for the Sn/Y particle size distribution.

2.13.3 Surface area method Brunauer-Emmett-Teller (BET)

One of the most used methods for determining a material's surface area and porosity is the BET method, which is also frequently used in catalyst characterisation. The BET

is based on three assumptions: adsorbents have flat surfaces, neither lateral nor vertical interactions exist, and the mechanism of adsorption is the same for all forms of adsorption. In contrast, the BET theory extends the Langmuir model by considering multilayer adsorption and the phenomenon of condensation, allowing it to describe adsorption on heterogeneous surfaces more accurately [35]. This enhancement accounts for interactions between adsorbed layers, making the BET model applicable to a broader range of materials. The total surface area is proportional to the volume of gas adsorbing on it [36]. In the study of catalysts, surface area often plays a significant role in determining the catalyst's reactivity [37]. For a catalyst, the more surface area available to the reacting gas or liquid, the greater the product conversion if often observed.[38] Water contaminants must be removed from solid surfaces before surface area or pore size measurements can be performed. Langmuir's theory assumes ideal monolayer adsorption of gas molecules. The BET theory takes into account multilayer adsorption and equilibrium between all layers (without interfering with them). Thus, Langmuir's equation applies for all layers. The following equation 2.10 is express the BET isotherm [39-40]:

$$\frac{\frac{P}{P_0}}{n(1-\frac{P}{P_0})} = \frac{1}{n_m C} + \frac{C-1}{n_m C}(\frac{p}{p_0}) \quad (eq.2.10)$$

As shown in the equation above, n is the specific adsorption quantity at the relative pressure $\frac{P}{P_0}$, Adsorbate equilibrium and saturation pressures are P and P_0, respectively at the temperature of adsorption. n_m is the monolayer capacity ((Amount of Adsorbate required to occupy all adsorption sites of a gas), and C is the BET constant. In the BET range, C can be used to determine the shape, size, and volume of an isotherm based on the enthalpies of adoption and liquefaction [41-42].

2.13.4 Inductively Coupled Plasma optical emission spectrometer (ICP-OES).

Trace elements in a sample, or a liquid mixture like in our case, can be quantified using coupled plasma optical emission spectroscopy or ICP-OES) [43]. As it detects metals at ppb levels, it can also be used to determine whether any metals have leached from a catalyst support into a reaction solution. An inductively coupled plasma ionizes a liquid sample in ICP-OES (figure 2.19). Electromagnetic coils are used to inductively heat a gas, usually argon, to create an inductively coupled plasma. As the sample passes through the plasma, the elements present are ionized. For quantification, the intensity of the peaks can be calibrated using standard known solutions [44].

ICP-OES analysis of postreaction solutions quantified total metal leaching from the supported catalyst. Samples were analysed by a SPECTROGREEN FMX46 ICP-OES. Samples were diluted by a factor of 2-15 in 1% nitric acid (made up from deionised water and Primar Plus - Trace Analysis Grade nitric acid). The instrument was calibrated using commercially available certified reference materials (Sigma-Aldrich/Supelco TraceCERT Standard for ICP; Fisher scientific Spex Certiprep standards; VWR/BDH inorganic reference standard). Samples were run alongside a daily factoring standard to correct for changes in conditions.

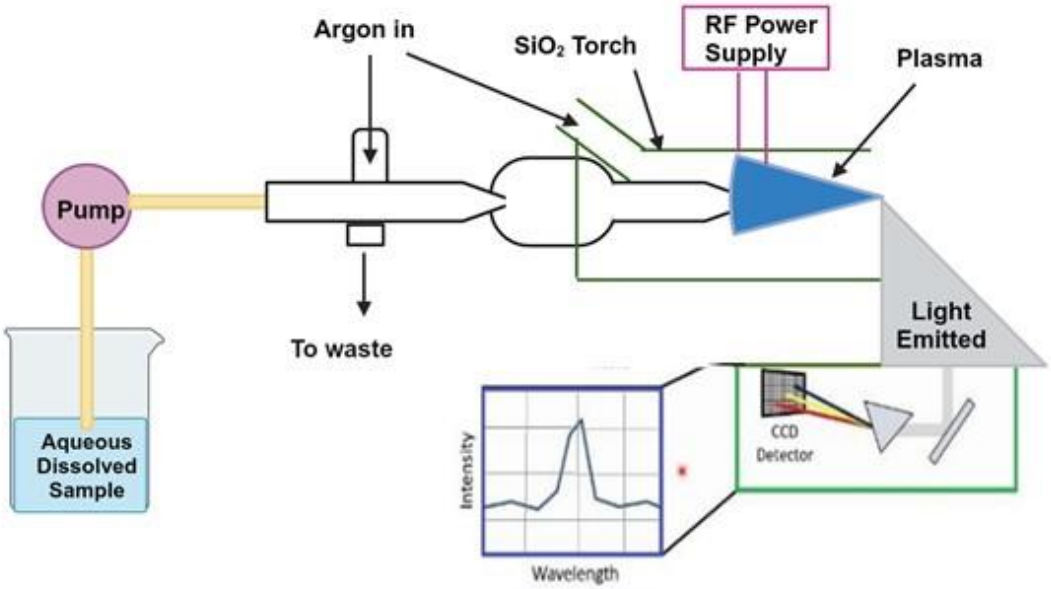

Figure 2.8: Schematics of an Inductively Coupled Plasma optical emission spectrometer (ICP-OES). High-temperature plasma sources atomize and excite samples, emitting characteristic wavelengths of light.

2.13.5 X-ray photoelectron spectroscopy (XPS)

X-ray photoelectron spectroscopy (XPS) is extensively utilized in surface characterization and catalysis, offering insights into elemental composition and oxidation states of various elements. This technique relies on the photoelectric effect, which occurs when high energy photons, specifically x-rays interact with a material resulting in the emission of photoelectrons from the near-surface region [45]. The operational principles are illustrated in figure 2.20. Each element possesses a distinct set of binding energies, which are defined as the energy differences between the initial and final states following electron emission from the atom [46]. These variations arise from differences in chemical potential and polarizability, enabling X-ray photoelectron spectroscopy (XPS) to identify and quantify the concentration and chemical states of elements present on the surface [47]. The kinetic energy of the emitted photoelectron ($\mathrm{E}k$) can be described by Einstein's law (eq. 2.11), where hv represents the energy of the incident radiation, Eb denotes the binding energy of the emitted electron at a specific energy level and ϕs is the work function of the spectrometer [46].

$$\mathrm{E}k = \mathrm{hv} - \mathrm{Eb} - \phi s \qquad (eq.\,2.11)$$

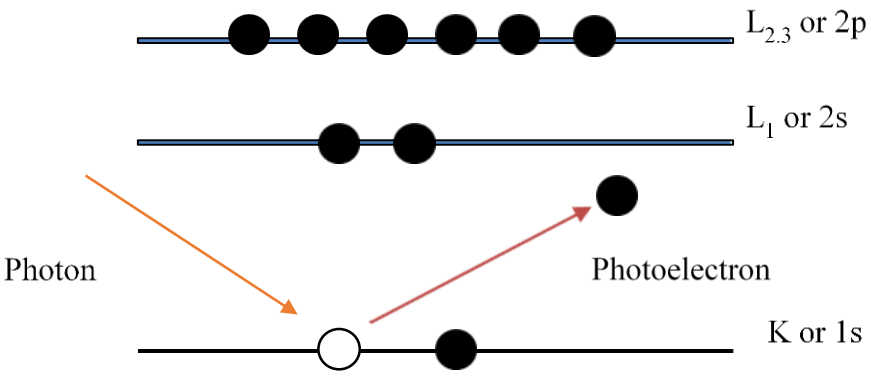

Figure. 2.20: The XPS emission process for a model atom involves the ejection of photoelectrons triggered by the X-ray source [46].

The Kratos Axis Nova spectrometer was used to perform X-ray photoelectron spectroscopy (XPS) utilising a monochromatised AlKα X-ray source (225 W) with an analyser pass energy of 20 eV for high resolution scans and 160 eV for survey scans. Charge neutralization was used to evaluate three places per sample. charge

correction was applied to all XPS spectra by setting the C1s C-C/H component to 284.8 eV [48].

2.14 Hydrocarbon analysis: quantitative assessment and statistical comparison

A statistical comparison is an essential tool for assessing the significance of differences between variables in scientific research and analysis. Analysing data statistically allows researchers to identify patterns, draw conclusions, and make informed decisions. In statistical comparison, data sets are evaluated to determine whether observed differences or associations are likely to be due to chance or statistically significant [49].

This study investigated methods of quantifying products using GC-MS and NMR approaches. As well as to be able to determine product conversion and selectivity and yields and gain a deeper understanding of the instrument's sensitivity towards various classes of compounds by obtaining quantitative information with this instrument [5]. To compare reaction mixtures and catalytic activity, statistical tests such as the t-test and F-test are employed. The null hypothesis (H_0) is a foundational concept in statistical hypothesis testing. It represents a default or baseline statement that there is no effect, difference, or relationship between variables in a given study. Essentially it makes the assumption that any observed data discrepancies are the result of chance rather than a real underlying influence. The purpose of testing the null hypothesis is to determine whether the data provide enough evidence to reject it, which would suggest that an alternative hypothesis (H_1) might be true. The null hypothesis states that there is no significant difference between the reaction mixtures or catalytic activities of different metal catalysts. The t-test assesses differences in means, while the f-test evaluates differences in variances (t-test and f-test shown in equation 2.13 and 2.13 respectively). As a result, statistical methods such as the t-test and F-test emerge as indispensable tools to evaluate the significance of data differences between different methodologies [50]. In each sample mixture, the average and standard deviation obtained from three repeated measurements, provide insight into the variability and precision of the analysis. For example, in catalyst efficiency the null hypothesis H_0 refer to the new catalyst has no effect on the rate of the chemical reaction compared to the existing catalyst. This means that any observed difference in reaction rates is

assumed to be due to random variation rather than the new catalyst's influence. Moreover, Experiments, while producing repeatable results, on a micro-scale, being able to interpret experimental data that shows some degree of variation depends entirely on statistical analysis.

As an example, a t-test was conducted to compare the purity results obtained from the titration method (100 ± 2) and the NMR method (98 ± 2) for the same sample. The purpose was to determine if the observed difference between the two methods was statistically significant. With an assumed sample size of five for each method, the calculated t-statistic was 1.58. Given the degrees of freedom (8) and a significance level of 0.05, the critical t-value is 2.306. Since the t-statistic is less than the critical value, we fail to reject the null hypothesis. This indicates that there is no significant difference in the purity measurements between the titration and NMR methods, and any observed variation is likely due to random chance rather than a true discrepancy between the two techniques. It is necessary to apply the t-test and f-test method and in the case of hypothesis testing with a t-test, we compare the difference between the means of the two groups relative to the variability within the groups (as captured by the standard deviation). The significance level (typically set at 0.05) defines the threshold for determining whether the observed differences are statistically meaningful or could have occurred by random chance. These results demonstrate the reliability and validity of both methods for analysing hydrocarbons quantitatively. The ratio of the squares of the standard deviations, or the ratio of two sample variances, can also be used to calculate significant levels for the f-test (eq.2.17) .Degrees of freedom (df) refer to the number of independent values or observations in a statistical calculation that are free to vary while still adhering to certain constraints, such as fixed totals or relationships among the data. In simpler terms, the number of independent data points that can be used to estimate a statistical parameter is known as degrees of freedom, such as the mean or variance. When calculating a statistic like the sample standard deviation or performing a t-test, the degrees of freedom are critical because they account for the number of independent pieces of data after certain parameters (e.g., the sample mean) have been fixed or estimated from the data [51]. The degrees of freedom in a two-sample t-test are usually determined by taking into account the sample sizes of the two groups under comparison. For example, if two independent samples have sizes n_1 and n_2 , the degrees of freedom for t-test shown in eq.2.12 ,

This accounts for the fact that each sample provides independent information, but two parameters (the sample means of the two groups) have been estimated from the data, reducing the degrees of freedom by 2 [52].

$$t = \frac{X_1 - X_2}{s\sqrt{\frac{1}{n_1} + \frac{1}{n_2}}} \qquad (eq. 2.12)$$

Where X_1 and X_2 are defined as means, $n_1 + n_2 - 2$ is degree of freedom.

$$F = \frac{{S_A}^2}{{S_B}^2} \qquad (eq. 2.13)$$

Where A, and B are defined such that ${S_A}^2$ is greater than or equal to ${S_B}^2$.

2.15 References

1 J. D. Grayson and B. M. Partridge, *ACS Catal.*, 2019, **9**, 4296–4301.

2 M. E. Ali, M. M. Rahman, S. M. Sarkar and S. B. A. Hamid, *J. Nanomater.*, 2015, **2014**, 209.

3 C. Deyrieux, P. Villeneuve, B. Baréa, E. A. Decker, I. Guiller, F. Michel Salaun and E. Durand, *Eur. J. Lipid Sci. Technol.*, 2018, **120**, 1800109.

4 P. Wiklund, C. Karlsson and M. Levin, *Anal. Sci.*, 2009, **25**, 431–436.

5 H. J. Hübschmann, *Handbook of GC-MS: fundamentals and applications*, John Wiley & Sons, 2015.

6 A. J. Van Es, J. A. Rijks, C. A. Cramers and M. J. E. Golay, *J. Chromatogr. A*, 1990, **517**, 143–159.

7 S. Bouchonnet, *Introduction to GC-MS coupling*, CRC Press, 2013.

8 J. Sneddon, S. Masuram and J. C. Richert, *Anal. Lett.*, 2007, **40**, 1003–1012.

9 F. Leemans and J. A. McCloskey, *J. Am. Oil Chem. Soc.*, 1967, **44**, 11–17.

10 W. Fan and J. Almirall, *Anal. Bioanal. Chem.*, 2014, **406**, 2189–2195.

11 V. Van den Bergh, I. Vanhees, R. De Boer, F. Compernolle and C. Vinckier, *J. Chromatogr. A*, 2000, **896**, 135–148.

12 C. Schummer, O. Delhomme, B. M. R. Appenzeller, R. Wennig and M. Millet, *Talanta*, 2009, **77**, 1473–1482.

13 S. C. Moldoveanu and V. David, *Gas Chromatogr. Sample Prep. Appl.*, 2018, 9.

14 K. J. Ng, B. D. Andresen, J. R. Bianchine, J. D. Iams, R. W. O'Shaugnessy, L. E. Stempel and F. P. Zuspan, *J. Chromatogr. B Biomed. Sci. Appl.*, 1982, **228**, 43–50.

15 A. M. Tsedilin, A. N. Fakhrutdinov, D. B. Eremin, S. S. Zalesskiy, A. O. Chizhov, N. G. Kolotyrkina and V. P. Ananikov, *Mendeleev Commun.*, 2015, **25**, 454–456.

16 J. N. Shoolery, *Anal. Chem.*, 1993, **65**, 731A-741A.

17 H. Friebolin, Basic one-and two-dimensional NMR spectroscopy, John Wiley & Sons, 2010.

18 P. Munnik, P. E. De Jongh and K. P. De Jong, *Chem. Rev.*, 2015, **115**, 6687–6718.

19 A. Cao, R. Lu and G. Veser, *Phys. Chem. Chem. Phys.*, 2010, **12**, 13499–13510.

20 J. C. Pritchard, Q. He, E. N. Ntainjua, M. Piccinini, J. K. Edwards, A. A. Herzing, A. F. Carley, J. A. Moulijn, C. J. Kiely and G. J. Hutchings, *Green Chem.*, 2010, **12**, 915–921.

21 L. Sun, L. Jiang, X. Hua, Y. Zheng, X. Sun, M. Zhang, H. Su and C. Qi, *J. Alloys Compd.*, 2019, **811**, 152052.

22 R. J. White, R. Luque, V. L. Budarin, J. H. Clark and D. J. Macquarrie, *Chem. Soc. Rev.*, 2009, **38**, 481–494.

23 I. Chorkendorff and J. W. Niemantsverdriet, *Concepts of Modern Catalysis and Kinetics*, Wiley, 2017.

24 D. L. Daggett, R. C. Hendricks, R. Walther and E. Corporan, *Most*, 2007, 2007–1196.

25 C. Ding, Y. He, J. Yin, W. Yao, D. Zhou and J. Wang, *Ind. Eng. Chem. Res.*, 2015, **54**, 1899–1907.

26 V. Raji, M. Chakraborty and P. A. Parikh, *Ind. Eng. Chem. Res.*, 2012, **51**, 5691–5698.

27 I. Hermans, P. A. Jacobs and J. Peeters, *J. Mol. Catal. A Chem.*, 2006, **251**, 221–228.

28 J. W. Niemantsverdriet, *Spectroscopy in catalysis: an introduction*, John Wiley & Sons, 2007.

29 G. Leofanti, G. Tozzola, M. Padovan, G. Petrini, S. Bordiga and A. Zecchina, *Catal. today*, 1997, **34**, 307–327.

30 E. S. Ameh, *Int. J. Adv. Manuf. Technol.*, 2019, **105**, 3289–3302.

31 L. Lambert and T. Mulvey, in *Advances in imaging and electron physics*, Elsevier, 1996, vol. 95, pp. 2–62.

32 P. L. Gai and E. D. Boyes, *Electron microscopy in heterogeneous catalysis*, CRC Press, 2003.

33 B. Imelik and J. C. Vedrine, *Catalyst characterization: physical techniques for solid materials*, Springer Science & Business Media, 2013.

34 R. F. Egerton, *Reports Prog. Phys.*, 2008, **72**, 16502.

35 M. Naderi, in *Progress in filtration and separation*, Elsevier, 2015, pp. 585–608.

36 S. Brunauer, P. H. Emmett and E. Teller, *J. Am. Chem. Soc.*, 1938, **60**, 309–319.

37 J. M. Thomas and W. J. Thomas, *Principles and practice of heterogeneous catalysis*, John Wiley & Sons, 2014.

38 G. Leofanti, M. Padovan, G. Tozzola and B. Venturelli, *Catal. today*, 1998, **41**, 207–219.

39 F. Ambroz, T. J. Macdonald, V. Martis and I. P. Parkin, *Small methods*, 2018, **2**, 1800173.

40 D. D. Do, H. D. Do and D. Nicholson, *Chem. Eng. Sci.*, 2010, **65**, 3331–3340.

41 Z. Kónya, V. F. Puntes, I. Kiricsi, J. Zhu, J. W. Ager, M. K. Ko, H. Frei, P. Alivisatos and G. A. Somorjai, *Chem. Mater.*, 2003, **15**, 1242–1248.

42 D. M. Antonelli and J. Y. Ying, *Chem. Mater.*, 1996, **8**, 874–881.

43 F. Vanhaecke, L. Balcaen and P. Taylor, *Inductively coupled plasma Spectrom. its Appl.*, 1999, 160.

44 A. W. Boorn and R. F. Browner, *Anal. Chem.*, 1982, **54**, 1402–1410.

45 M. Stöcker, *Microporous Mater.*, 1996, **6**, 235–257.

46 J. Chastain and R. C. King Jr, *Perkin-Elmer Corp.*, 1992, **40**, 221.

47 A. Proctor and P. M. A. Sherwood, *Anal. Chem.*, 1982, **54**, 13–19.

48 M. Haneda and A. Towata, *Catal. today*, 2015, **242**, 351–356.

49 R. Nuzzo, *Nature*, 2014, **506**, 150.

50 V. V. Nalimov, The application of mathematical statistics to chemical analysis, Elsevier, 2014.

51 M. P. Fay and M. A. Proschan, *Stat. Surv.*, 2010, **4**, 1.

52 M. Fiandini, A. B. D. Nandiyanto, D. F. Al Husaeni, D. N. Al Husaeni and M. Mushiban, *Indones. J. Sci. Technol.*, 2024, **9**, 45–108.

Chapter 3: Method development for the characterization of 1-phenyl ethyl hydroperoxide (EBHP)

3.1 Overview

One of the main intermediates in the partial oxidation of ethylbenzene oxidation is its alkyl hydroperoxide or 1-phenyl ethyl hydroperoxide for this specific substrate. This intermediate EBHP can undergoes decomposition when heated in the liquid phase [1-2]. Thus reliable data on the decomposition of these compounds in the liquid phase is rather limited. When hydrocarbons undergo autoxidation, they can generate a variety of products such as alcohols, ketones, peroxides, organic acids, and form these also condensation products. This process may also involve decarboxylation reactions, releasing CO_2. It can therefore be challenging to characterize these complex reaction mixtures and might lead to inaccurate results in some cases [3-4]. For example, it is usually required to convert fatty acids into esters before analysing them since the presence of alkyl acids and hydroperoxide limits the ability to use direct analytical techniques [5-6-7]. This is important because catalysis by design relies on altering catalysts to influence the chemical composition of a reaction mixture. Thus, if the analysis of the reaction mixture is inaccurate, the catalyst design is likewise not correct. In light of this, ethylbenzene alkyl hydroperoxide (EBHP) has been investigated in depth by using gas chromatography-mass spectroscopy (GC-MS). This study aims to study the reactivity of EBHP (otherwise also referred as R-OOH). Indeed, these compounds can break down to produce an alcohol (R-OH) and a ketone (R=O)[8], namely phenyl ethyl alcohol and acetophenone respectively However, there's a challenge concerning the decomposition of R-OOH, which might occur due to catalytic reactions or thermal processes, and as such potentially altering results concerning selectivity data. Therefore the scope of the work presented din this work is to determine accurate methods for the determination of the composition of this kind of reaction mixtures and in turn to be able to provide accurate catalytic data.

3.2 Titration methods for determination of 1-phenyl ethyl hydroperoxide content

In various analytical contexts, analysts are frequently tasked with identifying organic peroxides. For example, assessing the purity of peroxides is essential in their commercial production as industrial chemicals. Process control demands rapid methods capable of detecting peroxide which include pure peroxides, also intermediate and low concentrations as well. For example, trace methods are required when detecting peroxidation in solvents or incipient in oils. Depending on the system used, peroxides may be highly reactive, inactive, or very stable, and mixtures of peroxides may have similar or different characteristics [9]. In general, for specific target analyses, titration was used in this study as a standard to validate NMR result. Direct or forward titration can be impractical or have unclear endpoint detection. In such instances, titration is carried out indirectly by adding an excess of reagent. This reagent fully reacts with analysis, and the titration is then used to determine the quantity of remaining reagent in the solution. This method is known as back titration. Iodine liberation methods, a group of volumetric procedures reliant on the peroxide bond reduction through iodide. Practically all the peroxides initially of analytical significance could undergo reduction using this method, resulting in the quantitative liberation of iodine. In this study, sodium thiosulfate $Na_2S_2O_3$ was used, the standardization procedure for $Na_2S_2O_3$ relies on a redox idometric titration using potassium iodate as the primary standard. Potassium iodate, which acts as a strong oxidizing agent, is reacted with an excess of potassium iodide under acidic conditions, utilizing starch as an indicator, resulting in the release of iodine. This liberated iodine is then titrated back with sodium thiosulfate.

To determine the quantity of pure alkyl hydroperoxide transformed, EBHP was titrated. It is a back titration where sodium thiosulfate titrates iodine [10].

$$ROOH + 2I^- + 2H^+ \longrightarrow ROH + H_2O + I_2 \quad \text{(eq.3.1)}$$

$$I_2 + 2S_2O_3^{2-} \longrightarrow 2I^- + S_4O_6^{2-} \quad \text{(eq.3.2)}$$

The mixture's colour changes as a result of the first stage (eq.3.1). When the titration volume is reached, the mixture turns colourless (eq.3.2).

In this study, the idometric approach was employed to facilitate the investigation of the purity of alky hydroperoxides. The steps detailing this method were outlined in the previous chapter, specifically in section 2.4.2. Titration method was internally consistent, however, the results differed by 5%. Because the R-OH was generated through ROOH decomposition, the concentration of alkyl hydroperoxide varied across batches but consistently were within the range of 0.1 to 0.5 M for freshly prepared samples. Over time, the concentration of EBHP gradually decreased during storage[11]. Therefore, to validate the purity of EBHP, we used peroxide titration with 0.1 N Sodium thiosulphate to determine the amount of TBHP at 70% concentration in water. The results from this analysis are presented in the following table 3.1 as an example,

Table 3.1: The table below presents the results from this analysis, showing the repeated titration volumes (V) for each measurements as V_1, V_2 and V_3 of tBHP content using 0.04M $Na_2S_2O_3$, reaction condition before being titrated with 0.1 M $Na_2S_2O_3$ (1mL of tBHP in 1mL of acid, 4mL of KI added into narrow mouth flask with a taper stopper and heated at 69°C with slow magnetic stirring (300rpm) 10 min and leave it cool down before titrated.

	V_1	V_2	V_3	Mean	SD	RSD%
$V(Na_2S_2O_3)$ / mL	18.2	18.2	16.9	18	0.4	2
$n(Na_2S_2O_3)$ / mol	7.10^{-05}	$7.28.10^{-05}$	7.10^{-05}	$7.19.10^{-05}$		
n(tBHP detected) / mol				$3.59.10^{-05}$		
Actual purity %	70	70	67.5	69.3	1.56	0.02

Discrepancy: (Detected-expected)/expected*100% = -1%
Concentration of tBHP = 0.072 M

By comparing the results between the alkyl hydro peroxide we synthesized in the lab and tert-butyl peroxide with a known concentration, we found that the latter's purity fitted well with the specifications indicated on its bottle. Titration proved to be a reliable method for determining peroxide concentration. However, it has some limitations, For instance, using titration with iodine introduces additional challenges, such as the time required for preparation and the risk of iodine evaporation during the process, which can lead to inaccurate results. These issues necessitate repeated attempts and increasing the overall cost. Moreover, since EBHP is not 100% pure, this introduces additional challenges. The titration method is indeed laborious and cannot be applied to reaction mixtures due to potential interferences from alcohol. Furthermore, if various

types of ROOH species are present simultaneously, the titration would not be effective. Despite these drawbacks, titration remains a useful method. However, we aimed to develop a faster and easier method to carry out this study and capable to work in the presence of an actual reaction mixture. More details on this approach will be discussed in the next section.

3.3 Triphenylphosphine (TPP) methods for determination of 1-phenyl ethyl alkyl hydroperoxide (EBHP) content

Triphenylphosphine (TPP) into triphenylphosphine oxide (TPPO) by hydroperoxides, is proposed[12-13] as shown in eq. 3.3 :

$$ROOH + TPP_{excess} \longrightarrow ROH + TPPO \qquad \text{(eq.3.3)}$$

The details of sample preparation and principles have been discussed in detail in the previous chapter, specifically in section 2.4.2.2. The reaction of TPP with alkyl hydroperoxide has been studied. It has been demonstrated that this reaction rapidly completes at ambient temperature, which makes it an attractive method for measuring alkyl hydroperoxides. In this work, we have chosen to treat a sample of alkyl hydroperoxide with TPP (dilute solution) in chloroform with subsequent GC-MS analysis to quantify the TPPO produced from the reaction.

TPP is transformed into TPPO through oxidation by one equivalent of hydroperoxide, which itself is converted into the corresponding alcohol. Consequently, the level of hydroperoxides present in the sample equates to the amount of TPPO generated. Any excess TPP is then reacted with molecular sulphur to produce TPPS, providing a precautionary measure against potential over-determination resulting from any subsequent interaction of TPP with oxygen in the air, as shown in the following equation:

$$TPP + C_6H_5CH(CH_3)OOH \longrightarrow TPPO + C_6H_5CH(CH_3)OH \qquad \text{(eq.3.4)}$$

$$TPP + S \longrightarrow TPPS \qquad \text{(eq.3.5)}$$

Selecting the appropriate solvent for this reaction is crucial. For this particular study,

chloroform was ultimately chosen as the solvent for several reasons. Firstly, the resistance of chloroform to oxidation is notable. As a second benefit, it has a high capacity to dissolve mineral oils, even those that are extensively aged and oxidized, unlike alternatives such as toluene. Finally, and perhaps most significantly, chloroform is highly effective at dissolving sulphur and TPPS at elevated concentrations [14]. This attribute was particularly crucial as we aimed to prepare single reagent solutions capable of covering very low to very high range of analyse hydroperoxide levels (range of 10^{-4} M)[15]. Moreover, in this method, we used fluorene as an internal standard (IS) to provide more reproducibility for the result. Selecting the appropriate internal standard is also critical. It should possess excellent solubility within the combined reagent/product solution. Moreover, it should not interact with alkyl hydroperoxides and another product form in the system and should be readily accessible in high analytical purity. Following careful consideration, the decision was made to use fluorene. It was determined that fluorene did not present any chromatographic interference issues within the GC temperature program, even when analysing samples of the mixture. The findings from these determinations are present in figure 3.1.

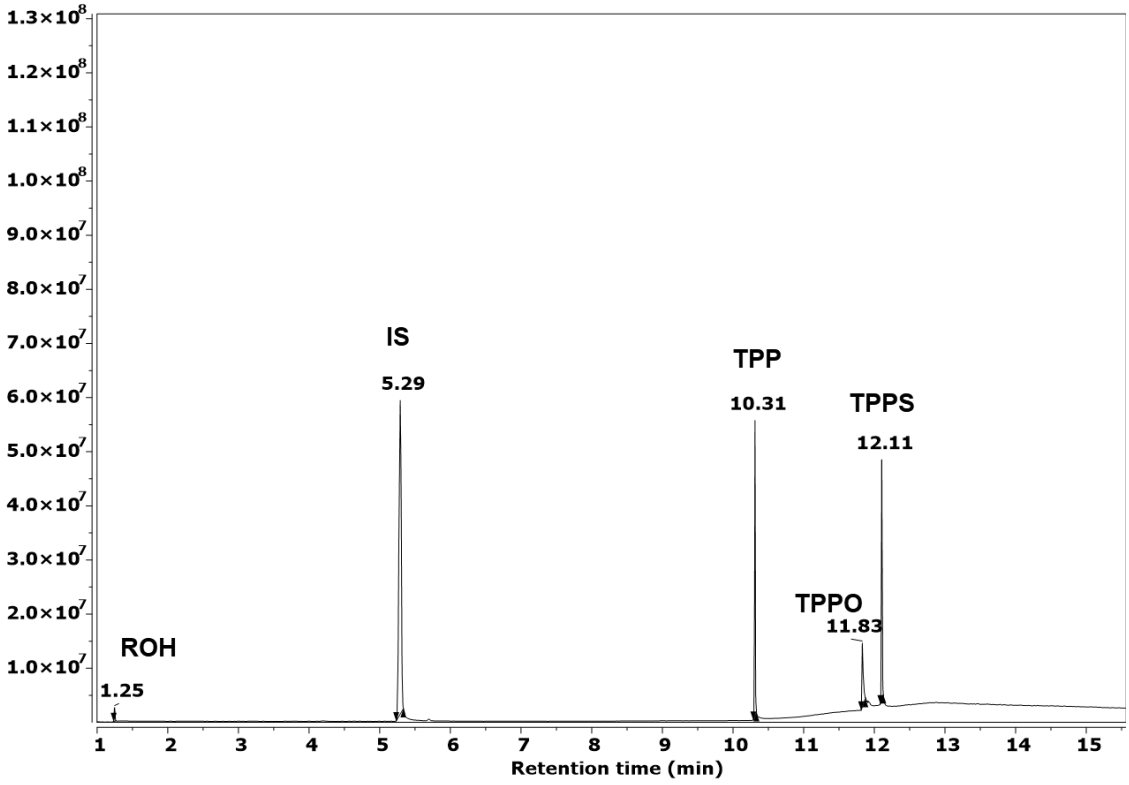

Figure 3.1: The chromatogram showing peaks that correspond to (from left to right) 1-phenyl ethanol (ROH), fluorene (internal standard IS) and triphenylphosphine (TPP), triphenylphosphine oxide (TPPO), triphenylphosphine sulphide (TPPS) at 100 °C injector temperature.

The TPP methods used in figure 3.1 demonstrated that the reaction is not quantitative. Regarding this latter point, the amount of TPPO formed did not match the quantity of alkyl hydroperoxide added (table 3.2). The injector temperature doesn't affect the retention time, but it affects the physical state of a species, under these conditions, the alcohol was eluted after 1.25 minutes. The lower temperature may cause incomplete vaporization of the sample leading to a less accurate separation. Additionally, the boiling points of all the compounds are above 200°C. Therefore we increased the injector temperature to 250°C and adjusted the oven temperature programme as outlined in table 3.2 for proper evaporation and separation.

Table 3.2 GC method parameters for TPP samples preparation

Detector Settings	Chromatographic conditions
Injector temperature	250°C
Oven T°C	50 -250°C
Split ratio	200:1
Injection volume	1µL
Carrier gas	He (1mL/min)

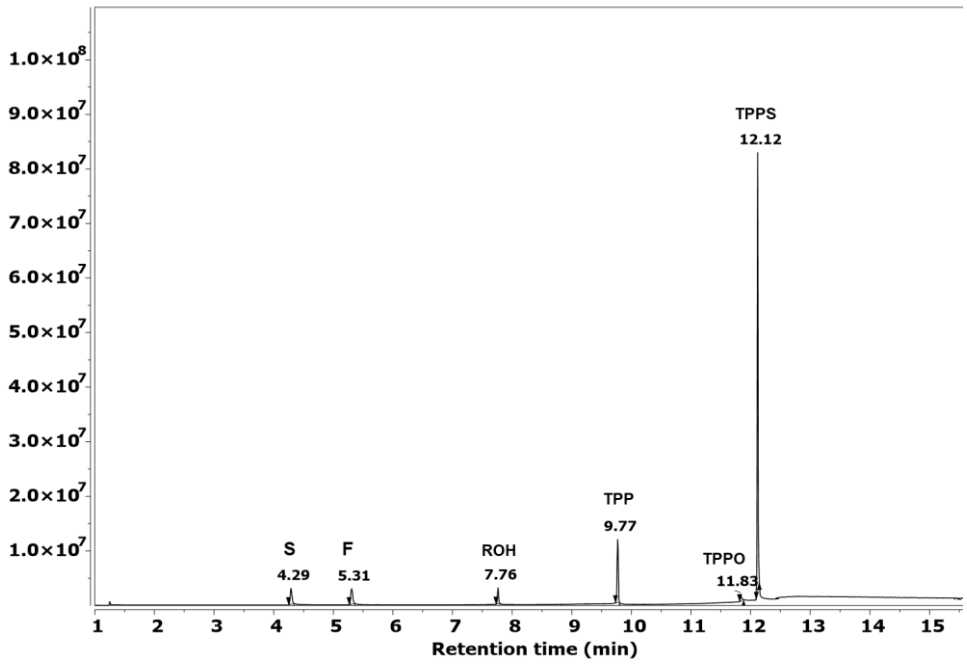

Figure 3.2: Chromatogram showing peaks that correspond to (from left to right) sulphur (S), fluorene (internal standard IS) and 1-phenylethanol (ROH), triphenylphosphine (TPP), triphenylphosphine oxide (TPPO), triphenylphosphine sulphide (TPPS) at 250 °C injector temperature.

Figure 3.2 above shows better separation of the compounds at an injector temperature of 250°C. This is because the boiling points of all compounds are above 200°C, and the higher temperature allows for complete evaporation and effective separation in the column.

The use of the GC-MS/TPP method to determine the EBHP purity has been done and the results from these determinations are shown in the following table 3.3.

Table 3.3: GC-MS/TPP result to determined 1-phenylethyl alkyl hydroperoxide purity using the area of internal standard IS (decane) to do this calculations.

TPPO area	IS area	TPPO/IS	Detected EBHP	Expected EBHP	Purity%
3.22×10^{7}	3.96×10^{8}	0.08	2.40×10^{-4}	7.47×10^{-4}	32
8.40×10^{7}	7.06×10^{8}	0.12	3.58×10^{-4}	7.47×10^{-4}	48
7.24×10^{7}	6.92×10^{8}	0.10	3.15×10^{-4}	7.47×10^{-4}	42

From table 3.3 and by seeing the purity result, we can conclude that the TPP method was employed to assess the purity of peroxide in comparison to the titration method. However, the results obtained from the TPP method yielded a significantly lower purity percentage, ranging between 40-35%, whereas the titration method indicated a purity level within the range of 96%. This discrepancy suggests that the TPP method is not as accurate for determining peroxide purity as the titration method as instead originally thought. Additionally, the stoichiometry of TPP may not be in excess with peroxide, highlighting another potential disadvantage of the TPP method in this context.

3.4 1-phenyl ethyl hydroperoxide stability

The stability of peroxides can be divided into different regimes: stability during storage, and thermal stability[16]. 1-phenyl ethyl hydroperoxide (EBHP) stability during storage refers to its ability to resist chemical oxidation throughout months or years of storage under ambient temperature. The ambient storage temperatures are relatively mild (generally ranging from 10 to 25°C). As a result of the relatively weak oxygen-oxygen linkage, peroxide molecules exhibit reactivity and spontaneous decomposition due to their relatively low bond-dissociation energy (20 - 50 KJ mol $^{-1}$)[17]. This weak O–O bond provides a favourable pathway for the decomposition of EBHP, leading to the formation of by-products. These oxygenated species and other contaminates introduced during storage, can have a negative effect on the future thermal stability of EBHP and data analysis study. As a result, this particular aspect of EBHP storage has been studied, and the stability test is illustrated in figure 3.3 for reference.

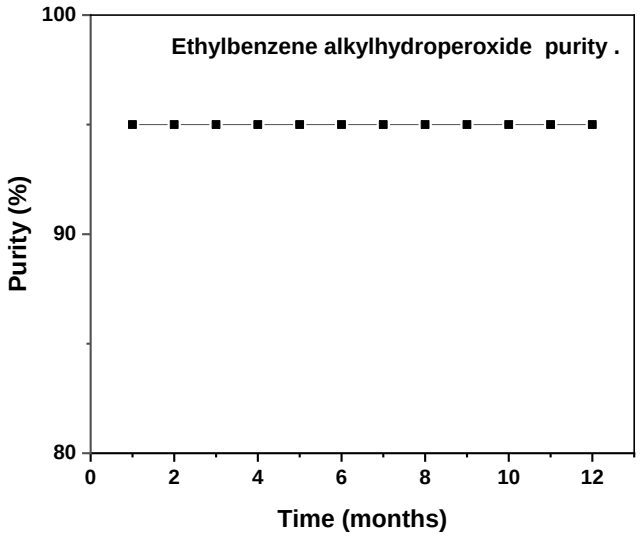

Figure 3.3: Stability of EBHP over time; variation in peroxides stability from one month to twelve months of storage, maintaining 96% purity throughout the study period.

The figure shows that the stability of EBHP was high over the year of storage at 96%. Analysis conducted at monthly intervals demonstrated minimal variation in the peroxide's stability, with its purity consistently maintained at 96% throughout the study period. This analysis was done by using ^{1}H-NMR with internal standard 1,1,2,2TCE, ensuring the reliability of using this peroxide in many investigations in this study.

3.5 GC-MS methods for determination of ethylbenzene alkyl hydroperoxide content

Detecting or determining peroxides and hydroperoxides holds significance across various fields, including the study of oxidation reactions of hydrocarbons by molecular oxygen in laboratory or industrial oxidation processes[18] . In non-catalytic oxidation processes involving hydrocarbons, hydroperoxides typically serve as the initial reactive intermediates. Ethylbenzene alkyl hydroperoxide is obtained by the non-catalysed oxidation of ethylbenzene at low temperatures (80 to 120 °C) [19]. However, the process also generates various additional by-products such as acetophenone, and 1-phenyl ethanol and requires further optimization regarding the conversion of ethylbenzene and selectivity of EBHP [20]. Therefore, to ensure that the observed quantities of acetophenone and 1-phenylethanol have not been generated through the decomposition of EBHP or its interactions with other reaction products within the column. Therefore, due to the thermal instability of peroxides, we have conducted a thorough investigation using GC-MS. An in-depth study of the stability of peroxide under various conditions in GC-MS will be carried out in this section.

3.5.1 Compounds Calibration in Gas Chromatography

One of the main analytical methods is gas chromatography, which is well known for its accuracy and sensitivity in isolation and measuring complex mixtures of compounds. The calibration curve is the key component of this analytical technique to ensure accurate and reliable measurements in GC analysis. The calibration curve establishes a link between a target compound’s concentration and matching detector response.to quantitatively analyse hydrocarbon oxidation samples, calibration curve measurements were conducted. Moreover, to ensure the accuracy of quantitative data, internal standards are necessary to adjust for any analytical and chemical losses that may occur during analysis. Thus, n-decane was used as the internal standard and Dichloromethane (DCM) as the solvent, ensuring the analysis falls within a linear concentration range. Our case involves Ethylbenzene alkyl hydroperoxide, Acetophenone and 1-phenylethanol were major products resulting from the oxidation of Ethylbenzene. The Ethylbenzene alkyl hydroperoxide has not been identified yet,

and there is a lot of investigation and study that will be presented in detail in this chapter. We conducted calibration curve measurements for other products such as Acetophenone, 1-phenylethanol, and ethylbenzene. An example of the calibration curve for Ethylbenzene is presented in the following figure 3.4.

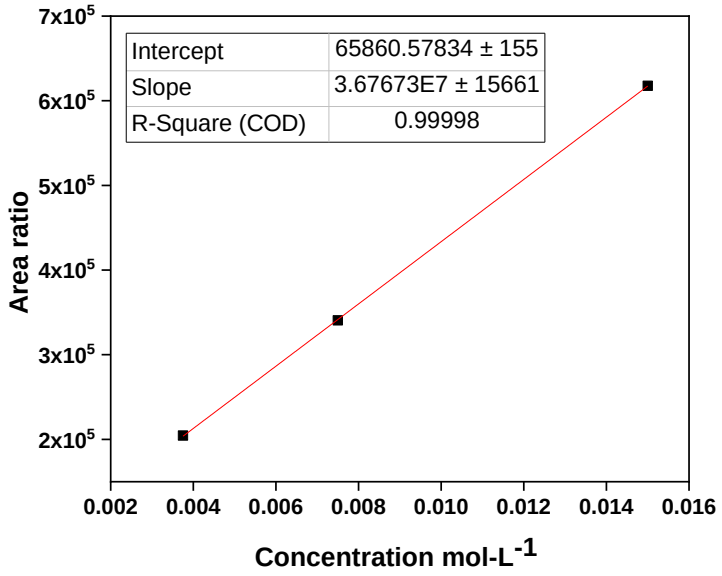

Figure 3.4: ethylbenzene calibration curve at different concentrations, the graph illustrates the calibration curve for ethylbenzene across varying concentrations. The x-axis represents concentration levels while the Y-axis depicts the ratio of the area of the analyte to that of the internal standard.

3.5.2 Investigating EBHP behaviour in GC-MS: effects of Injector Temperature

After synthesizing the alkyl hydroperoxide and ensuring its stability over time, we proceeded to utilize this pure EBHP for GC-MS analysis. It was better to start with a low injector temperature in order to achieve a very mild method and use split mode injection. Both split and splitless modes are forms of hot injection techniques, where the injector is maintained at a temperature sufficient to vaporize both the solvent and analytes in the sample [21]. This temperature remains constant throughout the entire GC run. Using split mode offers an advantage over splitless mode in that we employ a 1:100 ratio (adjustable in the software). This results in shorter analysis times compared to other methods, which is particularly beneficial for unstable compounds because their residence time in the hot injector is short [22]. Typically, a sample size of 1 µL is utilized, which helps to prevent any solvent not soluble in the stationary phase

from entering the column due to the minimal amount of solvent introduced. However, one drawback of splitless mode is its longer injection time, which can result in the decomposition of thermally labile compounds [22]. Following our initial use of GC using split mode, moved to the injector by applying different temperatures.

Upon injecting the pure peroxide, we anticipated observing a single peak in the chromatogram. However, contrary to our expectations multiple peaks appeared indicating the occurrence of decomposition (figure 3.5). The extent of this decomposition, whether partial or complete remains uncertain. Consequently, our investigation commences with an assessment of the injector component in the GC system. We initiated our study by applying six different injector temperatures 70 °C, 80 °C, 90 °C 120 °C, 150 °C and 250 °C. However, all injector temperatures produced the same result, with multiple peaks appearing in the chromatogram. Subsequent analysis of these peaks revealed them to be Acetophenone and 1-phenylathanol which are possible oxidation products of EBHP. Even though EBHP AP and 1-Ph have high boiling points 230 °C, 202 °C, and 204 °C, a low injector temperature isn't an issue. Cullis and Fersht noted that despite their high boiling points, most peroxides and hydroperoxides have high vapour pressures, thus rendering a high injector temperature not necessary [23]. After the injection, the result showed consistency in terms of the number of products appearing in the chromatograms. Following these results, we transitioned to further investigations using Gas Chromatography-Mass Spectrometry (GC-MS). The quantitative data related to the study decomposition of ethylbenzene alkyl hydroperoxide (eq. 3.6) in the GC-MS have been studied in detail. At the start, the work was carried out in the gas phase using concentration to calculate CMB% and the amount of EBHP at the start and after running GC-MS (table 3.4).

$$ROOH \longrightarrow RO + OH \qquad \text{(eq. 3.6)}$$

More details about radical species and their explanation in chapter 1.

The sample of pure EBHP was analysed with direct injections of 0.1 µL three times at each different injector temperature. This will generate an average value, and the procedure was carried out periodically to ensure the reliability of the analysis.

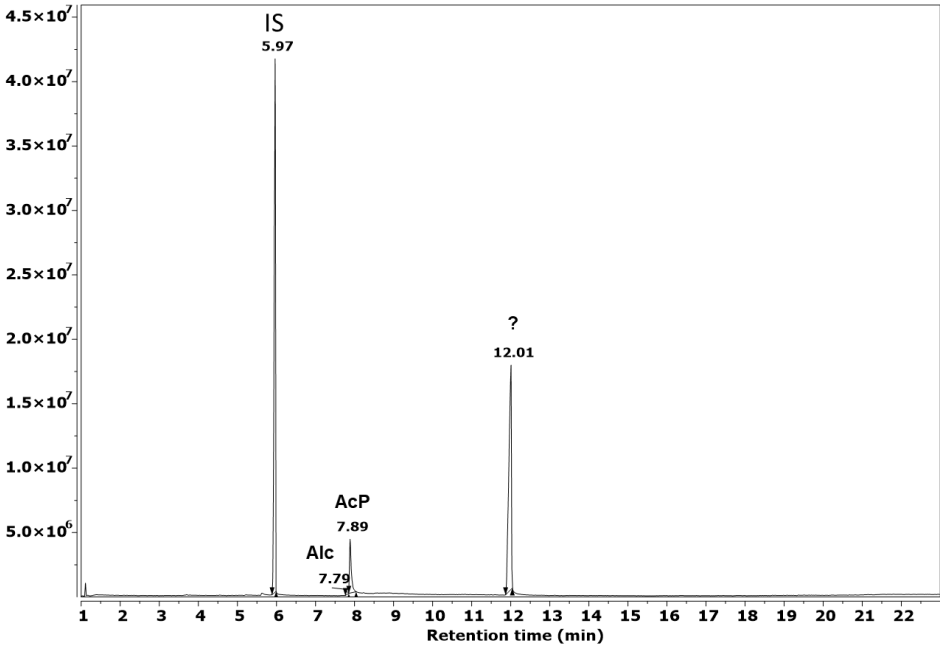

Figure 3.5: Chromatogram of EBHP 96% injected into GC-MS at six different injector temperatures 70°C, 80°C, 90°C and 120°C, 150°C and 250°, show consistent peaks corresponding to (from left to right), n-decane (internal standard IS) and 1-phenyl ethanol (ROH), Acetophenone (ACP), an unknown product with similar mass to Acetophenone.

Table 3.4: Represented the carbon mass balance of the decomposition of alkyl hydroperoxide 93% in the GC-MS at 5 different temperatures using the internal standard (Decane).

Injector temperature °C	CMB%
70	89 ± 2
80	89 ± 1
90	91 ± 1
120	89 ± 4
250	91 ± 1

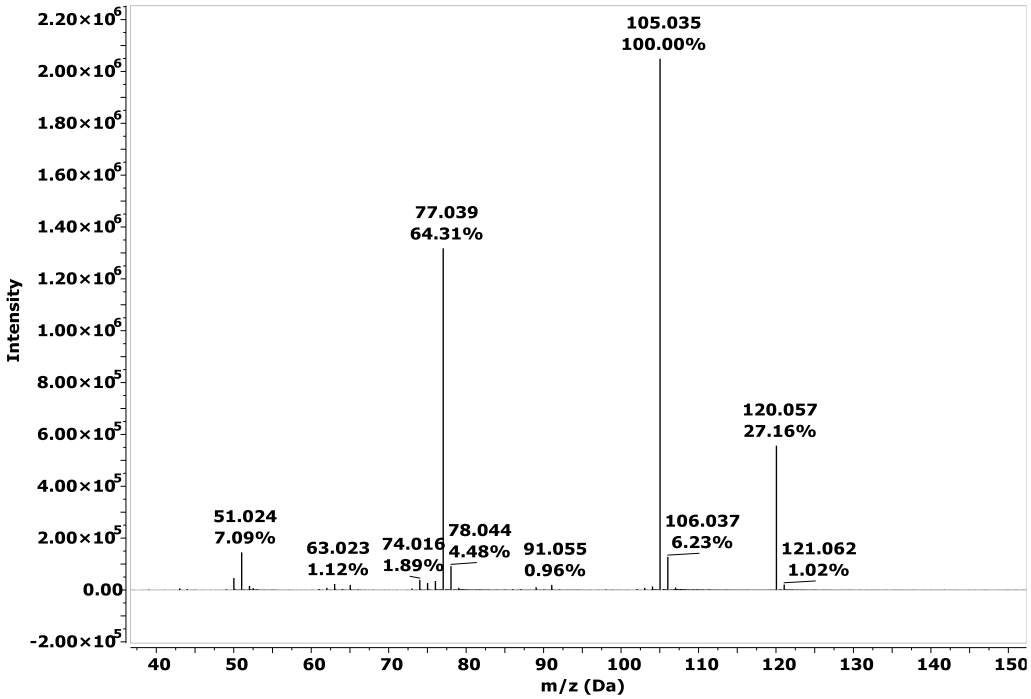

Figure 3.6: Representative mass spectrum of Acetophenone with a molecular weight of 120. Fragmentation: m/z = 120 corresponds to the molecular ion $[C_8H_8O]^+$, the peak at m/z= 105 corresponds to $[C_7H_5O]^+$ which is the base peak (due to the removal of a methyl group during the ionization process), additional fragmentation of C=O results in a shift from 105 to 77.

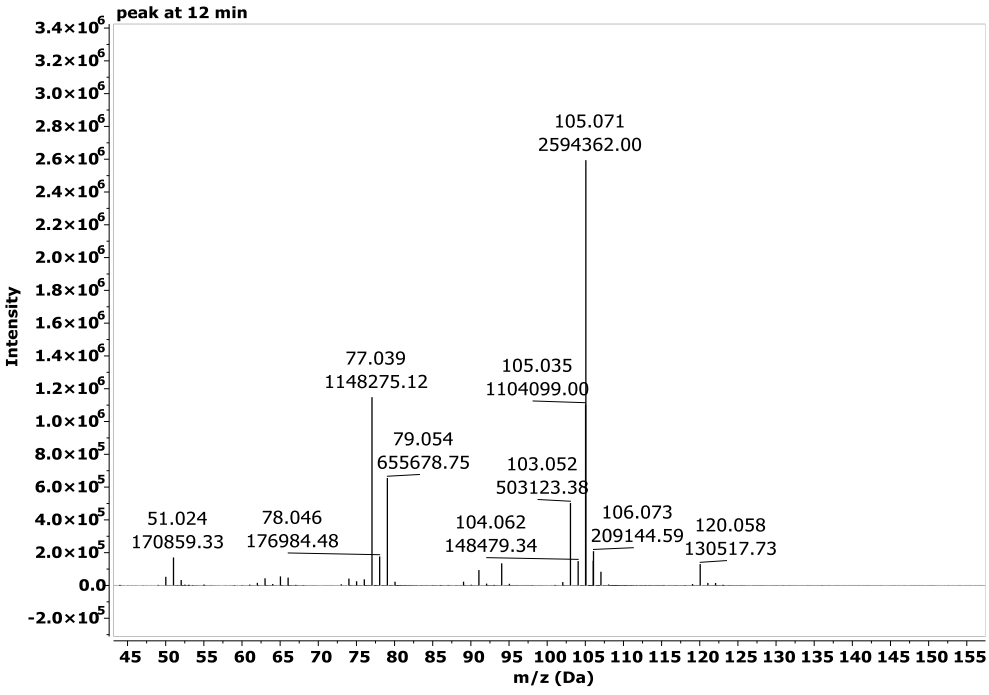

Figure 3.7: Representative mass spectrum of a compound similar to Acetophenone with a molecular weight of 120. Fragmentation: m/z = 120 corresponds to the molecular ion $[C_8H_8O]^+$ which could be generated due to the loss of H_2O from the molecular ion, the peak at m/z= 105 corresponds to $[C_7H_5O]^+$ which is the base peak (due to the removal of a methyl group during the ionization process), additional fragmentation of C=O results in a shift from 105 to 77.

From figures 3.6 and 3.7, a molecular mass spectrum is a plot of the relative abundance of an ion vs. the m/z ratio of the ion. The peak with the highest intensity in the spectrum is typically assigned a value of 100, while the intensities of smaller peaks are expressed as relative percentages. The molecular ion (m/z=120 as shown in both figures 3.5 and 3.6) provides the molecular weight of the compound. The base peak also identified as the ion abundance (m/z=105), indicates the most stable ion or ion fragment generated during the analytes ionization process. At this stage, Acetophenone and 1-phenylethanol with internal standard have been identified. This outcome is consistent information in the mass spectrum, indicating the peroxide decomposed totally or partly. Consequently, further analysis has been conducted to obtain structural insights into the molecule and verify its identity by comparison with national mass databases (NIST).

3.5.3 Investigating EBHP behaviour in GC-MS: effects of column

Based on our prior investigation, spanning injection temperatures from a low of 70°C to a high of 250 °C, we observed consistent reactivity in terms of the products appearing in the chromatograms. Consequently, we have shifted our focus towards studying decomposition within the column. Before moving to the effects of the column, it's important to address an issue arising from the close boiling points of acetophenone (AP) and alcohol (1-Ph), which often causes them to overlap. To resolve this challenge, we initially injected a mixture of pure Acetophenone and pure 1-phenylethanol into the GC. It became apparent that there was indeed an overlap between Acetophenone and 1-phenylethanol. Consequently, we focused on adjusting the oven column temperature and modifying the hold time near the temperature range relevant to AP and 1-Ph from zero to 3 minutes (table 3.5, 3.6 respectively). Upon analysis of the chromatogram, it became evident that the peaks were successfully resolved a process which took approximately 27 minutes (Figure 3.8). It is worth considering extending the hold time from zero to 3 minutes to further enhance resolution (table 3.7).

Table 3.5 GC column method (oven program) used for EBHP investigation before splitting AP and 1-Ph.

initial	Temp (°C)	Rate (°C min^{-1})	Hold time	He rate (mL min^{-1})	Total time
initial	50 -90	4	0	1.2	
initial	102	2	0	1.2	23
Final	250	30	2	1.2	

Table 3.6 GC column method (oven program) used for EBHP investigation after splitting AP and 1-Ph.

Initial	Temp (°C)	Rate (°C min^{-1})	Hold time	He rate (mL min^{-1})	Total time
Initial	50 -90	4	3	1.2	
	102	2	0	1.2	27
Final	250	30	2	1.2	

Table 3.7: Time and column temperature corresponding to components detected in GC analysis

Time (min)	Column °C	Component appears in GC
0	50	
1	54	
2	58	
3	62	
4	66	
5	70	Decane (IS)
6	74	
7	78	1-phenyl ethanol
8	82	Acetophenone
9	86	
10	90	
11	92	
12	94	Unidentified Peak

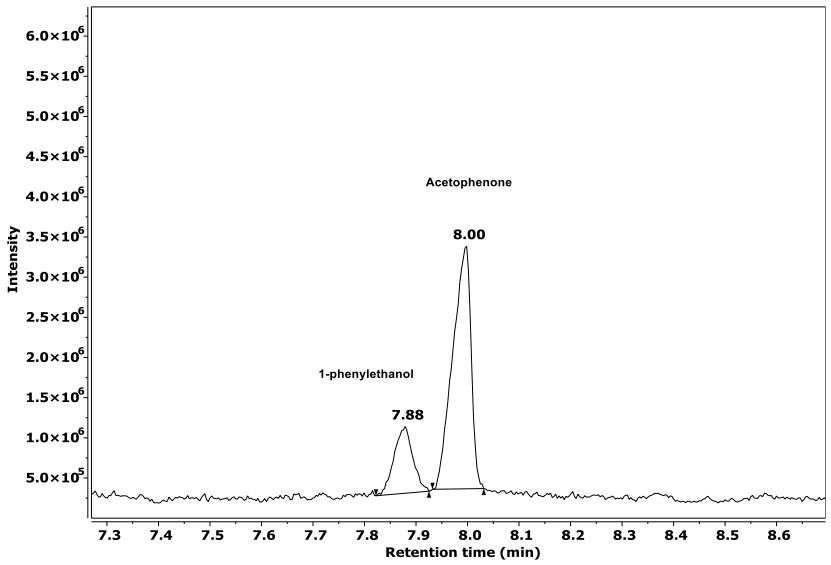

Figure 3.8: Chromatogram demonstrating an effective separation between acetophenone and 1-phenyl ethanol peaks, highlighting a successful resolution.

After confirming the efficacy of the method applied to the column, we proceeded to investigate the reactivity of alkyl peroxide during its passage through the column. Therefore, a pure sample of EBHP 96% were analysed to ensure that it had not undergone any reaction during the separation process. Recognizing that decomposition is influenced not only by temperature but also by column parameters. It was found that the lowest temperature that could be achieved by the column during our investigations, independently of the laboratory's temperature changes and without any cooling device, was 50 °C. Therefore, the column temperature was set to 50 °C. The results also indicate that the decomposition of EBHP within the column mirrors what occurs in the injector section of the GC, with the same products appearing. Furthermore, varying temperatures whether low or high did not affect and the decomposition is real. Moreover, the compound at 12 min in chromatogram cannot be identified for the reason mentioned in section 3.4.1 and this needs further investigation.

3.5.4 Investigating EBHP behaviour in MS: effects of Ion Source

Within the mass spectrometer volatile analytes separated by the gas chromatography undergo ionization and fragmentation, analysis, and identification according to their fragmentation patterns. Typically, mass spectrometers consist of three main parts: the ion source, the mass analyser, and the detector. The sensitivity, resolution, and speed of the mass spectrometer are determined by the characteristics of the mass analyser. Typical mass analysers encompass double focusing, ion traps, quadrupoles, and time-of-flight analysers. In this study, a time of flight mass analyser is used. The main goal of the ion source is to ionize and fragment the analyte in a given sample [24-25]. Electron impact ionization (EI) and chemical ionization (CI) are the two ionization techniques most frequently used in gas chromatography-mass spectrometry [26]. EI removes a valence electron from the atom with the lowest ionization energy through the bombardment of molecules with an electron beam. This leads to the creation of an often unstable radical cation that experiences rearrangement and/or fragmentation [27]. This mass fragmentation produces a characteristic mass spectrum for the analyte. Ionization by electron impact is the only technique used in this study. The ion source typically consists of a heating block, filament, and repelled. The heating block keeps the analyte in a vapour state by ensuring a consistent temperature. The filament produces high-energy electrons that can remove the valence electrons from the analyte and is typically kept at 70 eV. The analyte molecules fragment based on the kind of functional groups present and their structure. The pattern of fragmentation (intensity versus mass/charge ratio) is termed a mass spectrum and frequently exhibits uniqueness specific to the molecule. The ion fragments within the ion source are propelled towards the mass analyser via a narrow aperture by the repelled. The primary function of the pumps is to eliminate the carrier gas neutral particles, and negatively charged ions from the MS system, while also decelerating the analyte ions to facilitate fragmentation within the ion source. In conclusion, ion sources frequently identify the same species, though operational differences exist [28]. Therefore, it is often not possible to change the ion source to address a specific natural product analysis. Instead, the selection of an ion source is typically influenced by the accessibility of instrumentation and expertise [29].

3.5.5 Changing the flow rate

In order to verify the origin of the activity observed during the injection of EBHP in GC at a low injector temperature of 50 °C. This study was subjected to changing the flow rate from 1.2 to 2 mL/min. the result showed that increasing the flow rate accelerates the movement of compounds through the column, reducing the opportunity for interaction with the stationary phase [30]. Consequently, based on the data presented in the figures (3.9 and 3.10, 3.11) respectively, it is evident that the peak intensity weakens noticeably when transitioning from a flow rate of 1.2 to 2 mL min^{-1}.

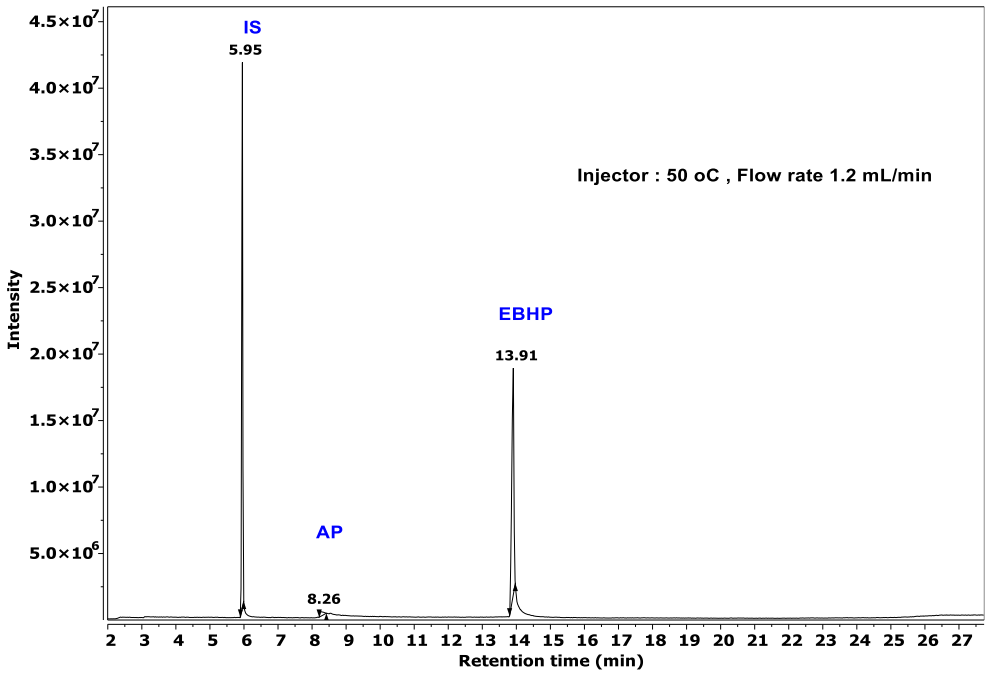

Figure 3.9: Decomposition of EBHP at low injector temperature of 50 °C and flow rate of 1.2 mL min^{-1}.

At a flow rate of 1.2 mL min^{-1} (figure 3.8) the positions of the peaks in the chromatogram changed according to the changing the carrier gas flow rate. Because the mobile phase is moving relatively slowly. Due to this slow flow rate, the analyte can interact for a longer time with the stationary phase. As a result, the retention time is longer as we see the peak of EBHP appear at 13.9 min. This flow rate makes a balance between analysis time and resolution.

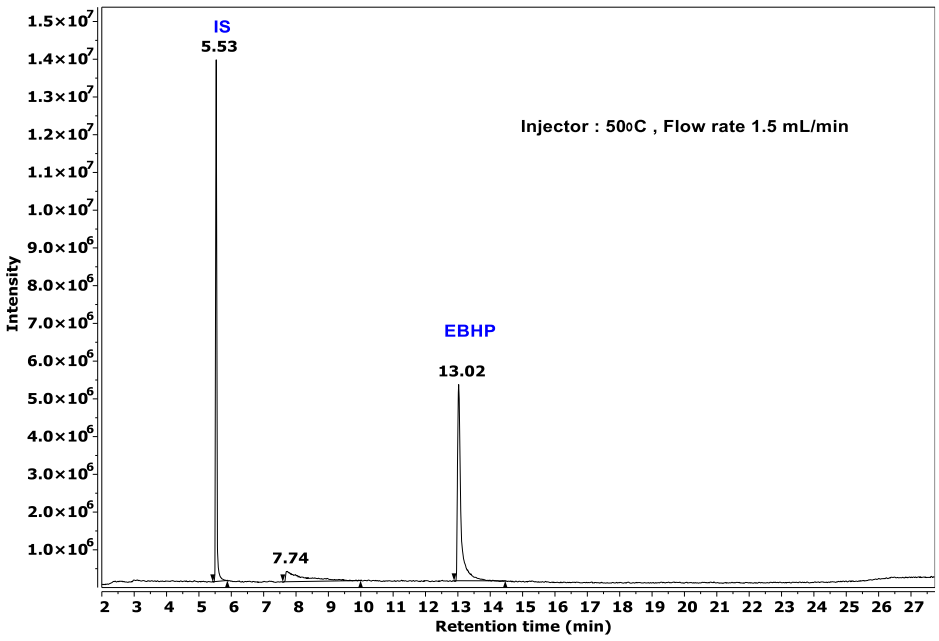

Figure 3.10: Decomposition of EBHP at low injector temperature of 50°C and flow rate of 1.5 mL min^{-1}.

At a flow rate of 1.5 mL min^{-1} (figure 3.9) increasing the flow rate accelerates the velocity of the mobile phase, and the analytes spend less time interacting with the stationary phase compared to the lower flow rate. As a result, retention times are shorter leading to faster elution of analytes from the column. In general, high flow rate leads to narrower peaks, increases resolution, but excessively high flow rate results in peak distortion. Lower flow rate improves separation (better interaction between analytes and stationary phase), but leads to peak broadening and longer analysis time.

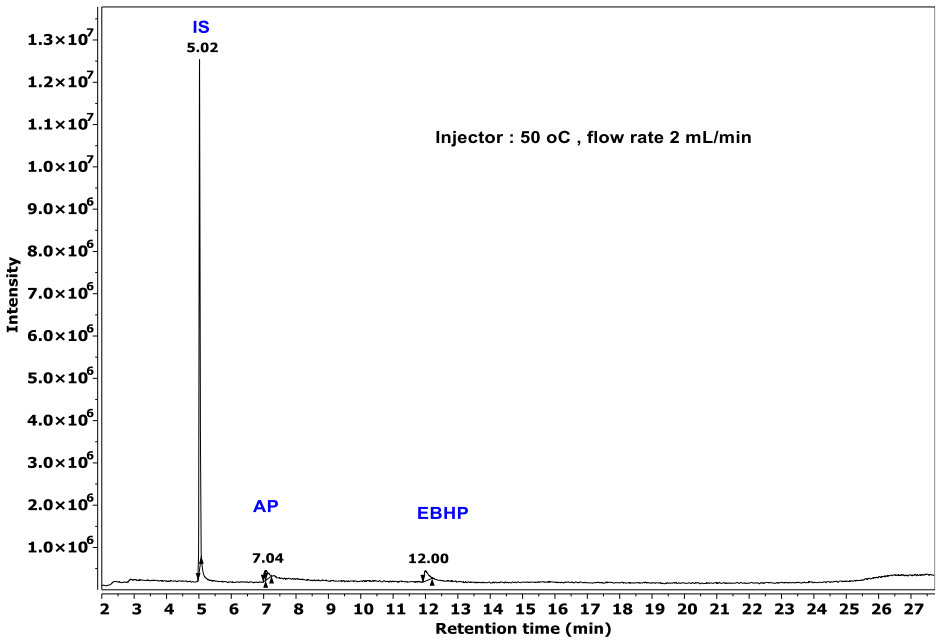

Figure 3.11: Decomposition of EBHP at low injector temperature of 50°C and flow rate of 2 mL min^{-1}

Further increasing the flow rate to 2 mL min^{-1} (figure 3.10) significantly increases the velocity of the mobile phase. This reduces the retention time, meaning the analytes have less time to interact with the stationary phase compared to the previous flow rates. Consequently, retention times are shorter, resulting in rapid elution of analytes from the column. However, at this higher flow rate, a poor separation is observed, because overall the peak position is closer for the analytes.

3.5.6 Changing DB-5MS-UI column to ZB-5MS

In order to establish the accurate determination of 1-phenyl ethyl hydroperoxide (EBHP) with other compounds that appear in the system. The non-polar ZB-5MS GC columns can separate the three compounds. EBHP are known for their chemical instability and propensity for decomposition, making their analysis challenging yet crucial in various applications. The ZB-5MS column, renowned for its versatility and suitability for a wide range of analytes, was selected for its compatibility with the compounds under investigation. However, it became apparent during the experimentation process that the ZB-5MS column exhibited extended separation times for the target compounds. As shown in figure 3.10, acetophenone a common decomposition product of EBHP appeared at 19 minutes, while EBHP appeared at 33.7 minutes. With such a long retention time, the method may not be as efficient or throughput-efficient as it could potentially impact its practical application. Furthermore, there was substantial noise in the chromatogram which may have effects and could compromise the accuracy of the data [26-31].

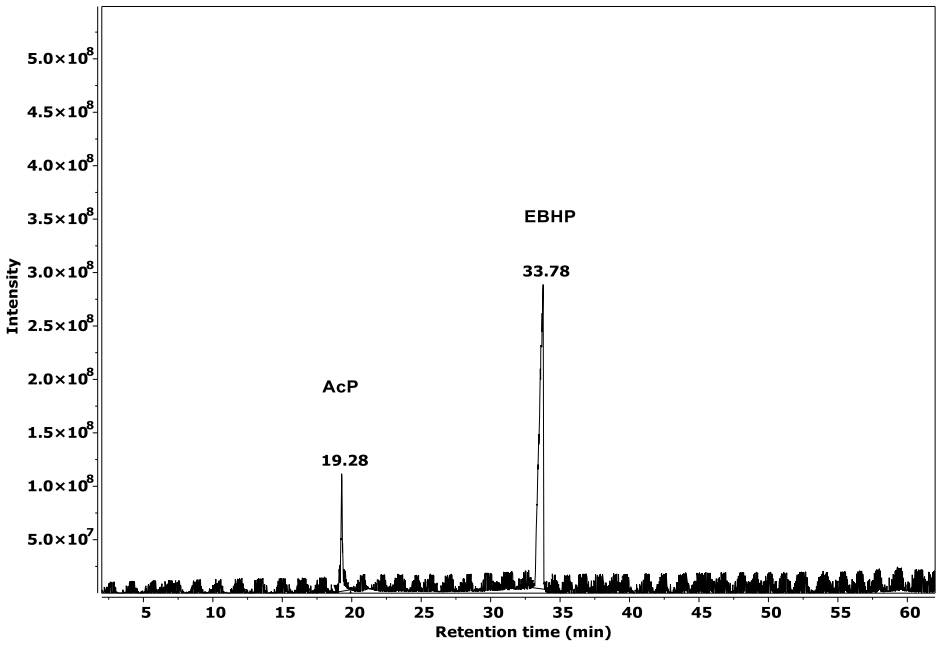

Figure 3.12: Chromatogram illustrating the separation of EBHP decomposition products utilizing a ZB-5ms column. Two peaks are observed: acetophenone elutes at 19.28 minutes, while EBHP elutes at 33.78 minutes. The chromatogram illustrates the extended retention times and noise levels encountered during the analysis.

3.5.7 Protecting group using BSTFA for GC-MS analysis

Even with the possibilities provided by the electronic searches in the mass spectrum libraries, the process of identifying molecules using mass spectroscopy is not an easy task [32]. Many different compounds might have a mass spectrum that closely matches more than one other compound, indicating a high degree of similarity [33]. In such instances, performing derivatization to yield a compound that generates more informative fragments in the mass spectrum proves highly beneficial [34-33]. Therefore from the observations discussed above, in order to clarify the identity of the peak present at 12 min in GC. We conducted a protecting group synthesis (scheme 3:1) for EBHP (method described in the previous chapter section 2.7). This study aimed to justify whether the observed peak indeed corresponds to EBHP by enhancing the stability of compounds. The derivatization by silylation utilizing various ratios (EBHP: Protected group), 1:1, 1:0.26, and 1:3. The analysis involved comparing the initial concentration with the concentration post-injection and subsequently converting the concentration of protecting group to ratios. The result demonstrates that the fragments from derivatized compounds can be used for the identification of the peak at 12 min. These significant findings are quantitatively accepted and will be presented here in this section in more detail.

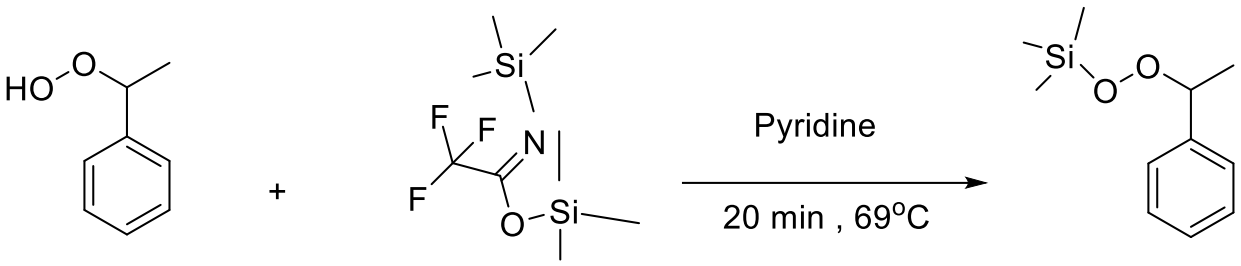

Scheme 3.1: The silyation reaction involves the EBHP reacting with BSTFA (N, O-bis (trimethylsilyl) trifluoroacetamide) in the presence of pyridine as a catalyst at 69 °C for 20 minutes. The result is the formation of the protected peroxide compound.

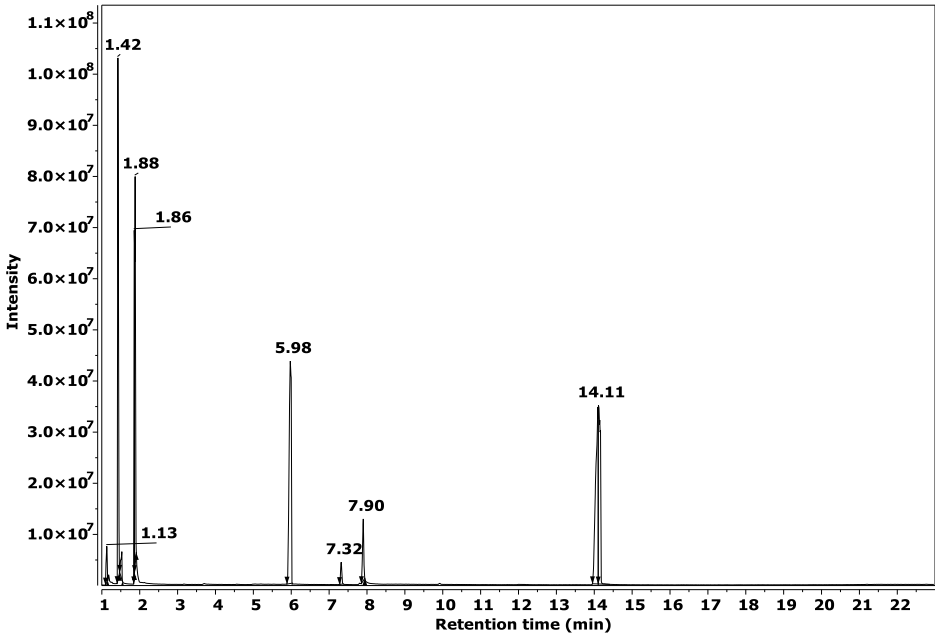

Figure 3.13: The GC fragmentation pattern for the protecting group with a ratio (1:1) shows peaks at specific retention times. Beginning with DCM at 1.42 min, followed by pyridine at 1.88 min, and the internal standard at 5.9 min. subsequently, BSTFA appears at 7.3 min, followed by acetophenone (AP) at 7.9 min. finally the protected compound at 14 min.

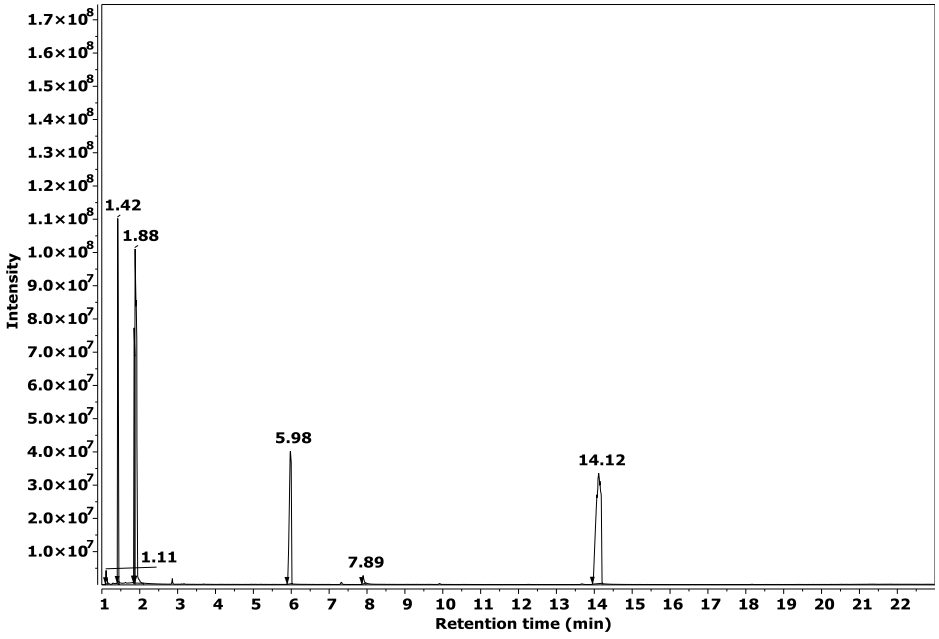

Figure 3.14: The GC fragmentation pattern for the protecting group with ratio (1:3)

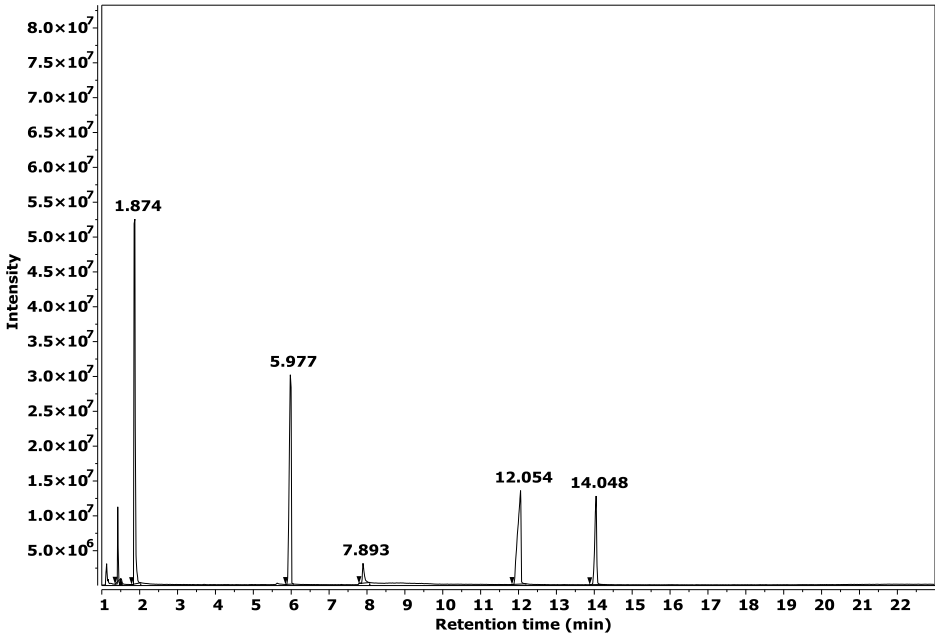

Figure 3.15: The GC fragmentation pattern for the protecting group with ratio (1:0.26)

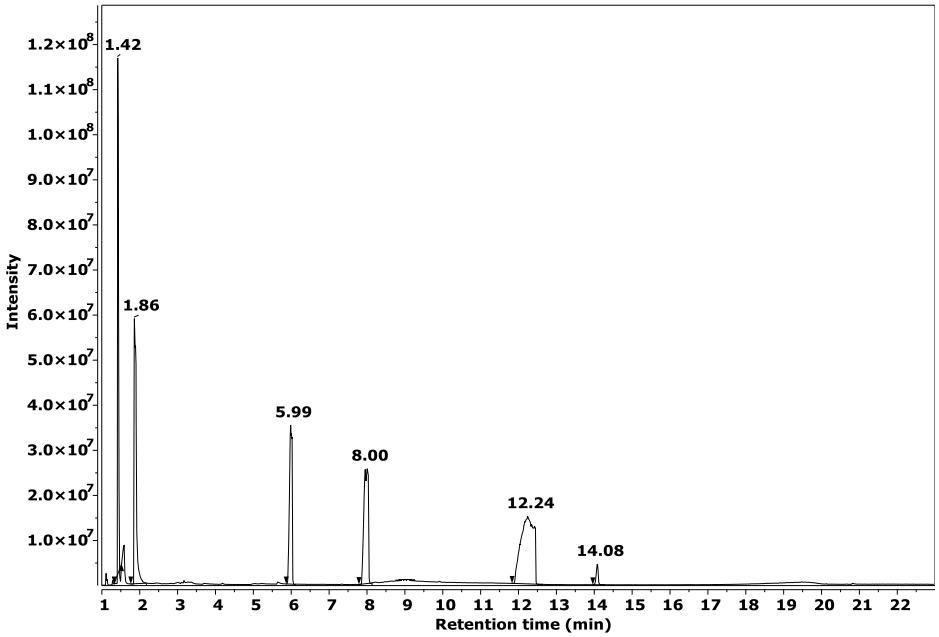

Figure 3.16: Representative mass spectrum of protecting group with ratio (4:0.25)

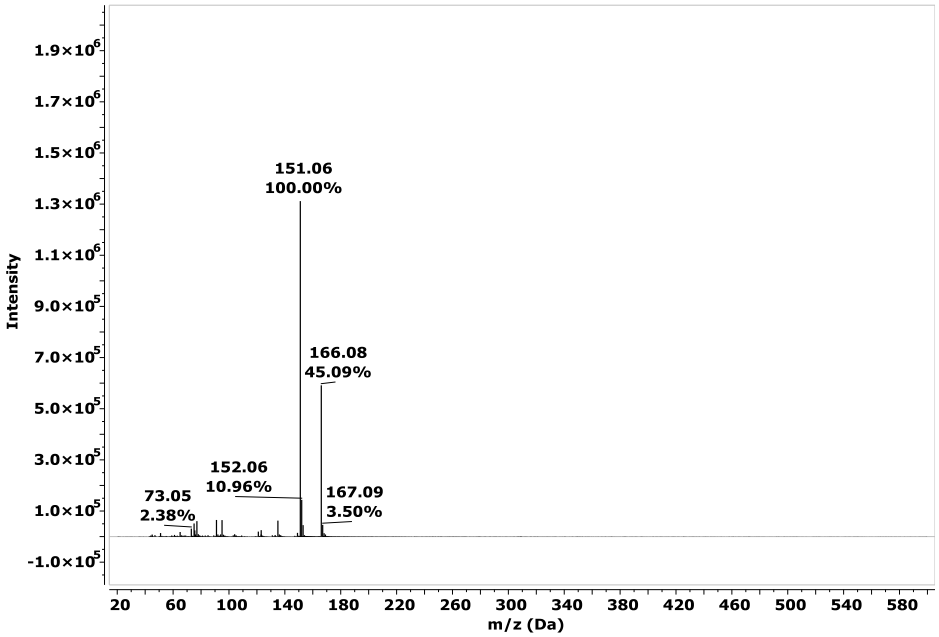

Figure 3.17: Representative fragmentation for BSTFA at 7.3 min, MS: m/z = 166.0817 corresponds to the silyated phenol $[C_9H_{14}OSi]^+$, the peak at m/z= 151.0602 corresponds to the ion $[C_8H_{11}OSi]^+$ (due to the loss of CH_3 group from the silyated compound), m/z 135.0277 corresponds to the ion $[C_7H_7OSi]^+$ (loss of the 2nd group of CH_3 from the silyated compound)and m/z 75.0274 and m/z 73.0479 correspond to the silyated group $[C_2H_7OSi]+$ and $[C_3H_9Si]^+$ respectively.

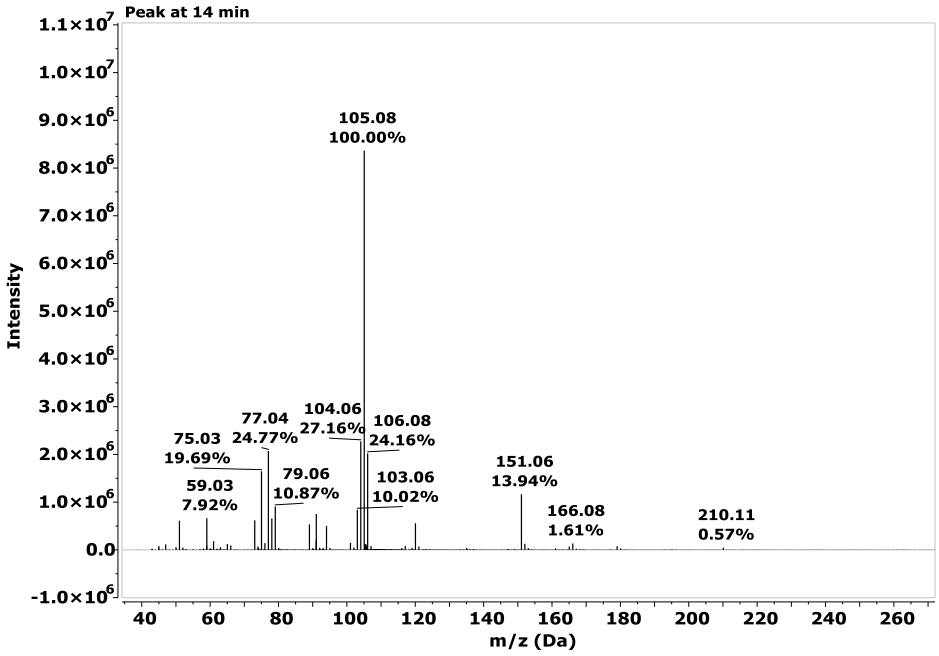

Figure 3.18: Representative mass spectrum of the protecting group with a molecular weight of 210.11. Fragmentation: m/z = 210.11 corresponds to the molecular ion $[C_{11}H_{18}O_2Si]^+$, the peak at m/z= 195.09 corresponds to the ion $[C_{10}H_{15}O_2Si]^+$ (loss of CH_3 group), m/z 166. 0856 corresponds to the ion $[C_9H_{14}OSi]$ + (loss of the 2nd CH_3 group and O) and m/z 151.0626 corresponds to the ion $[C_8H_{11}OSi]^+$ (loss of the 3rd CH_3 group and O).

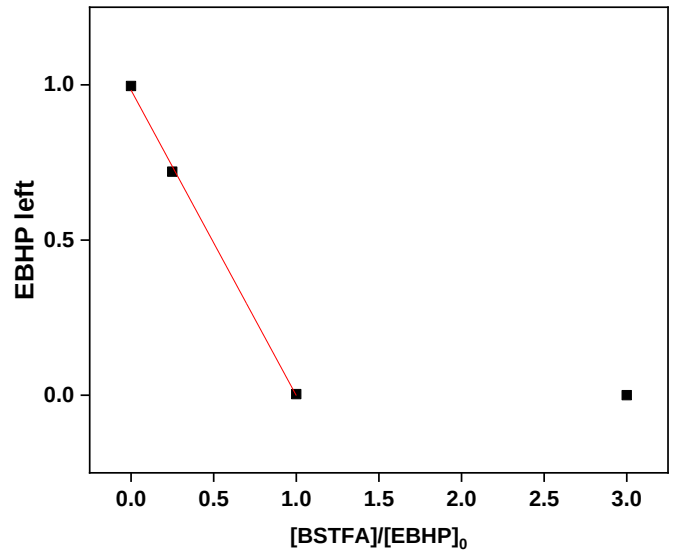

Figure 3.19: Graph illustrating the chromatographic analysis of residual EBHP at various ratios, aimed at identifying the peak observed at 12 minutes.

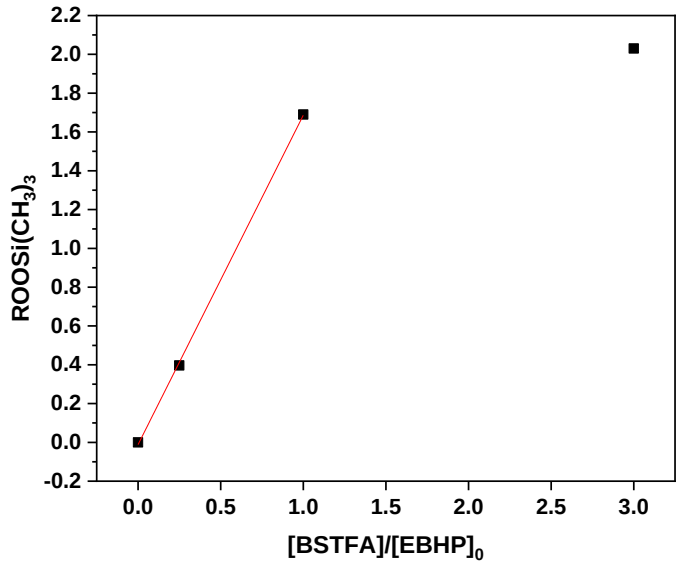

Figure 3.20: Graph illustrating the chromatographic analysis of the protected group at various ratios, aimed at identifying the peak observed at 14 minutes.

Figures 3.19 and 3.20 illustrate the results of various ratios of peroxide to the protecting group (1:1, 1:26, 1:3, and 4:0.25) and data analysis. Upon plotting the residual peroxide and the concentration of the protecting group, a distinct trend emerges. The concentration of residual peroxide consistently decreases, while that of the protecting group steadily increases [35]. This trend supports the inference that the peak observed at 12 minutes in the chromatogram corresponds to the peroxide compound. Considering the partial decomposition of EBHP during GC analysis, it becomes imperative to explore alternative techniques devoid of thermal or high-temperature requirements. Transitioning to methods such as NMR, which works at room temperature, could present a viable solution for accurate compound characterization without the risk of thermal decomposition [36], as long as in the absence of NMR peaks overlaps form the proton signal of relevant functional groups.

3.6 Method development for determination of alkyl hydroperoxide (EBHP) content in reaction mixtures by using NMR methods

Although, GC-MS analysis presents a complex analytical procedure, typically meticulous calibration for accurately quantifying compounds within a reaction mixture. Moreover, samples must undergo appropriate pre-treatment prior to analysis, leading to a relatively time consuming process. Moreover, in our case, this entails analysing alkyl hydroperoxides, a critical intermediate that under the analysis conditions of GC-MS, can undergo thermal decomposition into the corresponding ketones or alcohols upon sample injection. Commonly operating within a temperature of 150 to 250°C, it is probable that the samples analysed by GC-MS do not accurately represent the original samples from a reaction mixture. This is because the decomposition of alkyl hydroperoxides could lead to a perceived increase in selectivity for alcohol and ketone compounds. Considering this, our research has developed quantitative analysis using nuclear magnetic response spectroscopy (NMR). One significant benefit of NMR for our project is its capability to analyse reactive intermediates without experiencing thermal decomposition, as NMR analysis takes place at room temperature [43- 44].

3.6.1 ^{1}HNMR quantification: analytical approach

NMR is widely used because it has several unique advantages [45]. These include shorter analysis times, typically a matter of minutes, contrasting with the time-consuming nature of chromatographic methods, which can take up to an hour per sample [46]. NMR is formally non-destructive and preserves the physical characteristics of the sample [47]. However, it necessitates the use of a solvent for analyte recovery. Moreover, NMR analysis is conducted at room temperature enhancing its relevance for detecting compounds of interest [48]. It is crucial to consider a temperature range at room temperature or below, significantly lower than the thermal decomposition point of alkyl hydroperoxides, which serve as the main intermediates in our reactions. In addition, the preparation of the sample is very straightforward and convenient. ^{1}H-NMR can therefore be thought of as a rapid screening technique for the analysis of our reaction samples based on all of these features [49]. Given the discussion above and the practical considerations involved in analysing reaction mixtures containing a variety of substrates, ensuring the stability of the alkyl hydroperoxide, and swiftly gathering data for screening purposes, we have chosen to measure the products in

these mixtures using ^{1}H-NMR. As outlined in section 2.7.2 of Chapter 2, proton nuclear magnetic resonance ^{1}HNMR involves detecting hydrogen-1 nuclei, commonly referred to as protons, within a substance with the objective of elucidating the structure of organic molecules. This can be accomplished by examining the chemical displacement of hydrogen (H), which is influenced by factors such as the molecular configuration of the compound, the solvent used, and the temperature conditions [50].

3.6.2 Ethylbenzene alkyl hydroperoxide decomposition

As discussed earlier in this chapter, alkyl hydroperoxides EBHP is an essential step in the oxidation of hydrocarbons. Particularly when this happens through a free radical pathway, they are created when alkyl radicals ($R^{\bullet}$) react with O_2 to produce peroxyl radical species ($ROO^{\bullet}$), which are then combined with hydrocarbons (R–H) in an autoxidation process [51]. At present, research primarily emphasizes understanding the reaction pathways and mechanisms of different catalysts involved in direct hydrocarbon oxidation. Conversely, the decomposition of alkyl hydroperoxides has been relatively overlooked. These compounds, containing α-H near the C–OOH group which is easy to be autoxidized under typical conditions [52]. Therefore, the aim is to examine the decomposition pathway of an alkyl hydroperoxide, whether catalysed or not, and to utilize it directly as a substrate rather than obtaining it as an intermediate. We synthesized the alkyl hydroperoxide, following the procedure outlined in the previous chapter specifically in section 2.4. This synthesis of ethylbenzene alkyl hydroperoxide was utilized as a substrate, both in the presence and absence of a catalyst to evaluate its transformation into a ketone or alcohol as seen in figure 3.21, and NMR of pure EBHP 96% can be seen in figure 3.22.

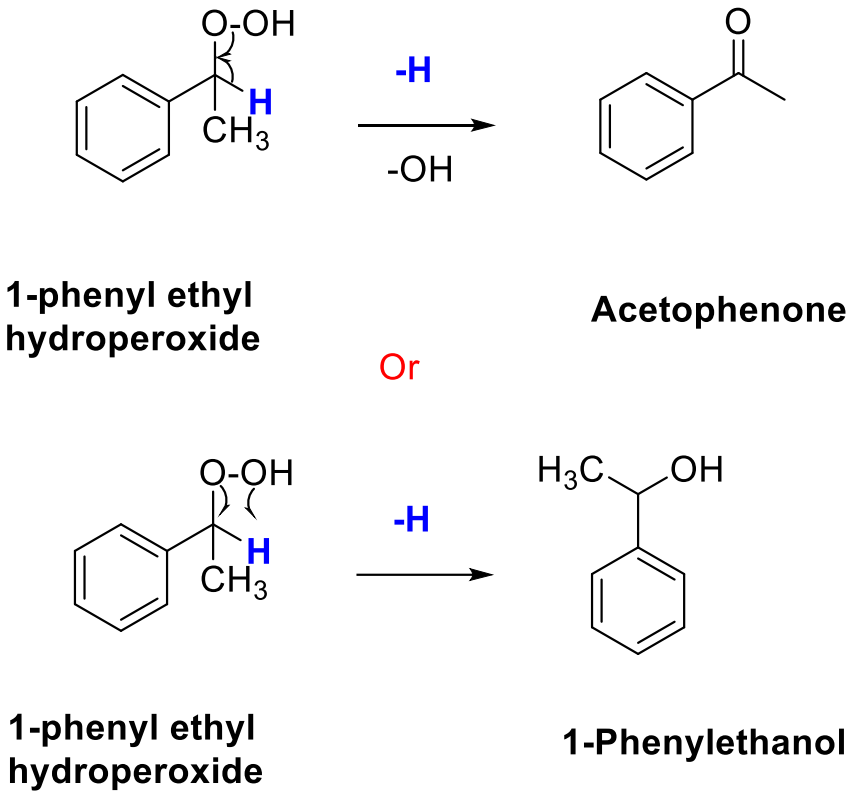

Figure 3.21: Ethylbenzene alkyl hydroperoxide decomposition pathway to ketone and alcohol.

The autoxidation of ethyl benzene alkyl hydroperoxide was carried out in the absence of any catalyst. This is a very important step to study the decomposition of the intermediate. In this study, the EBHP test was conducted using C_6F_8 as the solvent. This choice stemmed from the solvent's characteristic absence of proton signals in NMR spectra, facilitating clear observation of the peroxide signals without solvent interference. Moreover, taking into account the lengthy process involved in synthesizing 1-phenyl ethyl hydroperoxide, which yielded only minimal amounts, the use of a solvent was also introduced. However, the boiling point of C_6F_8 (104 °C) acted as a limiting factor, restricting our capacity to increase the reaction temperature beyond 80 °C. This constraint ensured that the temperature remained below the boiling point of the solvent thereby maintaining the integrity of the experimental setup and preventing any unwanted changes in the reaction conditions. Additionally, the solvent is inert and did not react with the compound and this was approved from other investigations. For this purpose, a temperature of 80 °C is employed for this reaction. The outcome showed that the decomposition did not proceed, with zero conversion observed. Based on these findings, which included the inertness of the solvent and the inability to increase the temperature beyond 80 °C due to the boiling point of C_6F_8,

we proceed with further investigation by employing different solvents. Toluene and 1, 2-dichlorobenzene were used as solvents, however, neither proved to be inert under the conditions of 100 °C 24h. Therefore, the study conducted using C_6F_8 was sufficient to validate the results obtained from the EBHP decomposition at 80 °C.

Therefore, this study highlights the decomposition of alkyl hydroperoxide at 80°C over a 24 h period. The intermediate formed during this process demonstrated remarkable stability, showing no formation of ketones or alcohols. This stability makes the intermediate a good standard for further investigations using our catalysis method. As depicted in figure 3.22, the purified ethylbenzene hydroperoxide (EBHP) achieved a high purity level of 96% with only 4 ± 1 % impurities primarily in the form of acetophenone. These impurities were carefully considered when analysing EBHP decomposition using GC-MS.

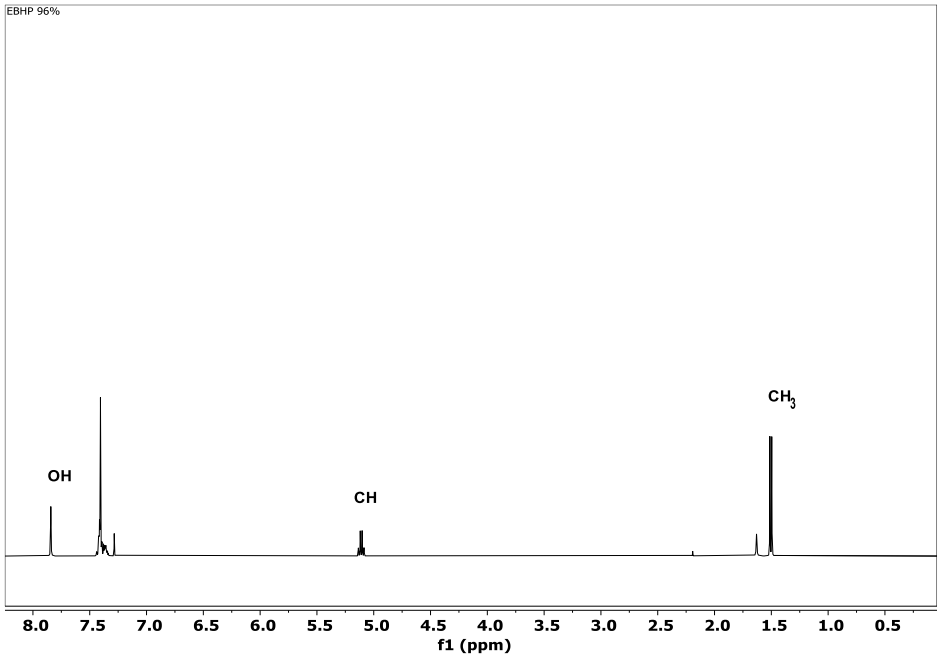

Figure 3.22: NMR spectrum of pure EBHP (96%) recorded in $CDCl_3$ at 400MHz, the spectrum showed peaks: 1H NMR (400 MHz, CDCl3) δ 7.80 (s, 1H), 7.38-7.45 (m, 5H), δ 5.11 (q, J=6.6, 1H), 1.50 (d, J= 6.6, 3H).

The conclusion of the investigation into EBHP oxidation demonstrates it is stability under controlled conditions at 80°C, without decomposition (as confirmed by a blank test). Further research directions are also outlined. Chapter 5 will provide a detailed study, including a thorough examination of additional catalysts and further investigations on this topic.

3.6.2.1 Analysis of EBHP the intermediate compound formed during Ethylbenzene oxidation

The reactivity of EBHP in the liquid phase during the oxidation of Ethylbenzene was investigated across temperatures ranging from 100 °C to 130 °C, with varying reaction times from 24 hours to 120 hours. As depicted in the figure 3.23, it is evident that 1-phenyl ethyl hydroperoxide emerges as the major product from the beginning of the reaction. Particularly in low-temperature oxidation at 100 and 110 °C, the selectivity reached 100%.

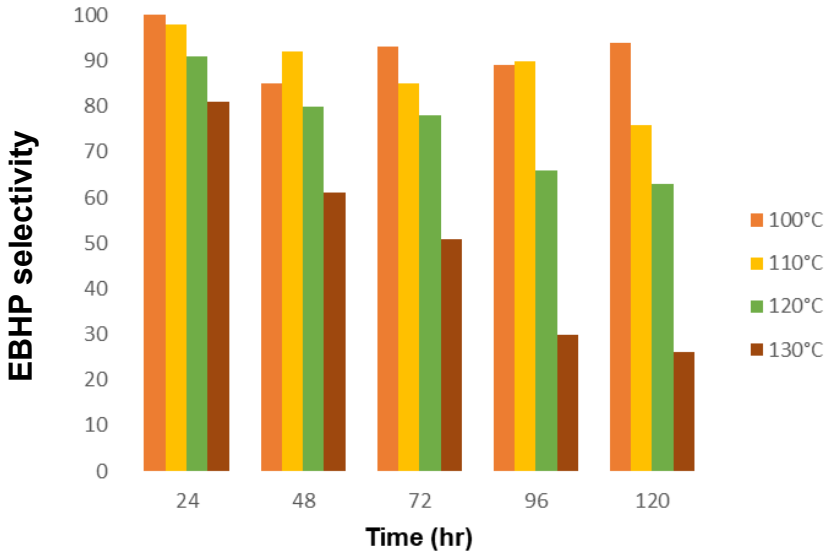

Figure 3.23: This illustrates changes in the observed selectivity of EBHP at varying temperatures 100C,110,120 and 130 (°C) and reaction times of 24,48,72 and 96 ,120 (h) under reaction conditions of 5 mL Ethylbenzene, 600 rpm stirring in the air (atm).

Temperature plays a crucial role in autoxidation influencing the stability of EBHP [53]. The data presented above reveals that at 100°C and 24h hours, the reaction rate remains unaffected by temperature, evidenced by the presence of 100% EBHP. This trend persists at 110°C as well, where no by-products are observed within this temperature range. This observation suggests favourable conditions for future catalysis tests, indicating minimal or no thermal decomposition of EBHP in these temperature settings. However, between 120°C and 130°C alkyl hydroperoxide gradually decomposes at 24 hours yielding ketones and alcohol. The compound's stability was further examined over extended periods under identical temperature conditions. Additionally, increasing the reaction temperature can potentially reduce selectivity due to radical pathways [54-55]. Hence, based on the presented data, alkyl

hydroperoxide exhibits stability at 130°C, however, over half of it is decomposed during the reaction. Considering the observed reactivity of EBHP, it becomes essential to further investigate the decomposition tendencies of EBHP. Chapter 5 will provide an in-depth study of this aspect focusing particularly on Ethylbenzene oxidation.

3.7 Validation of GC-MS methodology through comparative analysis with NMR spectroscopy: a statistical approach

In this section, we aim to validate the gas chromatography-mass Spectrometry (GC-MS) method by comparing it with Nuclear Magnetic Resonance (NMR) spectroscopy, a well-established analytical technique. Validation of analytical methods is crucial to ensure the accuracy and reliability of the results obtained [56 - 57]. By comparing the results obtained from both GC-MS and NMR methods, we can assess the consistency and reliability of the analysis. Among many statistical methods available, the t-test and f-test stand out as fundamental tools for hypothesis testing and assessing the validity of research findings [58]. To find out if there is a significant difference between the means of two groups, one effective inferential statistical method is the t-test [59]. This t test is widely used across various disciplines, the t-test allows researchers to evaluate the effectiveness of interventions, compare treatment outcomes, and assess the impact of independent variables on dependent measures [60-61]. It is important to validate hypotheses and draw robust conclusions from the data. The fundamental premise of the t-test lies in comparing the means of two groups while accounting for the inherent variability within each group [62-63]. By calculating the t-value, which represents the ratio of the difference between the group means to the standard error of this difference, researchers can determine the likelihood of observing such a difference by chance alone [64-65]. This probability known as the p-value serves as a crucial indicator of the statistical significance of the observed difference [66-67]. A low p-value supports the alternative hypothesis by showing that the observed difference is unlikely to have happened by accident [68]. Apart from the t-test, the F-test is also crucial for statistical analysis, especially when it comes to regression analysis and analysis of variance (ANOVA) [69-70]. The F-test serves as a versatile tool for comparing the variability between multiple groups or assessing the overall fit of a regression model [71-72]. At its core, the F-test evaluates the ratio of two variances: the variance between groups and the variance within group [73-74]. This ratio known as the F-ratio provides a measure of the extent to which the variability in the data can be attributed to the factors under investigation [75]. A high F-ratio suggests that the variability between groups exceeds the variability within groups indicating a significant effect of the independent variables on the dependent measure [76]. The importance of statistical testing including the t-test and F-test cannot be overstated in scientific research. These tests enable researchers

to evaluate hypotheses assess the validity of their findings and make evidence based decisions [77-78].

The validation of an analytical method is critical to ensuring its consistency, accuracy, and reproducibility. We can compare the NMR and GC-MS methods quantitatively using these statistical tests, so as to determine their suitability for specific analyses. An example will be presented in this section to compare the results from ^{1}HNMR and GC-MS. By utilizing the t-test, the main values obtained from each method will be compared in order to assess whether there is a statistically significant difference between them. We can use this comparison to determine if the two methods have comparable results or if one method consistently produces a significantly different value. Furthermore, we will compare the variances of the two methods using an F-test. The following example will present a detailed example demonstrating the use of these statistical tests. As a result of using these tools, we will demonstrate how method developers can rigorously evaluate and validate analytical methods and ensure that they meet the necessary standards of accuracy and precision.

To compare the carbon mass balance (CMB %) results between GC-MS and ^{1}HNMR for a reaction mixture of Ethylbenzene at 120 °C 24h, using a t-test: tow samples assuming equal variances. First, by stating the hypotheses: null hypothesis (H_0) represents there is no significant difference between the mean CMB% of the two methods (GC-MS and ^{1}H-NMR). On the other hand, the alternative hypothesis ($H\alpha$) showed that there is a significant difference between the mean CMB % of the two methods. Therefore, the data collected from GC-MS showed a carbon mass balance equal to 93 ± 3 and 96 ± 5 from ^{1}H-NMR. By applying the t-test formula for two samples (eq.3.7), X_1 and X_2 are the sample means.

$$t = \frac{X_1 - X_2}{s\sqrt{\frac{1}{n_1} + \frac{1}{n_2}}} \qquad (eq.3.7)$$

Therefore, X_1 (GC-MS) = 93 and X_2 (^{1}H-NMR) =96 and $S_1^2 = 3^2 = 9$, $S_2^2 = 5^2 = 25$

$$s^2 = \frac{(10-1)9 + (10-1)25}{10+10-2}$$

$$s^2 = \frac{306}{18}$$

$$S = \sqrt{17} \approx 4.12$$

After this step, we can calculate the t statistic:

$$t = \frac{93-96}{\sqrt{17\,(\frac{1}{10}+\frac{1}{10})}}$$

$$t = -1.63$$

Degrees of freedom:

$df = n_1 + n_2 = 18$

To calculate the critical value by using a t-table for a two-tailed test at α = 0.05 with 18 degrees of freedom, the critical value of t is ± 2.10, therefore by comparing the test statistic to the critical value $|t| = 1.63 < 2.10$, this mean that the calculated t-value (1.63) is less than the critical value (2.10) meaning there is no statistically significant difference between the mean CMB% obtained from the GC-MS methods and ^{1}H-NMR method. In our study, this data comparison might suggest that there is no significant difference between the two methods in terms of CMB%. However, due to the differing K/A ratios and the variations observed in the decomposition of EBHP during GC-MS analysis, we opted to use NMR for further evaluation. In fact, the advantages offered by NMR which employed for a quick analysis. Importantly, it allowed us to make an analysis at room temperature without encountering issues such as the thermal decomposition of 1-pheny ethyl alkyl hydroperoxide which occur in the gas chromatography.

3.8 Conclusion

Hydrocarbon oxidations hold significant promise across various industrial and academic research [79]. Serving as a fundamental chemical feedstock from which virtually all organic compounds originate, underscores the critical importance of study methods for their functionalization [80]. The main focus of this project lies in the selective oxidation of hydrocarbons to produce their corresponding ketones or alcohols. This process entails the targeted conversion of hydrocarbons into valuable intermediate products, emphasizing the project's aim to develop methodologies for this chemical reactivity[81]. Hence, catalysts must exhibit selectivity to minimize the generation of by-products. To assess a catalyst's selectivity accurately, a precise and quantitative analytical method (either spectroscopic or chromatography) is essential for determining the composition of the reaction mixture. The complete characterization of hydrocarbon reaction mixture both qualitative and quantitative is not an easy task [82-83]. In reality, these reactions typically yield dozens of products. A frequently employed method for determining the composition of such reaction mixtures is gas chromatography [84- 85]. However, despite their low detection limits, which can be as low as parts per billion (ppb) for GC-MS methods, these techniques are cumbersome, time consuming and may not yield accurate results without pre-preparation of reaction mixture prior to analysis [86-7]. In this context, this specifically refers to the analysis of alkyl hydroperoxides and any relative organic acid form in the system [87-5]. In fact in this study, alkyl hydroperoxide decomposes into ketones and alcohol under chromatographic conditions. Consequently, despite while the GC-MS method can achieve low detection limits, there is a risk that the analysed specimen will not accurately represent the original reaction mixture sample. In light of this and to manage the analysis of a large number of reaction mixtures, we study to develop a method to quantify and characterize our reaction mixtures. Therefore, at the start of this chapter, we studied the stability of alkyl hydroperoxide over the year and the result showed the consistency of its stability at 96%. Subsequently, we couldn't directly determine the concentration of alkyl hydroperoxide using GC-MS since these compounds undergo decomposition in the GC, resulting in the production of ketone and alcohol. Therefore, we shifted our focus to identifying alternative methods capable of calculating this concentration and purity. One of those methods we utilized was the iodometric titration to assess the peroxide purity. While effective, this method was

time-consuming and involved the use of a vapour solution such as iodine. Hence, we attempted to identify a more efficient method to validate our findings in a timely manner. Using TPP was one of the techniques we used; prior to GC analysis, the reaction solution sample was treated with an excess of TPP for 20 minutes at ambient temperature. The hydroperoxide is reduced to its corresponding alcohol. Consequently, the disparity in alcohol levels in the GC traces of reaction solution before and after triphenylphosphine reductions can't present the estimation of hydroperoxide amount. This is because the peroxide amount presented in the solution did not match the alcohol/ketone ratio prior to the reduction with TPP. Therefore, the titration method was significantly matched with the purity obtained from NMR and can be used. Following that, an efficient and accurate method for the quantification analysis of reaction mixtures from the oxidation of hydrocarbons was developed. The findings demonstrated that ^{1}H-NMR serves as a dependable and efficient approach for quantifying the intermediate products, particularly for the quantification of alkyl hydroperoxide. Notably, the analysis process was conducted at room temperature thereby preserving the thermal stability of alky hydroperoxide, unlike GC-MS. Additionally the statistical data analysis employing t-test and F-test confirmed the validity of quantitative analysis by ^{1}H-NMR method when applied to the oxidation of hydrocarbon (Ethylbenzene). In this context, ^{1}H-NMR emerges as a reliable method for quantitative analysis of ethylbenzene oxidation, particularly when focusing on the intermediate (EBHP). To some degree, in our study, this data comparison might suggest that there is no significant difference between the two methods in terms of CMB%. However, because the K/A ratio is different and not identical, and due to the decomposition of EBHP during GC-MS analysis, we chose to proceed with NMR for further assessment.

3.9 References

1 I. Opsenica, D. Opsenica, K. S. Smith, W. K. Milhous and B. A. Šolaja, *J. Med. Chem.*, 2008, **51**, 2261–2266.

2 J. L. Colodette, *Factors affecting hydrogen peroxide stability in the brightening of mechanical and chemimechanical pulps*, State University of New York College of Environmental Science and Forestry, 1987.

3 J. Luo, F. Peng, H. Yu, H. Wang and W. Zheng, *ChemCatChem*, 2013, **5**, 1578–1586.

4 I. Hermans, J. Peeters and P. A. Jacobs, *J. Org. Chem.*, 2007, **72**, 3057–3064.

5 L.-X. Xu, C.-H. He, M.-Q. Zhu, K.-J. Wu and Y.-L. Lai, *Catal. Letters*, 2007, **118**, 248–253.

6 B. P. C. Hereijgers and B. M. Weckhuysen, *J. Catal.*, 2010, **270**, 16–25.

7 M. A. Farajzadeh, N. Nouri and P. Khorram, *TrAC Trends Anal. Chem.*, 2014, **55**, 14–23.

8 W. Kanjina and W. Trakarnpruk, *J. Met. Mater. Miner, 2013, **23**, 31-35.*

9 R. D. Mair and A. J. Graupner, *Anal. Chem,* 1964, **36**, 194–204.

10 F. H. Dickey, J. H. Raley, F. F. Rust, R. S. Treseder and W. E. Vaughan, *Ind. Eng. Chem.*, 1949, **41**, 1673.

11 X. Zhang, S. Z. He, Z. M. Chen, Y. Zhao and W. Hua, *Atmos. Chem. Phys.*, 2012, **12**, 8951–8962.

12 J. Nouroozzadeh, J. Tajaddinisarmadi and S. P. Wolff, *Anal. Biochem.*, 1994, **220**, 403–409.

13 T. Nakamura and H. Maeda, *Lipids*, 1991, **26**, 765–768.

14 P. Wiklund, C. Karlsson and M. Levin, *Anal. Sci.*, 2009, **25**, 431–436.

15 C. Deyrieux, P. Villeneuve, B. Baréa, E. A. Decker, I. Guiller, F. Michel Salaun

and E. Durand, *Eur. J. Lipid Sci. Technol.*, 2018, **120**, 1800109.

16 F. Zhang, M. Chen, X. Jia, W. Xu and N. Shi, *Process Saf. Environ. Prot.*, 2019, **126**, 1–6.

17 D. E. Clark, *Chem. Health Saf.*, 2001, **8**, 12–22.

18 T. Willms, H. Kryk and U. Hampel, *J. Chromatogr. A*, 2016, **1458**, 126–135.

19 A. Ushakova, V. Zatsepin, M. Varfolomeev and D. Emelyanov, *J. Combust*, 2017.

20 S. Vetrivel and A. Pandurangan, *J. Mol. Catal. A Chem.*, 2004, **217**, 165–174.

21 R. A. Yokley, L. C. Mayer, R. Rezaaiyan, M. E. Manuli and M. W. Cheung, *J. Agric. Food Chem.*, 2000, **48**, 3352–3358.

22 O. D. Sparkman, Z. Penton and F. G. Kitson, *Gas chromatography and mass spectrometry: a practical guide*, Academic press, 2011.

23 C. F. Cullis and E. Fersht, *Combust. Flame*, 1963, **7**, 185–192.

24 C. Dass, Fundamentals of contemporary mass spectrometry, John Wiley & Sons, 2007.

25 E. De Hoffmann and V. Stroobant, *Mass spectrometry: principles and applications*, John Wiley & Sons, 2007.

26 A. Van Asten, *TrAC Trends Anal. Chem.*, 2002, **21**, 698–708.

27 A. E. Ashcroft, *Ionization methods in organic mass spectrometry*, Royal Society of Chemistry, 1997, **5**.

28 C. N. McEwen and R. G. McKay, *J. Am. Soc. Mass Spectrom.*, 2005, **16**, 1730–1738.

29 C. Bhardwaj and L. Hanley, *Nat. Prod. Rep.*, 2014, **31**, 756–767.

30 S. Z. Hussain and K. M. Khushnuma Maqbool, *Int. J. Curr. Sci.*, 2014, **13**, 116-126.

31 S. Sporstol, N. Gjos, R. G. Lichtenthaler, K. O. Gustavsen, K. Urdal, F. Oreld and J. Skei, *Environ. Sci. Technol.*, 1983, **17**, 282–286.

32 M. C. Wiener, J. R. Sachs, E. G. Deyanova and N. A. Yates, *Anal. Chem*, 2004, **76**, 6085–6096.

33 S. C. Moldoveanu and V. David, *Gas Chromatogr. Sample Prep. Appl*, IntechOpen, 2018, **9**.

34 R. Morabito, P. Massanisso and P. Quevauviller, *TrAC Trends Anal. Chem.*, 2000, **19**, 113–119.

35 M. J. Golden, *J. Am. Pharm. Assoc. (Scientific ed.)*, 1951, **40**, 119–122.

36 A. M. Tsedilin, A. N. Fakhrutdinov, D. B. Eremin, S. S. Zalesskiy, A. O. Chizhov, N. G. Kolotyrkina and V. P. Ananikov, *Mendeleev Commun.*, 2015, **25**, 454–456.

37 F. Cavani and J. H. Teles, *ChemSusChem*, 2009, **2**, 508–534.

38 Y. Su, Y. Li, Z. Chen, J. Huang, H. Wang, H. Yu, Y. Cao and F. Peng, *ChemCatChem*, 2021, **13**, 646–655.

39 B. K. Matuszewski, M. L. Constanzer and C. M. Chavez-Eng, *Anal. Chem.*, 2003, **75**, 3019–3030.

40 Ge. B. Shulpin, D. Attanasio and L. Súber, *J. Catal.*, 1993, **142**, 147–152.

41 M. Farré, M. Petrovic and D. Barceló, *Anal. Bioanal. Chem.*, 2007, **387**, 1203–1214.

42 L. Hermabessiere, C. Himber, B. Boricaud, M. Kazour, R. Amara, A.-L. Cassone, M. Laurentie, I. Paul-Pont, P. Soudant and A. Dehaut, *Anal. Bioanal. Chem.*, 2018, **410**, 6663–6676.

43 J. N. Shoolery, *Anal. Chem.*, 1993, **65**, 731A-741A.

44 F. Malz and H. Jancke, *J. Pharm. Biomed. Anal.*, 2005, **38**, 813–823.

45 R. Kaptein, R. Boelens, R. M. Scheek and W. F. Van Gunsteren, *Biochemistry*,

1988, **27**, 5389–5395.

46 H. Günther, *NMR spectroscopy: basic principles, concepts and applications in chemistry*, John Wiley & Sons, 2013.

47 S. K. Bharti and R. Roy, *TrAC Trends Anal. Chem.*, 2012, **35**, 5–26.

48 P. Giraudeau, *Magn. Reson. Chem.*, 2017, **55**, 61–69.

49 E. D. Becker, *High resolution NMR: theory and chemical applications,* Elsevier, 1999.

50 C. J. Jameson, *Annu. Rev. Phys. Chem.*, 1996, **47**, 135–169.

51 Y. Zhu, X.-W. Zhang, F. Wang, B. Xue and J. Xu, *Catalysts*, 2023, **13**, 828.

52 Y. Zhu, L. Yu, F. Wang, J. Xu and B. Xue, *ChemistrySelect*, 2023, **8**, e202301526.

53 L. Xiaowei, R. Jean-Charles and Y. Suyuan, *Nucl. Eng. Des.*, 2004, **227**, 273–280.

54 F. P. Fehlner and N. F. Mott, *Oxid. Met.*, 1970, **2**, 59–99.

55 D. J. Young, *High temperature oxidation and corrosion of metals*, Elsevier, 2008, **1**.

56 M. Yuwono and G. Indrayanto, *Profiles drug Subst. excipients Relat. Methodol.*, 2005, **32**, 243–259.

57 C. M. Riley and T. W. Rosanske, *Development and validation of analytical methods*, Elsevier, 1996.

58 J. P. Verma and A.-S. G. Abdel-Salam, *Testing statistical assumptions in research*, John Wiley & Sons, 2019.

59 M. P. Fay and M. A. Proschan, *Stat. Surv.*, 2010, **4**, 1.

60 N. A. Obuchowski Jr and H. E. Rockette Jr, *Commun. Stat. Comput.*, 1995, **24**, 285–308.

61 Q. Liu and L. Wang, *Behav. Res. Methods*, 2021, **53**, 264–277.

62 T. K. Kim, *Korean J. Anesthesiol.*, 2015, **68**, 540.

63 D. Semenick, *Strength Cond. J.*, 1990, **12**, 36–37.

64 X. U. Manfei, D. Fralick, J. Z. Zheng, B. Wang and F. Changyong, *Shanghai Arch. psychiatry*, 2017, **29**, 184.

65 M. Delacre, D. Lakens and C. Leys, *Int. Rev. Soc. Psychol.*, 2017, **30**, 92–101.

66 E. C. Hedberg and S. Ayers, *Soc. Sci. Res.*, 2015, **50**, 277–291.

67 H. O. Posten, in Robustness of statistical methods and nonparametric statistics, Springer, 1984, **1**, 92–99.

68 R. H. Browne, *Am. Stat.*, 2010, **64**, 30–33.

69 S. F. Sawyer, *J. Man. Manip. Ther.*, 2009, **17**, 27E-38E.

70 R. Christensen, *Analysis of variance, design, and regression: applied statistical methods*, CRC press, 1996.

71 R. Christensen, *Analysis of variance, design, and regression: Linear modeling for unbalanced data*, Chapman and Hall/CRC, 2018.

72 J. H. Bray and S. E. Maxwell, *Multivariate analysis of variance*, Sage, 1985.

73 M. J. Blanca, R. Alarcón, J. Arnau, R. Bono and R. Bendayan, *Behav. Res. Methods*, 2018, **50**, 937–962.

74 R. A. Alexander and R. P. DeShon, *Psychol. Bull.*, 1994, **115**, 308.

75 S. W. Huck and R. A. McLean, *Psychol. Bull.*, 1975, **82**, 511.

76 L. S. Kao and C. E. Green, *J. Surg. Res.*, 2008, **144**, 158–170.

77 W. P. Gardiner, *Statistical analysis methods for chemists: A software based approach*, Royal Society of chemistry, 2007.

78 V. V. Nalimov, *The application of mathematical statistics to chemical analysis*,

Elsevier, 2014.

79 I. A. Makaryan, E. A. Salgansky, V. S. Arutyunov and I. V Sedov, *Energies*, 2023, **16**, 2916.

80 H. Hojo, Y. Inohara, R. Ichitsubo and H. Einaga, *Catal. Today*, 2023, **410**, 127–134.

81 Y. Liu, Y. Zheng, D. Feng, L. Zhang, L. Zhang, X. Song and Z. Qiao, *Angew. Chemie*, 2023, **135**, e202306261.

82 M. S. Avila, C. I. Vignatti, C. R. Apesteguia and T. F. Garetto, *Chem. Eng. J.*, 2014, **241**, 52–59.

83 C. Resini, F. Catania, S. Berardinelli, O. Paladino and G. Busca, *Appl. Catal. B Environ.*, 2008, **84**, 678–683.

84 L. Chen, K. Zhu, L.-H. Bi, A. Suchopar, M. Reicke, G. Mathys, H. Jaensch, U. Kortz and R. M. Richards, *Inorg. Chem.*, 2007, **46**, 8457–8459.

85 M. W. Peters, P. Meinhold, A. Glieder and F. H. Arnold, *J. Am. Chem. Soc.*, 2003, **125**, 13442–13450.

86 H. Pobiner, *Anal. Chem.*, 1961, **33**, 1423–1426.

87 B. P. C. Hereijgers and B. M. Weckhuysen, *Catal. Letters*, 2011, **141**, 1429–1434.

Chapter 4: Catalytic and non-catalytic routes for the oxidation of ethylbenzene

4.1 Introduction

Partially oxidized hydrocarbons serve as crucial components in the production of plastics and synthetic fibers, while also playing a key role as intermediates in the synthesis of a wide range of everyday chemicals. These compounds are derived from natural gas and volatile petroleum fractions through processes of partial oxidation. Current partial oxidation methods utilize gas-phase or liquid-phase reactions with homogeneous catalysts, or involve catalysis occurring on solid surfaces. Due to the large scale of these processes, molecular oxygen is the only cost-effective oxidizing agent. However, when hydrocarbons react with oxygen molecules in the gas or liquid phase, or with activated oxygen species on solid catalysts, they typically produce a variety of products. As a result, maintaining selectivity in product formation continues to be a significant challenge. Therefore, this chapter primarily focuses on the oxidation of ethylbenzene which is widely used in various industrial processes, undergoes oxidation to produce valuable intermediates and end products such as 1-phenyl ethyl alkyl hydroperoxide (EBHP) and Acetophenone (AP) [1]. This chapter focuses on the investigation of catalytic systems using various metals such as Co, Mn, Fe, and others. The aim is to provide a deep understanding of how these metals perform in comparison to our chosen catalyst, which will be discussed in more detail in the next chapter. The initial stages of this study involved the ethylbenzene oxidation and, the determination of the activation energy of the ethylbenzene oxidation process to understand the reaction pathway. By understanding the reaction pathway, we can design catalytic systems for enhanced efficiency and selectivity.

Furthermore, many tests of transition metals and metal oxides as potential catalysts, along with testing different oxidising agents such as hydrogen peroxide (H_2O_2), tert-butyl hydroperoxide (tBHP), and molecular oxygen (O_2). The objective was to identify the most effective combination of catalyst and oxidant to promote the oxidation of ethylbenzene. Following these results, we studied the inhibitor effect in the ethylbenzene oxidation, and we have chosen 1-phenylethanol as a case study for this reaction.

4.1.1 Oxidation reaction of Ethylbenzene

When ethylbenzene undergoes oxidation, yielding various oxidized products, primarily, it yields acetophenone (AP) and 1-phenylethanol, as demonstrated in **Scheme 4.1**. The selective oxidation of the terminal carbon within the alkyl chain poses a challenge due to the stronger carbon hydrogen bond dissociation energy (98 Kcal mol^{-1}). Hence, the resulting products of terminal oxidation, as illustrated in **Scheme 4.2**, are not usually observed.

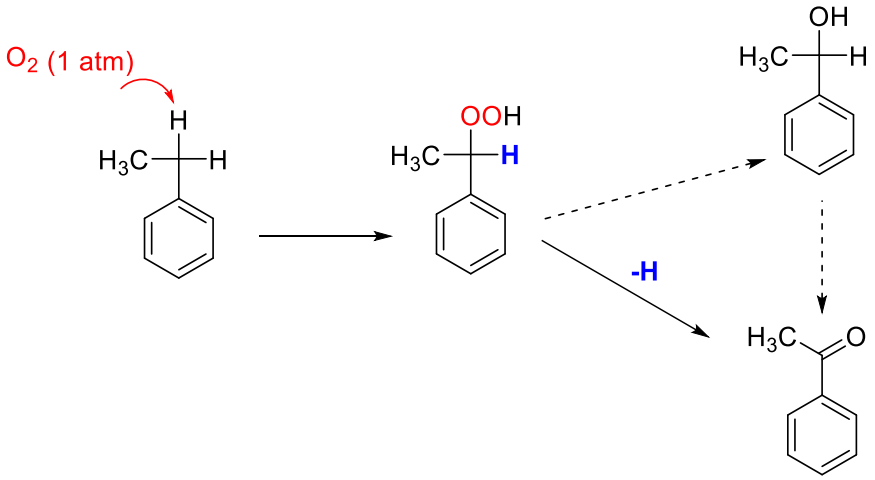

Scheme 4.1: A simplified pathway for the ethylbenzene oxidation to 1-phenyl ethyl alkyl hydroperoxide and this decomposes to acetophenone R=O and 1-phenylethanol R-OH.

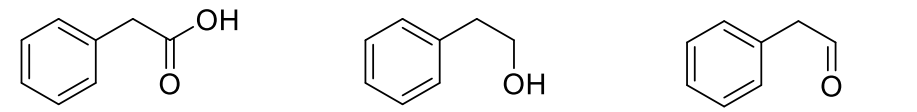

2-phenylacetic acid 2-phenylethan-1-ol 2-phenylacetaldehyde

Scheme 4.2: The products resulting from the terminal oxidation of the alkyl chain in ethylbenzene.

The selective oxidation of hydrocarbons is a process wherein hydrocarbons undergo conversion into specific oxygenated compounds only and ideally not considering CO_2, involving the breaking of a C-H bond. However, the typically high bond dissociation energy of the C-H bond (typically ranging from 295-470 kJ mol^{-1} [2-3] in hydrocarbons often necessitates the presence of a catalyst to facilitate the process by reducing the energy required for C-H bond dissociation, particularly under mild conditions such as

lower temperatures below 150°C and pressures below 10 bar [4-5] . In this scenario, it's important to note that hydrocarbon oxidation frequently exhibits low selectivity, leading to the production of significant waste and by-products. Introducing a catalyst proves advantageous as it enhances selectivity towards specific desired products or classes of products, thereby aiding in the advancement of energetically efficient and environmentally sustainable chemical processes. Heterogeneous catalysts typically comprise an active component, frequently a transition metal, along with a support and a promoter. The support plays a crucial role in influencing the catalyst's performance in several ways [6], such as preventing sintering or particle aggregation, influencing particle morphology and size, facilitating metal-support interactions, and storing oxygen to promote reactions [7]. The behaviour of support is determined by its intrinsic properties, such as basicity, surface area, and the presence of mixed oxidation states. From these perspectives, the support can exhibit a range of behaviours, varying from being chemically inert to acting as a promoter or inhibitor. Therefore, it is crucial to understand the distinct roles of the support in a specific model reaction independently from any metal nanoparticles. A comprehensive understanding of the support's effects on the reaction would enable clarity regarding the roles of doped metals in the oxidation process by comparison, which is essential for catalyst design. Metal oxides hold significant importance across various domains of chemistry, physics, and materials science [8-9], metal catalysts. This preference arises due to several factors: i) their enduring thermal and mechanical stability, which makes them suitable for prolonged usage and large-scale production, ii) the often-assumed pivotal role of high surface area in augmenting catalytic activity or facilitating the dispersion of deposited metal nanoparticles; and iii) the potential significance of oxygen vacancies in partial oxidation reactions, indicating different oxidation states [10-11]. Notably, the utilization of metal oxides in catalyst preparation represents a technologically advanced and economically crucial aspect. These oxides have been extensively applied in the formation of catalysts tailored for selective oxidation (such as cyclohexane and ethylbenzene), alkane oxidation, and selective dehydrogenation [12]. With the goal of innovating the discovery process for materials capable of selectively oxidizing hydrocarbons, our study investigated a variety of metal oxides with the intention of elucidating their capacity to improve selective hydrocarbon oxidation. Considering these factors, this chapter directs its attention towards exploring the catalytic capabilities of metal oxides such as Fe_2O_3, Mn_2O_3 and Cu_2O, MoO_3, Pt_2O and Ag_2O

and Cr_2O_3, widely recognized for their role as supports in hydrocarbon oxidation. This examination of the metal oxide's functions will serve as a groundwork for delving into the active metal, a discussion reserved for the next chapter.

4.1.2 Mechanism for the autoxidation of hydrocarbons

Autoxidation refers to the oxidation of hydrocarbons by means of using ground-state (triplet) molecular oxygen. This process generates organic hydroperoxide as primary intermediates through a radical chain pathway [13]. Enhancing the efficiency and selectivity of the selective oxidation of hydrocarbons using molecular oxygen is a significant industrial priority, aiming to produce valuable products. A notable example is the process where ethylbenzene converts into ethylbenzene hydroperoxide, serving as an important oxidising agent in the propylene oxide/styrene process, with an annual production of 5 million tons [14]. Understanding autoxidation mechanisms remains a big challenge due to their complexity. It's generally thought to involve a series of reactions where a ketone is formed (figure 4.3).

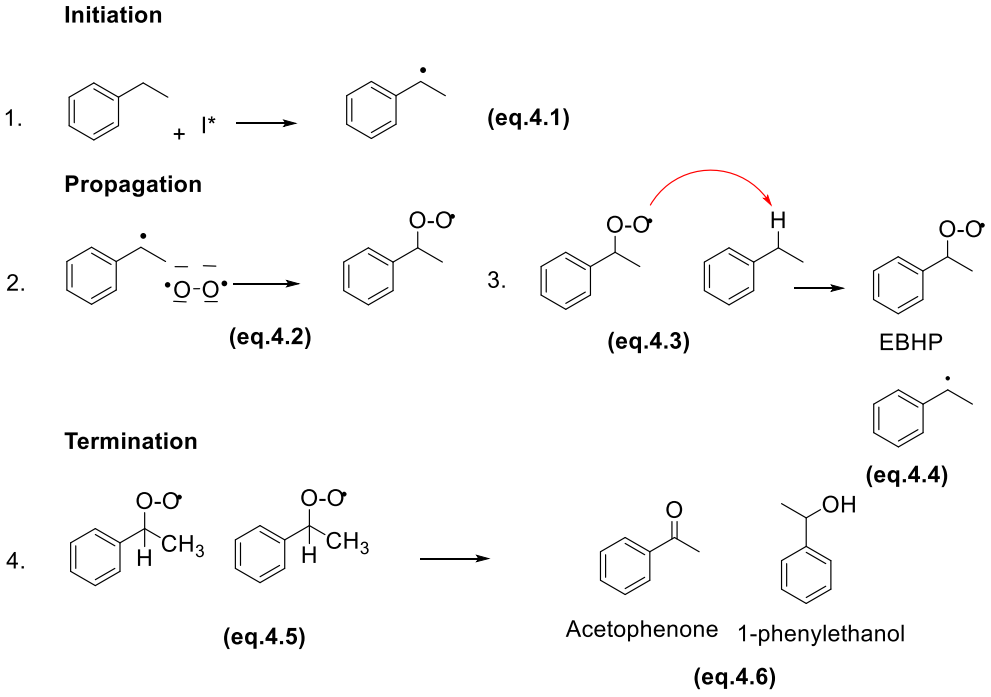

Figure 4.3: The autoxidation reaction mechanism proceeds in three key stages: initiation, propagation, and termination. In the initiation step, as shown in Equation 4.1, I* is an initiator, a low-energy C-H bond (such as in a CH_2 group) is broken, forming an alkyl radical (R•) and a hydrogen radical (H•). During propagation, the alkyl radical reacts with molecular oxygen (O_2) to form a peroxy radical (ROO•), which abstracts hydrogen from another hydrocarbon, generating a hydroperoxide (ROOH) and regenerating the alkyl radical, sustaining the chain reaction. Termination occurs when two radicals combine to form stable non-radical products, effectively stopping the reaction.

The oxidation of hydrocarbons, particularly when aiming for alcohols or ketones as target products like in ethylbenzene oxidation, tends to a lack of selectivity. This is because hydrocarbon oxidation often involves radical intermediates, particularly in non-catalytic processes. Once these radicals are generated, they readily react with molecular oxygen in an uncontrolled manner, producing a variety of by-products such as carboxylic acids and peroxides. This lack of selectivity in radical reactions leads to the formation of multiple undesired compounds. Therefore, ethylbenzene in Liquid-phase hydrocarbon oxidation produces hydroperoxide EBHP as the first products before alcohol and ketones (aldehydes) are formed as shown in (scheme 4.2). Alcohols and ketones are prone to oxidation, leading to the formation of acid and other by-products through degradation. This vulnerability stems from the high reactivity of α-hydrogen. Therefore, in the process of oxidizing hydrocarbons to alcohols and ketones, it's typically preferred to keep the conversion rate low to prevent the unwanted further oxidation of these products [15]. In light of these considerations, and to thoroughly assess the catalytic behaviours while optimizing the reaction conditions for the oxidation of ethylbenzene, we employed a diverse range of transition metal oxides in this study. Our initial experiments focused on the aerobic oxidation of ethylbenzene using Radleys reactors, where we carefully monitored how different catalysts influenced the reaction's selectivity and efficiency. As the study progressed, we shifted our attention towards studying the aerobic oxidation conditions of key intermediates formed during the reaction, such as 1-phenyl ethyl alkyl hydroperoxide (EBHP) and 1-phenylethanol. This choice was driven by the observation that selective formation of acetophenone (the desired product) was achievable under certain conditions. We also investigated the role of EBHP decomposition, which leads to the formation of both alcohol (1-phenylethanol) and ketone (acetophenone). A notable aspect of this process is that the alcohol can undergo further decomposition into acetophenone via radical reactions, highlighting the complexity of controlling product selectivity. To gain deeper insight into these transformations, we conducted a detailed investigation of the reaction pathways, focusing on how catalytic systems and reaction conditions could be fine-tuned to favour the formation of acetophenone while minimizing undesirable side reactions. By understanding the chemistry between these intermediates and the catalytic environment, we aimed to optimize the reaction for higher selectivity and yield of the desired ketone product.

4.2 Potential alternative oxidants for ethylbenzene oxidation

4.2.1 Hydrogen peroxide (H_2O_2)

H_2O_2 is commonly employed in liquid oxidation processes of organic compounds because of its environmentally safe and non-polluting characteristics [16-17]. From a chemical perspective, H_2O_2 is intriguing because its breakdown produces just one by-product, which is water. This unique characteristic lends the molecule an unmistakably eco-friendly quality. Therefore, we conducted an oxidation reaction for ethylbenzene using H_2O_2 as the oxidant, and the results compared to the reaction carried out with ethylbenzene alone without H_2O_2. This to study the ability of H_2O_2 to generate radical species, including hydroperoxyl and hydroxyl radicals, positions it as a promising oxidant and initiator for oxidation reactions. Given this potential, it is worthwhile to explore the outcomes of employing H_2O_2 under the specific oxidation conditions used for ethylbenzene. Surprisingly, no detectable activity was observed during the oxidation process. This lack of reactivity raises questions about the efficiency of H_2O_2 in this specific context. The underlying reasons for this inactivity will be examined in greater detail in section 4.5.2 of this chapter, where we will discuss the factors influencing the phase transfer and interaction dynamics of H_2O_2 with ethylbenzene and how these may contribute to the observed results.

4.2.2 Tert-butyl hydroperoxide (tBHP)

A key feature of radical reactions is that the reaction rate is contingent upon the initial concentration of the radical initiator [18]. Figure 4.4 demonstrates that by increasing the initial tBHP concentration (1.23×10^{-3} mol) to 5% and 10%, 20% the reaction rate increased dramatically at the beginning of the reaction. Indeed, at the higher tBHP amount the induction period reached a plateau. There was an increase in EB conversion with increasing tBHP added at a decreasing trend, from the graph, it can be seen that if more of tBHP is added, a plateau of conversion can be observed around 35%. As this increase is not linear per amount of tBHP and for 1 tBHP % the increase is already at 12% (i.e. >> 1%) this implies that tBHP act as a radical promoter in this reaction, the more tBHP present, the higher amount of radicals will be generated, however, larger volume of free radical will increase the reaction rate but also after certain limit, they will start to terminate each other and stop the reaction, leading to a plateau of conversion in the end.

In contrast, if a linear correlation between EB conversion and tBHP addition was observed, it would lead to a conclusion that tBHP act as an oxygen transfer agent, where conversion increased linearly based on the stoichiometric value.

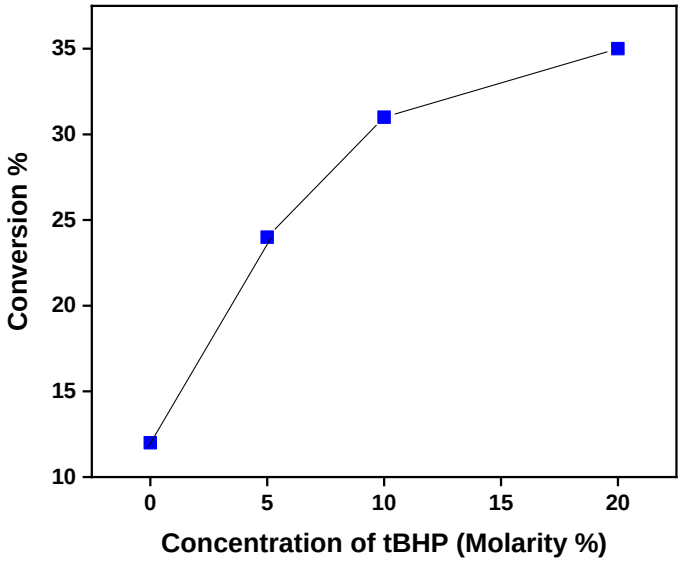

Figure 4.4: Effect of t-butyl hydroperoxide (tBHP) concentration on the conversion of ethylbenzene. The conversion increased with incremental additions of tBHP at concentrations of 5%, 10%, 15%, and 20%, eventually reaching a plateau at 35% tBHP concentration.

4.2.3 Oxygen (O_2)

Molecular oxygen (O_2) has been used in many studies to investigate oxidation reactions. Activation molecular O_2 presents a challenge compared to other oxidants due to the strength of the O–O bond. Nonetheless, there is a growing requirement to utilize environmentally friendly, cost-effective, and readily available oxidants such as molecular O_2 is increasing. The more easily activated nature of other oxidants makes them widely used. Typically, more harsh conditions, such as high temperatures are required to activate O_2. Developing an understanding of the activation mechanism and the interactions between O_2 , catalyst, and substrate would facilitate the creation of the system capable of activation O_2 [19-20]. The use of O_2 as an oxidant has been studied in this work and is better understood than other oxidant H_2O_2 and tBHP. Therefore, various oxidizing agents are frequently mentioned in the literature, with molecular oxygen (O_2), hydrogen peroxide (H_2O_2), and tert-butyl hydroperoxide (tBHP) being among the most common [21]. This oxidant has been questioned whether it acts as a radical initiator or promotes the autoxidation pathway. Each of these options has its

own advantages. Molecular oxygen is a well-established oxidant that is easily accessible and cost-effective. The presence of an O_2 source is essential for the oxidation of hydrocarbons into alcohols, aldehydes, and ketones. Other oxidant H_2O_2 has no toxicity; it is an inexpensive reagent. A great advantage of hydrogen peroxide is its ability to transfer oxygen atoms to substrates to produce water as a by-product [22-23]. In contrast to H_2O_2, the inclusion of the tBHP imparts organic characteristics to the molecule, enabling it to dissolve in both aqueous and organic substrates. However, the by-product generated from tBHP can be tert-butanol or methanol which can be reactive in the reaction and costly during separation process [24]. Frequently, the generation of a peroxide species serves as an initiate for oxidation, regardless of the oxidant employed. Consequently, certain reactions may exhibit comparable activity with different oxidants, whereas others will rely on the specific reagent utilized, along with variations in solvent, oxidant and catalyst [22]. Besides being oxidants, some species (H_2O_2 and tBHP) can also initiate radical reactions [25]. As a result of the homolytic cleavage of the molecule, radical species are formed, which can easily activate other molecules. Typically, these oxidants work through a radical mechanism. Controlling radical reactions poses significant challenges due to the nature of radical species, which are highly reactive, prone to chain reactions, sensitive to their surroundings, and susceptible to unwanted side reactions. Consequently, attaining selectivity and fine-tuning the conditions in radical-based chemistry demands a thoughtful approach, often involving advanced techniques and the use of specific catalysts to regulate radical activity efficiently. Thus, designing a catalyst that can effectively initiate the radical mechanism and control its propagation is of paramount importance in radical chemistry. The ability to manage the generation and activity of radical species directly impacts the selectivity and yield of desired products. Therefore, a thorough understanding of the reaction mechanisms occurring on the catalyst surface is essential for the development of new catalytic systems that can optimize these processes.

Radical reactions, particularly those involving the oxidation of hydrocarbons like ethylbenzene, can be significantly influenced by the choice of oxidant. Different oxidants can yield varying degrees of efficiency, selectivity, and reaction rates depending on the specific conditions under which the reaction takes place. For example, hydrogen peroxide (H_2O_2), tert-butyl hydroperoxide (tBHP), and molecular

oxygen (O_2) each exhibit unique properties and reactivity profiles that can affect the overall outcome of the oxidation process. By investigating the effectiveness of H_2O_2, tBHP, and O_2 in the oxidation of ethylbenzene, this study aims to identify the good conditions and catalytic systems that can maximize product yield while minimizing side reactions, alongside the use of various transition metal oxides, this study aims to identify the good conditions and catalytic systems that can maximize product yield while minimizing side reactions.

4.3 Oxidation using transition metal-based catalysts

Transition metal oxides are likely among the most fascinating categories of solids, exhibiting a diverse array of structures and properties [26-27]. The metal-oxygen bond can range from nearly ionic to strongly covalent or metallic. The distinct characteristics of transition metal oxides arise from the exceptional qualities of their outer d-electrons. The diverse range of electronic and magnetic properties exhibited by transition metal oxides is particularly remarkable. Thus, we discuss some of the important aspects of the properties of transition metal oxides of current interest [27] as shown in figure 4.5 and are commonly employed as supports for the fabrication of supported.

The following are some of the reasons that contribute to the unique characteristics of transition metal oxides that distinguish them from metallic elements, alloys, covalent semiconductors, and ionic insulators:The electronic bands of d-block transition element oxides are narrow due to the limited overlap between the metal d orbitals and oxygen p orbital (the bandwidths are typically of the order of 1 or 2 eV rather than 5 to 15 eV as in most metals). Secondly, electron correlation effects are significant, as anticipated due to the narrow electronic bands. The specific electronic structure of copper (Cu) in copper oxide (CuO) can be delineated using atomic-like states that correspond to its various oxidation states. In this context, copper can exist in several oxidation states, particularly Cu^{+}, Cu^{2+}, and Cu^{3+}. The electronic configuration for Cu^{+} is represented as [Ar] $3d^{10}$, indicating a fully filled 3d subshell. In contrast, the Cu^{2+} state exhibits an electron configuration of [Ar] $3d^{9}$, reflecting the removal of one electron from the 3d subshell. Further oxidation to Cu^{3+} results in a configuration of [Ar] $3d^{8}$, where two electrons have been removed from the 3d subshell. This variation in electronic configuration among the oxidation states of copper plays a critical role in determining the catalytic and electronic properties of copper oxide materials, influencing their behavior in various chemical processes. Finally, oxygen's ability to polarize is crucial. In solids, variations in oxygen states, like O^{-1}, are significant, influencing platonic and bipolaronic effects, allowing mobility and correlation in oxygen holes [28]. Therefore, given these unique properties of transition metals, we selected a range of transition metal catalysts for the oxidation of ethylbenzene. This selection included not only metal oxides but also non-hydrated and hydrated metal complexes. The diverse electronic structures and reactivity profiles of these transition metal

catalysts offer a promising path for enhancing the selectivity and efficiency of the oxidation process. By applying these catalysts in our study, we aim to explore their effectiveness and understand their roles in facilitating the conversion of ethylbenzene into desired products, thereby advancing our knowledge in the field of catalysis and radical chemistry.

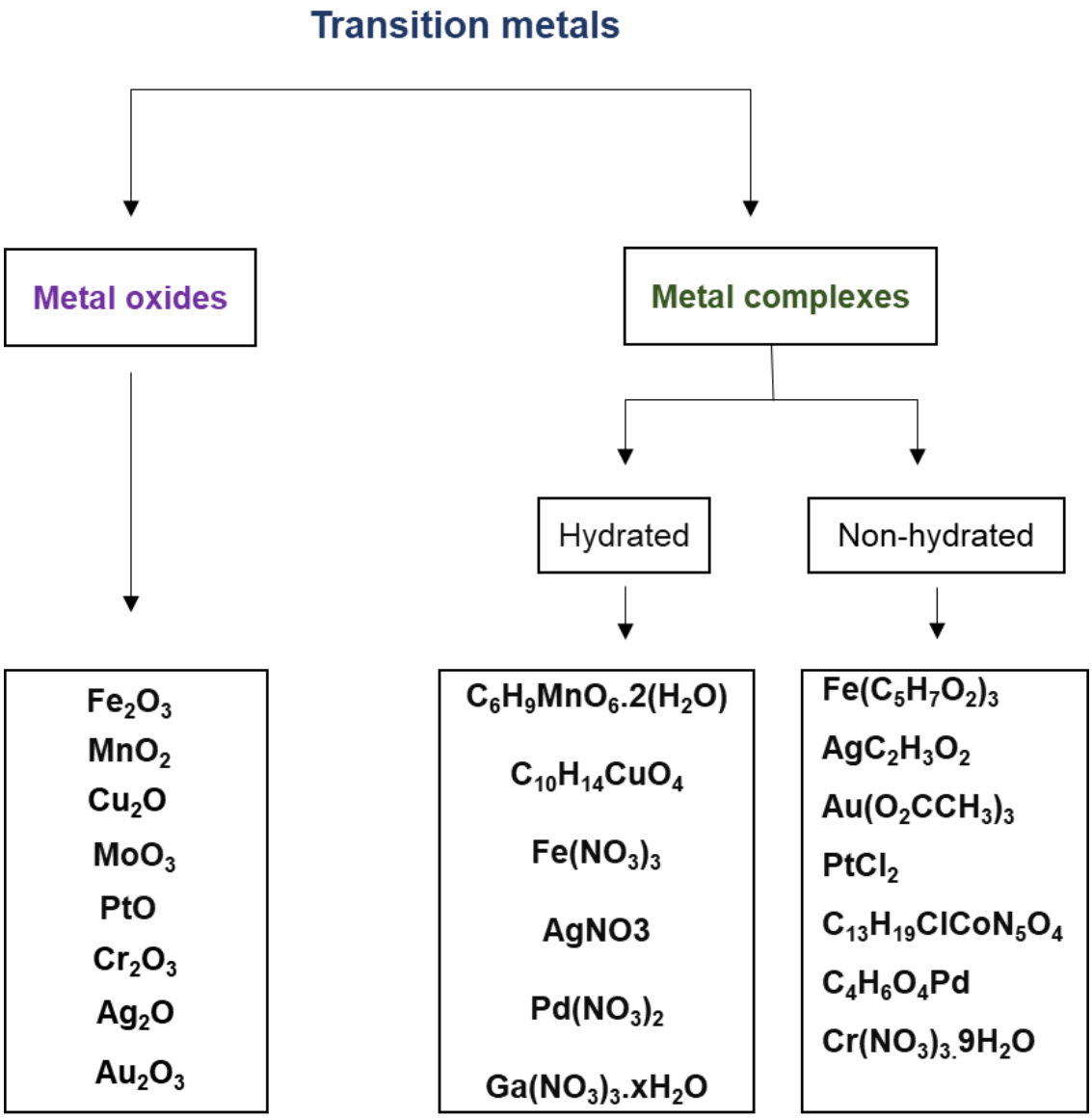

Figure 4.5 Selection of Transition Metals as Catalysts for Ethylbenzene Oxidation: This study explores a various array of transition metal catalysts for the oxidation of ethylbenzene, focusing on three key categories: metal oxides, non-hydrated metal complexes, and hydrated metal complexes.

4.4 Investigation of key variables in the oxidation reaction of Ethylbenzene

Understanding the key variables influencing the oxidation reaction of ethylbenzene is crucial for optimizing reaction conditions and improving product yields. The effectiveness of oxidation processes is often determined by a variety of parameters, and this section focuses on the investigation of several critical factors that affect the oxidation of ethylbenzene. Among these parameters are reaction conditions such as atmospheric pressure, temperature, and reaction time, all of which play significant roles in determining the reactivity and selectivity of the reaction. In particular, the use of an open-air system facilitates atmospheric pressure conditions, which can significantly impact the reactivity of ethylbenzene during oxidation. Temperature is another parameter that plays a crucial role in the catalytic process. It is one of the most influential factors affecting the equilibrium constant and the overall kinetics of the reaction. Specifically, the initiation step in hydrocarbon oxidation is significantly influenced by temperature, as higher temperatures generally increase reaction rates by providing the necessary energy to overcome activation barriers. Therefore, variations in temperature can change the reaction kinetics, yielding valuable insights into the activation energy required for the oxidation of ethylbenzene. By systematically studying the impact of temperature on the reaction, we aim to identify optimal conditions that enhance product formation. Moreover, the investigation of autoxidation in the absence of any catalyst serves as a baseline reaction for comparison with catalytic activity. This allows us to determine the intrinsic reactivity of ethylbenzene under varying conditions and evaluate the effectiveness of different catalysts. Additionally, the impact of reaction time on the oxidation process is examined to gain insights into the kinetics of ethylbenzene oxidation. To determine whether the reaction operates under a kinetic or diffusion regime, variations in stirring speed and the metal-to-substrate ratio were systematically implemented. For important comparisons between different catalysts to be valid, the system must remain within a kinetic regime; otherwise, mass transfer limitations may hinder the diffusion of the substrate to the catalyst's surface, which could subsequently impact the selectivity of the reaction. Once the optimal parameters are established, they will be fixed, allowing for the investigation of additional factors such as the weight percentage of the metal, the type of metal employed, the nature of the support material.

4.4.1 Effect of the temperature and time on autoxidation of ethylbenzene

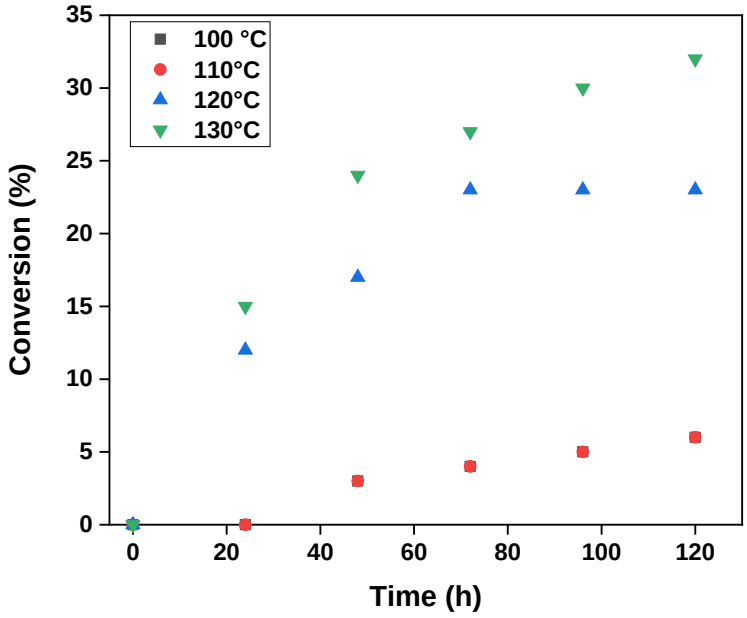

Figure 4.6: the conversion of ethylbenzene 3 mL without catalysis as background for this study, with temperature range 100°C and 110°C and 120°C to 130°C with different time started from 24h,48h and 72h and 96h ,120h, at a stirring rate 600 rpm, *p* = ambient.

The oxidation of alkanes under solvent-free, mild conditions presents significant challenges [29]. A temperature range of 110 °C to 140 °C was investigated. As illustrated in Figure 4.6, the blank test for ethylbenzene exhibited a conversion rate comparable to zero between 100 °C and 110 °C. Notably, at 120 °C, the conversion increased significantly to 9 ± 4 with a 1:1 ratio of K/A, which aligns with a radical pathway mechanism. Additionally, the reaction at 130 °C demonstrated a slight increase in conversion, reaching 20 ± 2. The data exhibit a sigmoidal trend characterized by an initial low gradient followed by a rapid increase in conversion, a pattern frequently observed in oxidation reactions [30-31]. This behaviour suggests that temperature acts as a significant limiting factor in the process. Therefore, using 130°C it is not favoured for this study due to its proximity to the boiling point of EB (136°C), potentially leading to evaporation, which could impact the catalytic study. Moreover, introduce the element of time is very crucial for studying whether the radical pathway progresses to completion. However, the data does not demonstrate any complete conversion, which could be attributed to other factors influencing the oxidation, such as inhibitors. More dissection of the inhibitory effects is provided in section 4.6. In every case, NMR measurements showed that the carbon mass balance was greater than 95% suggesting that there was no appreciable loss of volatile chemicals.

4.4.2 Blank test of ethylbenzene and activation energy

As outlined in this chapter, a range of reaction conditions and catalysts have been investigated for the oxidation of Ethylbenzene. High temperatures and radical initiators are commonly employed to activate the radical mechanism. Additionally, the comparison between O_2 as an oxidant and H_2O_2 and tBHP has been presented. Therefore, based on the data and results obtained in figure 4.3, we have determined that 120°C is the optimal temperature for this study. Temperatures above 120°C were not employed due to their proximity to the boiling point of ethylbenzene, which constrained any further temperature increases to avoid any potential losses of volatile compounds. Moreover, the standard reaction time of 24 hours is employed, primarily due to the slow reaction rates and extended induction periods.

In order to create a baseline for catalyst activity, oxidation studies were conducted to study the autoxidation of ethylbenzene. It was found that there was little to no conversion as shown in table 4.1.

Table 4.1 Ethylbenzene (EB) 99.8 % autoxidation in the absence of catalysis with magnetic stirring (600rpm) and 120 °C, 24 h, the products are Acetophenone (AP), 1-phenylethanol (1-Ph) and 1-phenyl ethyl hydroperoxide (EBHP).

Blank test	Conversion (%)	Observed selectivity (%)			CMB (%)
		AP	1-Ph	EBHP	
Ethylbenzene 99.8%	9 ± 3	10 ± 2	7 ± 1	85 ± 3	100± 2

The control test is very important because in the absence of autoxidation, the catalyst must exhibit optimal activity at 120 °C under atmospheric conditions. However, it is important to acknowledge that this is a challenging and ambitious target, as 120 °C is considered relatively low for the oxidation of saturated hydrocarbons. Furthermore, the degree and product distribution of autoxidation play a significant role in this context. If a catalyst demonstrates inactivity at lower temperatures yet exhibits changes in selectivity when compared to autoxidation conditions conducted without a catalyst, it indicates that the catalyst still influences the reaction.

The activation energy for the oxidation of ethylbenzene has been determined to be 36 kJ/mol. This parameter is essential as it represents the minimum energy required for the reaction to proceed, significantly influencing the reaction kinetics. To illustrate this concept, an Arrhenius plot can be constructed, displaying the natural logarithm of the reaction rate constant (ln k) against the inverse of the temperature (1/T) as shown in figure 4.6. The slope of this plot, derived from the Arrhenius equation, confirms the calculated activation energy value of 36 kJ mol^{-1}, demonstrating how temperature affects the rate of reaction. One main goal of kinetic analysis involves quantifying how the reaction rate changes with temperature. Typically, this parameter is explained using the Arrhenius activation energy [32] as shown in eq. 1.11 in chapter 1.

$$k = Ae^{\frac{-Ea}{RT}} \qquad (eq\ 1.11)$$

The activation energy for the ethylbenzene reaction (Figure 4.7) came out to be 36 ± 2 kJ mol^{-1} which is in agreement with the typical values range mentioned in many studies to be in range 26-43 KJ mol^{-1} [33-34].

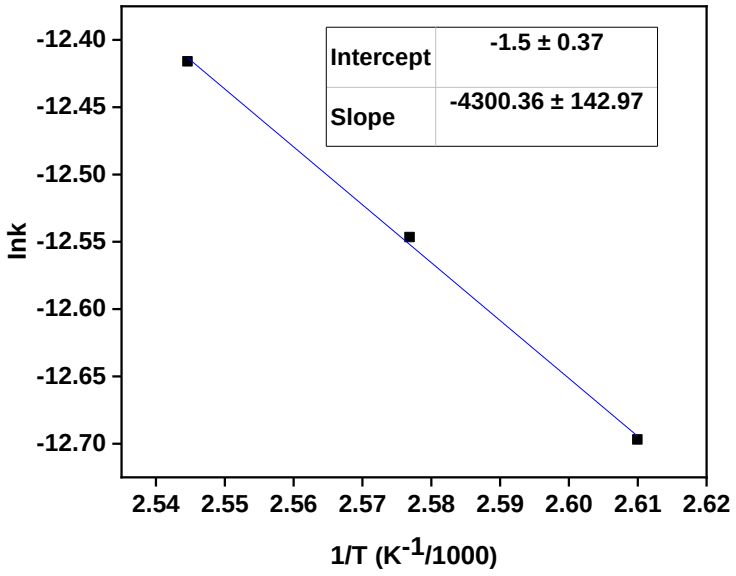

Figure 4.7: the reaction diagram illustrates the concept of activation energy with the ethylbenzene, determined to be 36 KJ mol^{-1} for this reaction, represents the energy barrier that must be overcome for the reaction to proceed.

For a reaction to take place, the relative translational motion of the reactants must overcome the activation energy, which is the height of the energy barrier [32].

4.4.3 Control test for ethylbenzene oxidation using metal oxide, complexes and salt

Many attempts have been undertaken to develop new catalytic systems for the mild oxidation of ethylbenzene, aiming for enhanced efficiency, selectivity. Given the importance of ethylbenzene as a precursor in various industrial processes as mentioned earlier in this chapter, finding efficient catalytic pathways for its oxidation under mild conditions has remained a significant area of research. Traditional methods often rely on harsh reaction conditions, high temperatures, and toxic reagents, which underscore the need for more benign and cost-effective alternatives. In this section, we apply several metal oxides, metal complexes, and salts as control tests to evaluate their effectiveness in promoting the oxidation of ethylbenzene under controlled, mild conditions. This preliminary screening of materials serves as a foundational step before developing a catalytic methodology. By conducting these control tests, the objective is to identify which of these materials, or combinations thereof, exhibit catalytic activity, and to assess their potential to activate ethylbenzene and facilitate its oxidation.

Table 4.2: Ethylbenzene oxidation at 120 °C, 24 h using various metal oxide arranged in order of their placement on periodic table and all CMB of reactions consistently equal to 100%.

Metal Catalyst (periodic table group)	Conversion (%)	Observed selectivity (%)		
		EBHP	AP	1-Ph
Cr_2O_3 (6)	4 ± 2	-	-	-
MoO_3 (6)	0	-	-	-
Mn_2O_3 (7)	19 ± 3	47 ± 3	19 ± 1	34 ± 1
Fe_2O_3 (8)	11 ± 3	46 ± 2	18 ± 8	39 ± 9
Pt_2O (10)	2 ± 1	0	0	0
Ag_2O (11)	36 ± 1	78 ± 2	19 ± 2	4 ± 2
Cu_2O (11)	13 ± 5	51 ± 1	23 ± 2	24 ± 2

Table 4.3: Ethylbenzene oxidation at 120 °C 24 h using different metal complexes and all CMB of reactions consistently equal to 100%. The metal is sorted by the group number of the metal in periodic table group.

Metal Catalyst (periodic table group)	Conversion (%)	Observed selectivity (%)			
		AP	1-Ph	EBHP	other
$C_6H_9MnO_6 \cdot 2H_2O$ (7)	32 ± 2	57 ± 2	29 ± 2	4 ± 1	9 ± 1
$Fe(NO_3)_3$ (8)	31 ± 2	62 ± 1	26 ± 1	3 ± 1	10 ± 1
$Pd(NO_3)_2$ (10)	6 ± 1	31 ± 1	23 ± 1	16 ± 1	30 ± 1
$C_{10}H_{14}CuO_4$ (11)	5 ± 2	21 ± 1	11 ± 2	42 ± 3	24 ± 1
$AgNO_3$ (11)	23 ± 1	36 ± 10	26 ± 11	36 ± 11	-

Table 4.4: ethylbenzene oxidation at 120 °C 24 h using salt and all CMB of reactions consistently equal to 100%. The metal are sorted by the group number of the metal in periodic table group.

Metal Catalyst (periodic table group)	Conversion (%)	Observed selectivity (%)			
		AP	1-Ph	EBHP	Other
$Cr(NO_3)_3.9H_2O$ (6)	36 ± 1	70 ± 1	14 ± 1	11 ± 3	2± 1
$Fe(C_5H_7O_2)_3$ (8)	20 ± 1	47 ± 1	26 ± 2	10 ± 2	15 ± 1
$C_{13}H_{19}ClCoN_5O_4$ (9)	21 ± 1	74 ± 2	20 ± 2	5 ± 1	-
Pd (II) acetate (10)	35 ± 1	42 ± 1	0	0	57± 1
$PtCl_2$ (10)	2 ± 1	21 ± 1	-	42 ± 3	30 ± 1
$AgC_2H_3O_2$ (11)	27 ± 1	72 ± 1	23 ± 1	4 ± 1	7±1
$Au(C_2H_3O_2)_3$ (11)	2 ± 1	56 ± 5	47 ± 7	-	-

In table 4.2, the use of metal oxide in ethylbenzene oxidation indicated zero conversion for group 6 metals, suggesting their inability to activate ethylbenzene. On the other hand, by moving to groups 7, 8 and 10 activity was observed; however, it is identical with blank test results of ethylbenzene as shown in table 4.1 section 4.4.2. We also studied ethylbenzene oxidation with group 11 metals and a good result was obtained by using silver. At the same conditions, Ag showed activity by decomposing the EBHP, resulting in the generation of AP with a 36% conversion rate and 78% selectivity towards AP. This is mean that the Ag favouring the abstraction of hydrogen from ethylbenzene, which constitutes the initial step of the oxidation process. All in all, the

analysis offers insight into the performance of various metal catalysts. The result obtained for Mn, Fe and Co for metal complexes and salt, showed a high activity that comes from the leaching of the metal into the solution. The observed catalytic activity is mainly due to the homogeneous species. Moreover, best result was obtained with Ag and more to follow about silver behaviour by next chapter.

4.5 Effect of different oxidants on ethylbenzene oxidation with different catalyst

4.5.1 Ethylbenzene oxidation with H_2O_2 and tBHP as oxidant

Ethylbenzene oxidation was studied with H_2O_2 using set of catalysts (metal oxide, complexes metal oxide) same metal observed in section 4.4. In all cases, H_2O_2 as oxidant was not active compared to tBHP. H_2O_2 seems to have for most cases a solubility limit in organic phase (more details in next section 4.5.2). Hence, we can conclude that H_2O_2 is not a good oxidant agent for ethylbenzene oxidation, and therefore was not used in this study.

Following the discussion in section 4.2.2, tBHP has been tested in the same condition using different concentrations of 1%, 5%, and 10% with an addition of metal oxide. The resulting conversion was plotted against the molar ratio of substrate to tBHP, as illustrated in the figure 4.1. An increase in ethylbenzene (EB) conversion was observed with the addition of tert-butyl hydroperoxide (tBHP), as depicted in Graph 4.1. The data indicate that as more tBHP is introduced into the reaction mixture, the conversion of ethylbenzene rises correspondingly. However, beyond a certain limit of tBHP addition, the conversion appears to reach a plateau at approximately 35%. This plateau suggests that the reaction may be experiencing a saturation effect, where the concentration of reactive radicals becomes sufficiently high. At this point, the radicals in the system can begin to recombine and terminate each other, thereby inhibiting further reaction progress. Based on these results, we proceeded to investigate the catalytic activity of Fe_2O_3 and Ag_2O under the same conditions and molar ratios. The results for Fe_2O_3 are illustrated in figure 4.8, while those for Ag_2O are shown in Figure 4.9. In the oxidation of ethylbenzene using Fe_2O_3, the conducted experiments revealed negligible activity at both 1% and 5% concentrations in terms of conversion, aligning closely with the results obtained from the blank test. Similarly, when Ag_2O was

employed in conjunction with tBHP, the results indicated minimal catalytic activity, with the conversion rate remaining below 35%. These findings suggest that neither Fe_2O_3 nor Ag_2O significantly enhances the oxidation of ethylbenzene under the tested conditions, indicating a need for further exploration of alternative catalysts to improve reaction efficiency.

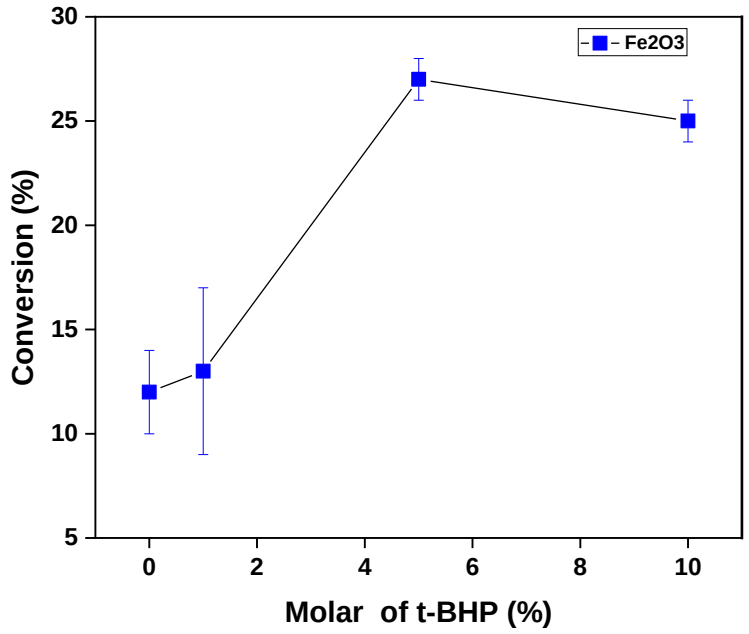

Figure 4.8: ethylbenzene oxidation at 120 °C 24 h using Fe_2O_3 with an addition of tBHP, range 0%, 1% and 5%, 10%.

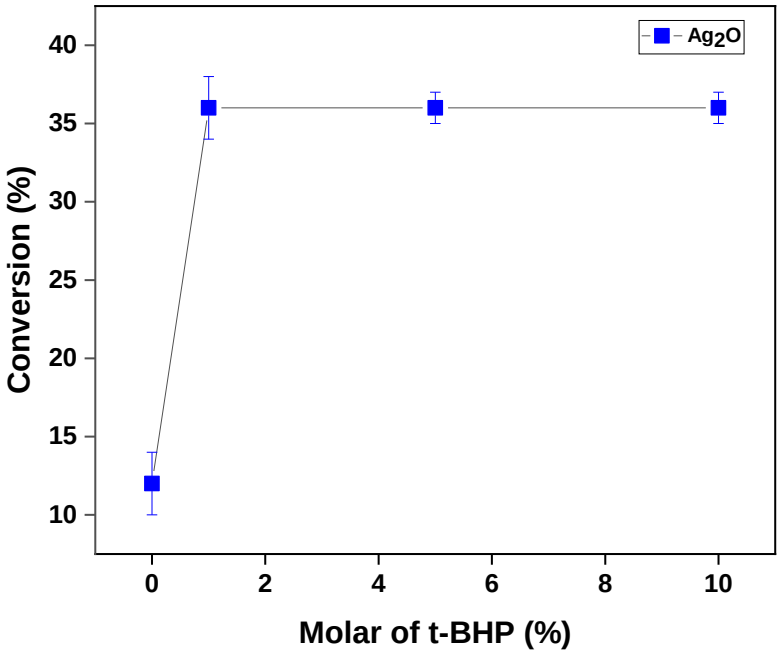

Figure 4.9: ethylbenzene oxidation at 120 °C 24 h using Fe_2O_3 with an addition of tBHP, range 0%, 1% and 5%, 10%.

4.5.2 Phase transfer of H_2O_2 and tBHP

The oxidation of ethylbenzene utilizing H_2O_2 and tBHP as oxidants has revealed significant insights into the phase transfer dynamics and their implications for reaction efficiency. Therefore, this lack of observable impact from the hydrogen peroxide prompted us to further investigate its role in the reaction. To confirm the influence of H_2O_2, we performed additional experiments as described in chapter 2, section 2.10. The preceding results indicate that the transfer of H_2O_2 from the aqueous phase to the organic phase of ethylbenzene was notably limited, which has profound implications for the oxidation reaction. Despite various attempts to enhance the transfer of H_2O_2, including stirring conditions and variations in temperature, the NMR data suggested minimal interaction between H_2O_2 and ethylbenzene, particularly at room temperature. This lack of effective phase transfer underlines a critical limitation in utilizing H_2O_2 as an oxidant in this reaction. The inefficacy of H_2O_2 to migrate into the organic phase implies that its potential as a radical initiator is severely restricted, which likely contributes to the observed low conversion rates of ethylbenzene during oxidation. Conversely, tBHP demonstrated a more favourable performance, as indicated by the increased conversion of ethylbenzene with its addition. However, results also highlighted that beyond a certain concentration of tBHP, a plateau in conversion was reached, suggesting that excessive tBHP could lead to radical termination and reduced reactivity. This phenomenon emphasizes the delicate balance required in optimizing tBHP concentrations to enhance radical generation without leading to diminished reaction rates.

4.6 Effect of an alcohol in ethylbenzene oxidation

4.6.1 Overview

By adding small quantities of some compounds, such as inhibitors, oxidation is retarded. The impact of inhibitors on chain reaction can be generally defined by their molecules reacting with reactive free radicals, replacing them with less active ones, or even trapping them, and thus ultimately slowing down the chain process. In general, radical X● can react with hydrocarbon RH and give rise to a free radical:

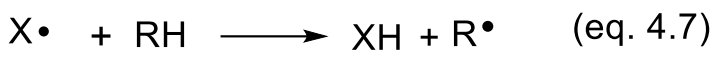

(eq. 4.7)

(eq. 4.8)

If the X● radical, derived from the inhibitor, is inactive, then for a reaction to proceed, it must interact with another species. Most inhibitors in this type of reaction operate by reacting with the ROO● radicals, which are considered the primary chain carriers. This interaction initiates the reaction but halts further chain propagation. Even with a significant addition of a weak inhibitor, the reaction will continue at a certain rate due to the role of X● radicals in sustaining the chain propagation [35]. To investigate the potential of 1-phenylethanol as an inhibitor, we first conducted reactions without it as a benchmark. We examined its inhibitory effects on reactions such as ethylbenzene, followed by additional experiments where we introduced 1-phenylethanol at concentrations of 1%, 5%, and 10% in the presence of 1 atm of air during the ethylbenzene reaction. These results were compared to control tests that included only 1-phenylethanol. The result does not show any difference between EB blank tests (table 4.1) comparing with the addition of 1-phenylethanol. As such, the results revealed no significant difference between blank test of ethylbenzene and the inclusion of 1-phenylethanol as an additive. Moreover, we carried out more investigation using a variety of metal oxide and metal complexes and salt with the ethylbenzene oxidation.

4.6.2 Investigation of 1-phenylethanol inhibitory role in the oxidation of ethylbenzene

The impact of inhibitors (antioxidants) on hydrocarbon oxidation, particularly during the initiation steps, also plays a role in the termination of the reaction. This effect depends on whether enough free radicals (chain initiators) are produced to counteract the chain-breaking action of the inhibitor. Experimental evidence supports the idea that the effect of inhibitors is relative rather than absolute. For instance, compounds like phenols or alcohols, which prolong the initiation inhibition phase, may have minimal influence on a reaction that has already reached a steady state [36]. As discussed earlier, 1-phenylethanol is one of the by-products formed during the oxidation of ethylbenzene. To determine whether 1-phenylethanol acts as an inhibitor in this reaction, an investigation was conducted to assess its potential inhibitory effect. A blank test of ethylbenzene oxidation was first performed without any added 1-phenylethanol, providing a baseline for comparison. The conversion rate of ethylbenzene in the blank test was measured at 9 ± 4%, and this value was used as the reference point for all subsequent comparisons. To investigate the inhibitory role of 1-phenylethanol, varying concentrations (5%, 10%, and 20% molar ratio) of alcohol were added to ethylbenzene, and the oxidation reaction was carried out under identical conditions. The reaction was run for 24 hours, after which samples were collected and analyzed using NMR spectroscopy. Upon completion of the reactions and analysis of the NMR data, no significant differences were observed when comparing the results to the blank test conducted with ethylbenzene alone, without any catalyst. This indicates that the presence of alcohol, at the concentrations tested, does not appear to significantly inhibit the oxidation of ethylbenzene under the experimental conditions employed.

The blank test showed a conversion of ethylbenzene at 9 ± 4%, which aligns with the results presented in table 4.5. This suggests that alcohol does not significantly inhibit the oxidation reaction. However, the fact that the reaction did not proceed to full completion indicates that while alcohol may not be a strong inhibitor, it could still have a minor inhibitory effect, reducing the overall efficiency of the reaction without fully preventing it.

Table 4.5: Outlines the trials where 3 mL of ethylbenzene were mixed with different concentrations (5%, 10%, and 20%) of 1-phenylethanol for 24 h 120 °C 600rpm.

Trial	Ethylbenzene (mL)	1-phenylethanol molar concentration (%)	EB Conversion (%)
1	3	5	8 ± 1
2	3	10	12 ± 1
3	3	20	12 ± 1

4.6.3 1-phenylethanol blank test

The alcohol blank test plays a crucial role in this study, serving as an essential baseline for understanding the reaction pathways involved in the oxidation of ethylbenzene. During the oxidation process, both 1-phenylethanol and acetophenone are typically formed as intermediates or products. As previously described in scheme 4.1, 1-phenylethanol can be further oxidized to acetophenone, providing an additional pathway in the reaction mechanism.

The alcohol blank test is particularly important because it allows us to study the behaviour of 1-phenylethanol in the absence of other reagents or catalysts. This, in turn, helps us evaluate whether the conversion of 1-phenylethanol to acetophenone occurs naturally under the reaction conditions or requires catalytic assistance. Understanding the factors affecting this conversion is critical for designing efficient catalysts that can promote the desired transformation while avoiding unwanted side reactions. Moreover, since the ultimate goal of catalytic development is to achieve high selectivity toward a specific product, in our case acetophenone, the insights gained from this blank test will guide the optimization of catalyst design. Under the selected experimental conditions (120 °C for 24 hours), the blank test for 1-phenylethanol revealed that the conversion was effectively zero. This indicates that, in the absence of a catalyst, 1-phenylethanol does not exhibit significant activity towards the formation of acetophenone. This result will serve as a benchmark for evaluating future reactions of 1-phenylethanol with various metal oxides, metal complexes, and salts, establishing a clear baseline for comparison.

4.6.4 1-phenylethanol oxidation using metal catalysts

The possible pathway that can be taken during the oxidation of 1-phenylethanol is that 1-phenylethanol can be converted to acetophenone by an acid-base reaction at OH level, then an H removal to the C in alpha (figure 4.10) or can be undertake other pathway (dehydration) of the alcohol by removing water to form styrene.

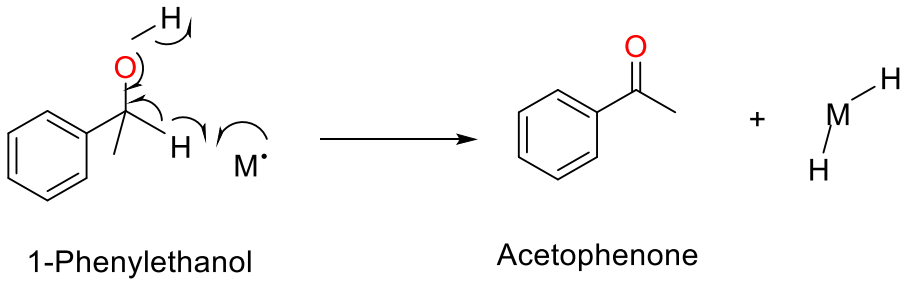

Figure 4.10: Possible H-abstraction route for 1-phenylethanol: forms acetophenone and water if M represents an oxygen species, or a hydride if M is a metal.

Therefore, many metals have been investigated in this study. Understanding this pathway is crucial for the final yield of acetophenone derived from the oxidation of ethylbenzene (EB). Consequently, understanding this process adds value to designing catalysis that selectively produces acetophenone without being influenced by alcohol. Therefore, to design a catalyst that is selective for the desired product, we investigate the oxidation of 1-phenylethanol over various metals from different periodic groups, as illustrated in table 4.7. These different periodic groups exhibit varying activities in oxidation reactions, highlighting the importance of selecting the appropriate metal for catalytic processes. The results indicate that the metal catalysts employed from periodic groups 6, 7, 8, and 9 exhibit negligible activity in the oxidation of 1-phenylethanol, with the exception of Co and Cr. Both of these transition metals demonstrated notable catalytic activity, leading to the conversion of 1-phenylethanol to acetophenone. Specifically, the conversion rates observed for these metals fall within the range of 22% to 33%. The lack of activity observed in the majority of the other metal catalysts is advantageous for our conditions, suggesting that these metals do not facilitate the necessary reaction pathways for the conversion of 1-phenylethanol to acetophenone. Understanding this selectivity is crucial for determining the final yield and selectivity of acetophenone, as it indicates that the reaction does not proceed along alternative pathways that could convert the alcohol into acetophenone. On the other hand, platinum group metals Pd and Pt take different routes. The high

conversion present (more than 60%) comes from dehydrogenation of alcohols to ethylbenzene, which is endothermic and reversible (in the presence of excess of water) [37] . Although the role of noble metals may not be central to the current investigation, the insights gained from their inactivity can be valuable for future research undertakings. Understanding the different catalytic behaviours of various metal groups can inform the development of new catalytic systems for alternative reaction pathways or different catalytic applications in future studies. In contrast, the noble metals Ag, Au, and Cu demonstrate negligible activity in the oxidation of 1-phenylethanol, as shown in Table 4.7. This lack of activity is particularly significant for this study, as it indicates that these metals do not participate in the abstraction of hydrogen from alcohol, resulting in zero conversion to acetophenone. As our primary focus in this study is on Ag, it is important that this noble metal did not participate in the abstraction of hydrogen from alcohol, resulting in zero conversion to acetophenone. Moreover, silver it is more selective to radical pathways than acid base. This finding is significant for the design of effective catalytic systems, as it highlights the limitations of silver in promoting the desired oxidation reactions. The inability of silver to facilitate the conversion of 1-phenylethanol into acetophenone indicates that alternative catalytic strategies may be necessary when utilizing this metal. Understanding the specific catalytic behavior of Ag is essential for optimizing its application in catalysis, particularly in oxidation reactions. The lack of activity observed in this study may suggest that silver’s unique electronic and structural properties do not favour the reaction pathways required for effective hydrogen abstraction from alcohols. Further discussion regarding the characteristics and potential applications of silver as a catalyst will be provided in the next chapter.

Table 4.7: Oxidation of 1-phenylethanol (3 mL) at 120 °C for 24 h, 600 rpm, using different metal oxides categorized by their respective groups in the periodic table. The metal is sorted by the group number of the metal in periodic table group.

Metal oxide (Periodic table group)	**EB Conversion %**
$Cr(NO_3)_3.9H_2O$ (6)	33 ±1
Cr_2O_3 (6)	33 ±1
MoO_3 (6)	1 ±1
$MoO_3.H_2O$ (6)	11 ±1
MnO_2 (7)	1 ±1
Fe_2O_3 (8)	1 ±1
$C_{13}H_{19}ClCON_5O_4$ (9)	22 ± 1
Pd II acetate (10)	99 ± 2
$C_{10}H_{14}CuO_4$ (11)	2 ± 1
$AgNO_3$ (11)	0
Ag_2O (11)	0
Cu_2O (11)	0

4.7 Conclusion

This study has provided valuable understandings into the selective partial oxidation of ethylbenzene to acetophenone and 1-phenylethanol, focusing on improving reaction conditions and identifying key pathways. By investigating the effects of various reaction times and temperatures, we were able to better understand the radical-driven oxidation mechanism and determine the optimal conditions for ethylbenzene oxidation which were found to be 120 °C 24 h. Control tests with 9 ± 4 % conversion were utilized as a baseline for comparison, ensuring accurate assessment of the experimental results. A detailed analysis of potential oxidants including oxygen, hydrogen peroxide (H_2O_2), and tBHP, revealed that oxygen was the primary active oxidant in the reaction. In contrast hydrogen peroxide (H_2O_2) did not participate in the reaction mixture. This was attributed to the phase transfer limitations of H_2O_2, which failed to migrate into the ethylbenzene phase, thus explaining its negligible impact on ethylbenzene conversion. In contrast, tert-butyl hydroperoxide (tBHP) was shown to act as an effective radical promoter in the oxidation process. The results confirmed that increasing the concentration of tBHP led to the generation of more radicals, enhancing the reaction rate. However, after reaching a certain limit, excess radicals began to terminate each other, ultimately leading to a plateau in conversion. Based on these observations, oxygen (O_2) was selected as the preferred oxidant for further investigations. Following the identification of the most suitable oxidant, we extended our research to the use of different metal oxides, metal complexes, and salts to act as catalysts. All of these metals except Ag did not exhibit promising activity toward the activation of the C–H bond in ethylbenzene (EB) or the decomposition of 1-phenyl ethyl alkyl hydroperoxide (EBHP), as explained. Most of them leached into the solution and acted as homogeneous catalysts, which is not the focus of this work. The catalytic activity varied across the different metals, with particular interest in Ag, which demonstrated significant activity. This finding holds significant potential and will be further explored in the following chapter to provide a deeper understanding of Ag's role in catalysing ethylbenzene oxidation. Additionally, an investigation into potential inhibitory factors, specifically the role of 1-phenylethanol, revealed no substantial inhibitory effects on the oxidation process. While minor inhibitory effects cannot be entirely ruled out, their influence appears to be negligible under the experimental conditions. Additionally, since 1-phenylethanol is one of the key by-products formed during the oxidation of

ethylbenzene, its role in the reaction mechanism warrants closer examination. The oxidation of ethylbenzene typically proceeds via a free radical mechanism, which, in an ideal scenario, should continue until completion. However, in our reaction, full conversion was not observed, suggesting potential factors that may be influencing the reaction's progress even within our reaction time. One such factor might be the presence of alcohol, which could potentially act as inhibitor by trapping the ROO• species, which are considered the chain carrier species. This leads to the initiation of the reaction, but it prevents further progression of the chain reaction affecting the efficiency of the oxidation process. To investigate this possibility, a series of control tests were conducted to establish a baseline for comparison. Following the control experiments, varying concentrations of 1-phenylethanol (5%, 10%, and 20% molar ratio) were added to ethylbenzene to observe their effect on the reaction. The results indicated that, even with the addition of alcohol, the reaction did not proceed to full completion. This suggests that while alcohol may not act as a strong inhibitor, it could still exert a minor inhibitory effect, reducing the overall efficiency of the oxidation reaction. The fact that the reaction did not reach completion terminate fully implies that alcohol may interfere with the radical mechanism to some extent as described earlier. As a result, fewer radicals are available to drive the reaction to completion, thereby decreasing the overall conversion of ethylbenzene to the desired product. Moreover, understanding the role of alcohols in this process is crucial for future catalyst design. If 1-phenylethanol, are produced during the reaction and subsequently act as mild inhibitors, the efficiency of the catalytic system could be compromised. This finding highlights the importance of managing the accumulation of such by-products in oxidation reactions to maintain high catalytic performance. Further future studies could explore methods to mitigate this inhibitory effect, perhaps by adjusting the reaction conditions or developing catalysts that are less susceptible to inhibition by alcohol.

4.8 References

1 S. Vetrivel and A. Pandurangan, *J. Mol. Catal. A Chem.*, 2004, **217**, 165–174.

2 G. A. Olah and Á. Molnár, *Hydrocarbon chemistry*, John Wiley & Sons, 2003.

3 S. J. Blanksby and G. B. Ellison, *Acc. Chem. Res.*, 2003, **36**, 255–263.

4 F. Cavani, *Catal. Today*, 2010, **157**, 8–15.

5 R. Liu, H. Huang, H. Li, Y. Liu, J. Zhong, Y. Li, S. Zhang and Z. Kang, *Acs Catal.*, 2014, **4**, 328–336.

6 B. R. Cuenya, *Thin Solid Films*, 2010, **518**, 3127–3150.

7 J. R. Croy, S. Mostafa, H. Heinrich and B. R. Cuenya, *Catal. Letters*, 2009, **131**, 21–32.

8 J. A. Rodriguez and M. Fernández-García, *Synthesis, properties, and applications of oxide nanomaterials*, John Wiley & Sons, 2007.

9 H. H. Kung, *Transition metal oxides: surface chemistry and catalysis*, Elsevier, 1989.

10 A. Gavriilidis, B. Sinno and A. Varma, *J. Catal*, 1993, **139**, 41–47.

11 S. Chang, M. Li, Q. Hua, L. Zhang, Y. Ma, B. Ye and W. Huang, *J. Catal.*, 2012, **293**, 195–204.

12 V. Raji, M. Chakraborty and P. A. Parikh, *Ind. Eng. Chem. Res.*, 2012, **51**, 5691–5698.

13 H. STEINER, *Nature*, 1965, **208**, 420.

14 I. Hermans, J. Peeters and P. A. Jacobs, *J. Org. Chem.*, 2007, **72**, 3057–3064.

15 I. Uryga-Bugajska, D. Borman, M. Pourkashanian, E. Catalanotti and C. Wilson, *Proc. Inst. Mech. Eng. Part G J. Aerosp. Eng.*, 2011, **225**, 874–885.

16 A. V. Shijina and N. K. Renuka, *React. Kinet. Catal. Lett.*, 2008, **94**, 261–270.

17 Ge. B. Shulpin, D. Attanasio and L. Súber, *J. Catal* , 1993, **142**, 147–152.

18 J. A. M. Simões, A. Greenberg and J. F. Liebman, 1996, **109**, 175-176.

19 L. Boisvert and K. I. Goldberg, *Acc. Chem. Res.*, 2012, **45**, 899–910.

20 G. Henrici-Olivé and S. Olivé, *Angew. Chemie Int. Ed. English*, 1974, **13**, 29–38.

21 Y. Su, Y. Li, Z. Chen, J. Huang, H. Wang, H. Yu, Y. Cao and F. Peng, *ChemCatChem*, 2021, **13**, 646–655.

22 I. W. C. E. Arends, R. A. Sheldon, M. Wallau and U. Schuchardt, *Angew. Chemie Int. Ed. English*, 1997, **36**, 1144–1163.

23 M.-J. Cheng, K. Chenoweth, J. Oxgaard, A. Van Duin and W. A. Goddard, *J. Phys. Chem. C*, 2007, **111**, 5115–5127.

24 J. Zhang, Z. Wang, Y. Wang, C. Wan, X. Zheng and Z. Wang, *Green Chem.*, 2009, **11**, 1973–1978.

25 X. Liu, Y. Ryabenkova and M. Conte, *Phys. Chem. Chem. Phys.*, 2015, **17**, 715–731.

26 C. N. R. Rao, *Annu. Rev. Phys. Chem* , 1989, **40**, 291–326.

27 C. N. R. Rao and J. Gopalakrishnan, *New directions in solid state chemistry*, Cambridge University Press, 1997.

28 Y. Tokura and N. Nagaosa, *Science*, 2000, **288**, 462–468.

29 L. Chen, K. Zhu, L. H. Bi, A. Suchopar, M. Reicke, G. Mathys, H. Jaensch, U. Kortz and R. M. Richards, *Inorg. Chem*, 2007, **46**, 8457–8459.

30 A. Schwartz, L. L. Holbrook and H. Wise, *J. Catal* , 1971, **21**, 199–207.

31 T. F. Garetto, E. Rincón and C. R. Apesteguia, *Appl. Catal. B Environ.*, 2007, **73**, 65–72.

32 M. Menzinger and R. Wolfgang, *Angew. Chemie Int. Ed. English*, 1969, **8**, 438–171

444.

33 A. P. Unnarkat, J. Sonani, J. Baldha, S. Agarwal, K. Manvar, A. R. Faraji and M. Arshadi, *Chem. Pap.*, 2022, **76**, 995–1008.

34 M. Osman, M. M. Hossain and S. Al-Khattaf, *Ind. Eng. Chem. Res.*, 2013, **52**, 13613–13621.

35 E. T. Denisov, *Russ. Chem. Rev,* 1970, **39**, 31.

36 C. E. Frank, *Chem. Rev.*, 1950, **46**, 155–169.

37 M. Burgener, T. Mallat and A. Baiker, *J. Mol. Catal. A Chem,* 2005, **225**, 21–25.

Chapter 5: Ethylbenzene oxidation using Ag/Nb_2O_5 as a catalyst

5.1 Introduction

As discussed in chapter 1, ethylbenzene can undergo partial oxidation to yield several valuable products , including acetophenone , alcohol as illustrated in figure 5.1 [3-4]. This process is crucial for the manufacture of pharmaceuticals, agrochemicals, foods, and cosmetics [5-6].

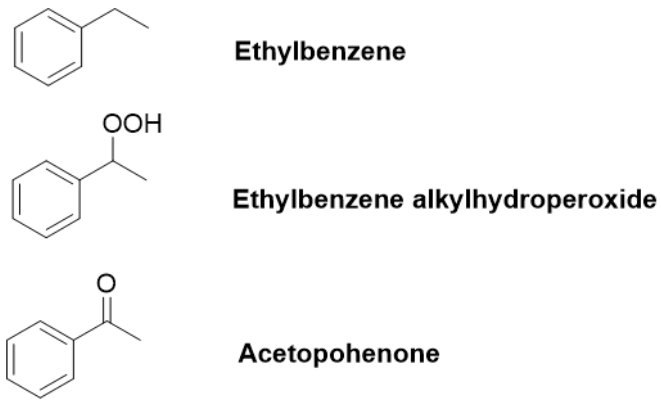

Figure 5.1: This figure shows the potential main by-products from the oxidation of ethylbenzene (EB), including the intermediate (EBHP), and acetophenone.

Given its significance, this study focuses on the selection of catalysts and investigation of their reactivity in the oxidation of ethylbenzene using molecular oxygen. Specifically, it studies the selectivity and stability of some catalytic systems under different reaction conditions to understand the oxidation process. The selection of this reaction as a model serves as the primary means to evaluate the catalytic performance of the prepared catalysts for the following reasons: i) the primary products resulting from the oxidation of ethylbenzene, acetophenone and 1-phenylethanol, serve as valuable intermediates in industrial organic synthesis; ii) the oxidation process can be readily accomplished using an experimental setup used at ambient conditions, thus utilizing molecular oxygen directly from the atmosphere, and in turn facilitating the experimental set ups and eliminating the initial requirement for pressurized systems; iii) based on literature research, the catalysts mainly employed in the oxidation of ethylbenzene are cobalt based salts or materials of Mn and Cu [3-7] thus provide a benchmark for comparison for our materials However, at the same time, there is only a limited number of publications documenting the oxidation of ethylbenzene using supported metal catalysts such as Nb_2O_5 and Ag and molecular oxygen. Hence, and

to provide continuity with the autoxidation studies reported in chapter 3 and 4, the oxidation of ethylbenzene was used to study the catalytic reactivity of supported Ag catalysts. This study also aims to understand the reactivity of Ag itself in the reaction, with the aim to identify new catalysts for a selective C–H activation and oxidation. In particular by focusing on which part of the oxidation process can be Ag activated, either the initiation by cleavage of the C–H bonds in ethylbenzene, or also if taking part in the subsequent, and selective, decomposition of intermediates. To this scope, various parameters were adjusted to enhance the conversion [8]. Such as temperature, oxygen partial pressure, metal to substrate ratio, and stirring speed were varied and study to assess their impact on catalytic performance like the conversion rate and selectivity towards acetophenone.

In this context it is worth noting that the use of supported metal oxide catalysis, containing metals such as Au, Pt, Pd and Ru has garnered significant attention over the past decades for these types of reactions due to their unique properties compared to bulk metals [9-10-11].

Among the metals studied thus far, Ag has received only limited attention for the partial oxidation of saturated hydrocarbons such as ethylbenzene in the liquid phase [12]. Additionally, there is insufficient understanding of its effects during the reaction. Currently, Ag, in the form of Ag nanoparticles supported over Al_2O_3, is utilized in industry for the process of ethylene epoxidation, yielding ethylene oxide with up to 80% selectivity, and for the dehydrogenation of methanol to formaldehyde [13-14].

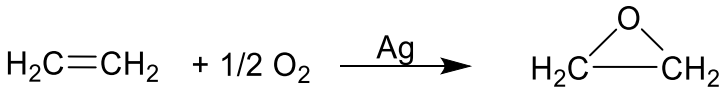

Scheme 5.1: Silver oxide-catalysed oxidation of ethylene-to-ethylene oxide (known as ethylene epoxide) at temperature 230°C with pressure 1.5 MPa, 4 h.

These industrial applications indicate potentially expanded uses supported silver catalysts, particularly for oxidation reactions. In fact, Ag has the capability to activate oxygen, leading to the formation of superoxide species ($O_2^{\bullet-}$) as a result of oxygen adsorption on silver species [15-16], this mechanism is often observed in the partial oxidation of organic compounds, including hydrocarbons. Moreover, existing literature suggest that the combined effect of Ag with a supporting material can influence the

distribution of oxygen vacancies within both the bulk and surface regions of metal oxides, such as cerium oxide, CeO_2 [17], with these vacancies being able to affect the oxidation process either by abstracting H species or trapping peroxides The deposition of Ag onto metal oxides, such as CeO_2 and TiO_2, leads to the creation of oxygen vacancies, which subsequently enhances the reductive adsorption of O_2 [17-18]. Additionally, when compared to other noble metals like Au, Pt, Pd, and Ru, Ag emerges as a promising candidate for industrial applications due to its relatively lower cost (£300 per gram). In this chapter, we will aim to evaluate the potential use of supported silver catalysts on various metal oxides, particularly focusing on Nb_2O_5, alongside other metal oxides such as CeO_2, TiO_2, and SiO_2 for comparison. These catalysts will be tested for their efficacy in the selective oxidation of ethylbenzene, as well as for cyclic hydrocarbons, like or branched aromatics like *p*-xylene (see chapter 6). Our goal is to generate data that can facilitate the identification of structure and activity correlation, and ultimately facilitate the design of catalysts.

5.2 Ethylbenzene oxidation test at atmospheric pressure using an open system

Studying autoxidation without the presence of catalysts as described in chapter 4, serves as a baseline or benchmark for comparing catalyst activity. Reaction parameters are modified to strike a balance between ethylbenzene conversion and selectivity, observing their impact on alcohol or acetophenone selectivity, which are the desired products of our study. Temperature is like one of the most crucial factors in the catalytic process, influencing the equilibrium constant and initial step of hydrocarbon oxidation. Moreover, the impact of the reaction time is studied to understand the kinetics of ethylbenzene oxidation, and it is also relevant to underline that a reaction needs to be under a kinetic regime to enable a comparison between different catalysts. Otherwise, mass transfer might become the predominant factor affecting the reaction and in turn the meaningfulness of conversion rates, and in some cases even selectivity. Hence, the stirring speed and metal to substrate ratio (M: S) were varied during the tests conducted under atmospheric pressure O_2. During the study on the quantity of ethylbenzene alkyl hydroperoxide from ethylbenzene in chapter 3 in section 3.5.2.1, tests were conducted at various temperatures: 100 °C, 110 °C, 120 °C and 130 °C for 24 h, 48 h, 72 h, 96 h and 120 h, 144 h. Based on the observed activity it was decided to consider a temperature of 120 °C and a reaction time of 24 h. This decision was influenced by the fact that temperatures above 120 °C would approach the boiling point of ethylbenzene which is 136 °C. Operating at temperatures near the boiling point would result in significant evaporation of ethylbenzene. Additionally, the study aimed to facilitate comparison with previous research findings [19-12]. Consequently, all subsequent reactions were performed at 120 °C for different reaction times (figure 5.2).

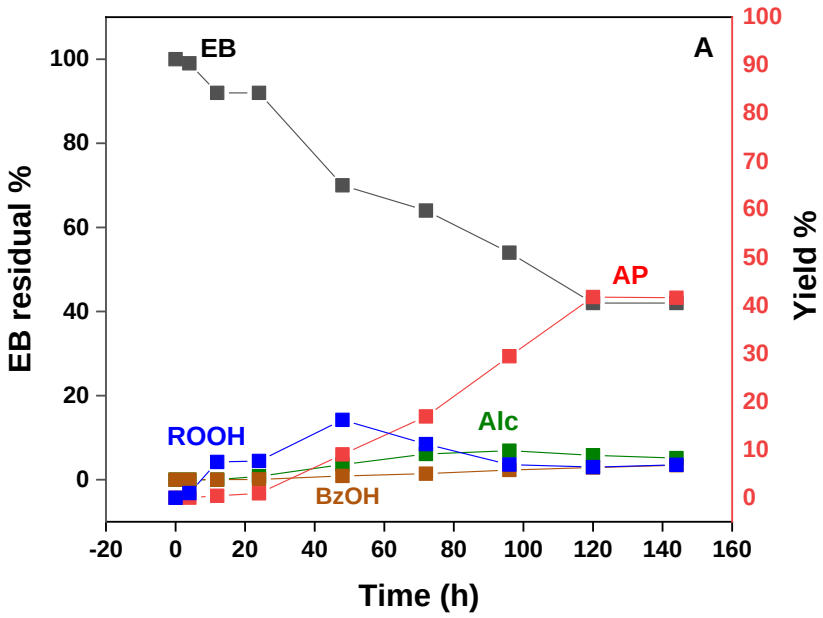

Figure 5.2: Ethylbenzene oxidation (in the absence of catalyst), at temperature 120 °C and different reaction time (24 h,48 h,72 h ,96 h 120 h and 144 h), at a stirring rate 600 rpm, *p* = ambient.

The consumption of ethylbenzene without catalysts begins very slowly as shown in figure 5.2, and gradually decreases to 40% over 144 hours. This process follows a free radical mechanism producing equal amounts of acetophenone and 1-phenyl ethyl alcohol with a K/A ratio of around 1, resulting from the decomposition of intermediate 1-phenyl ethyl alkyl hydroperoxide. This compound shows a typical intermediate evolution trend as at first it is formed (and only limited amounts of alcohol and ketone are present) to reach a maximum at about 50 h, then it is consumed. It is possible to observe that when the consumption of this intermediate starts then the formation of ketone and alcohol starts to take off, with a predominance of ketone thus showing these are direct decomposition products from 1-phenyl ethyl alkyl hydroperoxide. Interestingly though, the reaction doesn't seem to reach completion which might be due to an inhibition effect form the alcohol (see section 4.6). From this perspective, it might be possible to optimize the product distribution to produce more acetophenone by using Nb_2O_5 [20]. This catalyst might enhance the efficiency and selectivity of the reaction. Additionally, it is important to note that the conversion in the absence of catalyst is very low with 9 ± 4 % conversion observed at 24 h and 1 atm air pressure. Therefore, in the next section we will investigate the role of Nb_2O_5 in the autoxidation of ethylbenzene to better understand its potential impact on this process. Once we have a thorough understanding of this process, we will then apply silver doping to this support and use it in our study.

5.3 Overview of designing catalysts: metal nanoparticles supported by metal oxides

Heterogeneous catalysts sometimes consist of three main elements: an active component, usually a transition metal, a support material and a promoter. The support plays a crucial role in influencing the performance of the catalyst in different ways [20-21]. For instance, it can prevent sintering of supported species , impact the shape and size of particles that can be deposited on its surface, inhibit or facilitate interactions between the metal and support and in case of oxidation reactions store oxygen to enhance reaction rates either from the lattice or by adsorption and proximity effect [22]. The particular nature of a support hinge on its inherent characteristics, such as its basicity, surface area and the presence of varied oxidation states [23]. From these viewpoints, a variety of catalytic behaviours can be witnessed, spanning from chemically inactive to acting as a promoter or even as an inhibitor. In this context, it becomes crucial to elucidate the functions of the support in a particular model reaction independent of any metal oxide.

In this regard, metal oxides are frequently employed as supports or catalysts in a variety of chemical reactions because of their unique properties , which include high surface area, thermal stability, and the capacity to promote redox reactions [24]. Furthermore, their surface oxygen can act as a catalyst for oxidation reactions. The ability of a metal to change its oxidation state during the reversible storage and release of oxygen in catalytic reactions is known as its oxygen storage capability [17]. These properties make them particularly suitable for oxidation processes including the oxidation of ethylbenzene. At present, the utilization of metal oxides in catalysis preparation stands among the most advanced and economically significant technique [25]. These oxides have been utilized in crafting catalysts for selective oxidation reactions such as those involving ethylbenzene or cyclohexane [26]. Aiming to innovate in the discovery of materials capable of selective hydrocarbon oxidation, we concentrated on using Nb_2O_5, either as a support for metal oxide or directly in hydrocarbon oxidation. As a support, our expectations are grounded in previous research that demonstrated surface niobium oxide-support interaction (SOSI) [27] and strong metal support metal support interaction (SMSI) [28]. Regarding the use of pure Nb_2O_5, niobium oxides are currently attracting significant interest in heterogeneous

catalysis, where they are employed either as catalyst components or as additives to catalysts [29]. For example: niobium oxide was utilized to synthesize a gelled material, which was subsequently subjected to lyophilisation, yielding a novel polyoxoniobate catalyst (L-AmNbO) containing peroxo groups. The catalytic performance of this newly developed catalyst was evaluated through oxidation reactions of cyclohexene. Under the influence of the L-AmNbO catalyst, the oxidation of cyclohexene with hydrogen peroxide achieved a conversion rate of 90% after 12 hours at 75 °C, with a selectivity of approximately 50% for 1,2-cyclohexanediol [30]. Additionally, Nb_2O_5 is a metal oxide that can exist in various crystallographic forms such as orthorhombic (T-phase) and monoclinic (H-phase), amorphous, each potentially exhibiting different reactivity. It is known for its resistance to hydrolysis which is relevant since partial hydrocarbon oxidation produces water. Niobium centres can exist in multiple oxidation states including 2^+, 4^+ and 5^+, corresponding to NbO, NbO_2 and Nb_2O_5 oxides respectively. Due to these properties, Nb_2O_5 has been investigated as a catalyst support for metal involving Ag. However, despite this background and potential, there are limited reports on the use of Nb_2O_5, either as a support or as a bare metal oxide, for the direct oxidation of hydrocarbons by molecular oxygen without the presence of an initiator or solvent. This gap in the literature prompted us to consider an investigation into the potential reactivity. We will then examine whether Nb_2O_5 possesses catalytic properties and compare it with conventional metal oxides like CeO_2, TiO_2, and SiO_2, which are well known supports in hydrocarbon oxidation.

5.3.1 An investigation into the reactivity of Nb_2O_5 in ethylbenzene oxidation

As highlighted in the previous discussion, catalysts based on Nb_2O_5 are infrequently employed for the oxidation of hydrocarbons using molecular O_2 in the absence of a solvent [31-32]. In this section, we will study the potential of employing Nb_2O_5 to develop a catalyst specifically for the aerobic oxidation of hydrocarbons. This section reports the performance of Nb_2O_5 in the solvent free system for the aerobic oxidation of ethylbenzene. Based on our experimental procedures (see chapter 2 section 2.9.1), the initial catalytic tests were conducted at a temperature of 120 °C and a reaction temperature of 24 hours under atmospheric pressure with a condenser open to air.

The findings demonstrate that Nb_2O_5 inhibits the reaction under atmospheric air conditions showing 0% conversion compared to the blank test's 9 ± 4 %conversion. This absence of activity indicates that this material not only doesn't contribute to the initiation the reaction under these specific conditions. But it would appear to have even an inhibiting effect. This aligns with previous findings indicating that Nb_2O_5 is generally considered chemically inert in the oxidation of hydrocarbons [29]. However, there are also reports suggesting that it (Nb_2O_5) can be activated in the photo oxidation process for alcohol oxidation, when solvent like acetonitrile is present [33]. Conversely, since this material can influence both the conversion and selectivity in distinct ways, there is speculation that it may interact with the intermediate 1-phenyl ethyl alkyl hydroperoxide. Increased consumption of this intermediate (EBHP) could potentially enhance the selectivity to a desired product, like for example the ketone due to the acid surface properties of Nb_2O_5. Hence, according to the current study there is a proposition that Nb_2O_5 contributes to the breakdown of 1-phenyl ethyl alkyl hydroperoxide intermediate into acetophenone. This hypothesis will be further study by directly examining the decomposition of a particular hydroperoxide (1-phenyl ethyl alkyl hydroperoxide) in the presence of Nb_2O_5.

5.3.2 An investigation into the reactivity of Nb_2O_5 in 1-phenyl ethyl alkyl hydroperoxide

To better understand the decomposition pathway of 1-phenyl ethyl alkyl hydroperoxide EBHP, it is important to study their behaviour both in the presence and absence of a catalyst. Instead of obtaining these compounds as intermediates using them directly as substrates can provide clear insights. We synthesized 1-phenyl ethyl alkyl hydroperoxide as discussed in chapter 2 section 2.4 and used it as a substrate to examine its transformation into acetophenone or 1-phenyl ethanol with and without a catalyst. For this purpose, we performed a reaction involving the oxidation of 1-phenyl ethyl alkyl hydroperoxide using bare NbO_5 (figure 5.3).

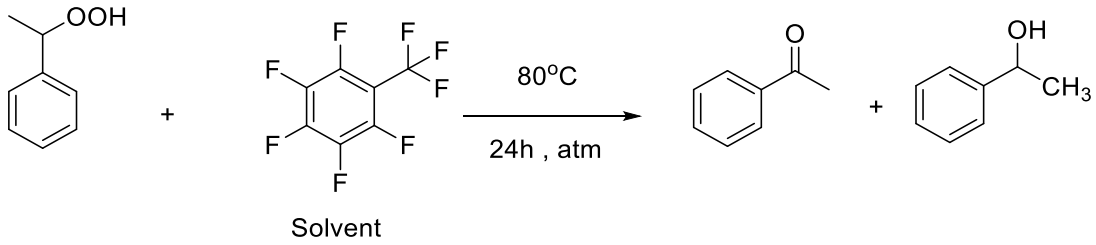

Figure 5.3: Test were initially conducted at 80 °C under atm O_2 using 100 µL of EBHP and 2 mL of perfluorotoluene (C_7F_8) as the solvent for 24 h. This is to study the reactivity of Nb_2O_5 in the decomposition of EBHP. The potential by-products from the decomposition of (EBHP) the intermediate to form acetophenone and 1-phenyl ethanol.

The solvent Perfluorotoluene (C_7F_8) is inert in this reaction, has a relatively high boiling point 104°C and because having no H is an ideal solvent to be used for ^{1}H-NMR experiments and as such indirectly enhance the NMR signal of the reaction mixture was used to address the lengthy synthesis process of 1-phenyl ethyl alkyl hydroperoxide which yields only a very small amount. It was observed that in the absence of catalysts, there were no significant changes in the blank test even after 24 hours of reaction time, with a decomposition rate of 0% under these conditions. However, the presence of Nb_2O_5 significantly enhanced the decomposition of 1-phenyl ethyl alkyl hydroperoxide, achieving values up to 97%. In the decomposition of EBHP by molecular O_2, Nb_2O_5 resulted in a K/A ratio above 2.5 as seen in table 5.1.

Regarding the role of Nb_2O_5 in the oxidation reaction of ethylbenzene, it can be concluded that Nb_2O_5 exhibits no activity in directly oxidizing ethylbenzene as shown 0% conversion. Furthermore, in the absence of an initiator as such it is not able to activate a primary C–H bond, and in turn it doesn't promote the initiation process. On

the other hand, with the date, we have provided so far it is a support capable to intervene during the reaction by enhancing the decomposition of the alkyl hydroperoxide intermediate and even more with a specificity the ketone thus allowing to conclude this support is involved in the abstraction of the H in alpha to the COOH group.

Table 5.1: Comparison of the blank test (in the absence of catalyst) and the Nb_2O_5 catalysed test for the decomposition of 1-phenyl ethyl hydroperoxide (EBHP) under specified conditions: a temperature of 80°C, 24h, and stirring speed of 600rpm, including selectivity for 1-phenylethanol (1-Ph), Acetophenone (AP) and 1-phenyl ethyl alkyl hydroperoxide (EBHP), and carbon mass balance (CMB %), n.d stands for not detected., under our reaction conditions.

Test	EBPH decomposition (%)	Observed selectivity (%)			CMB (%)
		AcP	Alc	EBHP	
Blank test	0	n.d.	n.d.	100 ± 2	100 ± 5
Nb_2O_5	97 ± 3	70 ± 2	28 ± 3	2 ± 2	

This result was surprising as there are no known instances in the literature of bulk niobium oxide functioning as a catalyst for this decomposition. Typically, a support material should be inert during the catalytic process to prevent unwanted side reactions and the formation of additional by products. In this respect Nb_2O_5 doesn't promote parallel initiation routes, but if a support material can promote the decomposition of the intermediate, it warrants further study. Therefore, to determine whether the catalytic behaviours observed for Nb_2O_5 are a peculiarity for this material, an array of metal oxides including CeO_2, TiO_2 and SiO_2 was considered. Details of these comparative tests will be provided in the following section.

5.3.3 Assessing the catalytic activity of CeO_2, TiO_2 and SiO_2 in the oxidation of ethylbenzene and decomposition of 1-phenyl ethyl hydroperoxide

The specific properties of Nb_2O_5 in relation to various hydrocarbons remain only partially understood at present, prompting further investigation into the effects of CeO_2, TiO_2 and SiO_2 and they were tested for the oxidation of ethylbenzene and cyclooctane and *p*-xylene as the most relevant substrates for this project.

CeO_2 is recognized in photochemistry as a metal oxide utilized in oxidation reactions such as those involving methane and cyclohexane [34-35]. While TiO_2 is commonly employed as a support in the oxidation of cyclohexane or alcohols [36-37]. While SiO_2

alone is not active the oxidation of ethylbenzene and cyclohexane. Additionally, these metal oxides are frequently used as supports. It is important to note that not all of these metal oxides are expected to exhibit activity in the tested reactions [38-39]. This underscores the purpose of these control test which include species like SiO_2 that are not anticipated to demonstrate activity. These tests serve to validate the activity observed with Nb_2O_5. The conversion rate of blank autoxidation (table 5.2) is approximately 9 ± 4 %, however no conversion observed in the presence of TiO_2 which is same with Nb_2O_5, indicating that both are inhibitor in the oxidation process. As TiO_2 is known to present oxygen vacancies [40] we speculate this could be the case also for Nb_2O_5 and such the inhibition effect could be due to some trapping effect. Nonetheless, CeO_2 and SiO_2 both exhibit reactivity for oxidation across a range of blank tests indicating that they neither inhibit nor promote the reaction. CeO_2 is known for its exceptional oxygen storage capacity, which is associated with the ease of forming and repairing oxygen vacancies on the surface of solid ceria [41]. SiO_2 shows no significant activity compared to autoxidation, as all parameters remain consistent within experimental error. Thus, it does not enhance selectivity toward EBHP. In contrast, CeO_2 is capable of decomposing EBHP, potentially through redox or acid-base mechanisms, leading to the formation of ketones. Further investigations are needed to explore these pathways. We aimed to understand the potential catalytic effects of these metal oxides on this decomposition reaction.

Table 5.2: Comparison of ethylbenzene oxidation conversion rates and observed selectivity: blank test vs. TiO_2, CeO_2 and SiO_2 at 120°C for 24hours, including by products: 1-phenylethanol (1-Ph), Acetophenone (AP) and 1-phenyl ethyl hydroperoxide (EBHP), and carbon mass balance (CMB %), n.d stands for not detected.

Test	EB Conversion (%)	Observed selectivity (%)				CMB (%)
		AP	1-Ph	EBHP	other	
Blank test	9 ± 3	10 ± 2	7 ± 2	85 ± 3	n.d	97 ± 5
TiO_2	0	n.d	n.d	n.d	n.d	
CeO_2	6 ± 3	23 ± 2	9 ± 2	68 ± 3	n.d	
SiO_2	7 ± 3	8 ± 2	4 ± 2	87 ± 3	n.d	

We then used these same metal oxides to test their capabilities for the decomposition of EBHP compared to Nb_2O_5 (table 5.3).

Table 5.3: Comparison of 1-phenyl ethyl alkyl hydroperoxide decomposition rates and observed selectivity: blank test (in the absence of catalyst) vs. TiO_2, CeO_2 and SiO_2 at 120°C for 24hours, including selectivity for 1-phenylethanol (1-Ph), Acetophenone (AP) and 1-phenyl ethyl hydroperoxide (EBHP), and carbon mass balance (CMB %), n.d stands for not detected.

Test	EBPH decomposition (%)	Observed selectivity (%)			CMB (%)
		AP	1-Ph	EBHP	
Blank test	0	n.d	n.d	100 ± 2	100 ± 2
CeO_2	36 ± 3	15 ± 2	11 ± 2	70 ± 3	
TiO_2	30 ± 3	20 ± 2	6 ± 2	70 ± 3	
SiO_2	9 ± 3	10 ± 2	7 ± 2	85 ± 3	

The difference is also observed in the decomposition of alkyl hydroperoxide indicating that the addition of Nb_2O_5 promotes the transformation of alkyl hydroperoxide to acetophenone with a selectivity of 75 % Whereas the other metal oxides show less reactivity in decomposing the intermediate and without apparent selectivity control, thus implying a limited surface substrate interaction with a reaction dominated by the statistics of the free radical pathway. From this perspective, using Nb_2O_5 as a support for our catalyst is interesting. More experimental will be used in this chapter with the addition of Ag to the metal oxides Nb_2O_5, CeO_2, TiO_2 and SiO_2, to assess the potential application of supported silver over metal oxides, primarily Nb_2O_5 as a catalyst for the selective oxidation of ethylbenzene.

5.4 Comparative study of supported Ag catalysts on Nb_2O_5, Fe and Mn for ethylbenzene oxidation

In this section we conducted a systematic study to demonstrate the activity of Ag as well as which of the possible Ag species may be active or take part in the reaction. We examined Mn, Fe and Ag doped into Nb_2O_5, as well as other metal oxides (CeO_2, TiO_2 and SiO_2) for comparison. Mn and Fe are known for their ability to oxidize hydrocarbons, as evidenced by their reactivity in the oxidation of methane [42]. From our data Ag indicates a promising industrial potential for supported Ag catalysts [43-44]. Therefore, the reactivity of Ag for ethylbenzene oxidation is illustrated in figure 5.4.

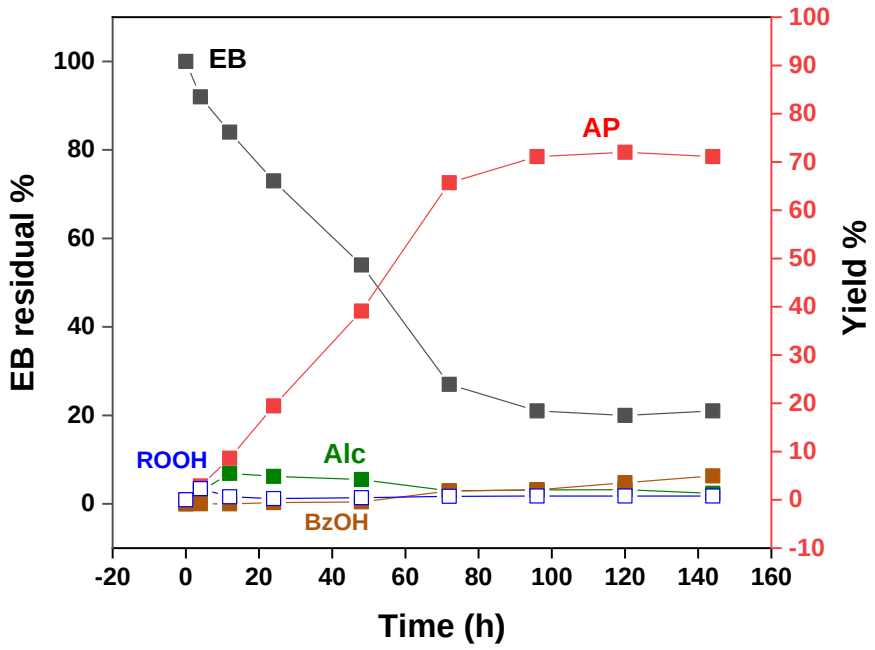

Figure 5.4: Ethylbenzene oxidation by using Ag_2O, at temperature 120 °C and different reaction time (24 h,48 h,72 h ,96 h 120 h and 144 h), at a stirring rate 600rpm, p=ambient. Based on our discussion about the reactivity of Nb_2O_5 in ethylbenzene alkyl hydroperoxide in section 5.3, and the activity of Ag species in the oxidation of ethylbenzene, we hypothesize that Nb_2O_5 is capable of decomposing intermediates, while Ag species can initiate the C-H bond I ethylbenzene as seen in figure 5.4.

Unlike the case of the activity of Ag as shown in figure 5.4, in this case consumption down to 20% is observed. Notably, the intermediate behavior of EBHP formation and decomposition follows entirely different trends. A small maximum is reached just after 15 hours (unlike about 50 h) this is a consequence of a fast consumption of this intermediate and corroborated by the simultaneous steep growth of the ketone. This suggests a combined effect by both the support and Ag capable to abstract the H-alpha to the peroxide to from the ketone. Figure 5.5 presents a simplified proposed mechanism for the reaction of Ag/Nb_2O_5.

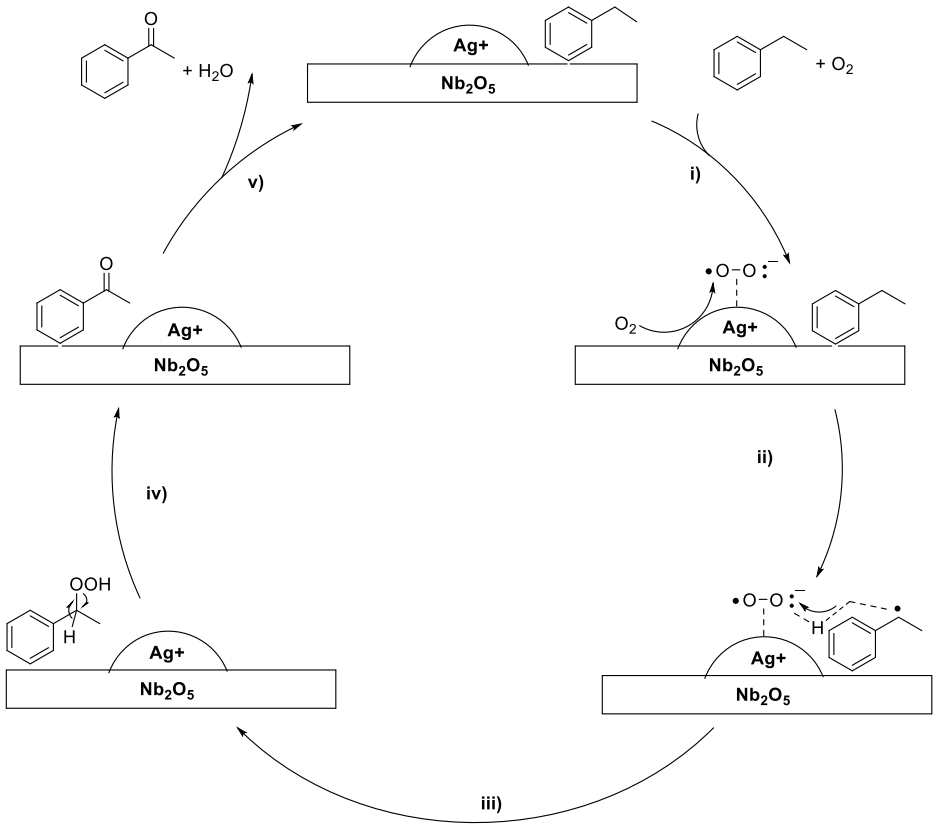

Figure 5.5: A simplified proposed mechanism for the reaction of Ag/Nb_2O_5 in the oxidation of cyclooctane using molecular oxygen.

To investigate the reactivity of Ag on the support Nb_2O_5, we then compared Ag/Nb_2O_5 with that of Ag deposited on support such as TiO_2 and CeO_2 (table 5.4)

Table 5.4: comparison of ethylbenzene oxidation conversion rates and observed selectivity: silver doped into. TiO_2, CeO_2 and SiO_2 at 120 °C for 24 hours, by products: 1-phenylethanol (1-Ph), Acetophenone (AP) and 1-phenyl ethyl hydroperoxide (EBHP), and carbon mass balance (CMB %), n.d. stands for not detected.

Test	EB Conversion%	Observed selectivity (%)				CMB %
		AP	1-Ph	EBHP	other	
Ag/Nb_2O_5	29 ± 3	71 ± 2	20 ± 2	0	n.d	100 ± 2
Ag/CeO_2	25 ± 3	65 ± 2	29 ± 2	6 ± 3	n.d	
Ag/TiO_2	24 ± 3	54 ± 2	26 ± 2	21 ± 3	n.d	

While the conversion remained similar across different supports, within the selected experimental timescale, the observed selectivity varied with K/A ratio 4:1. Specifically, no alkyl hydro peroxide was left when using Ag/Nb_2O_5 whereas some alkyl hydro peroxide was still present with Ag/CeO_2 and Ag/TiO_2. This finding supports our hypothesis that Ag initiates ethylbenzene and Nb_2O_5 has an active role in the selective decomposition of the alky hydro peroxide. After testing silver on these supports, we then conducted similar experiments by replacing Ag with Fe as seen in table 5.5.

Table 5.5: comparison of ethylbenzene oxidation conversion rates and observed selectivity: iron doped into. TiO_2, CeO_2 and SiO_2 at 120°C for 24hours, by products: 1-phenylethanol (1-Ph), Acetophenone (AP) and 1-phenyl ethyl hydroperoxide (EBHP), and carbon mass balance (CMB %).

Test	Conversion (%)	Observed Selectivity (%)				CMB(%)
		AP	1-Ph	EBHP	Styrene	
Fe/ Nb_2O_5	7 ± 3	50 ± 2	16 ± 2	0	27	
Fe/CeO_2	22 ± 3	67 ± 2	27 ± 2	7 ± 3	n.d	100 ±2
Fe/TiO_2	23 ± 3	69 ± 2	26 ± 2	6 ± 3	n.d	

As can be seen in table 5.5, iron-doped niobium oxide exhibits a different activity compared to doped Nb_2O_5 with silver. The conversion rate of Fe/Nb_2O_5 differs from that of the iron salt (result discussed in chapter 4, table 4.3 and 4.4), and the undoped niobium oxide. However, the product distribution remains the same as that of the undoped material. Therefore, these are the primary contributors to the catalytic activity. This suggests that iron is not responsible for the observed conversion. Additionally, the leaching of iron into the solution may contribute to the conversion. However, despite iron's potential influence on conversion, the selectivity remains similar to that of Ag/Nb_2O_5. This further supports our hypothesis that the support material, not the iron, plays the key role in controlling selectivity for this reaction. Moreover, as discussed earlier, Nb_2O_5 plays an important role in the decomposition of the intermediate. This is clearly evident from the table 5.5, where no ethylbenzene alkyl hydroperoxide remains in the reaction. We have then used the same approach for manganese as supported metal. a conversion of up to nearly 30% with a selectivity above 70% to the ketone were observed, the activity of Mn may indicate the presence of leaching, this metal may leach into solution, as shown by the activity observed in table 5.6. To study leaching effect, we conducted a control test using manganese (II)

acetate tetra hydrate, which is soluble in the reaction mixture and acts as a homogeneous catalyst. The results as seen in table 5.7 match with the previous result of Mn presented in table 5.6 and this corroborates our hypothesis, and this is homogenous effect. As expected, these materials are highly selective towards acetophenone, however, our catalysis Ag/Nb_2O_5 demonstrates comparable activity, making it a valuable competitor for selective oxidation.

Table 5.6: comparison of ethylbenzene oxidation conversion rates and observed selectivity: Manganese doped into. TiO_2, CeO_2 and SiO_2 at 120 °C for 24 hours, by products: 1-phenylethanol (1-Ph), Acetophenone (AP) and 1-phenyl ethyl hydroperoxide (EBHP), and carbon mass balance (CMB %).

Test	EB Conversion (%)	Observed selectivity (%)				CMB (%)
		AP	1-Ph	EBHP	other	
Mn/TiO_2	26 ± 3	76 ± 2	24 ± 2	0	n.d	100 ± 5
Mn/Nb_2O_5	28 ± 3	76 ± 2	24 ± 2	0	n.d	
Mn/CeO_2	28 ± 3	77± 2	23 ± 2	0	n.d	

Table 5.7: Ethylbenzene oxidation conversion rates and observed selectivity of using homogenise solution of Mn at 120°C for 24hours, by products: 1-phenylethanol (1-Ph), Acetophenone (AP) and 1-phenyl ethyl hydroperoxide (EBHP), and carbon mass balance (CMB %).

Test	EB Conversion (%)	Observed selectivity (%)			CMB (%)
		AP	1-Ph	EBHP	
$(CH_3COO)_2Mn{\cdot}4H_2O$	31 ± 3	73 ± 2	27 ± 2	0	100 ± 5

After confirming the leaching effect of Mn in the solution, we proceeded to explore a bimetallic system by doping both Fe and Ag into the support. In this setup, Fe is expected to activate the C–H bond of the hydrocarbon (RH) to initiate the reaction, while Ag is anticipated to decompose EBHP by cleaving the C–H bond adjacent to the OOH group (table 5.8). The result did not demonstrate any difference activity from what was previously observed with Ag/Nb_2O_5. Interestingly, the activity was more similar to Ag/Nb_2O_5 suggesting that the catalytic activity originates from silver which initiates the reaction, while Nb_2O_5 plays a significant role in decomposing the intermediate. This implies that the presence of silver is responsible for catalytic

initiation, while the metal oxide support particularly Nb_2O_5, facilitates the breakdown of intermediates.

Table 5.8: Comparison of ethylbenzene oxidation conversion rates and observed selectivity: Ag and Fe doped into. TiO_2, CeO_2 and SiO_2 at 120°C for 24h, by products: 1-phenylethanol (1-Ph), Acetophenone (AP) and 1-phenyl ethyl hydroperoxide (EBHP), and carbon mass balance (CMB %).

Test	Conversion (%)	Observed selectivity (%)			CMB (%)
		AP	1-Ph	EBHP	
Ag-Fe/TiO2	25 ± 3	73 ± 2	23 ± 2	4 ± 2	98 ± 3
Ag-Fe/ CeO_2	25 ± 3	72 ± 2	25 ± 2	4 ± 2	
Ag-Fe/ Nb_2O_5	29 ± 3	80 ± 2	21 ± 2	0	

5.4.1 Comparative study of supported Ag catalysts on Nb_2O_5, Fe and Active Ag species over Nb_2O_5

In view of the active role expressed by Ag we wanted to gather information on which Ag species, like Ag^0 or Ag^+ could be responsible for the activity that we observe. To achieve this, a series of control teste were conducted, and the outcomes of these experiments are detailed in the following graphs. This was towards the reactivity for EB oxidation (figure 5.6.)

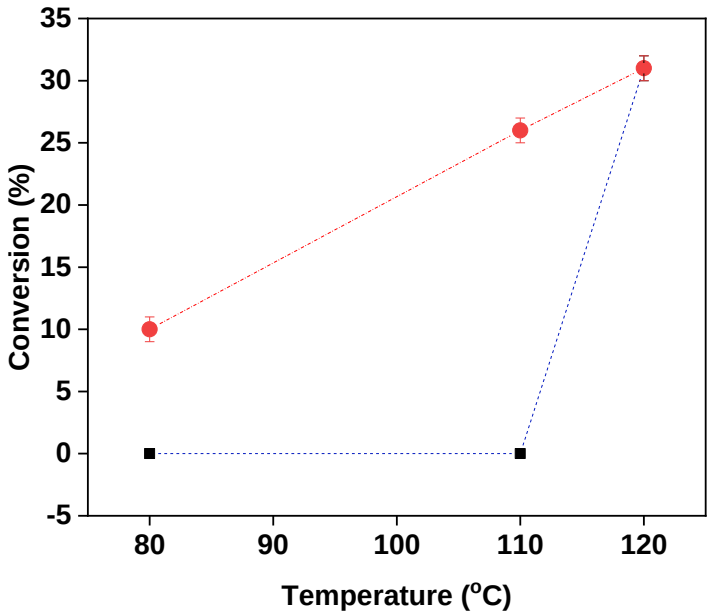

Figure 5.6: The catalytic activity of Ag^0 (---) and Ag^+ (---) in ethylbenzene oxidation at temperatures 80°C, 110°C and 120°C for 24h, (dash line to guide the eye).

As we can observe from the graphs above Ag^0 exhibited no reactivity within the temperature range of 80 °C to 110 °C. However, at 120 °C, activity was detected, similar to that of Ag^+. This suggests that at higher temperatures Ag^0 might be oxidizing to Ag^+, leading to the observed catalytic activity. The high temperature facilitates the oxidation of Ag^0 to its ionic form Ag^+, which is responsible for the reactivity. Therefore, the activity seen at 120 °C could be attributed to the Ag^+ species rather than Ag^0. Furthermore, we also tested Ag^0 with EBHP and observed no decomposition of the intermediate. Considering this, we can confirm that Ag^+ ion act as an initiator for breaking the C–H bond in ethylbenzene, presenting a promising application of Ag^+ in hydrocarbon oxidation.

Moreover, it's typically observed that the activation of C–H bonds by abstraction of H atoms can be achieved through various means, such as Superoxide species linked to metal centres or metal oxides, peroxide species such alkoxy or peroxyl radicals, and unsaturated metal centres in homogeneous catalysis. It is clear from the discussion of how supported Ag particles activate O_2 that newly generated superoxide species can abstract C–H bonds to initiate the reaction when adsorbed oxygen species are activated by Ag^+ sites. Additionally, studies have indicated the incapacity of Ag–O to active C–H bonds in ethylene oxidation, supporting the explanation that the initiation of ethylbenzene oxidation is indeed due to superoxide species [14]. Additionally, research suggests that catalytic systems containing Ag can perform as effectively as organic radicals in initiating the oxidation of ethylbenzene [45]. Thus, an initiator may not be required for such a catalytic system.

5.4.1.1 Repeatability test with low amount of Ag/Nb_2O_5 and stop and go reaction

Table 5.9: Comparison of ethylbenzene oxidation conversion rates and observed selectivity: blank test vs. Ag/Nb2O5 (1:1000) at 120°C for 24hours, including by products: 1-phenylethanol (1-Ph), Acetophenone (AP) and 1-phenyl ethyl hydroperoxide (EBHP), and carbon mass balance (CMB %), n.d stands for not detected.

Test	EB Conversion (%)	Observed selectivity (%)				CMB (%)
		AP	1-Ph	EBHP	other	
Blank test	9 ± 3	10 ± 2	7 ± 2	85 ± 3	n.d	97 ± 5
Ag/Nb_2O_5 (1:1000)	21	50	15	39	n.d	
Ag/ Nb_2O_5 (1:100)	29 ± 2	78 ± 1	22 ± 1	0		

Table 5.10: Stop and go reaction: Ethylbenzene 3 mL +1:100 Ag/Nb_2O_5 run for 12h then stop and run NMR and then recover EB only and carry reaction for 24h, 120°C

Test	EB Conversion (%)	Observed selectivity (%)				CMB (%)
		AP	1-Ph	EBHP	other	
12h, EB +1:100 (Ag/Nb_2O_5	12	63	25	8	n.d	97 ± 5
24h recover EB only	21	50	14	41	n.d	

Table 5.10 show after the removal of the catalyst, the reaction continues to progress due to the presence of residual alkyl hydroperoxides in the solution, which act as initiators. However, the reaction rate is significantly reduced, indicating that the catalyst plays a critical role in driving the reaction. This highlights the dual contribution while residual species sustain the reaction to a limited extent, the catalyst substantially enhances the process.

Regarding selectivity, the relatively small amount of EBHP produced suggests that the catalyst surface- whether Ag, Ag^{+} or $Nb^{2}O^{5}$ is primarily responsible for this process. Specifically, the catalyst facilitates the decomposition of ROOH into R=O as inferred from the last row of the first table (5.9). This underscores the catalysts' role in decomposing the majority of ROOH with the additional R=O (distinct from that formed via autoxidation) being catalytically driven. When analysing Table 1, the results are more insightful when compared to Table 2. For example, with a 1:100 ratio, the activity decreases but not proportionally to the reduction in active sites (i.e., 10 times fewer active centres). This behavior suggests potential diffusion limitations. However, the altered selectivity in this case implies the presence of either residual effects or an auto-oxidation component. Notably, the second row of Table 5.9 closely aligns with the second row of Table 5.10, further supporting this hypothesis.

5.5 Results of ICP-MS analysis for leaching determination

Leaching in the context of catalysis refers to the process by which metal species from the catalyst surface and enter the surrounding solution. This phenomenon holds significant importance in catalytic reactions as leached metal species can influence both the catalytic activity and the ability to maintain high performance of the catalyst. It is well established that leached metal ions can actively participate in reactions, thereby showing additional catalytic effects beyond those of the original catalyst material. ICP-MS was utilised in our study to measure the metals present in the catalysts, specifically Ag species. This involved treating the catalysts with concentrated HNO_3 to extract the metals and analyse the reaction mixtures, which might contain active metal leaching component as described in chapter 2 section 2.12.4. With this understanding of leaching in mind, initial control test was conducted to evaluate the potential role of Ag^+ ions that could leach into the solution during catalytic processes. The same procedures used for ethylbenzene oxidation were applied with $AgNO_3$ as the catalyst. It is significant to notice that the metal salt used in these control tests was usually far less than 0.5 mg. An $AgNO_3$ solution that was concentrated in water was made in order to reduce experimental error. The appropriate volume of Ag was then measured and poured into a round bottom flask. The flask was dried at 100 °C until all the water evaporated, and then after cooling the organic substrate was added. Subsequently, ICP-MS analysis of the solutions after the reaction was completed reveals the results presented in the following table 5.9.

Table 5.9: Analysis via ICP-MS of solutions post oxidation reaction of ethylbenzene at 120°C, 24h, and using 5 wt% Ag supported on various metal oxide substrates (Nb_2O_5, TiO_2, CeO_2 and SiO_2)

Catalyst	Relative percentage of Ag to original doped metal (5 wt%)
Ag/Nb_2O_5	0.21
Ag/CeO_2	3
Ag/TiO_2	7
Ag/SiO_2	8

Since the reaction mixtures are organic solutions, and the samples for ICP-MS analysis need to be in aqueous solution, the detection of potential leached species was performed through an extraction procedure from the organic phase into water.

Specifically, 1 mL of the reaction mixture was extracted into 10 mL of deionized water by thorough mixing for 2 hours at room temperature followed by separating the aqueous phase for analysis.

ICP-MS data was collected of the reaction mixture of ethylbenzene at 120 °C 24 h. The result demonstrated that the silver amount detected for catalytic test with Ag/Nb_2O_5 was less than 5% with 0.2% appeared in solutions. This indicates that the catalytic activity is heterogeneous in nature because all of the silver has stayed on the surface.

Other test for the other silver supported in CeO_2 and TiO_2 and SiO_2 shown leaching in range of 5-10%. This mean that some of the silver leached into the solution and the activity observed is homogeneous in nature. To ensure the accurate result we moved to quantify the result of leaching via ICP-MS as we can see in the following section.

5.5.1 Quantification of leaching via ICP-MS analysis

It is important to ensure that the metals loaded into the catalyst (such as Silver in Ag/Nb_2O_5, WI) remain stable and do not lead under catalytic conditions. This is particularly critical for heterogeneous catalyst, as their ability to be reused is a primary advantage. Consequently, if substantial leaching occurs from batch to batch a loss in activity will be noticeable [46]. Moreover, there is chance that the metal released through leaching could demonstrate activity when in solution [47]. this could result in some level of homogeneous catalysis taking place which has caused debates regarding mechanisms among palladium catalysts [48]. Since the objective of this project is to create a heterogeneous catalyst with confined active sites, any non-confined leachates catalysing reactions freely would be highly undesirable. For further analysis of potential leaching, we conducted additional test. The result from the ICP analysis indicate the relative percentage of silver to the original doped metal (5 wt%). Now we need to assess if there is any leaching observed from this amount, specifically for Ag/Nb_2O_5 at 0.21. To investigate this, additional test was conducted as detailed in the table 5.10.

Table 5.10: To study the effect of leaching, ethylbenzene oxidation reaction were conducted at 120°C 24h using different ratios 1: 10^5 and 1: 10^6 of $AgNO_3$. Including selectivity for 1-phenylethanol (1-Ph), Acetophenone (AP) and 1-phenyl ethyl hydroperoxide (EBHP), and carbon mass balance (CMB %).

Test	EB conversion (%)	Observed selectivity (%)			CMB (%)
		AP	1-Ph	EBHP	
$AgNO_3$ 1:10^5	16 ± 2	12 ± 2	7 ± 2	81 ± 2	100 ± 5
$AgNO_3$ 1:10^6	13 ± 2	13 ± 2	9 ± 2	78 ± 2	

When using $AgNO_3$ at a ratio of 1:10^5, a 16% conversion rate was observed. Conversely at a ratio of 1:10^6 a 13% conversion rate was noted. This indicate that the catalysis partially acts as a homogeneous catalyst, but its impact is minimal. To confirm this result, a leaching control test using a 'stop and go' protocol was conducted. The test showed a 23% conversion after 48 h, with the catalyst present for the first 24 hours and then removed. This conversion rate is slightly higher than the 19% observed in bare autoxidation (see chapter 4, figure 4.3). Therefore, although a homogeneous contribution cannot be entirely ruled out, its effect appears to be minimal. To ensure if these results are comparable to the original test for Ag/Nb_2O_5, a t-test needs to be applied for this comparison.

To perform a t-test, we need the means and standard deviations of the two samples, which are the conversions obtained from the Ag/Nb_2O_5 catalyst and the conversion from the reactions contains $AgNO_3$ at different ratios. For Ag/Nb_2O_5 vs. 1:10^5 $AgNO_3$ ratio the t-values is 9.19, and for Ag/Nb_2O_5 vs. 1:10^6 $AgNO_3$ ratio the t-values is 9.19 too. Since the t-values for both comparisons are greater than the critical t-value, we reject the null hypothesis indicating that there is a significant difference between the average conversions of the Ag/Nb_2O_5 catalyst and the reaction containing $AgNO_3$ at different ratios. Based on the results of the t-test, the leaching of Ag into the solution did not influence the catalytic activity. Therefore, it is likely that the observed catalysis remains is heterogeneous in nature.

Following the leaching tests, to develop a catalytic cycle incorporating both Ag^0 and Ag^+ for future catalytic applications, we conducted reactions at different calcination

temperatures to study their impact on activity in ethylbenzene oxidation. Therefore, to investigate the effects of different silver species (Ag^0 and Ag^+) and the influence of Ag^+ leaching from WI-Ag/Nb_2O_5 a series of test were conducted.

During the preparation of Ag/Nb_2O_5 using the impregnation method $AgNO_3$ decompose into metallic Ag through the following steps equation 5.1 and 5.2 [49] :

$$2AgNO_3 \rightarrow Ag_2O + 2\ NO_2 + 0.5\ O_2 \quad \text{(eq.5.1)}$$

$$Ag_2O \rightarrow 2\ Ag + 0.5\ O_2 \quad \text{(eq.5.2)}$$

In this scenario, it is likely that both Ag_2O and metallic Ag coexist after calcination at 180 °C for 4 hours. The result in table 5.11 demonstrate that the conversion does not improve as seen after calcination at 300 °C and there is remaining presence of peroxide at this temperature. Additionally, it is observed that conversion improves and selectivity for ketones increases, while selectivity for alky hydroperoxide decrease to 0%, following the calcination of Ag_2O + Nb_2O_5. The calcination process at 300 °C promotes the transformation of Ag_2O into Ag [50- 51].

Table 5.11: Ethylbenzene reaction mixture using Ag/Nb_2O_5 at different calcination temperatures (180°C and 300°C) at 120C for 24hours. Including selectivity for 1-phenylethanol (1-Ph), Acetophenone (AP) and 1-phenyl ethyl hydroperoxide (EBHP), and carbon mass balance (CMB %).

Test	EB Conversion (%)	Observed selectivity (%)			CMB (%)
		AP	1-Ph	EBHP	
Ag/ Nb_2O_5 (180°C)	19 ± 3	68 ± 2	16 ± 2	16 ± 2	98 ± 5
Ag/ Nb_2O_5 (300°C)	29 ± 3	71 ± 2	29 ± 2	0	

The finding also demonstrate that Ag^0 did not change the oxidation process. This mean that Ag nanoparticles (Ag^0) in WI-Ag/Nb_2O_5 did not impact the reaction. It is believed that Ag^+ sites in WI-Ag/Nb_2O_5 could activate oxygen to form superoxide oxygen species to initiate oxidation or promote the process via direct hydrogen abstraction.

5.6 Ethylbenzene oxidation reaction using tBHP as oxidant

In chapter 4 section 4.2.2, we discussed that for ethylbenzene (EB) reaction using tert-butyl hydroperoxide (tBHP), it implies that this oxidant act as a radical promoter in this reaction. Building on this understanding, further tests have been conducted using tBHP. Therefore, we aim to study the effect of tBHP in this reaction in greater detail.

Table 5.12: Oxidation of Ethylbenzene with varying amounts of tBHP molar concentration (1%, 5%, 10% and 20%) at 120C 24hours with a stirring rate of 600 rpm. including selectivity for 1-phenylethanol (1-Ph), Acetophenone (AP) and 1-phenyl ethyl hydroperoxide (EBHP), and carbon mass balance (CMB %).

Molar % of tBHP	EB Conversion (%)	Observed selectivity (%)			Yield (%) of AP	CMB (%)
		AP	1-Ph	EBHP		
0	12 ± 3	10 ± 2	7 ± 2	85 ± 2	1	
1	25 ± 3	73 ± 2	10 ± 2	17 ± 2	18	
5	24 ± 3	78 ± 2	5 ± 2	24 ± 2	19	98 ± 3
10	31 ± 3	19 ± 2	8 ± 2	73 ± 2	5	
20	35 ± 3	22 ± 2	10 ± 2	73 ± 2	8	

We used table 5.12 above as a reference for our results using Ag_2O catalyst in Ethylbenzene oxidation.

Table 5.13: Oxidation of Ethylbenzene with varying amounts of tBHP molar concentration (1%, 5%, 10% and 20%) using Ag_2O at 120C 24hours with a stirring rate of 600 rpm.

Molar (%) of tBHP	EB Conversion (%)	Observed Selectivity (%)			Yield (%) of AP	CMB (%)
		AP	Alc	EBHP		
0	12 ± 2	10 ± 2	7 ± 1	85 ± 3	1	
1	36 ± 2	75 ± 2	24 ± 1	1 ± 3	29	100 ± 5
5	36 ± 1	74 ± 1	25 ± 1	1 ± 1	27	
10	36 ± 2	72 ± 2	29 ± 1	0	26	

As we know tBHP decomposes easily into radical species; the more tBHP that decomposes the more radical species are produced. These radical species can react with ethylbenzene, but they can also react with each other to form non radical species. Consequently, tBHP could be consumed without being utilized to oxidize ethylbenzene. It can be seen from table 5.13 that the presence of Ag by itself showed

the same activity, regardless of whether the amount of tBHP was increased or not. We conducted catalytic test using Ag_2O alone for ethylbenzene oxidation, and the results matched those in table 5. 13 with 37 ± 1 conversion. This indicates that tBHP did not contribute to any activity. Therefore, it can be observed that with addition of more tBHP, a conversion plateau observed. Additionally, the conversion reaches a point where further increase is not achievable. This may indicate either an inhibitor effect or the termination of radicals, which stop the progression of the reaction. Hence, it appears that tBHP was not used as the primary oxidant in our reaction.

5.7 Ethylbenzene oxidation reaction using H_2O_2 as oxidant

TBHP is a strong oxidant and is frequently more effective than H_2O_2 and O_2. The decomposition of tBHP or H_2O_2 into radical species can lead to the formation of by-products. However, the by-product of H_2O_2 is water, which typically does not interfere with the desired products. In contrast, the by-products of tBHP, such as tert-butanol or methanol can be reactive and may inhibit the reaction, depending on the reaction conditions used [52]. Therefore, we conducted a study on the reactivity of H_2O_2 in ethylbenzene oxidation to better understand its behaviour and potential effectiveness as an oxidizing agent in this chemical reaction. H_2O_2 is recognized as a good oxidant because of its capability to generate radical species, such as hydroperoxyl and hydroxyl radicals. Ethylbenzene oxidation was conducted using the same conditions as before, H_2O_2 instead of tBHP. However, no activity was observed, and the reaction results consistent with the blank test, showing only 12% conversion. An experiment was undertaken to understand why this phenomenon occurred, as explained in chapter 2 section 2.10. Regarding the mixture of H_2O_2 and ethylbenzene, even after a few hours of stirring, no transfer of H_2O_2 to the ethylbenzene phase was detected via NMR, it remained in the aqueous phase. Therefore, it can be concluded that tBHP is a more complex organic molecule than H_2O_2 and commonly utilized in oxidation processes [53]. The presence of the tert-butyl group gives tBHP organic properties making it soluble in both aqueous and organic substrates, unlike H_2O_2 [54-55]. Therefore, H_2O_2 is not soluble in ethylbenzene, providing an explanation for the reaction did not occur. Hence, the selection of an oxidizing agent should be based on the substrate involved the desired products, and the specific reaction conditions [56].

5.8 Assessment of catalyst reusability

Industrial catalysts need to exhibit not only high activity but also stability. Ideally, theses catalysts should be long lasting or capable of regeneration at low cost without losing their effectiveness. In laboratory batch processes, the reusability of a catalyst is determined by recovering it after each reaction and using it repeatedly, a process that can be conducted as many times as required. Therefore, the catalyst containing 5 wt% Ag/Nb_2O_5 was recovered after reaction, following the process mentioned in chapter 2, section 9. The outcomes from repeated reuses of the same catalyst are shown in table 5.14. The conversion achieved with the reused catalyst remains generally stable, with only a slight decrease noted on the third use. Our catalyst Ag/Nb_2O_5 shows the best activity for ethylbenzene oxidation, achieving a conversion rate of 29 ± 3 and a selectivity of 78% for acetophenone after 24 hours. Therefore, the use of 5 wt% Ag/Nb_2O_5 catalyst was found to maintain stability over multiple uses without any loss of conversion, which was attributed to the absence of sintering. Following each use, the catalyst was cleaned with acetone to eliminate residual products which stay on the surface. After multiple uses, the selectivity changes slightly too with reuse. The selectivity for the acetophenone decrease from 78% on the first use to 64% by the third use. The loss of selectivity might be due to a build-up of product on the catalyst surface that washing with acetone does not remove. Understanding the cause of this change could be valuable for developing catalysts selective for ethylbenzene.

Table 5.14: Table showing the results of the reusability test for the oxidation of ethylbenzene using Ag/Nb_2O_5 catalyst at 120 °C for 24 h with a stirring rate of 600 rpm. The first and second, third test data are presented, illustrating the ethylbenzene conversion rates and selectivity for each test condition. Including selectivity for 1-phenylethanol (1-Ph), Acetophenone (AP) and 1-phenyl ethyl hydroperoxide (EBHP), and carbon mass balance (CMB %).

No. of test	Catalyst	EB Conversion (%)	Observed selectivity (%)			CMB (%)
			AP	1-Ph	EBHP	
1	Ag/ Nb_2O_5	29 ± 3	78 ± 2	22 ± 2	0	100 ± 3
2	Ag/ Nb_2O_5	29 ± 3	71 ± 2	29 ± 2	0	
3	Ag/ Nb_2O_5	23 ± 3	64 ± 2	28 ± 2	6	

5.9 Control tests for diffusion

Heterogeneous catalysis plays a crucial role in both academic research and industrial processes. This importance stems from the catalyst being in a different phase than the reactants, typically a solid catalyst interacting with gaseous or liquid reactants. One of the critical factors influencing the efficiency and rate of catalytic reactions is diffusion. It is a constant phenomenon that entails the movement of reactants from the fluid phase to the catalyst surface and the movement of products from the catalyst surface back into the fluid phase [57-58]. This can be a significantly important factor influencing the reaction rate or selectivity, particularly in large scale production [59]. In this study, the oxidation process needs to be in a kinetic regime to enable comparison among different tests. Therefore, the stirring speed and the molar metal to substrate ratio (M: S) were varied to determine whether the reaction is governed by kinetic or diffusion processes.

5.9.1 Impact of stirring speed on ethylbenzene oxidation

Another factor that could potentially limit the reaction is the stirring speed. As the stirring speed increases, the diffusion of reactants to the catalyst may also increase. If the stirring is not sufficient, then the diffusion limitation can arise. Therefore, the impact of stirring speed has been studied to determine the conditions under which inefficient stirring may lead to mass transfer limitations.

Mixing under specific conditions affects both reaction rates and product distribution [60]. To assess its impact on ethylbenzene oxidation, the influence of stirring speed on mass transfer was investigated across a range from 400 rpm to 800 rpm. Overly high or insufficient stirring speeds could result in incomplete mixing of the reaction slurry or lead to splashing inside the round bottom flask.

Figure 5.7 illustrate that there are no changes in conversion as the speed increases from 400 rpm to 800 rpm. The conversion remains consistently around 26 ± 2, taking into account the experimental error, suggesting that oxygen diffusion does not limit oxidation in this range. To ensure thorough mixing of the reaction mixture without splashing, a stirring speed of 600 rpm is employed in our study.

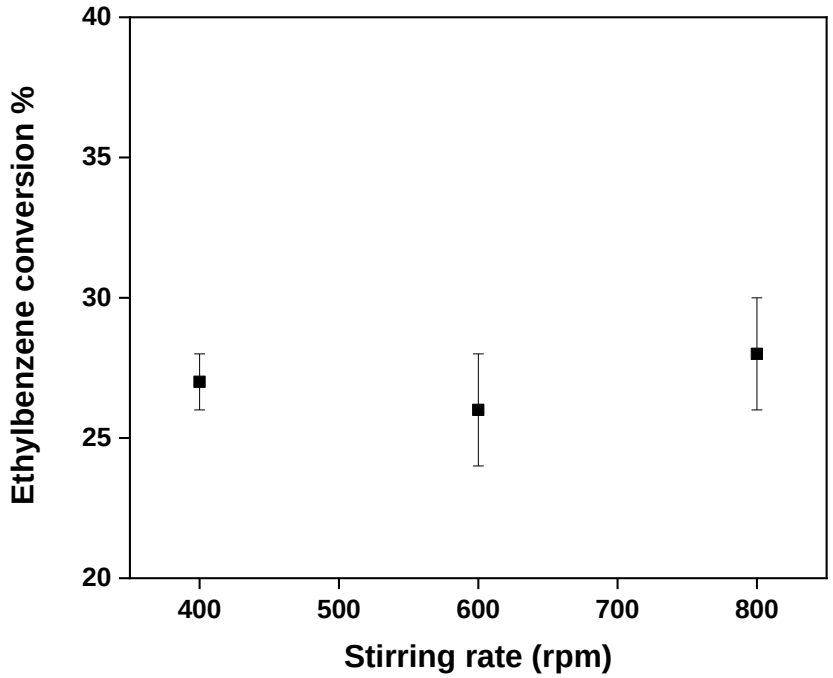

Figure 5.7: Effect of stirring speed (400 to 800 rpm) on ethylbenzene conversion using Ag_2O catalyst under fixed conditions (120 °C, 24 h, and atmospheric pressure).

5.9.2 Impact of varying metal to substrate ratios (M: S) on the oxidation of ethylbenzene.

To study the effect of the M:S ratio on ethylbenzene oxidation and ensure that the oxidation occurs without diffusion limitations, a series of reactions with different M ratios were conducted using O_2 (atm), under fixed conditions (120 °C, 24 hours with a stirring speed of 600 rpm).

The reaction results (figure 5.6), indicate that there was no notable increase in ethylbenzene conversion observed with an increase in the quantity of catalyst employed (M molar ratio), ranging from 0 to 1:1000, when taking the error into account. This suggests that either under the current conditions, the reaction was dominated by diffusion limit (mass transfer effect), or the conversion of ethylbenzene oxidation had reached its maximum after a 24 h reaction period. Considering this phenomenon, an M ratio of 1:100 was selected as the maximum substrate amount or minimum catalyst amount to avoid entering a diffusion limitation regime.

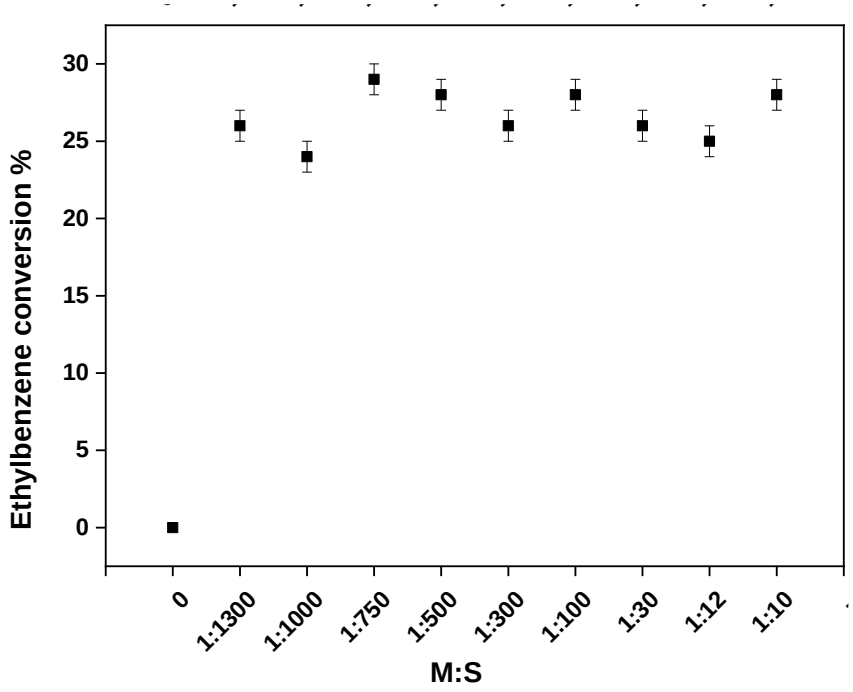

Figure 5.8: Effect of metal to substrate ratios on ethylbenzene conversion using Ag_2O catalyst under fixed conditions (120 °C, 24 h, and atmospheric pressure).

Based on the data from the tests conducted to study diffusion by varying the metal to substrate ratio and stirring speed, it is evident that we are not experiencing diffusion limitations. However, this conclusion cannot be definitively approved due to the potential impact of silver on the catalytic structure. The transformation of silver from Ag^0 to Ag^+ change the dynamics of the surface, which in turn may influence the diffusion behaviour. Moreover, changes in oxygen concentration can significantly affect the amount of intermediate species present, thereby changing the rate of the parallel termination pathway. Considering these factors and to gain more understanding of the present pathway, we have decided to carry out additional experiments. These experiments will introduce O_2 into the system up to the saturation point of the hydrocarbon. This approach aims to provide more detailed data and insights into the effects of oxygen concentration on the catalytic process and ensure that diffusion limitations are thoroughly investigated under different conditions.

5.10 XRPD patterns of WI-Ag/Nb_2O_5

As a form of quality control and in an attempt to identify structure activity correlations between the catalytic results we have observed and the bulk structure for some of our materials some characterization by means of XRPD was carried out (figures 5.10)

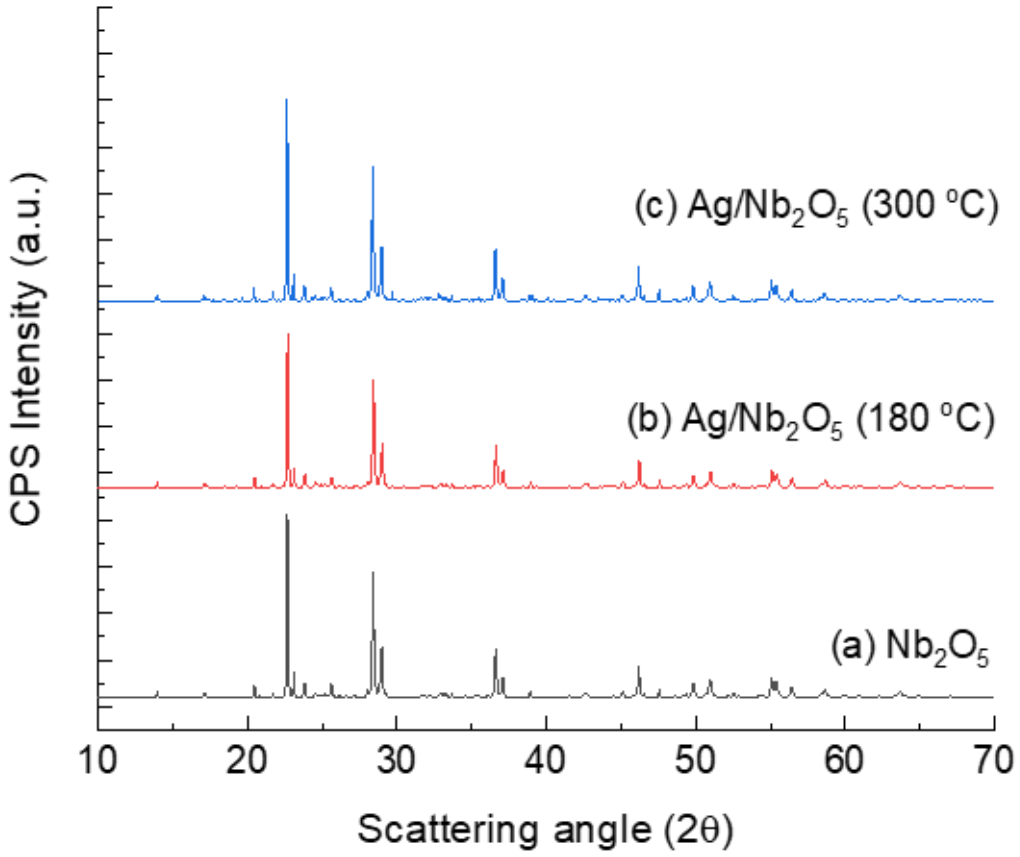

Figure 5.10: XRD patterns of Ag/Nb_2O_5 with a nominal 5 wt% loading, synthesized using the wet impregnation method. **a**. Nb_2O_5 with a purity/grade 99.9% was utilised; **b**, WI-Ag/ Nb_2O_5 catalyst was calcined at 180°C for 16h; and **c.** WI-Ag/ Nb_2O_5 catalyst was calcined at 300°C for 16h**.**

The observed XRD pattern of Nb_2O_5 with peaks 22.5°, 28.3°, 36.5°, 46.1°, and 50.9° 2θ is consistent with an orthorhombic structure (also known as T-Nb_2O_5) and with other patterns protected in the literature [18]. This is the most stable of the Nb_2O_5 phases (the others being monoclinic and hexagonal), and it also implies that the provided metal oxide from the supplier was obtained from an ethoxide precursor in a temperature range around 800 ºC.

No characteristic reflections for Ag or Ag_2O were detected. These were expected to be approximately 38.1° and 44.3° 2θ for the (111) and (200) reflections for Ag respectively and at (110) at approximately 32.8° and 54.9° 2θ for Ag_2O respectively [64]. However, as the presence of Ag was confirmed by ICP-MS, this implies small or dispersed Ag/Ag_2O species as in part corroborated by TEM (see section 5.12).

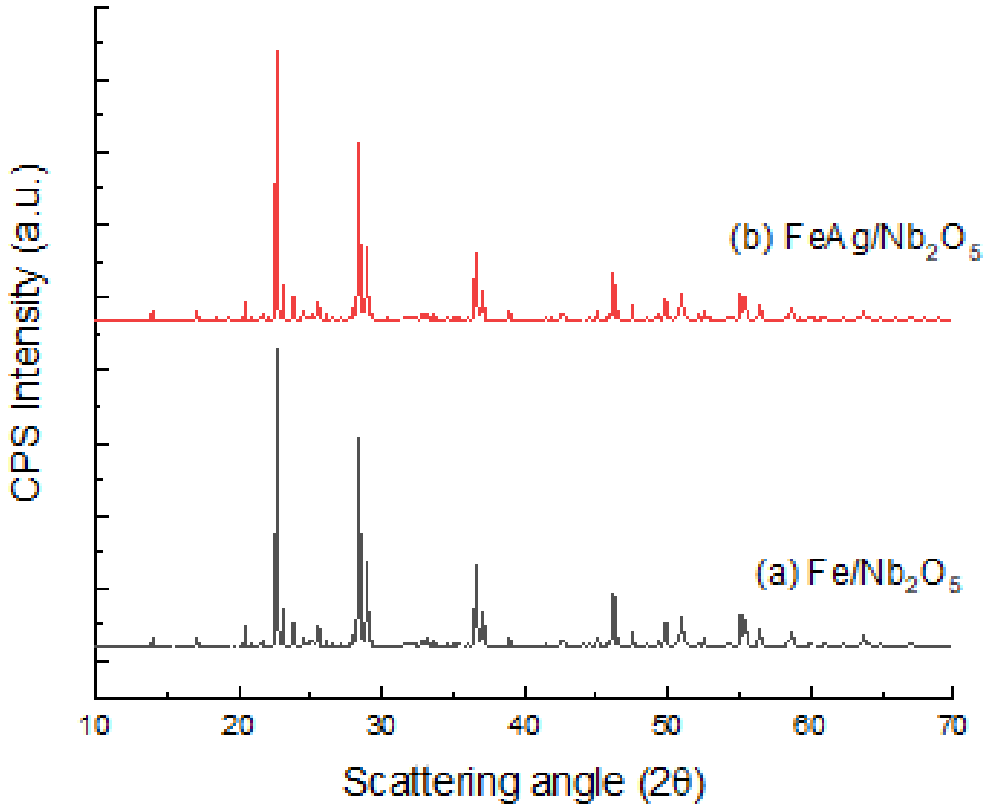

Figure 5.11: XRD patterns of Fe-Ag/Nb_2O_5 and Fe/Nb_2O_5 with a nominal 5 wt% loading, synthesized using the wet impregnation method. **a**. WI- Fe/Nb_2O_5 catalyst was calcined at 500°C for 16h; and **b.** WI-Fe-Ag/ Nb_2O_5 catalyst was calcined at 500 °C for 16 h**.**

The observed XRD pattern of Nb_2O_5 with peaks 22.5°, 28.3°, 36.5°, 46.1°, and 50.9° 2θ is consistent with an orthorhombic structure (also known as T-Nb_2O_5) and with other patterns protected in the literature. The spices are highly dispersed. The expected

reflections for Fe would be as Fe_2O_3 because the sample has been obtained by calcination in air (this is an important note and has to be added).In this case the expected reflections for the alpha form (or hematite) which is the most stable would have been at approximately 24.1°, 35.6° and 40.9° for the (102), (104) and (113) reflections respectively.

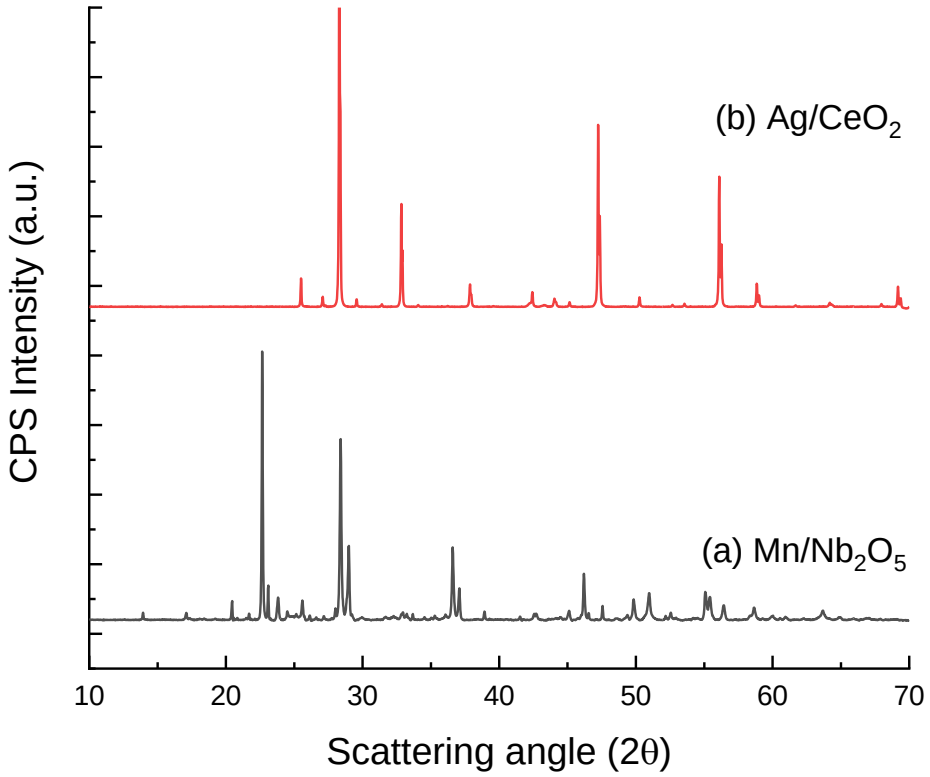

Figure 5.12: XRD patterns of Mn/Nb_2O_5 and Ag/CeO_2 with a nominal 5 wt% loading, synthesized using the wet impregnation method. **a**. WI- Mn/Nb_2O_5 catalyst was calcined at 300°C for 16h; and **b.** WI-Ag/CeO_2 catalyst was calcined at 300°C for 16h**.**

The observed XRD pattern of Nb_2O_5 with peaks 22.5°, 28.3°, 36.5°, 46.1°, and 50.9° 2θ is consistent with an orthorhombic structure (also known as T-Nb_2O_5) and with other patterns protected in the literature [18]. The spices are highly dispersed. The expected reflections for Mn would be as MnO_2 because the sample has been obtained by calcination in air and this is is the most stable of the many Mn metal oxides. In this case the expected reflections for the alpha form (a rutile-like) which is the most stable form of MnO_2 would have been at approximately 22.1° and 22.1° 2θ for the (110) and (101) reflections respectively. Also for he Ag/CeO_2 this is diagnostic of sample with well dispersed, i.e. no detectable Ag particles and for CeO_2 this shows typical signals at 28.5°, 33.0°, 47.5°, and 56.3° 2θ for the (111), (200), (220) and (311) reflections respectively and consistent with the most stable fluorite-like structure.

5.11 Transmission electron microscopy (TEM) images of Ag/Nb_2O_5

The TEM method is widely utilized for measuring surface area and is particularly prominent in the field of catalyst characterization [65]. To further establish the correlation between the catalytic activity of Ag/Nb_2O_5, synthesized via the wet impregnation (WI) method, and its properties (e.g., silver loading, particle size), transmission electron microscopy (TEM) analysis was conducted. The resulting images are presented in figure 5.13. Small Ag nanoparticles in the range of 4-5 nm were detected.

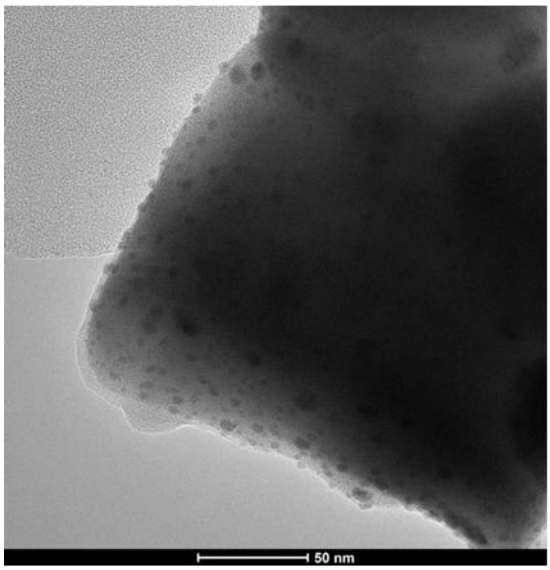

Bright Filed TEM for Ag 1 wt% over Nb_2O_5

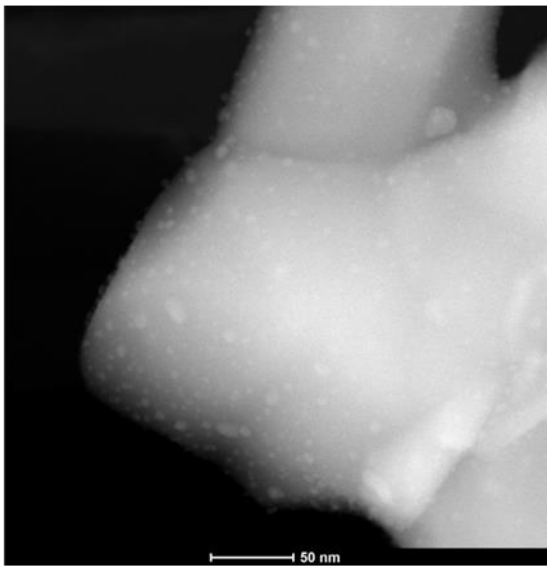

Dark field TEM for Ag 1 wt% over Nb_2O_5

Figure. 5.13: Representative TEM images of WI-Ag/Nb_2O_5 (5 wt% loading). The particle size distribution was measured, revealing a range centred around 50 nm.

5.13 X-ray photoelectron spectroscopy of WI-Ag/Nb_2O_5

We propose that the enhanced catalytic activity of WI-Ag/Nb_2O_5 may be associated with the presence of Ag_2O particles or Ag at surface level. To investigate the oxidation states of the silver species within this catalyst, X-ray photoelectron spectroscopy (XPS) was utilized, and the results are presented in figure. 5.14 and 5.15.

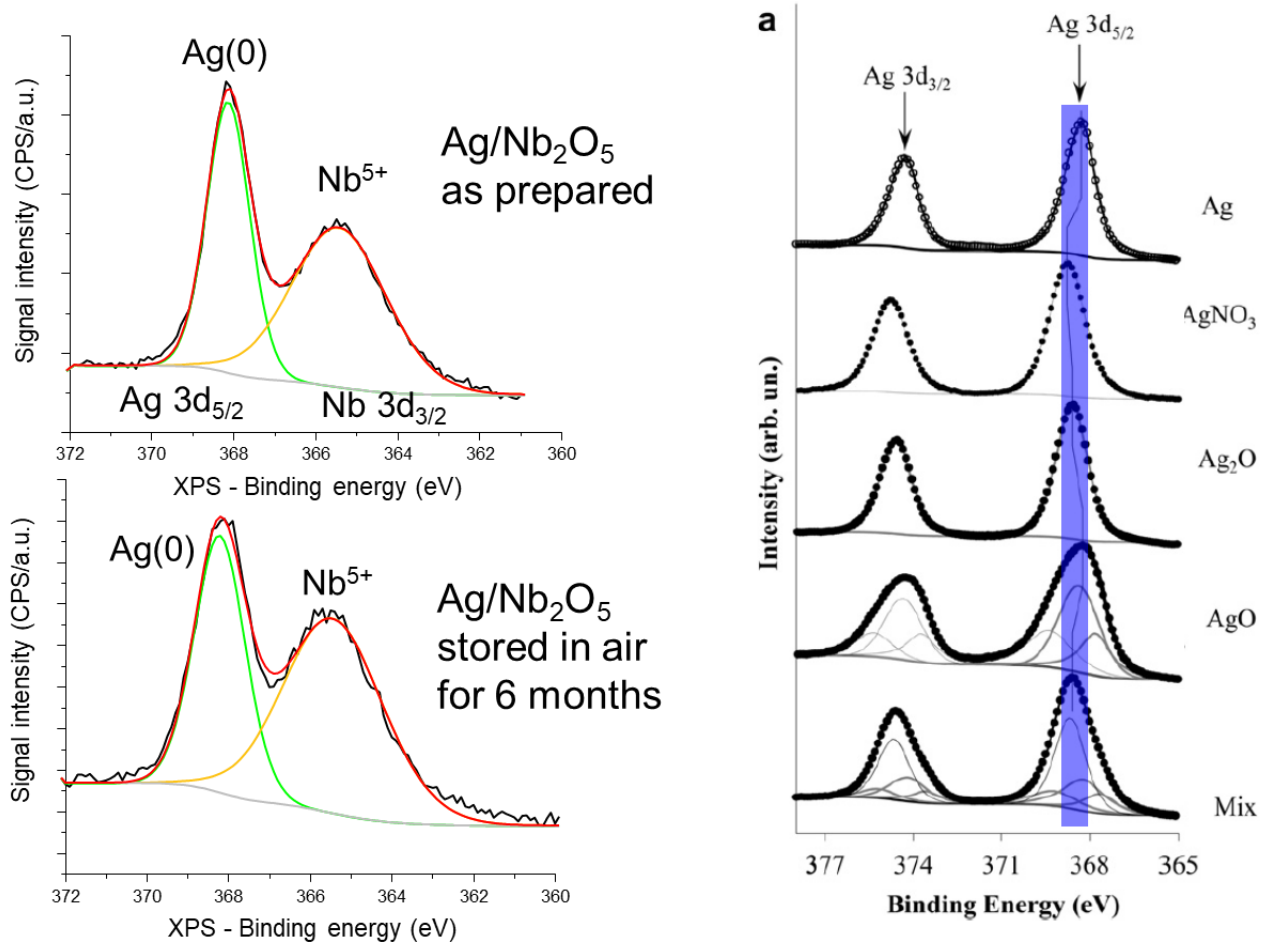

Figure 5.14: XPS spectra of the Ag/Nb_2O_5 catalyst (fresh) in the top and after stored 6 months. There is no presence of Ag^+.

At surface level, in our context metal support interface, no obvious presence of Ag+ centres, but this cannot be ruled out completely [66]. Therefore, Auger spectroscopy and possible $O_2^{\bullet-}$ formation is suggest that if the process; $M + O_2 \rightarrow M^{n+} + O_2^{\bullet-}$ takes place this may form AgO_x , and it should be possible to detect some Ag^+ (AgO_x) after reaction. Auger spectroscopy resolved the kinetic energy of photo emitted electrons more than XPS and can resolve Ag^0/Ag^+ species.

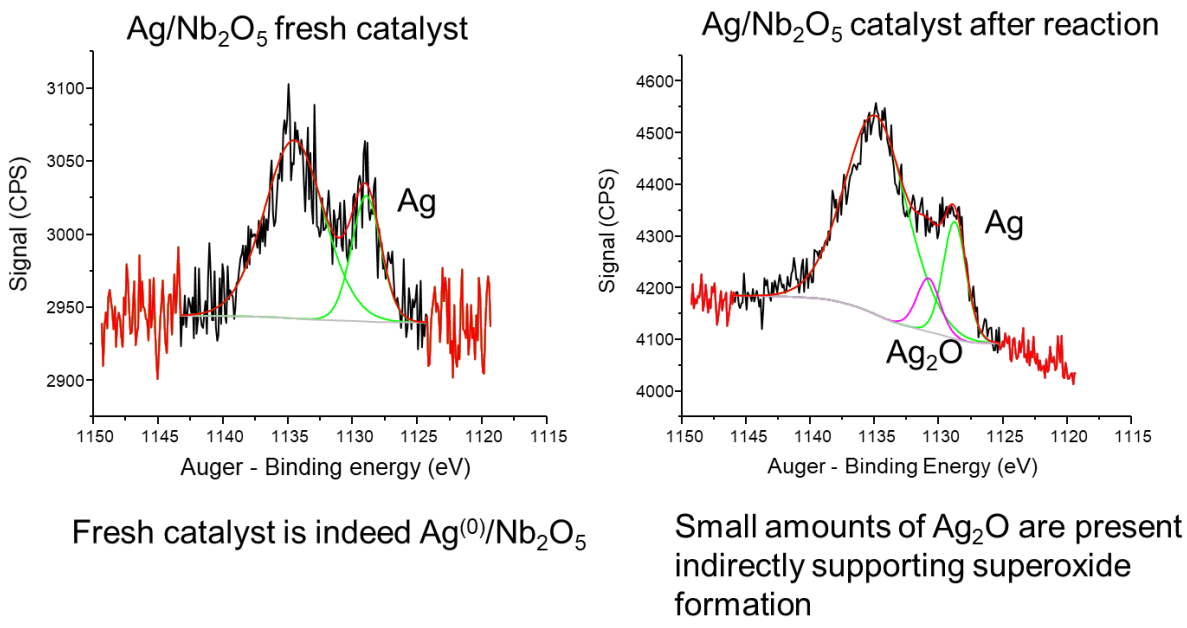

Figure 5.15: XPS spectra of the Ag/Nb_2O_5 catalyst before (fresh) and after the reaction. The presence of a small amount of Ag is indicated, with the peaks highlighted in pink on the right side of the graph, showing the Ag signals in both the fresh and used catalysts.

The Ag/Nb_2O_5 catalyst demonstrates remarkably high selectivity toward ketone formation, independent of the substrate used. It is capable of initiating the reaction and driving the selectivity of EBHP species towards ketone production. Ag (0) plays a crucial role in activating molecular oxygen (O_2) to form superoxide ($O2^{\bullet -}$). During the reaction, the catalyst undergoes structural changes, with both active species exhibiting different selectivities. The regeneration of Ag ensures that the catalyst remains active, maintaining its efficiency in the reaction process (figure 5.16).

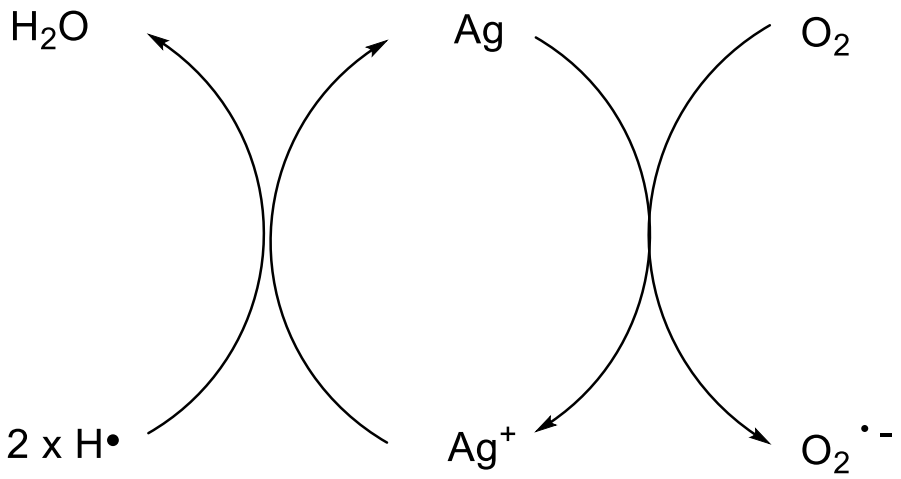

Figure 5.16: the catalyst can change structure during the reaction Ag to Ag_2O via $O2^{\bullet -}$ and Ag_2O to Ag via $H^{\bullet}$.

5.14 Conclusion

This chapter focused on the oxidation of ethylbenzene using Ag/Nb_2O_5 as a catalyst. We began with a control test of ethylbenzene oxidation in air, serving as a baseline for comparison. Without any catalyst, ethylbenzene consumption proceeded slowly, reaching 40% conversion over 144 hours. This uncatalyzed reaction followed a free radical mechanism, producing equal amounts of acetophenone and 1-phenylethyl alcohol, with a K/A ratio of approximately 1. These products result from the decomposition of the intermediate 1-phenylethyl alkyl hydroperoxide. Initially, the intermediate accumulates and reaches a maximum around 50 hours, after which it is consumed, leading to the formation of ketone and alcohol, with ketone as the dominant product. This suggests that the ketone and alcohol are direct decomposition products of the hydroperoxide intermediate. Interestingly, the reaction did not reach completion, likely due to an inhibition effect from the alcohol. The data suggest that product distribution could potentially be optimized for increased acetophenone production through the use of Nb_2O_5. However, under atmospheric conditions, Nb_2O_5 inhibited the reaction, showing 0% conversion, compared to the blank test's 9 ± 4% conversion. This indicates that Nb_2O_5 does not directly oxidize ethylbenzene, as it lacks the ability to activate a primary C–H bond and consequently does not promote the initiation process. Instead, we hypothesize that Nb_2O_5 plays a role in enhancing the decomposition of the alkyl hydroperoxide intermediate rather than initiating the reaction. On the other hand, Ag exhibited catalytic activity, initiating the C–H bond activation in ethylbenzene oxidation. Further investigation revealed that Ag+ is likely responsible for initiating the reaction driving the oxidation process. The Ag/ Nb_2O_5 catalyst demonstrated high selectivity toward ketone formation, regardless of the substrate used, and effectively directed the selectivity of EBHP species toward ketone production. Structural changes in the catalyst during the reaction, as well as the regeneration of Ag, ensured the continued activity and efficiency of the catalyst throughout the process. These findings were supported by a range of analytical techniques, including XPS, XRD, and TEM, providing valuable insights into the behaviour and performance of the Ag/ Nb_2O_5 catalyst in ethylbenzene oxidation. From XPS data it's clear that Ag can change structure during the reaction, TEM show the particle size distribution was measured, revealing a range centred on 50 nm, and XRD data show an orthorhombic structure (also known as T-Nb_2O_5).

5.15 References

1 K. Lin, J. Wang, S. Qiao and Z. Guo, *ACS Sustain. Chem. Eng.*, 2024, **12**, 6719–6727.

2 V. Berg, M. Geske, O. Korup, M. Schmidt, F. Rosowski, A. Karpov, M. Kraemer and R. Horn, *Ind. Eng. Chem. Res, 2024, **63**, 3891-3909.*

3 M. O. Azeez, S. A. Nafiu, T. A. Olarewaju, A. B. Olabintan, A. Tanimu, Y. Gambo and A. Aitani, *Ind. Eng. Chem. Res.*, 2023, **62**, 12795–12828.

4 W. L. Luyben, *AIChE J.*, 2011, **57**, 655–670.

5 Z. Razmara, F. Razmara and S. Shahraki, *Inorg. Chem. Commun.*, 2024, **161**, 112078.

6 G. Shi, Y. Feng, S. Xu, Q. Lu, Y. Liang, E. Yuan and L. Ji, *New J. Chem.*, 2021, **45**, 13441–13450.

7 Y. Su, H. Liu, H. Wang, J. Huang, H. Yu, Q. Zhang, Y. Cao and F. Peng, *Chem. Eng. J.*, 2024, **479**, 147594.

8 J. C. Rooke, T. Barakat, S. Siffert and B.-L. Su, *Catal. today*, 2012, **192**, 183–188.

9 M. Nasrollahzadeh, M. Sajjadi, M. Shokouhimehr and R. S. Varma, *Coord. Chem. Rev.*, 2019, **397**, 54–75.

10 C. Della Pina, E. Falletta, L. Prati and M. Rossi, *Chem. Soc. Rev.*, 2008, **37**, 2077–2095.

11 R. Saha and G. Sekar, *Appl. Catal. B Environ*, 2019, **250**, 325–336.

12 B. Han, PhD thesis work, The University of Sheffield, 2021.

13 T. Pu, H. Tian, M. E. Ford, S. Rangarajan and I. E. Wachs, *ACS Catal.*, 2019, **9**, 10727–10750.

14 C. T. Campbell and M. T. Paffett, *Surf. Sci*, 1984, **139**, 396–416.

15 A.-Q. Wang, C.-M. Chang and C.-Y. Mou, *J. Phys. Chem. B*, 2005, **109**, 18860–18867.

16 L. Y. Margolis and V. N. Korchak, *Russ. Chem. Rev* , 1998, **67**, 1073–1082.

17 S. Wu, Y. Yang, C. Lu, Y. Ma, S. Yuan and G. Qian, *Eur. J. Inorg. Chem.*, 2018, **2018**, 2944–2951.

18 L. Brugnoli, A. Pedone, M. C. Menziani, C. Adamo and F. Labat, *J. Phys. Chem. C*, 2020, **124**, 25917–25930.

19 J. Railton, PhD thesis work, the University of Sheffield, 2020.

20 B. R. Cuenya, *Thin Solid Films*, 2010, **518**, 3127–3150.

21 J. R. Croy, S. Mostafa, H. Heinrich and B. R. Cuenya, *Catal. Letters*, 2009, **131**, 21–32.

22 W. Lee, H. Koo, J. Sun, J. Noh, K.-S. Kwon, C. Yeom, Y. Choi, K. Chen, A. Javey and G. Cho, *Sci. Rep.*, 2015, **5**, 17707.

23 J.-W. Jun, Y.-W. Suh, D. J. Suh and Y.-K. Lee, *Catal. Today*, 2018, **302**, 108–114.

24 H. H. Kung, Transition metal oxides: surface chemistry and catalysis, Elsevier, 1989.

25 J. A. Rodriguez and M. Fernández-García, *Synthesis, properties, and applications of oxide nanomaterials*, John Wiley & Sons, 2007.

26 C. Mateos-Pedrero, H. Silva, D. A. P. Tanaka, S. Liguori, A. Iulianelli, A. Basile and A. Mendes, *Appl. Catal. B Environ.*, 2015, **174**, 67–76.

27 G. Deo and I. E. Wachs, *J. Catal.*, 1994, **146**, 323–334.

28 K. Kunimori, Z. Hu, T. Uchijima, K. Asakura, Y. Iwasawa and M. Soma, *Catal. Today*, 1990, **8**, 85–97.

29 I. Nowak and M. Ziolek, *Chem. Rev.*, 1999, **99**, 3603–3624.

30 C. G. O. Bruziquesi, B. G. José Filho, H. F. V Victoria, K. Krambrock, H. S. Mansur, A. A. P. Mansur, P. Chagas, A. C. Silva and L. C. A. Oliveira, *Catal. Commun.*, 2022, **171**, 106511.

31 H. Schäfer, R. Gruehn and F. Schulte, *Angew. Chemie Int. Ed. English*, 1966, **5**, 40–52.

32 C. Nico, T. Monteiro and M. P. F. Graça, *Prog. Mater. Sci.*, 2016, **80**, 1–37.

33 S. Furukawa, T. Shishido, K. Teramura and T. Tanaka, *J. Phys. Chem. C*, 2011, **115**, 19320–19327.

34 T. Lopez-Ausens, M. Boronat, P. Concepción, S. Chouzier, S. Mastroianni and A. Corma, *J. Catal.*, 2016, **344**, 334–345.

35 S. Colussi, P. Fornasiero and A. Trovarelli, *Chinese J. Catal.*, 2020, **41**, 938–950.

36 J. T. Carneiro, T. J. Savenije, J. A. Moulijn and G. Mul, *J. Photochem. Photobiol. A Chem.*, 2011, **217**, 326–332.

37 X. Yang, X. Wang, C. Liang, W. Su, C. Wang, Z. Feng, C. Li and J. Qiu, *Catal. Commun.*, 2008, **9**, 2278–2281.

38 J. Xie, Y. Wang, Y. Li and Y. Wei, *React. Kinet. Mech. Catal.*, 2011, **102**, 143–154.

39 V. Raji, M. Chakraborty and P. A. Parikh, *Ind. Eng. Chem. Res.*, 2012, **51**, 5691–5698.

40 X. Pan, M. Yang, X. Fu, N. Zhang and Y. Xu, *Nanoscale*, 2013, **5**, 3601–3614.

41 J. Paier, C. Penschke and J. Sauer, *Chem. Rev.*, 2013, **113**, 3949–3985.

42 M. Conte, X. Liu, D. M. Murphy, K. Whiston and G. J. Hutchings, *Phys. Chem. Chem. Phys.*, 2012, **14**, 16279–16285.

43 L. Kundakovic and M. Flytzani-Stephanopoulos, *Appl. Catal. A Gen.*, 1999, **183**, 35–51.

44 S. Miao, Y. Wang, D. Ma, Q. Zhu, S. Zhou, L. Su, D. Tan and X. Bao, *J. Phys. Chem. B*, 2004, **108**, 17866–17871.

45 X. Liu, M. Conte, Q. He, D. W. Knight, D. M. Murphy, S. H. Taylor, K. Whiston, C. J. Kiely and G. J. Hutchings, *Chem. Eur. J.*, 2017, **23**, 11834–11842.

46 H. Gruber-Wölfler, P. F. Radaschitz, P. W. Feenstra, W. Haas and J. G. Khinast, *J. Catal.*, 2012, **286**, 30–40.

47 R. A. Sheldon, M. Wallau, I. Arends and U. Schuchardt, *Acc. Chem. Res.*, 1998, **31**, 485–493.

48 H.-U. Blaser, A. Indolese, A. Schnyder, H. Steiner and M. Studer, *J. Mol. Catal. A Chem.*, 2001, **173**, 3–18.

49 E. Aneggi, J. Llorca, C. de Leitenburg, G. Dolcetti and A. Trovarelli, *Appl. Catal. B Environ.*, 2009, **91**, 489–498.

50 J. F. Weaver and G. B. Hoflund, *Chem. Mater.*, 1994, **6**, 1693–1699.

51 Q. Wu, M. Si, B. Zhang, K. Zhang, H. Li, L. Mi, Y. Jiang, Y. Rong, J. Chen and Y. Fang, *Nanotechnology*, 2018, **29**, 295702.

52 G. B. Shulpin and G. V Nizova, *React. Kinet. Catal. Lett.*, 1992, **48**, 333–338.

53 J. M. Escola, J. A. Botas, J. Aguado, D. P. Serrano, C. Vargas and M. Bravo, *Appl. Catal. A Gen.*, 2008, **335**, 137–144.

54 A. Dhakshinamoorthy, M. Alvaro and H. Garcia, *J. Catal.*, 2009, **267**, 1–4.

55 J. Zhang, Z. Wang, Y. Wang, C. Wan, X. Zheng and Z. Wang, *Green Chem.*, 2009, **11**, 1973–1978.

56 N. Montoya Sánchez and A. de Klerk, *Appl. Petrochemical Res.*, 2018, **8**, 55–78.

57 C. Resini, F. Catania, S. Berardinelli, O. Paladino and G. Busca, *Appl. Catal. B Environ.*, 2008, **84**, 678–683.

58 Y. Luo, *Comprehensive handbook of chemical bond energies*, CRC press, 2007.

59 P. Zhang, Y. Gong, H. Li, Z. Chen and Y. Wang, *Nat. Commun.*, 2013, **4**, 1593,

60 J. R. Bourne, *Org. Process Res. Dev.*, 2003, **7**, 471–508.

61 M. Che and J. C. Védrine, *Characterization of Solid Materials and Heterogeneous Catalysts: From Structure to Surface Reactivity,* Wiley-VCH Verlag GmbH & Co. KGaA, 2012, **1–2**.

62 S. U. Nandanwar, S. Rathod, V. Bansal and V. V. Bokade, *Catal. Letters*, 2021, **151**, 2116-2131.

63 K. M. Parida and S. S. Dash, *J. Mol. Catal. A Chem.*, 2009, **306**, 54–61.

64 Z. H. Dhoondia and H. Chakraborty, *Nanomater. Nanotechnol.*, 2012, **2**, 15.

65 F. Ambroz, T. J. Macdonald, V. Martis and I. P. Parkin, *Small methods*, 2018, **2**, 1800173.

66 A. M. Ferraria, A. P. Carapeto and A. M. B. do Rego, *Vacuum*, 2012, **86**, 1988–1991.

Chapter 6: Use of Ag/Nb_2O_5 for oxidation of cyclooctane and *p*-xylene

6.1 Introduction

The selective oxidation of hydrocarbons is an essential technique for introducing functional groups, enabling the production of various oxygenated compounds such as aldehydes, alcohols, ketones, and carboxylic acids. This process has been reported to effectively functionalize C–H bonds in hydrocarbons through oxidation, particularly when using heterogeneous catalysts [1-2]. The development was inspired by the high selectivity and efficiency observed in the oxidation of ethylbenzene using Ag/Nb_2O_5. As a result of the experimental findings from the oxidation of ethylbenzene in chapter 5, the selective decomposition of EBHP species through the abstraction of hydrogen at the alpha position has demonstrated significant potential for directing the formation of desired products [3-4]. Considering these results, we aim to investigate the capability of our catalysis Ag/Nb_2O_5 for the selective oxidation of another hydrocarbon. Therefore, in this chapter we studied the selective oxidation of cyclooctane and *p*-xylene. Two substrates chosen for their relevance in industrial applications [5-6] and their structural characteristics that may favour selective product formation [7-8]. For example, the aerobic oxidation of *p*-xylene in acetic acid media using co-catalysis of metalloporphyrin and $Co(OAc)_2$ to yield TPA as shown in the following figure 6:1:

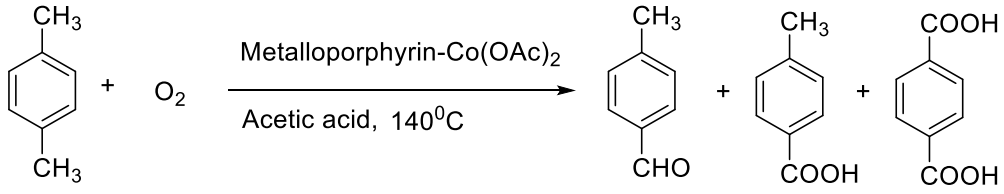

Figure 6.1: p-xylene oxidation catalyzed by metalloporphyrin–Co $(OAc)_2$ with air in acetic acid. The reaction used metalloporphyrin in combination with $Co(OAc)_2$ as the catalyst. The primary oxidation products were p-toluic aldehyde, p-toluic acid, and terephthalic acid as shown in the figure respectively.

The reason cyclooctane was chosen was that it is cyclic, which will have a lower C–H activation energy compared to linear alkanes (a difference of up to 84% kJ mol^{-1}) [9-10] . A key input in the production of polymers and pharmaceuticals is cyclooctane and cyclohexane oxidation, which are both industrially relevant reactions requiring selectivity and producing sought-after products [11-12-13]. In this reaction, all reactive positions are identical, and the main oxidation product is cycloctanone [7-14]. Unlike

cyclohexane which requires high pressure to oxidize into cyclohexanone [15-16], cyclooctane offers a potential pathway to cycloctanone under milder conditions, thereby providing an opportunity to examine the catalyst's ability to promote selective oxidation without producing ring-opened by-products. Similarly, p-xylene was chosen for its potential to be oxidized to para-terephthalic acid (PTA), a crucial precursor in the production of polyethylene terephthalate (PET) plastics and fibres [17-18] . Achieving high para selectivity in this reaction is challenging [19], as it requires minimizing the formation of unwanted by products, which can complicate the reaction mixture [20-21.] Therefore, Ag/Nb_2O_5 support was given particular attention in this work. By investigating these substrates, we aim to gain insights into the mechanisms of selectivity control and assess the efficacy of the catalysts in promoting desired oxidation pathways. ^{1}H-NMR used to characterise the reaction mixture and for quantitative the analysis. In a similar manner to the procedure outlined for ethylbenzene oxidation in chapter 3, a method was developed to calculate the conversion, selectivity, and carbon mass balance for the oxidation of cyclooctane and *p*-xylene.

6.2 Optimizing cyclooctane oxidation conditions

In the polymer industry, aryl and cyclic hydrocarbons serve as major raw materials for making precursors and high-value intermediates such as acids and ketones, which are used in producing fibres, plastics, and coatings [22-23-24]. The oxidation of cyclooctane by molecular O_2 is the model reaction used in our work to evaluate the catalytic capabilities of produced catalysts for the following reasons: i) it is well known that cyclooctane oxidation produces cycloctanone, cyclooctanol, and cyclooctyl peroxide as seen in scheme 6.1, which are valuable intermediates in industrial organic synthesis; ii) in addition, an experimental set-up open to air could be used to allow for the oxidation process, thus also utilizing molecular oxygen from air instead of pressurised systems initially; iii) according to findings from the literature, cyclooctane is mostly oxidized with polyoxometalates [25-26] or cobalt-based catalysts [27], to make ketones or alcohols with supported metal catalysts utilizing molecular oxygen (O_2); and iv) given that cyclooctane and cyclohexane have similar physical and chemical properties, it is anticipated that the catalytic results of oxidation of cyclooctane will yield valuable information for the study of oxidation of cyclohexane using the supported

metal catalysts that have been designed. This will allow us to expand the use of catalysts for oxidation of other hydrocarbons if it is possible. Thus, in order to study more about the catalytic reactivity of Ag/Nb_2O_5 catalysts, the primary investigation into cyclooctane oxidation has been conducted.

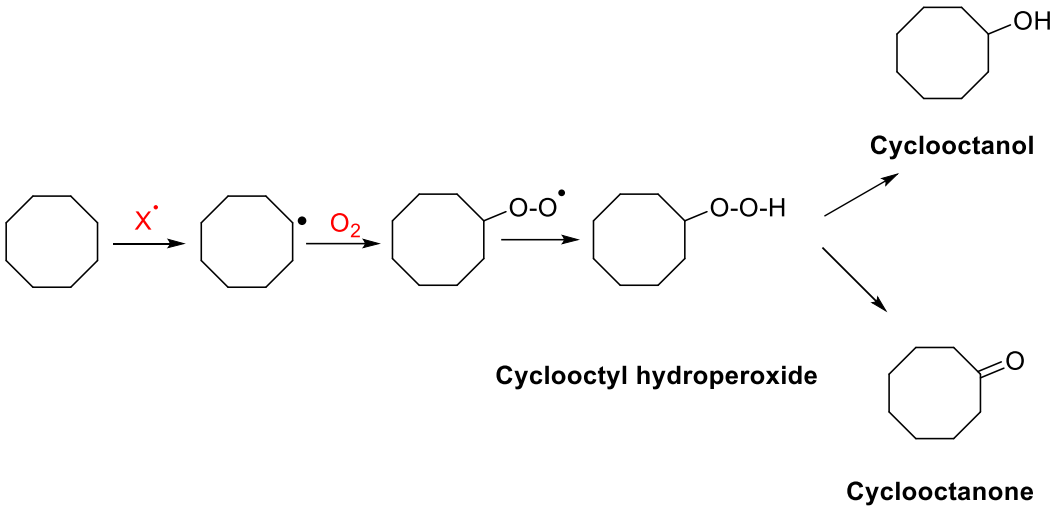

Scheme 6.1: The aerobic autoxidation of cyclooctane with an initiator (X•) follows a free-radical pathway where an R• radical reacts with O_2 to form a hydroperoxide radical. Cyclooctyl hydroperoxide, an intermediate, can further transform into alcohol, ketone, or other by-products.

6.2.1 Catalytic test at atmospheric pressure

Autoxidation without a catalyst is studied as a background process for comparison with catalyst activity, as covered in section 1.2.1 of chapter 1. In order to achieve an optimal balance between conversion and selectivity, we varied the parameters and observed their effects on selectivity toward alcohols and ketones (which is the target product in this work). Based on previous research with ethylbenzene in chapter 4, we identified the most effective parameter set, which included conducting the reaction for 24 hours at 120 °C with stirring at 600 rpm.

6.3 Oxidation of cyclooctane using Ag/Nb_2O_5

In this study, WI-Ag/Nb_2O_5 5 wt% was used for the oxidation of cyclooctane. In contrast to the blank autoxidation process this catalyst promotes the oxidation of cyclooctane. In fact, no significant conversion was observed for the autoxidation process without a catalyst, even after 24 hours. In the blank tests conducted at temperatures below 120°C, specifically at 100°C and 110°C, no conversion was observed. Similarly, when the temperature was increased to 120°C the results still showed no activity. Therefore,

as mentioned earlier in this chapter, we identified parameters which included conducting the reaction for 24 h at 120 °C with stirring at 600 rpm. To run out the reaction, when the test was run with our catalyst Ag/Nb_2O_5 the results showed a conversion of up to 27 ± 3%. This indicates that Ag/Nb_2O_5 actively participates in the reaction and reduces the activation energy required for the C–H bond activation. Therefore, Ag^+ ions might act as initiators for the dissociation of the C–H bond in cyclooctane, suggesting a promising role for Ag^+ in hydrocarbon oxidation. Following up on our discussion of the activation of O_2 by supported Ag particles in chapter 1, we conclude that the newly formed superoxide species ($O_2^{\bullet-}$) can abstract a C–H bond to initiate the reaction. The Ag/Nb_2O_5 catalyst effectively facilitates the conversion of cyclooctane at 120 °C, achieving a conversion rate of approximately 27%.

6.3.1 A possible Ag/Nb_2O_5 reaction pathway for the oxidation of cyclooctane

As shown in chapter 5, Section 5.4, we have provided evidence that both Ag^0 and Ag^+ are formed within the free radical system as shown in chapter 1 scheme 1.1. Each species was tested separately to assess their individual reactivity. The results clearly indicate that the source of reactivity in the oxidation of ethylbenzene originates from Ag^+ rather than Ag^0. The trend observed in the graphs presented here further supports this conclusion, showing that Ag^0 does not participate in the initiation of C–H bond activation or the decomposition of ethylbenzene hydroperoxide (EBHP). In contrast, Ag^+ is involved in the initiation process, while the supported catalyst, Nb_2O_5, might be responsible for the decomposition of the peroxide, as detailed in chapter 5, section 5.3.2.

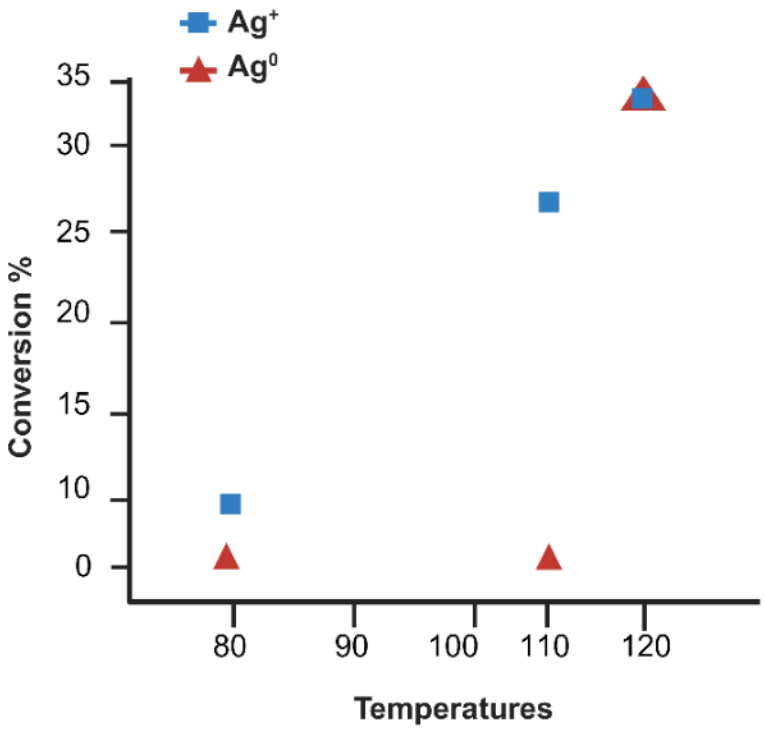

Figure 6.2: The figure illustrates the catalytic activity of Ag^0 (red) and Ag^+ (blue) in the oxidation of ethylbenzene, plotted as conversion percentage against temperature. The reaction was carried out at three different temperatures: 80 °C, 110 °C, and 120 °C, with each experiment running for 24 hours.

In figure 6.2 we demonstrated the differences in catalytic performance between the two species Ag^+ and Ag^0. To further support these data, additional investigations into the selectivity between Ag^0 and Ag^+ in ethylbenzene oxidation were conducted. The results are presented in the following tables, with each table divided according to different temperature conditions: 80 °C, 110 °C, and 120 °C, respectively.

Table 6.1: Oxidation of ethylbenzene at 80°C 24h using two species Ag^+ and Ag^0, including observed selectivity for 1-phenylethanol (1-Ph), Acetophenone (AP) and 1-phenyl ethyl alkyl hydroperoxide (EBHP), and carbon mass balance (CMB %), n.d stands for not detected..

Test	EB Conversion (%)	Observed selectivity (%)			CMB (%)
		1-Ph	AP	EBHP	
Blank test	n.d	n.d	n.d	n.d	100 ± 1
Ag^0	n.d	n.d	n.d	n.d	
Ag^+	10 ± 1	32 ± 2	62 ± 2	6 ± 3	

Table 6.2: Oxidation of ethylbenzene at 110°C 24h, using two species Ag^+ and Ag^0, including selectivity for 1-phenylethanol (1-Ph), Acetophenone (AP) and 1-phenyl ethyl hydroperoxide (EBHP), and carbon mass balance (CMB %), n.d stands for not detected.

Test	EB Conversion (%)	Observed selectivity (%)			CMB (%)
		1-Ph	AP	EBHP	
Blank test	n.d	n.d	n.d	n.d	100 ± 3
Ag^0	n.d	n.d	n.d	n.d	
Ag^+	10 ± 1	14 ± 2	79 ± 2	5 ± 3	

Table 6.3: Oxidation of ethylbenzene at 120 °C, 24 h, using two species Ag+ and Ag^0, including selectivity for 1-phenylethanol (1-Ph), Acetophenone (AP) and 1-phenyl ethyl hydroperoxide (EBHP), and carbon mass balance (CMB %).

Test	EB Conversion %)	Observed selectivity (%)			CMB (%)
		1-Ph	AP	EBHP	
Blank test	9 ± 4	7 ± 1	10 ± 2	85 ± 3	100 ± 3
Ag^0	32 ± 1	15 ± 2	82 ± 2	4 ± 2	
Ag^+	32 ± 1	15 ± 2	82 ± 1	4 ± 2	

These findings shown that Ag (0) plays an important role in activating molecular oxygen (O_2) to generate superoxide ($O_2^{\bullet-}$). Throughout the reaction, the catalyst undergoes structural changes, with both active species (Ag^0 and Ag^+) showing different selectivities. The regeneration of Ag ensures the catalyst's continued activity, preserving its efficiency in the reaction process (more details in chapter 5). Based on the results and discussions presented in the preceding sections, a simplified reaction mechanism for the oxidation of cyclooctane using Ag/Nb_2O_5 as the catalyst is proposed and depicted in Scheme 6.1. This proposed mechanism is grounded in the observed experimental data, which highlight the distinct roles of both silver species (Ag^0 and Ag^+) in the reaction pathway and the catalytic contribution of Nb_2O_5. The mechanism provides a key step involved in the cyclooctane oxidation process, including the initiation, propagation, and termination stages, as well as the decomposition of intermediates. Further details of the mechanistic steps are outlined

and illustrated in the following scheme 6.2

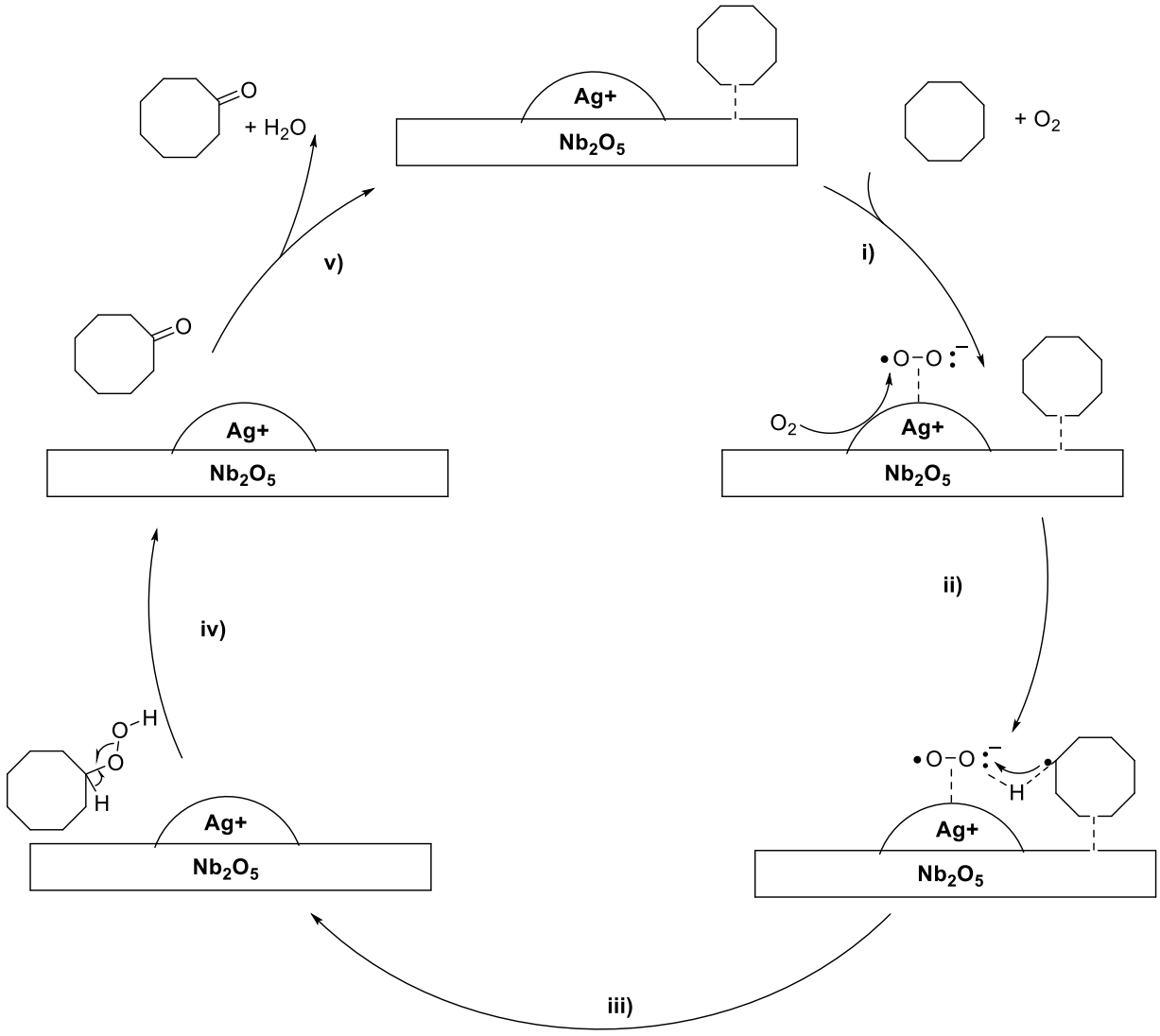

Scheme 6.2: A simplified outline of the reaction pathway for Ag/Nb_2O_5 in the oxidation of cyclooctane with O_2. By integrating the catalytic behavior of Ag and the role of the Nb_2O_5 support, the mechanism offers insight into how these components facilitate the oxidation of cyclooctane under the experimental conditions.

The proposed mechanism, as shown in scheme 6.2, suggests that the Ag/Nb_2O_5 catalyst has the capability to initiate the oxidation of similar types of hydrocarbons. We carried out the cyclooctane oxidation reaction under mild conditions at atmospheric pressure in a solvent-free system, which proved effective. In contrast, other studies have required higher pressures to activate similar reactions using different catalysts

[28]. This finding indicates the applicability of Ag/Nb_2O_5 to activate the specific substrate studied at this condition (120 °C, atm). We propose that in this reaction mechanism, molecular oxygen (O_2) is activated by Ag species (Ag_2O, Ag^+) on the Nb_2O_5 surface as the Ag–O interaction is more effective [29]. The newly formed superoxide species adsorb onto the surface of Ag particles where they extract H atoms from cyclooctane to initiate the reaction. This enhancement helps explain why selectivity for the ketone is higher with Ag particles compared to Nb_2O_5 alone. The Ag species facilitate more efficient oxidation processes leading to an increased formation of cycloctanone relative to other products. To further investigate this result and to better understand the roles of Ag and Nb_2O_5 in the reaction mechanism, 1-phenylethyl hydroperoxide (PEHP) was selected as a substrate for detailed study. The catalytic behavior of Nb_2O_5 alone and in combination with Ag, specifically in the form of WI-Ag/Nb_2O_5, was examined under an oxygen atmosphere (O_2) to elucidate how each component contributes to the reaction. By using PEHP as a model compound, we aimed to isolate and analyze the specific effects of the silver species and the niobium oxide support on the decomposition of the hydroperoxide and the overall oxidation process. The results provided awareness into the distinct functions of each catalyst in initiating and propagating oxidation reactions. Further details, including reaction conditions and mechanistic insights, are discussed in chapter 5.

6.4 Oxidation of *p*-xylene and its application

From petroleum feed-stock and natural gas, oxygen-containing compounds such as alcohols, ketone and carboxylic acids can be produced by direct oxidation with air (O_2) [30-31]. Among the carboxylic acids produced from hydrocarbons, terephthalic acid (TPA), derived from p-xylene, is currently one of the fastest-growing chemicals as an ingredient in PET (polyethylene terephthalate) [32-33]. Terephthalic acid (1, 4-benzendicarboxylic acid, TPA), is a crucial in the polyester industry for manufacturing polyester terephthalate, commonly referred to as PET [34-35]. While a large share of global terephthalic acid production is used for PET, it also has various other uses [33], including in textiles, polyester staple fibres, filament yarns, as a component in paints, coating resins, and as a raw material in the pharmaceutical sector (see figure 6.3).

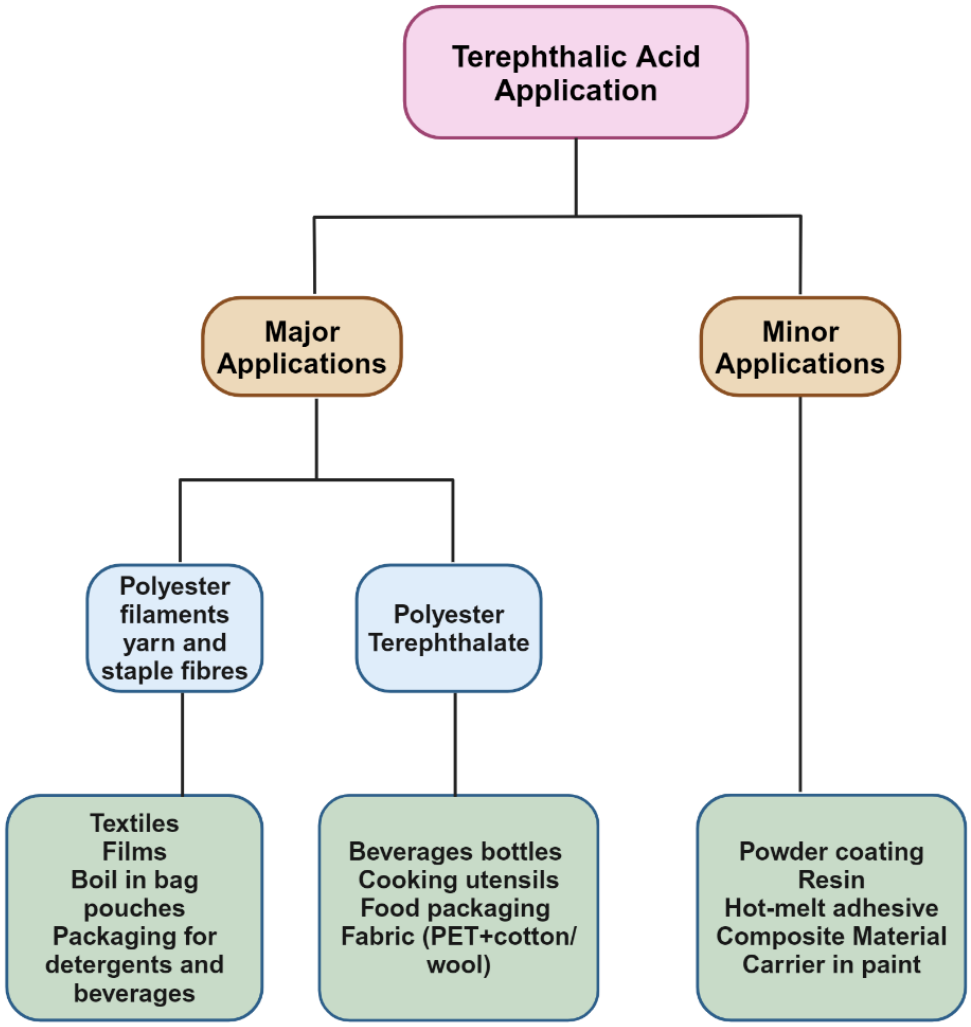

Figure 6.3: Terephthalic acid applications (1, 4-benzenedicarboxylic acid, TPA). Adapted from [36].

6.4.1 Terephthalic Acid: oxidation pathway

Terephthalic acid's history and necessity are closely related to the manufacture of polyester [37-38], which has fuelled advancements and extensive study in this area. Fractional distillation of naphtha yields p-xylene, which is used as a raw ingredient in petroleum-based terephthalic acid. The oxidation of *p*-xylene to terephthalic acid can typically be categorized into two steps: the fast oxidation of *p*-xylene to p-toluic acid, followed by the slower oxidation of p-toluic acid to terephthalic acid. The distinct shift in the oxidation rate is linked to the varying stability of the radicals generated during the reaction of alkyl benzene with molecular oxygen [39]. The oxidation of *p*-xylene is the primary pathway for producing terephthalic acid. These by-products is illustrated in the following (scheme 6.3).

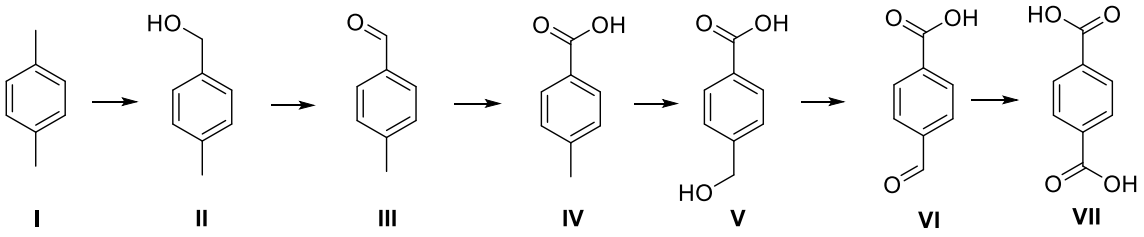

I: *p*-xylene
II: 4-methylbenzyl alcohol
III: *p*-tolualdehyde
IV: *p*-toluic acid
V: *p*-carboxylbenzyl alcohol
VI: 4-carboxylbenzaldehyde
VII: Terephthalic acid (TPA)

Scheme 6.3: The reaction pathway and resulting products from the oxidation of p-xylene [40-41].

The research aimed to investigate the oxidation mechanism by revealing the step-by-step pathway that the reactants, alkane and hydrocarbon, follow, identifying aldehydes as intermediates in the process. Although these early studies began producing terephthalic acid, the lengthy reaction times made them impractical for industrial use, therefore, using heterogeneous catalysis is indeed. The liquid phase oxidation of *p*-xylene was one of the earliest commercially and industrially feasible processes for generating terephthalic acid [5-42]. This was achieved with temperatures between 160 °C and 200 °C and pressures between 8 and 13 bar, using diluted nitric acid (30–40%) as the oxidant. For example, in the AMOCO process, *p*-xylene oxidation is carried out

using a homogeneous catalyst composed of three ions: cobalt, manganese, and bromide. Acetic acid serves as the solvent, while oxygen or air is used as the oxidant as can be seen in scheme 6.4. The setup created an explosive and hazardous environment, causing the terephthalic acid to become contaminated with colored impurities. After that , this method was replaced the dangerous nitric oxidation route with a favour solvent free air oxidation process for *p*-xylene (at temperatures between 140 °C and 180 °C and pressure between 5 and 8 bar using cobalt as a catalyst [43-44-45]. Consequently, research has focused on developing new catalytic systems for the oxidation of *p*-xylene that are less harmful to the environment and less corrosive. This has been done to advance our understanding of these new catalysts, enabling

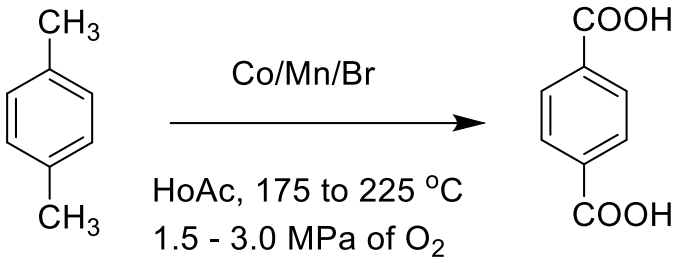

Scheme 6.4: Commercial Production of Terephthalic Acid: The AMOCO *p*-xylene Oxidation Process [46].

The oxidation of *p*-xylene under milder conditions. As a result, we applied Ag/Nb_2O_5 in the oxidation of *p*-xylene, achieving promising results that helps for future research and further development. This approach not only demonstrates the potential of Ag/Nb_2O_5 as an effective catalyst but also opens new ways for optimizing and refining the process in subsequent studies.

Commercially significant polyesters are formed by polymerizing a dibasic acid with a glycol. Especially, the polymers derived from terephthalic acid and ethylene glycol are a crucial category of synthetic fibres. Terephthalic acid (TPA) is typically produced through the oxidation of *p*-xylene using air or oxygen. There were 26 million tons of polyester terephthalate (PET) manufactured worldwide in 2012, with its growth estimated at 5% annually. Currently, about 70% of the TPA used worldwide is produced by catalytic oxidation of *p*-xylene (figure 6.4). However, this technology faces several challenges in producing fibre-grade TPA. The catalyst system must provide the maximum TPA yield in mild operating conditions. Additionally, purification from oxidation by-products and catalyst residues is often necessary to achieve fibre-grade TPA.

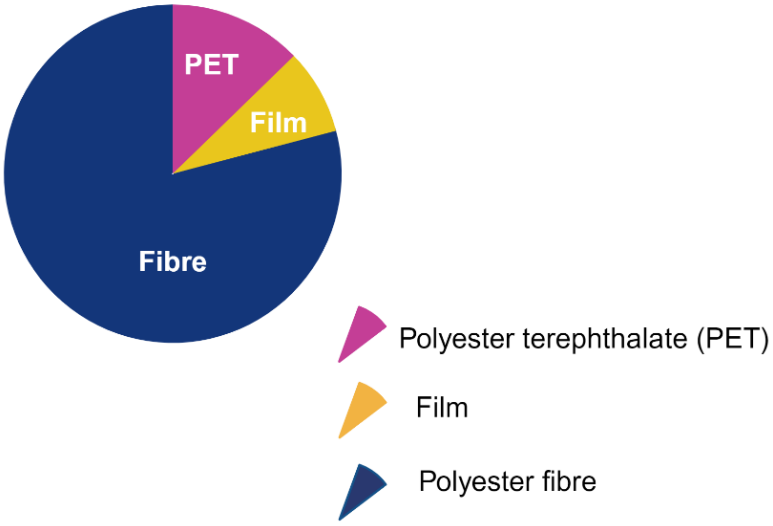

Figure 6.4: Global consumption of terephthalic acid (2011-2012) [36].

6.5 Oxidation of *p*-xylene by using Ag/Nb_2O_5

Under atmospheric pressure and in the presence of 1 bar oxygen (O_2), investigation into the catalytic activity was carried out using an open-system reactor and batch reactors with oxygen flow. A detailed explanation of this experimental setup is provided in chapter 2 section 2.9. For the *p*-xylene oxidation, we are utilizing our catalysed reaction according to the discussion we had for cyclooctane oxidation with Ag/Nb_2O_5. In light of this, preliminary control tests were conducted to evaluate the role of Ag^+ species in initiating the reaction and Nb_2O_5 with the unoccupied oxygen sites may cause O_2 to be activated and produce superoxide species [47]. Therefore , the result suggested that the Ag^+ species (Ag_2O) could facilitate the formation of the intermediate during the oxidation of cyclooctane, and also that superoxide species can form during this process (O_2^-) [48-49]. Based on the promising results from cyclooctane oxidation and the significance of ethylbenzene oxidation, we also carried out our preliminary study of the catalytic activity of the catalysts for *p*-xylene oxidation under two conditions (atmospheric pressure and 1 bar), at a fixed temperature of 120 °C and a reaction time of 24 hours. The reaction results for conversion and selectivity using Ag/Nb_2O_5 are presented in the following figure 6.5.

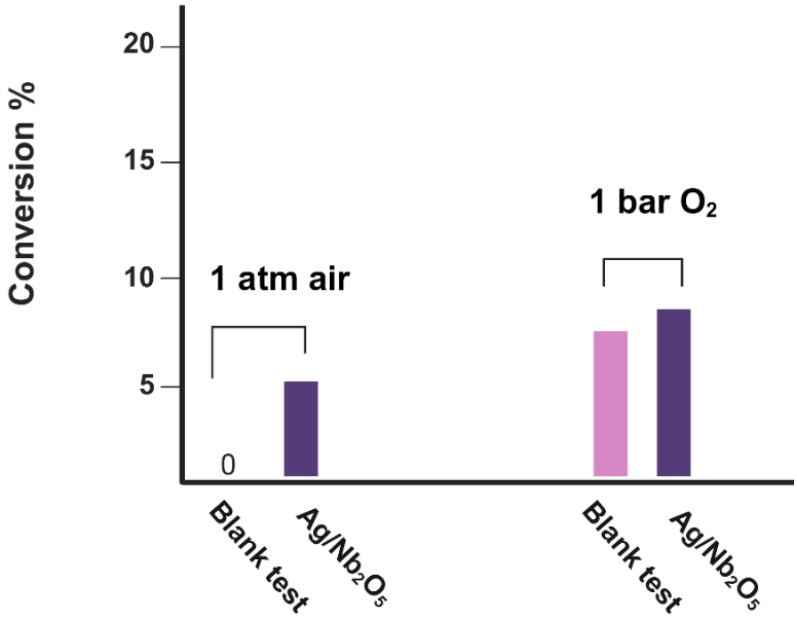

Figure 6.5: *p*-xylene oxidation by Ag/Nb_2O_5, the test was carried out at 120°C 24h at atmospheric pressure and 1 bar pressured oxygen.

According to the results shown in figure 6.5, the experimental data illustrate the oxidation of *p*-xylene under various conditions. The conversion rates demonstrate that Ag/Nb_2O_5 strongly promotes the oxidation of *p*-xylene when compared to the blank test. Specifically, under atmospheric pressure, the blank test exhibited no conversion at 1 atm, while the catalyzed reaction achieved 4% conversion rates. Additionally, when subjected to pressurized oxygen the blank test yielded 7% conversion while 9 % at 1 bar O_2. These findings highlight the significant catalytic efficiency of Ag/Nb_2O_5 in facilitating the oxidation process across different oxygen environments. Despite initial observations suggesting similar conversion rates in both the blank and catalysed reactions, the overall data clearly indicate that Ag/Nb_2O_5 enhances the oxidation of *p*-xylene. To further evaluate the impact of our catalyst on product selectivity, a detailed analysis was performed, comparing the selectivity of products formed in both the blank and catalysed reactions. The results of this selectivity analysis are presented in the subsequent (graph 6.6), which enables an assessment of the catalytic influence of Ag/Nb_2O_5. This comparison is essential for understanding whether the catalyst not only improves the conversion rate but also directs the reaction towards more desirable products.

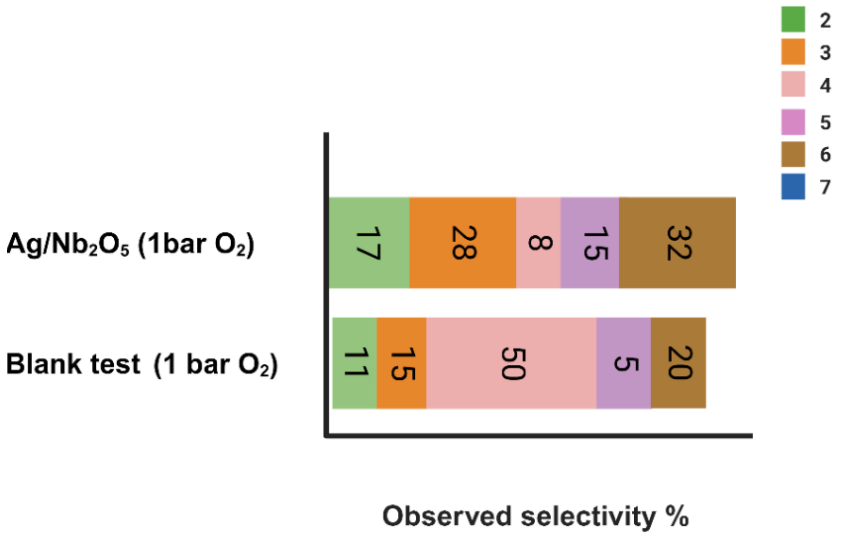

Figure 6.6: The observed selectivity for the oxidation of p-xylene was analyzed by comparing the selectivity obtained from the blank test with that of the Ag/Nb_2O_5 catalyst, both conducted under identical conditions at 1 bar of O_2. This comparative analysis allows for a clearer understanding of how the presence of the catalyst influences product distribution in the reaction. The selectivity of by-products is highlighted in distinct colours for clarity■: p-Methyl benzyl alcohol, ■: p-Tolualdehyde, ■: p-Toluic acid, ■: p-Hydroxymethylbenzoic acid, ■: p-Carboxybenzaldehyde, ■: Terephthalic acid

From the graph 6.5, the selectivity distribution between the blank test and our Ag/Nb_2O_5 catalyst showed a difference in reactivity. Particularly, during the reaction, the blank test produced a high amount of p-toluic acid, reaching 50% selectivity. In contrast, the use of Ag/Nb_2O_5 catalyst significantly reduced the production of p-toluic acid to just 8%. This variation in product distribution indicates that our catalyst plays a crucial role in influencing selectivity during the oxidation of *p*-xylene. The overall differences in selectivity further demonstrate the effectiveness of Ag/Nb_2O_5 in direct the reaction towards more desirable products. Taking this result into account, we proceed to investigate the roles of our catalyst under different reaction conditions, specifically comparing atmospheric conditions and 1 bar of O_2. The findings from this investigation are illustrated in the following figure 6.7.

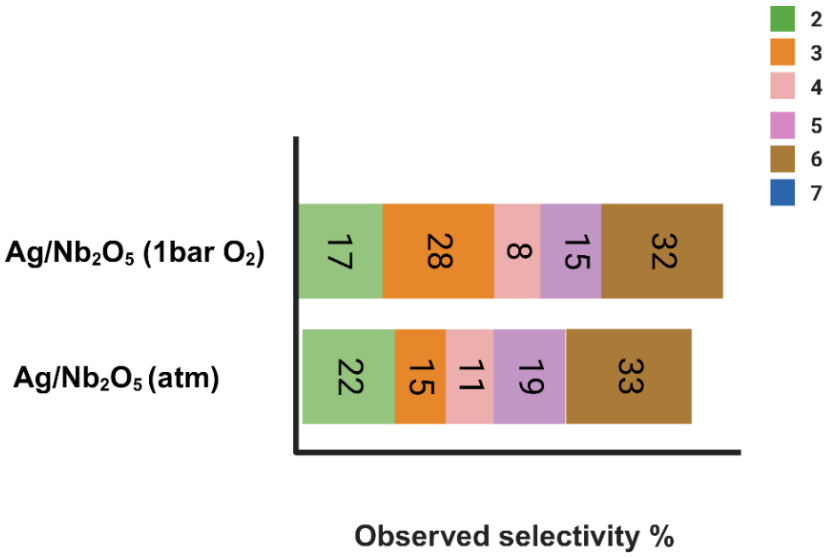

Figure 6.7: Observed selectivity of *p*-xylene oxidation using the same catalyst Ag/Nb_2O_5 under different conditions (atmospheric pressure and 1 bar O_2). The selectivity of by-products is highlighted in distinct colors for clarity: ■: p-Methyl benzyl alcohol, ■: p-Tolualdehyde, ■: p-Toluic acid, ■: p-Hydroxymethylbenzoic acid, ■: p-Carboxybenzaldehyde, ■: Terephthalic acid.

The distribution of selectivity is different when comparing the selectivity distribution of the blank test, as shown in figure 6.6. By examining both catalytic activities under atmospheric conditions and at 1 bar of oxygen figure 6.7, it is evident that the catalyst plays a significant role in the selectivity process by facilitating the decomposition of intermediates. As previously discussed at the beginning of this chapter, this process leads to a complex reaction mixture. This highlights the importance of the catalyst in influencing not only the conversion rates but also the specific product distribution formed during the oxidation of *p*-xylene. However, the target product which is terephthalic acid was absent in the product mixtures. This could be due to intermediate acids, such as p-toluic acid and *p*-carboxybenzaldehyde, participating in dehydration reactions with alcohols, leading to their consumption before terephthalic acid could form. The absence of terephthalic acid in the product mixture could be attributed to several factors, which need further investigation in future work. One possible reason is that insufficient reaction time may result in the formation of intermediates without their full conversion to the desired product. Extending the reaction duration might facilitate the complete conversion of these intermediates to terephthalic acid. Additionally, the choice of solvent can significantly influence both the reaction pathway and product distribution. Testing different solvents [40] may uncover conditions that favour the formation of terephthalic acid, thereby enhancing the overall yield of the desired product. Moreover, the stability of intermediates such as *p*-toluic acid and *p*-

carboxybenzaldehyde could also contribute to their preferential formation over terephthalic acid. Investigating the stability and reactivity of these intermediates will provide valuable results into how to modify the reaction pathway to promote the production of terephthalic acid. Moreover, for future work, a possible approach would be to test terephthalic acid itself in combination with the alcohols formed during the reaction to determine if dehydration occurs. This could help elucidate the interactions between the product and the reaction environment, providing further understanding of the factors influencing the formation of terephthalic acid. Addressing these aspects in future studies will be crucial for optimizing the reaction conditions and achieving the desired product.

6.6 Ag/Nb_2O_5 versus Mn/CeO_2 for p-xylene oxidation

Polyester is mainly produced from terephthalic acid (TPA), which is synthesized through the liquid phase catalytic oxidation of *p*-xylene oxidation [50-51-52]. The liquid phase oxidation of p-xylene has been investigated using a variety of methods, but around 70% of the terephthalate feedstock generated worldwide is made with a catalyst system that was created through scientific design, commonly referred to as the Amoco process, Nearly all new plants utilize this method [53-54]. The oxidation of p-xylene typically uses one or two multivalent metal salts (commonly Co or Mn) and bromine as a source of free radicals [55] . In this procedure, acetic acid is employed as the solvent. With air serving as the oxygen source and a pressure of 1-2 MPa, the reaction temperature ranges from 160 to 200 °C [56]. As previously illustrated in scheme 6.3, the reaction passes through a number of intermediates, including *p*-tolualdehyde (TALD), *p*-toluic acid (*p*-TOA), and 4-carboxybenzaldehyde (4-CBA). The fundamental principle behind catalytic oxidation-reduction involves electron transfer from the reductant to the catalyst, followed by a faster transfer from the catalyst to the oxidant compared to direct electron transfer between the reductant and oxidant. For this catalysis to occur, the metal must possess two distinct oxidation states, neither of which is overly stable relative to the other. The oxidation and reduction of saturated molecules often result in the formation of free radicals. Transition metals like Cu, Co, and Mn are capable of catalysing these oxidations. Among such reactions are hydrocarbon and organic molecule autoxidation, which initially produce hydroperoxides through free-radical chain mechanisms [17]. In comparison to numerous previous research studies, we aimed to carry out the reaction under milder conditions using our catalyst to activate the primary C-H in *p*-xylene. Additionally, we tested Mn supported in Nb_2O_5 and Mn/CeO_2 to determine whether there were any differences from the results of earlier work. In the oxidation of p-xylene, much of the existing research utilizes manganese (Mn) as a catalyst under high pressure and extended reaction times [40-5]. However, in our study, we employed silver (Ag) as a catalyst in competition with Mn, operating under significantly milder conditions 120 °C for 24 hours and at low pressure. While Mn showed slightly lower conversion rates (4%) compared to our silver-based catalyst (8%) using 1 bar O_2. However, by changing the support Nb_2O_5 to CeO_2 the result slightly changed and the conversion of Mn/CeO_2 show 12% comparing to Ag/CeO_2 (9%), As in the case of CeO_2, surface chemisorbed

molecular oxygen connected to the oxygen vacancies can produce active oxygen species [57-58]. This highlights an opportunity for further optimization and development of our catalytic system. Particularly, our aim represents a unique development, as no previous studies have demonstrated the activation of *p*-xylene under such mild conditions in a solvent-free system. Most reported methodologies rely on the use of metal salts in acetic acid or acetonitrile to achieve this oxidation [59], making our catalysis with solvent-free system a promising alternative for future research.

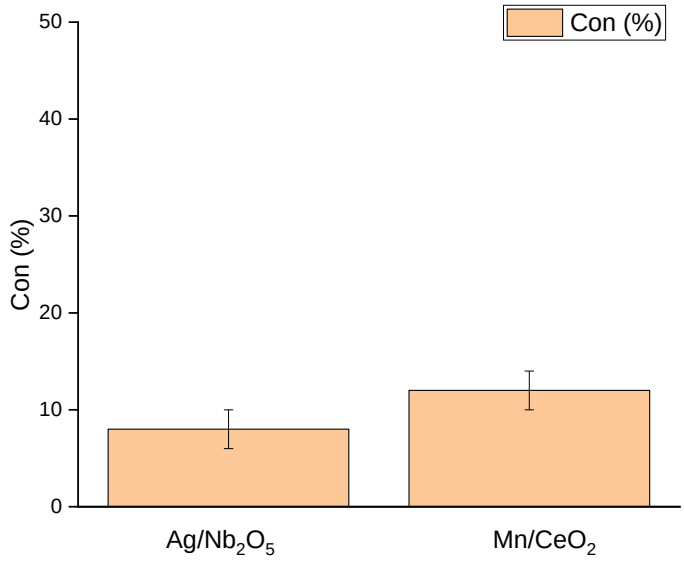

Figure 6.8: Conversion of *p*-xylene oxidation (3 mL) using Ag/Nb_2O_5 vs Mn/CeO_2 under same conditions (atmospheric pressure), 600 rpm, 24h, and 120°C.

6.7 Conclusion

The application of Ag/Nb_2O_5 catalysis for ethylbenzene oxidation yielded highly promising results, demonstrating effective activation of ethylbenzene with increased selectivity toward the desired product acetophenone with K/A ratio 3:1. This prompted us into further investigation into other hydrocarbons, including cyclooctane and *p*-xylene, using the same Ag/Nb_2O_5 catalyst for oxidation at atm and using O_2 pressure. In this study, both cyclooctane and *p*-xylene were activated under mild conditions (120 °C for 24 hours) using atm and O_2 (1 bar). Firstly, cyclooctane oxidation at mild temperature 120°C, using Ag/Nb_2O_5 at atm pressure show a promising result with a conversion of up to 27 % with 60% selectivity for AP, K/A (3/1), which is particularly important compared to other studies that require higher temperatures, elevated pressures [59]. Using 1 bar O_2 for cyclooctane oxidation resulted in a conversion of up to 25%, with a selectivity of 46% towards acetophenone (AP). This indicates that increasing the oxygen pressure beyond the saturation point may not significantly enhance the reaction's efficiency. Moving forward to p-xylene oxidation, the reaction yields intriguing results. The conversion rates demonstrate that, in comparison to the blank test, the presence of the Ag/Nb_2O_5 catalyst significantly enhances the oxidation of p-xylene, achieving a conversion of up to 5%, and further increasing to 9% under 1 bar of O_2. These findings highlight the promising potential of Ag/Nb_2O_5 as an effective catalyst in a solvent-free system. This is particularly noteworthy when contrasted with other studies, which have employed corrosive solvents such as acetic acid and required high reaction temperatures of up to 200 °C to achieve similar outcomes. Our results present a compelling case for the use of Ag/Nb_2O_5 in p-xylene oxidation, as the reaction proceeds under milder conditions, with lower temperatures and without the need for harsh solvents. This not only reduces environmental impact but also improves the overall sustainability of the process. The ability to perform selective oxidation of *p*-xylene under these conditions opens new opportunities for catalyst development and optimization. It suggests the potential for expanding the application of Ag/Nb_2O_5 to other hydrocarbon oxidation processes, thereby contributing to the advancement of greener and more efficient catalytic systems. This shift towards milder reaction conditions aligns with the growing demand for environmentally friendly chemical processes and demonstrates the potential for Ag/Nb_2O_5 to play a key role in future innovations in selective oxidation reactions.

6.8 References

1 X. Cao, T. Han, Q. Peng, C. Chen and Y. Li, *Chem. Commun.*, 2020, **56**, 13918–13932.

2 F. Roudesly, J. Oble and G. Poli, *J. Mol. Catal. A Chem.*, 2017, **426**, 275–296.

3 H. A. Ball, H. A. Johnson, M. Reinhard and A. M. Spormann, *J. Bacteriol.*, 1996, **178**, 5755.

4 F. A. Daniher, *Org. Prep. Proced.*, 1970, **2**, 207–210.

5 P. Raghavendrachar and S. Ramachandran, *Ind. Eng. Chem. Res.*, 1992, **31**, 453–462.

6 M. S. S. Balula, I. C. M. S. Santos, M. M. Q. Simões, M. G. P. M. S. Neves, J. A. S. Cavaleiro and A. M. V Cavaleiro, *J. Mol. Catal. A Chem.*, 2004, **222**, 159–165.

7 N. Theyssen and W. Leitner, *Chem. Commun.*, 2002, 410–411.

8 Q. Fan and X. Yan, *Soft Comput.*, 2015, **19**, 1363–1391.

9 R. D. Bach and O. Dmitrenko, *J. Am. Chem. Soc.*, 2004, **126**, 4444–4452.

10 Y. Luo, *Comprehensive handbook of chemical bond energies*, CRC press, 2007.

11 H. X. Yuan, Q.-H. Xia, H.-J. Zhan, X.-H. Lu and K.-X. Su, *Appl. Catal. A Gen.*, 2006, **304**, 178–184.

12 A. Szymańska, W. Nitek, M. Oszajca, W. Łasocha, K. Pamin and J. Połtowicz, *Catal. Letters*, 2016, **146**, 998–1010.

13 A. Abutaleb and M. A. Ali, *Rev. Chem. Eng.*, 2022, **38**, 769–797.

14 K. N. Sedenkova, K. S. Andriasov, S. A. Stepanova, I. P. Gloriozov, Y. K. Grishin, T. S. Kuznetsova and E. B. Averina, *European J. Org. Chem.*, 2018, **2018**, 879–884.

15 U. Schuchardt, D. Cardoso, R. Sercheli, R. Pereira, R. S. da Cruz, M. C.

Guerreiro, D. Mandelli, E. V Spinacé and E. L. Pires, *Appl. Catal. A Gen.*, 2001, **211**, 1–17.

16 I. M. Denekamp, M. Antens, T. K. Slot and G. Rothenberg, *ChemCatChem*, 2018, **10**, 1035–1041.

17 M. Arshadi, M. Ghiaci, A. A. Ensafi, H. Karimi-Maleh and S. L. Suib, *J. Mol. Catal. A Chem.*, 2011, **338**, 71–83.

18 J. L. Emdee, K. Brezinsky and I. Glassman, *J. Phys. Chem.*, 1991, **95**, 1626–1635.

19 A. G. Caloyannis and W. F. Graydon, *J. Catal.*, 1971, **22**, 287–296.

20 M. Hronec and Z. Hrabe, *Ind. Eng. Chem. Prod. Res. Dev.*, 1986, **25**, 257–261.

21 S. Nicolae, F. Neaţu and M. Florea, *Comptes Rendus. Chim.*, 2018, **21**, 354–361.

22 S. S. Mahajan, M. M. Sharma and T. Sridhar, *Ind. Eng. Chem. Res.*, 2005, **44**, 1390–1395.

23 J. Chen, H. Yang and C. Wu, *Org. Process Res. Dev.*, 2004, **8**, 252–255.

24 F. Eschenröder and H. Vogel, Chem. Eng. Technol. Ind. Chem. Equipment-Process Eng., 1998, **21**, 671–678.

25 R. Karcz, P. Niemiec, K. Pamin, J. Połtowicz, J. Kryściak-Czerwenka, B. D. Napruszewska, A. Michalik-Zym, M. Witko, R. Tokarz-Sobieraj and E. M. Serwicka, *Appl. Catal. A Gen.*, 2017, **542**, 317–326.

26 W. Trakarnpruk, A. Wannatem and J. Kongpeth, *J. Serbian Chem. Soc.*, 2012, **77**, 1599–1607.

27 X. Wang, B. Lei, L. Ma, L. Zhu, X. Zhang, H. Zuo, D. Zhuang and Z. Li, *Chem. Asian J.*, 2017, **12**, 2799–2803.

28 L. Matachowski, K. Pamin, J. Połtowicz, E. M. Serwicka, W. Jones and R. Mokaya, *Appl. Catal. A Gen.*, 2006, **313**, 106–111.

29 L. Brugnoli, A. Pedone, M. C. Menziani, C. Adamo and F. Labat, *J. Phys. Chem. C*, 2020, **124**, 25917–25930.

30 L. Y. Margolis, in *Adv. Catal.*, Elsevier, 1963, **14**, 429–501.

31 R. A. Sheldon and R. A. Sheldon, *Chem. from Synth. Gas Catal. React. CO*, 1983, **2**, 1–20.

32 A. Bohre, P. R. Jadhao, K. Tripathi, K. K. Pant, B. Likozar and B. Saha, *ChemSusChem*, 2023, **16**, e202300142.

33 B. Saha and J. H. Espenson, *J. Mol. Catal. A Chem.*, 2005, **241**, 33–38.

34 R. Nisticò, *Polym. Test.*, 2020, **90**, 106707.

35 B. Lepoittevin and P. Roger, *Handb. Eng. Spec. Thermoplast.*, 2011, **3**, 97–126.

36 N. A. M. Fadzil, M. H. A. Rahim and G. P. Maniam, *Chinese J. Catal.*, 2014, **35**, 1641–1652.

37 M. Heidari, A. Sedrpoushan and F. Mohannazadeh, *Org. Process Res. Dev.*, 2017, **21**, 641–647.

38 J. W. Patton and N. F. Seppi, *Ind. Eng. Chem. Prod. Res. Dev.*, 1970, **9**, 521–524.

39 E. A. Karakhanov, A. L. Maksimov, A. V Zolotukhina and V. A. Vinokurov, *Russ. J. Appl. Chem.*, 2018, **91**, 707–727.

40 M. Li, F. Niu, X. Zuo, P. D. Metelski, D. H. Busch and B. Subramaniam, *Chem. Eng. Sci.*, 2013, **104**, 93–102.

41 D. S. Kim, Y. H. Shin and Y.-W. Lee, *Chem. Eng. Commun.*, 2015, **202**, 78–84.

42 X. Zuo, F. Niu, K. Snavely, B. Subramaniam and D. H. Busch, *Green Chem.*, 2010, **12**, 260–267.

43 R. J. Sheehan, *Ullmann's Encycl. Ind. Chem.,* Wiley-VCH Verlag GmbH & Co.

KGaA. 2024.

44 E. Karakhanov, A. Maximov, A. Zolotukhina, V. Vinokurov, E. Ivanov and A. Glotov, *Catalysts*, 2019, **10**, 7.

45 Q. Lyu, J. Dong, R. He, W. Sun and L. Zhao, *Chem. Eng. Sci.*, 2021, **232**, 116340.

46 R. A. F. Tomas, J. C. M. Bordado and J. F. P. Gomes, *Chem. Rev.*, 2013, **113**, 7421–7469.

47 T. Nanba, S. Masukawa, A. Abe, J. Uchisawa and A. Obuchi, *Appl. Catal. B Environ.*, 2012, **123**, 351–356.

48 A. Wang, C. Chang and C. Mou, *J. Phys. Chem. B*, 2005, **109**, 18860–18867.

49 L. Y. Margolis and V. N. Korchak, *Russ. Chem. Rev.*, 1998, **67**, 1073–1082.

50 C. A. Lin, in *Polyesters and Polyamides*, Elsevier, 2008, 62–96.

51 P. Rodgers, J. Appl. Polym. Sci., 1993, **48**, 1061-1080.

52 G. P. Karayannidis, A. P. Chatziavgoustis and D. S. Achilias, *Adv. Polym. Technol. J. Polym. Process. Inst.*, 2002, **21**, 250–259.

53 D. I. Collias, A. M. Harris, V. Nagpal, I. W. Cottrell and M. W. Schultheis, *Ind. Biotechnol.*, 2014, **10**, 91–105.

54 E. E. Kwon and J. Lee, *J. Clean. Prod.*, 2024, **469**, 143210.

55 S. A. Chavan, S. B. Halligudi, D. Srinivas and P. Ratnasamy, *J. Mol. Catal. A Chem.*, 2000, **161**, 49–64.

56 W. Partenheimer, *Catal. Org. React.*, 1990, **40**, 321-330.

57 S. Wu, Y. Yang, C. Lu, Y. Ma, S. Yuan and G. Qian, *Eur. J. Inorg. Chem.*, 2018, **2018**, 2944–2951.

58 M. Machida, Y. Murata, K. Kishikawa, D. Zhang and K. Ikeue, *Chem. Mater.*, 2008, **20**, 4489–4494.

59 S. A. H. Zaidi, *Appl. Catal.*, 1986, **27**, 99–106.

Chapter 7: Conclusions and future work

The high relevance of aerobic oxidation of alkyl-substituted benzenes to their corresponding ketones has driven researchers to study and develop the catalytic systems [1]. In this thesis, the main model system was the oxidation of ethylbenzene under mild conditions, investigating the transformation of hydrocarbons in solvent free system to specific products like it ketone acetophenone. This work is significant as hydrocarbon oxidation typically requires high temperature and pressure, which can lead to energy inefficiency and undesirable by-products. By utilizing solvent free system and air condition with bio-catalysis, we aimed to overcome these limitations, specifically targeting the decomposition of intermediates such as 1-phenyl ethyl alkyl hydroperoxide, a critical compound in oxidation pathways [2-3].. Our work aims to be a significant step toward more sustainable and selective oxidation processes in hydrocarbon chemistry.

Quantitative and qualitative analysis of the 1-phenyl ethyl alkyl hydroperoxide using gas chromatography-mass spectrometry (GC-MS) revealed an unexpected complication: the decomposition of the intermediate EBHP to AP and 1-Ph during the injection process rather than as part of the reaction itself. This finding highlighted the limitations of traditional high-temperature analytical techniques for studying sensitive intermediates. To address this issue, we developed an alternative method using nuclear magnetic resonance spectroscopy. This NMR approach allowed for the analysis of EBHP at room temperature [4], eliminating the thermal decomposition observed in the GC-MS analysis. By avoiding the need for high temperatures, this method provided a more accurate representation of the reaction dynamics and intermediate stability. And in turn be able to accurately assess the composition of reaction mixtures which is fundamental for catalyst development. Therefore, from this point on the main goal of this research project was to create new supported nanoparticle catalysts that could selectively oxidise hydrocarbons to yield the desired products (alcohol or ketone), which are important building blocks for the industrial production of fibres and plastics at mild temperatures (120 °C) and atm air pressures (O_2). With this goal in mind, the entire project has been completed by incorporating the following elements:

1) In this study a calculation method for determining the conversion and selectivity in the oxidation of ethylbenzene, *p*-xylene, and cyclooctane using ^{1}H-NMR spectroscopy was developed and validated. The method enabled the accurate quantification of reaction products yielding a conversion of 30 % and selectivity of 75 % for acetophenone in the oxidation of ethylbenzene. Similarly, the oxidation of *p*-xylene demonstrated a 5 % conversion, while cyclooctane oxidation achieved a conversion of 27 % with a 60 % selectivity for AP. The validation of the method was achieved through a close carbon mass balance (CMB), which accounted for 99 % within the experimental error less than ± 5. This result were further study through GC-MS analysis as discussed in details in chapter 3.

2) An investigation into the effects of reaction conditions, such as temperature and O_2 pressure, on the oxidation of ethylbenzene and cyclooctane and *p*-xylene, both with and without catalysts, was conducted to determine ideal conditions for catalyst testing and to study the autoxidation process as a benchmark. For example, Ethylbenzene oxidation was performed at 100°C and 120°C , 130 °C for 24 hours in atm pressure and under 1, 2 bar O_2 (Chapter 4), while cyclooctane and *p*-xylene oxidation was carried out at 120 °C for 24 hours in atm and under 1 bar O_2 (Chapter 6).

3) This thesis investigates the decomposition behavior of 1-phenyl ethyl alkyl hydroperoxide through the synthesis of the intermediate and its subsequent analysis. The study focuses on the synthesis of EBHP intermediate, which is then analyzed using Gas Chromatography-Mass Spectrometry (GC-MS) to gain insights into its stability, decomposition pathways. After the synthesis of the alkyl hydroperoxide intermediate, the sample is injected into the GC-MS system for both qualitative and quantitative analysis. The quantitative analysis revealed a variation in the ketone to alcohol (K/A) ratio with a ratio of ~ 4:1 which can be attributed to the decomposition of EBHP at the injection point during GC-MS analysis. This thermal decomposition of EBHP during injection highlights a significant limitation of GC-MS for accurately quantifying this intermediate. To address this limitation, ^{1}H-NMR was used as an alternative analytical technique as it operates at room temperature and eliminates the decomposition of EBHP.

4) It has been demonstrated that Nb_2O_5 facilitates the decomposition of 1-phenyl ethyl alkyl hydroperoxide (EBHP) in Ethylbenzene oxidation, a previously unreported effect. Based on this observation, supported metals (Ag) over Nb_2O_5 was designed for hydrocarbon oxidation. When Ethylbenzene was oxidised, the catalysts showed high catalytic activity, especially when it came to producing ketones and alcohols. They demonstrated its potential for use in this industry by achieving 70% selectivity for acetophenone in ethylbenzene oxidation with 30% conversion. Additionally, both cyclooctane and p-xylene were activated under mild conditions (120°C for 24 hours) using atm and O_2 (1 bar). Firstly, cyclooctane oxidation at mild temperature 120°C, using Ag/Nb_2O_5 at atm pressure show a promising result with a conversion of up to 27 % with 60% selectivity for AP, K/A (3/1), which is particularly important compared to other studies that require higher temperatures, elevated pressures a structure-activity relationship was established by examining the properties of supported metal nanoparticles such as metal loading, particle size, and oxidation state using characterization techniques including XRPD, TEM, XPS, and ICP-MS.

In particular, the catalytic reactivity of Nb_2O_5 was thoroughly examined in the oxidation of Ethylbenzene, which could produce alcohols and ketones. It was concluded that Nb_2O_5 is indeed reactive in this process. Based on these control tests, the influence of Nb_2O_5 and Ethylbenzene was ruled out, confirming the catalytic activity of Nb_2O_5 in the oxidation of Ethylbenzene. Using XPRD and XPS analysis showed that Nb_2O_5 maintained high stability by withstanding acid attack, with Nb primarily existing as Nb^{5+} rather than Nb^{4+}, eliminating the influence of Nb^{4+} species. Furthermore, the decomposition of 1-phenylethyl alkyl hydroperoxide in the presence of Nb_2O_5 suggested that Nb_2O_5 plays a role in the breakdown of 1-phenyl ethyl alkyl hydroperoxide. These results highlight the potential of Nb_2O_5 in hydrocarbon oxidation, a field that has garnered little attention and requires further investigation for deeper understanding. Building on the investigation into the catalytic activity of Nb_2O_5, a new supported metal material was created and utilized for hydrocarbon oxidation. This approach has not been previously reported in the literature. In this study, silver (Ag) was supported on Nb_2O_5 using a wet impregnation method and applied to the oxidation of ethylbenzene, cyclooctane, and *p*-xylene. These reaction results suggest that the Ag/Nb_2O_5 catalyst system shows great promise for the oxidation of hydrocarbons, particularly for the production of ketones and alcohols. Ketones, in particular, are

valuable precursors for manufacturing materials such as nylon and fibers. Additionally, the investigation into the roles of Ag species and Nb_2O_5 in the reaction pathway shown that (Ag_2O, Ag^+) could activate molecular oxygen to produce superoxide species. These superoxide are probably bound to metal centres or metal oxides, facilitating the abstraction of hydrogen atoms from hydrocarbons to initiate oxidation. Furthermore, Ag^+ acted as an initiator for C-H bond cleavage whereas Ag species (Ag^0) is formed during the reaction but did not take part in the reaction. This was illustrated by the reaction of ethylbenzene, where using Ag_2O and Ag^0 at 80°C and 100°C and 120°C for 24 hours resulted in 0% conversion with Ag^0 and 35% conversion with Ag+, thereby confirming our findings. The intermediate alkyl hydroperoxides formed after the initiation step can be decomposed by Nb_2O_5 to produce alcohols and ketones. It is important to note that the cleavage of the O-O bond in EBHP can generate alcohols, which is likely associated with Nb_2O_5. Meanwhile, the abstraction of α-H from EBHP leads to ketones, a process enhanced by the presence of Ag (+) in the catalysts. This was evidenced by the observation that alkyl hydroperoxide was a major product in control tests using solid $AgNO_3$ or Ag_2O, whereas Ag/Nb_2O_5 favoured the production of acetophenone. Additionally, it is worth noting that WI-Ag/Nb_2O_5 demonstrated a good stability with minimal Ag leaching (0.02%) during ethylbenzene oxidation, indicating its potential for further development in this reaction. ICP-MS analysis showed minimal leaching of Ag (0.02%) indicating that the catalyst is highly stable and effectively retains its active metals. As a result, our research has developed a bifunctional catalyst for the selective oxidation of ethylbenzene. Based on these results, we believe Ag/Nb_2O_5 holds significant promise for hydrocarbon oxidation and could also be adapted for the oxidation of alcohols in future studies.

Prospects for future investigation: This study provides a basis for future research efforts, offering avenues for further exploration. Following investigations could focus on gaining deeper understanding into the catalytic oxidation process and selectivity control. Potential areas for future research include:

I. Evaluation of catalyst efficiency in hydrocarbon oxidation reactions.

For future work, applying the developed heterogeneous catalyst Ag/Nb_2O_5 to other hydrocarbons (e.g., cumene, toluene) or alcohols, would be a valuable step in assessing its broader efficiency. The oxidation of cumene holds substantial

importance in the chemical industry. The desired product, cumene hydroperoxide (CHP), serves as a key precursor for various chemicals such as phenol, acetone, and propylene oxides [5-6]. Toluene oxidation is a key industrial process, transforming this simple aromatic hydrocarbon into valuable products like benzyl alcohol, benzaldehyde, benzoic acid, and benzoates. These oxidation products are crucial, as they are widely used in daily life for manufacturing perfumes, dyes, plasticizers, flame retardants, preservatives, pesticides, and pharmaceuticals. Among these, benzaldehyde is the most commonly produced. Benzaldehyde production can indeed exceed 90,000 tons per year globally [7]. By studying both cumene and toluene, valuable insights can be gained into the catalytic process, enhancing the understanding of oxidation reactions and broadening the potential applications of this catalyst. This extension could provide insights into the catalyst's performance across different substrates, potentially leading to optimized processes for a wider range of hydrocarbon oxidation reactions.

II. Investigation of inhibitor effect

It is essential to investigate the inhibitory effects observed in the current study, as the reaction did not proceed to completion. The presence of inhibitors can significantly influence reaction kinetics, and understanding their impact is crucial for optimizing reaction conditions. The objective of this investigation is to identify the inhibitors affecting the reaction and to quantify their impact on the overall reaction rates. Because of this, we can use different kinds of alcohol, like isopropanol or phenol as both can be react similar to 1-phenylethanol in ethylbenzene oxidation, and this will help to carry out additional research into the inhibitory effects of different alcohols. In order to do this, we suggest incorporating isopropanol into ethylbenzene reaction mixture at 120°C 24h. By analyzing the role of isopropanol or phenol as an inhibitor, we can gain insights into how it interacts with the reaction components and influences the overall kinetics. Such comparative analysis will provide a clearer picture of the efficacy of different inhibitors in this reaction system.

III. Protocols for the deposition of Nb to form NbOx, over CeO_2

Given the synergistic effect resulting from the robust oxygen buffering capacity of cerium dioxide (CeO_2) combined with the significant redox activity of niobium (Nb), we

can explore the deposition of Nb to form niobium oxide (NbO) on the surface of CeO_2 [8]. This composite material could facilitate the selective oxidation of ethylbenzene (EB) to acetophenone (AcPO) using molecular oxygen, without the need for solvents or additives. To synthesize NbO_x over a CeO_2 substrate using a sol-gel method, the process involves the preparation of a niobium ethoxide-based precursor. The initial step includes dispersing the niobium ethoxide in an alcohol medium, where it is allowed to mix briefly. Once the suspension is stable, CeO_2 is incorporated into the mixture. The resulting composite is subjected to thermal treatment and stirring to ensure uniform deposition of NbO_x over the CeO_2 surface. This process produces the desired niobium oxide coating over the cerium oxide support, which can be employed for various hydrocarbon oxidation applications. The enhanced reactivity of the catalyst can be attributed to the synergistic roles of CeO_2 and Nb. CeO_2 likely contributes to the initiation of the reaction and increases the overall conversion due to its high oxygen storage capacity, facilitating the supply of active oxygen species during the oxidation process. Meanwhile, Nb plays a crucial role in decomposing reaction intermediates, thereby promoting the selective oxidation pathways. This combination of CeO_2 ability to activate oxygen and Nb catalytic decomposition properties creates an efficient catalytic system, improving both the activity and selectivity of the reaction.

7.1 References

1 X. Liu, Y. Ryabenkova and M. Conte, *Phys. Chem. Chem. Phys.*, 2015, **17**, 715–731.

2 J. Luo, F. Peng, H. Yu, H. Wang and W. Zheng, *ChemCatChem*, 2013, **5**, 1578–1586.

3 A. Peng, M. C. Kung, R. R. O. Brydon, M. O. Ross, L. Qian, L. J. Broadbelt and H. H. Kung, *Sci. Adv.*, 2020, **6**, eaax6637.

4 H. Günther, NMR spectroscopy: basic principles, concepts and applications in chemistry, John Wiley & Sons, 2013.

5 S. U. Nandanwar, S. Rathod, V. Bansal and V. V. Bokade, *Catal. Letters*, , DOI:10.1007/s10562-020-03474-8.

6 S.-J. Shen, A.-H. Tseng, C.-C. Shi and B.-Y. Yu, *Chem. Eng. Res. Des.*, 2023, **200**, 602–614.

7 R. Wu, S. Pan, Y. Li and L. Wang, *J. Phys. Chem. A*, 2014, **118**, 4533–4547.

8 J. Liu, R. Meng, P. Jian and R. Jian, *ACS Sustain. Chem. Eng.*, 2020, **8**, 16791–16802.